

# Synthesis and characterization of iron-clathrochelates and their applications in materials science

Présentée le 17 janvier 2020

à la Faculté des sciences de base  
Laboratoire de chimie supramoléculaire  
Programme doctoral en chimie et génie chimique

pour l'obtention du grade de Docteur ès Sciences

par

**José Luis BILA**

Acceptée sur proposition du jury

Prof. J. Waser, président du jury  
Prof. K. Severin, directeur de thèse  
Prof. A. Coskun, rapporteur  
Dr C. Bucher, rapporteur  
Prof. M. Mazzanti, rapporteuse



# Acknowledgements

It has been four long years of hard work of with a lot of laughter and tears. I am very happy to see the end and I have to acknowledge that it wouldn't be possible without the external support I received from various people. Therefore, I would like to express my gratitude by sharing my happiness with all of them.

First, I would like to express my gratitude to my thesis director, Prof. Kay Severin for giving me the opportunity to pursue my doctoral studies in his research group. He was always very patient and open to discussions; his experience and advices have certainly been my academic success determinants.

I would like to thank prof. Ali Coşkun, prof. Marinella Mazzanti and Dr. Christophe Bucher for devoting their time to read and correct my thesis as well as being part of my examination jury. A special thanks goes to prof. Jérôme Waser for accepting the role of president during my private defense.

I always enjoyed my time at the doctoral school's office and I have to thank Anne-Lene Odegaard for always being available to help with everything. Similarly, life would not be easy without our lovely secretary Christina Zammanos; thanks a lot for all your help. I would like to extend my gratitude to all collaborators at the BCH building; Dr. Laure Menin, Dr. Daniel Ortiz and Francisco Sepulveda from the Mass Spectrometry facility and Dr. Pascal Mieville and Emilie Baudat from the NMR facilities. Thank you for always working towards finding the proper solutions to my clathrochelate problems. The results from the X-ray facility were certainly a key to a sad or a happy day. I would like to thank Dr. Rosario Scopelliti and Dr. Farzaneh Fadei-Tirani for always trying their best to deliver the latter. Additionally, I would like to thank Dr. Euro Solari for helping me and everyone else with all the technical problems inside and outside the lab. He is definitely a champion in handling and mounting crystals.

A special thanks to Dr. Mathieu Marmier for his patience and dedication at my early PhD days. He taught me many tricks, which helped me, succeed in the late stages of my PhD. I would like to thank all old members of LCS; Dr. Nicolas Luisier, Dr. Suzanne Jansze, Dr. Marcus Papmayer and Dr. Loic Jean-Bourquin for being welcoming. I thank Dr. Giacomo Cecot, Dr. Léonard Eymann (hallelujah reverend) and Dr. Yizhu Liu for all the scientific discussions and mostly importantly for all the loud and nonstop singing in BCH 3409.

My lovely colleagues and special friends Ophélie and Erica always had my back and I am very lucky to have met them during my LCS years. I thank you for all the scientific and emotional support you gave me even without noticing. I would like to thank all current LCS members: my brother from another mother Cesare (Barbie girl), Carl, Alik, Pavel, Christian, Dong, Ruijin, Iris, Anastasia and Aude for all coffee break discussions etc. My quasi-LCS friend Sebastian Mauries, thank you for the fun days and concerts.

I would like to thank all my friends from the other EPFL labs with whom I spent so much time: PBL (Eva, Kaltrina, Alice, Giacomo and Filippo), LMOM (Vincent, Audrey, Giuseppe, Enzo, Bilal and Julien) and SUNMIL (Sergio,

Ahmet, Elif and Özgün). I thank Ahmet, Elif and Özgün for all the good discussions about life and complaints about politics.

While at the EPFL, I was very fortunate to be part of The Consulting Society where I met many people: Robert (dictator), Rayan, Tijana, Sherif, Philipp, Firas, Benoit, Wassim, Charles and Adrien. Thank you all for being part of such an amazing experience. A special thanks to Tijana and Kevin for their friendship inside and outside of the association.

I am always happy to talk about my first and best friend in Lausanne, Thiemo. It has been a pleasure meeting you and I always enjoyed your company. A special thanks to Mariana for always taking care of Thiemo and trying to learn German just to make him happy. I would like to thank my friends and colleagues from capoeira; Raul (Peixe) and Sonia (Amazonas) for all the good times spent trying to learn new moves and songs. I would like to thank my Turkish friends: Özgür, Çağır, Özge and Ömer for all the great times we have spent together in Lausanne, from the Rakı nights to the barbeques. I would like also to thank Öykü, Ezgi and Alper for their invaluable friendship.

I would like to thank my whole family for supporting me in the best way they could. I would not be here without my aunt Beatriz Bila, who raised me and always made sure I had an education and all means to succeed in life. Special thanks to my parents-law and brother-in law (Halil) for always being supportive in the most difficult times.

I do not have words to express my gratitude to my lovely wife, Hale Bila. She has definitely been my rock for the past 11 years. I am extremely lucky to have met and married you and I thank you for everything you have done for me. I can only say I love you so much and I dedicate this thesis to you.



# Abstract

This thesis focuses on the design and the synthesis of mono- and dinuclear iron clathrochelate complexes and their applications in materials science.

Dinuclear iron clathrochelate complexes can be synthesized in different oxidation states: *i.* as negatively charged  $\text{Fe}^{\text{II}}\text{-Fe}^{\text{II}}$  complexes or *ii.* as neutral  $\text{Fe}^{\text{II}}\text{-Fe}^{\text{III}}$  complexes. These compounds display interesting magnetic properties. The negatively  $\text{Fe}^{\text{II}}\text{-Fe}^{\text{II}}$  complexes are antiferromagnetic, whereas the neutral  $\text{Fe}^{\text{II}}\text{-Fe}^{\text{III}}$  complexes are paramagnetic. In addition, an interconversion between the two redox states can be achieved, both chemically and electrochemically. The functionalization of clathrochelate complexes with electron-donating groups was found to stabilize the higher oxidation states ( $\text{Fe}^{\text{III}}\text{-Fe}^{\text{III}}$ ), which was evidenced electrochemically. However, the deliberate preparation and isolation of  $\text{Fe}^{\text{III}}\text{-Fe}^{\text{III}}$  complexes was not achieved. Dinuclear iron clathrochelate complexes were successfully employed as redox-active compounds for redox flow batteries, and they displayed high battery voltages and Coulombic efficiencies.

Iron clathrochelate complexes are stable under the harsh conditions of metal-catalyzed coupling reactions (e.g. Suzuki or Sonogashira reactions). The high stability makes them suitable building blocks for the preparation of networks displaying permanent porosity. Both mononuclear and dinuclear iron clathrochelate-based networks displayed apparent BET surface areas between 235 and 593  $\text{m}^2\text{g}^{-1}$ . Moreover, all clathrochelate-based porous networks displayed high thermal and chemical stabilities. Mononuclear iron clathrochelate building blocks can be decorated with chiral ligands, resulting in homochiral porous networks with apparent BET surface areas up to 548  $\text{m}^2\text{g}^{-1}$ . Such materials were found to selectively adsorb D-tryptophan from water.

Porous networks based on iron clathrochelates can also be synthesized *via* polycondensation reactions. This synthetic strategy involves the combination of an iron salt, a dioxime ligand, and a capping boronic acid. The resulting Fe-templated condensation reactions give networks with apparent BET surface areas up to 927  $\text{m}^2\text{g}^{-1}$ . Similarly, these materials display high chemical and thermal stabilities. Additionally, they were found to efficiently adsorb chromium (VI) from water.

## Keywords

Clathrochelate complexes, supramolecular chemistry, redox-active complexes, coordination polymers, paramagnetic complexes.

# Résumé

Cette thèse porte sur la conception et la synthèse de complexes de clathrochélates de fer mono- et dinucléaires et leurs applications en science des matériaux.

Les complexes de clathrochélates de fer dinucléaires peuvent être synthétisés dans différents états d'oxydation: *i.* comme complexes  $\text{Fe}^{\text{II}}\text{-Fe}^{\text{II}}$  chargés négativement ou *ii.* comme complexes  $\text{Fe}^{\text{II}}\text{-Fe}^{\text{III}}$  neutres. Ces composés présentent des propriétés magnétiques intéressantes. Les complexes  $\text{Fe}^{\text{II}}\text{-Fe}^{\text{II}}$  sont antiferromagnétiques, tandis que les complexes  $\text{Fe}^{\text{II}}\text{-Fe}^{\text{III}}$  neutres sont paramagnétiques. De plus, une interconversion entre les deux états redox peut être réalisée, à la fois chimiquement et électrochimiquement. La fonctionnalisation des complexes de clathrochélates avec des groupes donneurs d'électrons a permis de stabiliser les états d'oxydation supérieurs ( $\text{Fe}^{\text{III}}\text{-Fe}^{\text{III}}$ ), ce qui a été démontré par une voie électrochimique. Cependant, la préparation délibérée et l'isolement des complexes  $\text{Fe}^{\text{III}}\text{-Fe}^{\text{III}}$  n'ont pas été réalisés. Des complexes de clathrochélates de fer dinucléaires ont été utilisés avec succès comme composés redox-actifs pour les batteries à flux, et ils ont montré des tensions de batterie et des efficacités Coulombiques élevées.

Les complexes de clathrochélates de fer sont stables dans les conditions des réactions de couplage catalysées par des métaux (par exemple, les réactions de Suzuki ou Sonogashira). Leur stabilité élevée en fait des composantes de base appropriés pour la préparation de matériaux présentant une porosité permanente. Les matériaux à base de clathrochélates de fer mono- et dinucléaires présentent des surfaces apparentes BET comprises entre 235 et 593  $\text{m}^2 \text{g}^{-1}$ . De plus, tous les matériaux poreux à base de clathrochélates présentaient une stabilité thermique et chimique. Les clathrochélates de fer mononucléaire peuvent être décorés avec des ligands chiraux, ce qui donne des matériaux poreux homochiraux avec des surfaces apparentes BET jusqu'à 548  $\text{m}^2 \text{g}^{-1}$ . On a constaté que de tels matériaux adsorbent sélectivement le D-tryptophane de l'eau.

Les matériaux poreux à base de clathrochélates de fer peuvent également être synthétisés par des réactions de polycondensation. Cette stratégie de synthèse implique la combinaison d'un sel de fer, d'un ligand dioxime et d'un acide boronique. Les réactions de condensation qui en résultent donnent des matériaux avec des surfaces apparentes BET allant jusqu'à 927  $\text{m}^2 \text{g}^{-1}$ . De même, ces matériaux présentent des stabilités chimiques et thermiques élevées. De plus, on a constaté qu'ils adsorbent efficacement le chrome (VI) de l'eau.

## Mots clés

Complexes de clathrochélates, chimie supramoléculaire, Complexes paramagnétiques, polymères de coordination, composés redox-actifs.

# Abbreviation and Symbols

°	degree
1D	one-dimensional
2D	two-dimensional
3D	three-dimensional
Å	Ångström
Ar	aryl
av.	average
°C	degree Celsius
<i>ca.</i>	<i>circa</i>
calcd	calculated
d	doublet
dd	double doublet
ddd	double double doublet
DMSO	dimethyl sulfoxide
DOSY	diffusion-ordered NMR spectroscopy
dppf	1,1'-Ferrocenediyl-bis(diphenylphosphine)
dt	double triplet
$\delta$	chemical shift
e.g.	<i>exempla gratia</i>
en	ethylenediamine
ESI-MS	electrospray ionisation mass spectrometry
Et	ethyl
<i>et al.</i>	<i>et alia</i>
g	gram
h	hour
HRMS	high-resolution mass spectrometry
Hz	Hertz

<i>J</i>	coupling constant
K	Kelvin
kDa	kilodalton
kJ	kilojoule
m	multiplet, or minute
<i>m</i>	meta
M	molar (mol.L <sup>-1</sup> )
<i>m/z</i>	mass:charge ratio
Me	methyl
mg	milligram
MHz	megahertz
mL	millilitre
mM	millimolar (mmol. L <sup>-1</sup> )
mmol	millimole
mol	mole
μmol	micromole
<i>n</i>	number or normal
n-Bu	normal-butyl
nm	nanometre
NOESY	nuclear Overhauser effect NMR spectroscopy
NMR	nuclear magnetic resonance
<i>o</i>	ortho
OTf	triflate, trifluoromethanesulfonate
<i>p</i>	para
Ph	phenyl
ppm	parts per million
q	quartet
ref	reference
RT	room temperature

s	singlet
t	triplet, or time
T	temperature

Note: additional abbreviation for specific compounds are defined within the manuscript.

# Table of contents

<b>Chapter 1 Introduction .....</b>	<b>1</b>
1.1 Mononuclear, boronate ester-capped clathrochelate complexes.....	1
1.1.1 Applications in supramolecular chemistry and materials science .....	5
1.2 Dinuclear, boronate ester-capped clathrochelate complexes .....	8
1.2.1 Applications in supramolecular chemistry and materials science .....	9
1.3 Aims of the project.....	14
<b>Chapter 2 Homo- and heterodinuclear iron clathrochelate complexes .....</b>	<b>17</b>
2.1 Synthesis and characterization of dinuclear iron clathrochelate complexes containing terminal 4-pyridyl groups.....	17
2.2 Synthesis and characterization of dinuclear iron clathrochelate complexes containing different functional groups in the ligand periphery .....	24
2.3 Heterometallic clathrochelate complexes .....	29
<b>Chapter 3 Dinuclear iron clathrochelates as redox-active compounds for redox flow batteries.....</b>	<b>33</b>
3.1 Introduction .....	33
3.2 Clathrochelate complexes.....	38
3.3 Clathrochelate-based redox flow batteries.....	44
<b>Chapter 4 Porous networks based on iron clathrochelate complexes .....</b>	<b>49</b>
4.1 Introduction .....	49
4.2 Clathrochelate complexes as building blocks for porous networks .....	50
4.3 Porous networks based on mononuclear iron clathrochelate complexes.....	52
4.4 Porous materials based on iron clathrochelate complexes .....	66
<b>Chapter 5 Porous materials based on Fe-templated polycondensation reactions .....</b>	<b>69</b>
5.1 Introduction .....	69
5.2 Synthesis and characterization of porous networks containing Fe clathrochelate complexes .....	70
5.3 Removal of Cr (VI) from water .....	77
5.4 Batch adsorption experiments .....	77
<b>Chapter 6 Conclusion and outlook .....</b>	<b>81</b>
<b>Chapter 7 Experimental details.....</b>	<b>83</b>
7.1 General.....	83
7.2 Experimental procedures .....	84
7.1.1 Experimental procedures from chapter 2 .....	84
7.1.2 Experimental procedures from chapter 3 .....	91
7.1.3 Experimental procedures from chapter 4 .....	97
7.1.4 Experimental procedures from chapter .....	104
<b>Chapter 8 Appendix .....</b>	<b>108</b>
8.1 Crystallographic tables .....	108

## Table of contents

---

<b>Chapter 9 References.....</b>	<b>112</b>
<b>Curriculum vitae .....</b>	<b>120</b>

# Chapter 1 Introduction

In 1964, Curry and Busch defined clathrochelates as a new class of coordination compounds where a saturated metal ion is trapped in a cage by coordinating ligands.<sup>[1]</sup> However, recent developments in this field have led to a more specific definition of a clathrochelate as a coordination complex, in which the metal ion is encapsulated and saturated by coordination to donor atoms making it isolated from the external environment. The first synthesized clathrochelates matching this definition were macrobicyclic Co<sup>III</sup> tris-dioximates complexes comprising a single metal ion bound by three dioximate ligands with geometries between trigonal prismatic and trigonal antiprismatic, and two apical capping groups.<sup>[2]</sup> The synthesis of clathrochelates is straightforward and metal-directed. The one-pot synthesis can be achieved by an initial formation of a tris-dioximato precursor complex in situ and finalized by the capping reaction. The capping group is a strong Lewis acid capable of forming a covalent adduct with the oxygen atoms of the dioxime ligands.<sup>[3,4]</sup> Metals such as Co, Fe and Ru, and capping groups such as B, Sn, Ge, and Sb have been incorporated (selected examples are shown in Figure 1.1).<sup>[5-7]</sup> Boronate ester-capped clathrochelates are frequently used since they offer several advantages in terms of functionalization and commercial availability of boronic acid precursors.<sup>[4]</sup> Several metal ion and capping group combinations have been presented to date. However, many of them are not directly relevant to this thesis. Therefore, in this chapter we will discuss selected advances in boronate ester-capped clathrochelate complexes focusing on their applications.

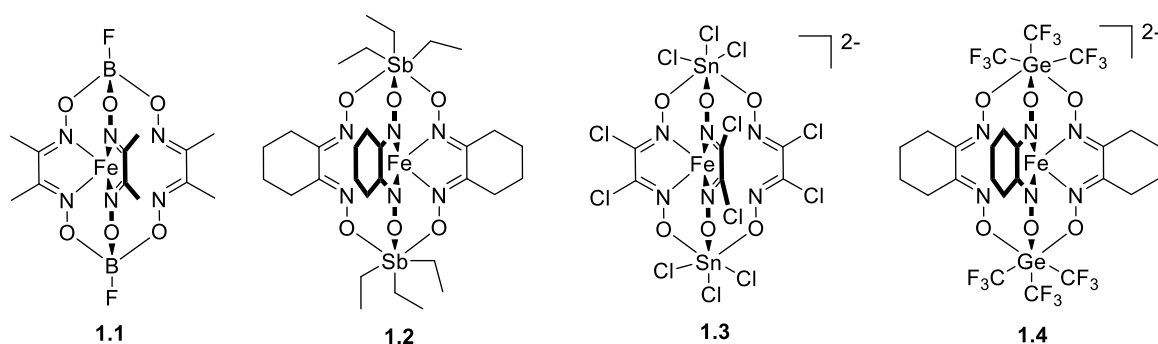


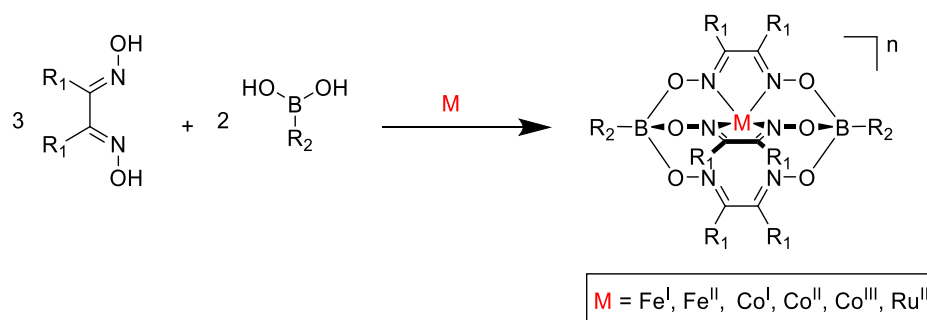
**Figure 1.1** - Representative mononuclear iron clathrochelates with different capping groups.

## 1.1 Mononuclear, boronate ester-capped clathrochelate complexes

Mononuclear, boronate ester-capped clathrochelate complexes can be obtained by combining a metal ion, a 1,2-dioxime ligand, and a boronic acid (Scheme 1.1). Depending on the functional groups present on the boronic acids and oximes, the overall hydrophobicity and electrochemical behaviour may be altered. The lateral groups can be modified via the dioxime ligand, and the capping groups through different boronic acids. For instance,



polyhalogenated cobalt and iron clathrochelates present valuable physical and physicochemical properties such as spin crossover, electrocatalytic activity, and high chemical reactivity.<sup>[8]</sup>



**Scheme 1.1** - Synthesis of mononuclear, boronate ester-capped clathrochelate complexes.

The group of Voloshin has developed straightforward strategies for the synthesis of various polyhalogenated clathrochelate complexes, which are suitable precursors for the preparation of a wide range of cage complexes of given symmetry and functionality. They found that the most convenient multistep synthetic pathway for their preparation includes *i*) direct template condensation of a dihalogeno- $\alpha$ -dioxime with boronic acid and the metal ion *ii*) its stepwise nucleophilic substitution reactions often with N-, O-, P-, S- and C-nucleophiles (Figure 1.2).<sup>[6,7,9]</sup>

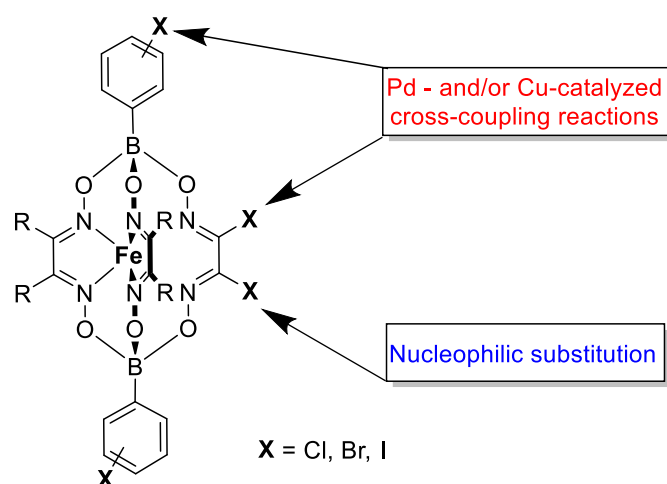


**Figure 1.2** - Post-synthetic functionalization of mononuclear iron clathrochelates..

The incorporation of halogens (I-, Br- and Cl-) also offers the possibility to perform Suzuki–Miyaura and Sonogashira coupling reactions. Voloshin et al reported palladium- and copper-catalyzed<sup>[10]</sup> reactions, and the reactivity of the leaving halogen group in the quasiaromatic complex framework correlates with their ability to undergo an oxidative addition (selected examples are shown in Figure 1.3). Such strategies have been employed by several groups and two books on this topic provide a comprehensive overview.<sup>[11,12]</sup>

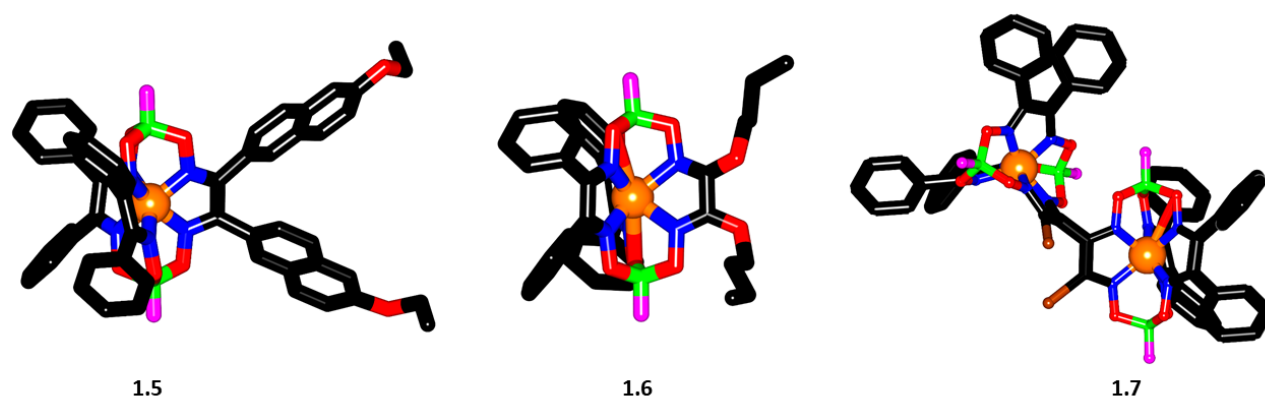


**Figure 1.3** - Representative molecular structures obtained from different post-synthetic strategies. **1.5** - Suzuki-Miyaura coupling **1.6** - nucleophilic substitution and **1.7** - Sonogashira coupling reactions. Color-coding: C: black; B: green; Fe: orange; Br: brown; N: blue; O: red; F: pink. Hydrogen atoms and solvent molecules have been omitted for clarity.

The possibility to introduce functional groups paved the way for the design of clathrochelate-based inhibitors with shapes closely matching the macromolecular surfaces, including protein–protein and protein–DNA interaction interfaces. Hence, clathrochelate complexes are prospective antiviral, anticancer and antifibrillogenic candidates.<sup>[13]</sup>

For instance, Voloshin et al. reported the synthesis and characterization of monoribbed-functionalized Fe<sup>II</sup> clathrochelate complexes large enough to ensure the significant binding to nucleic acids owing to van-der-Waals interactions. The *in vitro* studies showed that they were able to inhibit the transcription of T7 RNA polymerase (T7 RNAP) even in the nanomolar range.<sup>[14]</sup> Copper-promoted reductive homocoupling of quasi-aromatic Fe<sup>II</sup> dibromoclathrochelates yielded in C-C conjugated bisclathrochelates able to efficiently inhibit the transcription in the T7 RNAP system with IC<sub>50</sub> values below the submicromolar range. This places clathrochelate complexes among the most potent metal-based transcription inhibitors to date.<sup>[15]</sup> Mono- and bis-boronate ester-capped clathrochelates were investigated as anti-fibrillogenic agents. Kovalska et al found that mono- and bis-clathrochelate complexes significantly change the kinetics of insulin fibrilization, reduce the number of fibrils formed (up to 70%), while causing a decrease in their diameter. Additionally, they prevent the lateral aggregation of mature fibrils and the formation of super fibrillar clusters.<sup>[16]</sup> Another study investigated Fe<sup>II</sup> clathrochelates as potential molecular three-dimensional scaffold for the design of CD-sensitive reporters able to recognize specific elements of protein surfaces. Here, they demonstrated that inherently achiral Fe<sup>II</sup> clathrochelates functionalized by six ribbed carboxyphenylsulfide groups (Figure 1.4) are able to discriminate between serum albumins of relative structure (human and bovine albumins) by giving distinct ICD spectra.<sup>[17]</sup> It is worth noting that the role of the metal ion is purely structural and their activity is due to the caging ligand.<sup>[13]</sup>

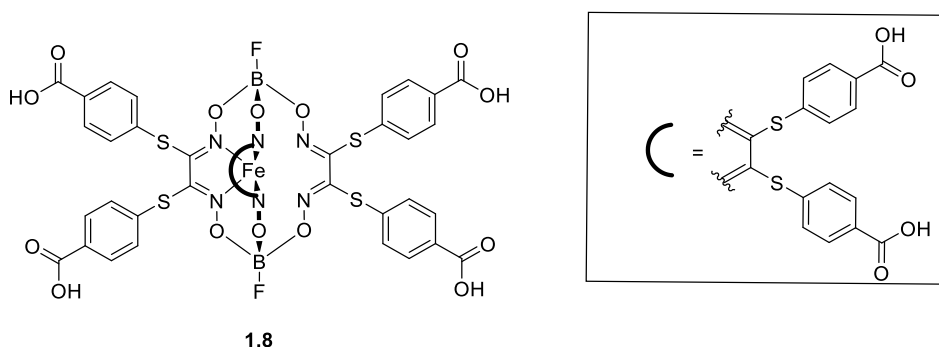


**Figure 1. 4** - Polyfunctionalized, mononuclear iron clathrochelate complex used for chiral distinction of HSA and BSA.<sup>[17]</sup>

The synthetic versatility of clathrochelate complexes offers new prospects for tuning their electrochemical properties. Dolganov et al. reported that the presence of terminal 4-pyridinyl moieties in Fe<sup>II</sup> clathrochelate complexes makes them promising homogeneous electrocatalyst for the molecular hydrogen formation in aqueous solutions. Although molecular hydrogen production can be achieved at low pH, this system presents high overpotentials.<sup>[18]</sup> More efficient catalysts can be prepared by encapsulating a cobalt ion in three oxidation states (+1, +2 and +3).<sup>[8]</sup> In fact, the specially designed hexachloro- and hexabromo-containing Co<sup>II</sup> boronate ester-capped clathrochelates were efficient for the production of molecular hydrogen from H<sup>+</sup> ions in high yields. The efficiency of this electrocatalytic process can be enhanced by an immobilization of the complexes with terminal mercapto groups on a surface of the working gold electrode.<sup>[8,19,20]</sup>

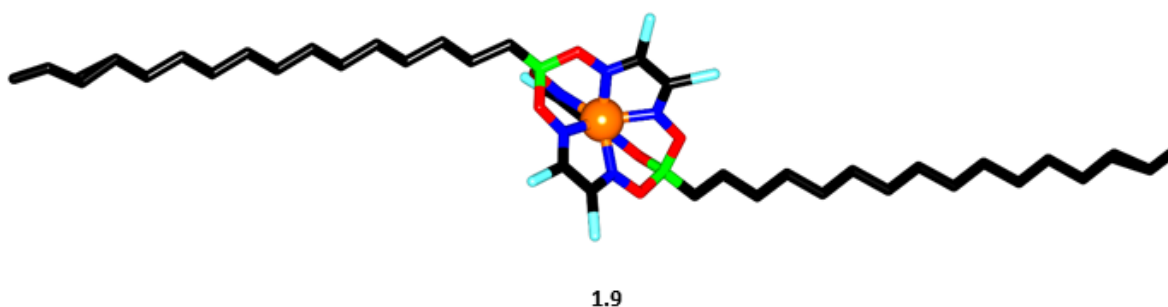


**Figure 1.5** - Molecular structure of Co<sup>II</sup> hexachloroclathrochelate complex. Color coding: C: black; B: green; Fe: orange; Cl: cyan; N: blue; O: red. Hydrogen atoms and solvent molecules have been omitted for clarity

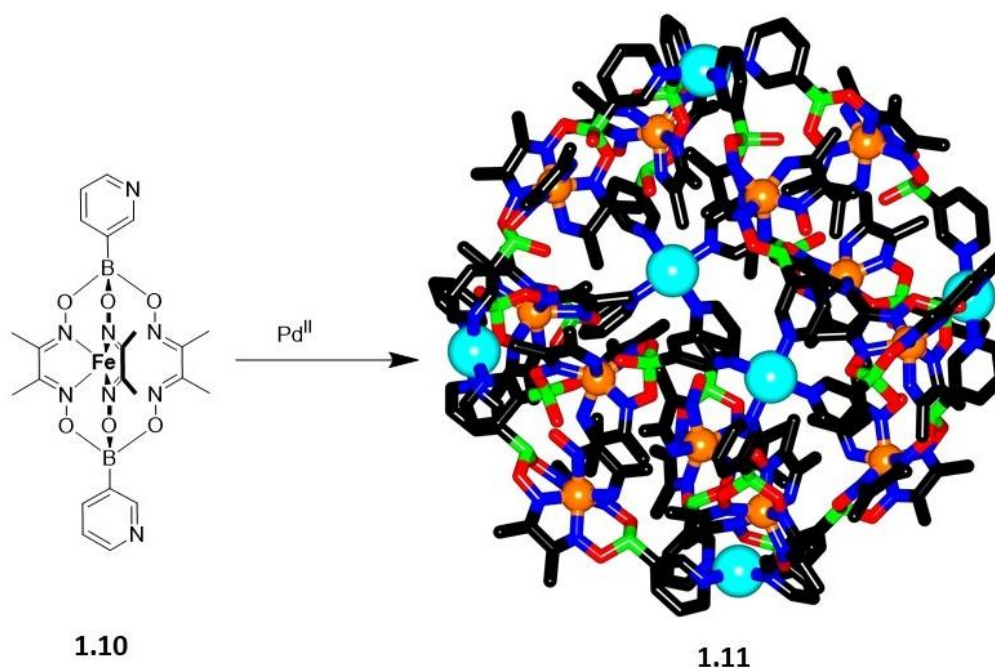
Co<sup>II</sup> Hexachloroclathrochelates with trigonal prismatic geometry of the complexes were reported to have large negative value of the zero-field splitting energy, which results in large anisotropy at room temperature (Figure 1.5). Such clathrochelates are promising for their application as paramagnetic tags.<sup>[21]</sup>

Boronate ester-capped clathrochelates are typically very stable towards ligand exchange reactions, hydrolysis, and air. The possibility to build a robust cage complex from a single center in all directions simultaneously, in combination with several functional groups, offers an advantage to design complex structures relevant for many applications in supramolecular chemistry and materials science, as discussed in more detail in the next section.<sup>[4]</sup>

### 1.1.1 Applications in supramolecular chemistry and materials science

Supramolecular coordination complexes are discrete nanostructures, which are obtained by self-assembly of ligands and metal salts or complexes.<sup>[22–26]</sup> The structure and function of a supramolecular assembly is determined by the building blocks from which it is derived.<sup>[27]</sup> Boron-capped mononuclear clathrochelate complexes were explored as candidate building blocks for supramolecular self-assemblies because they offer control over the steric and functional properties. Decorating clathrochelate complexes with terminal functional groups such as pyridyl or carboxylic acids allows their use as metalloligands.

Severin et al. reported the syntheses and the structures of clathrochelate-based metalloligands with terminal 3-pyridyl groups. Reactions of these ligands with Pd<sup>II</sup> afford large octahedral coordination cages (Scheme 1.2).



**Scheme 1.2** - Formation of linear clathrochelate-based molecular cage complexes with Palladium salts. Color coding: C: black; B: green; Fe: orange; Pd: cyan; N: blue; O: red. Hydrogen atoms and solvent molecules have been omitted for clarity.

The lateral size of the metalloligands prevents the formation of macrocyclic structures.<sup>[28]</sup> However, the formation of macrocycles can be achieved deliberately by combining 4-pyridyl functionalized clathrochelates with rhenium salts.<sup>[3]</sup> In another study, it was demonstrated how the ligand aspect ratio of clathrochelates is a decisive factor for the self-assembly of coordination cages. Palladium and iron based cages were explored, and pyridyl groups were used as terminal groups. In both cases, they observed a switch towards a higher nuclearity structure when the length-to-width ratio of the ligand was reduced (Figure 1.6).<sup>[29]</sup>

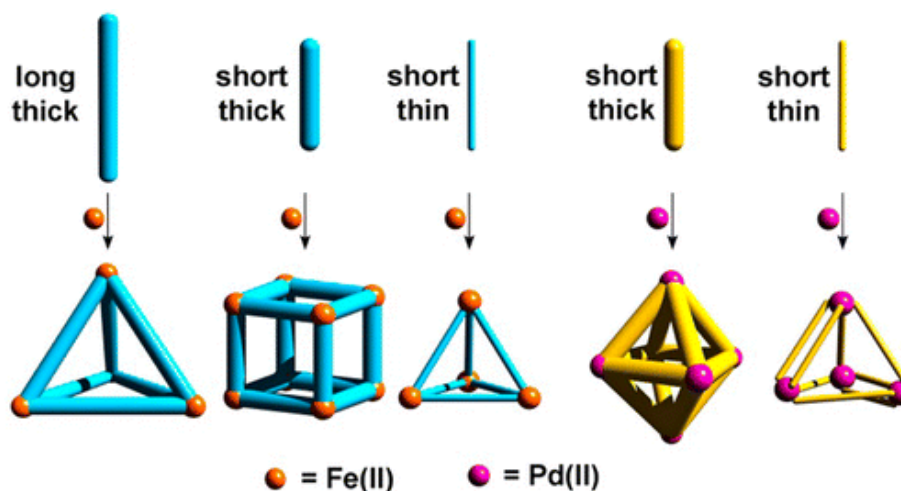
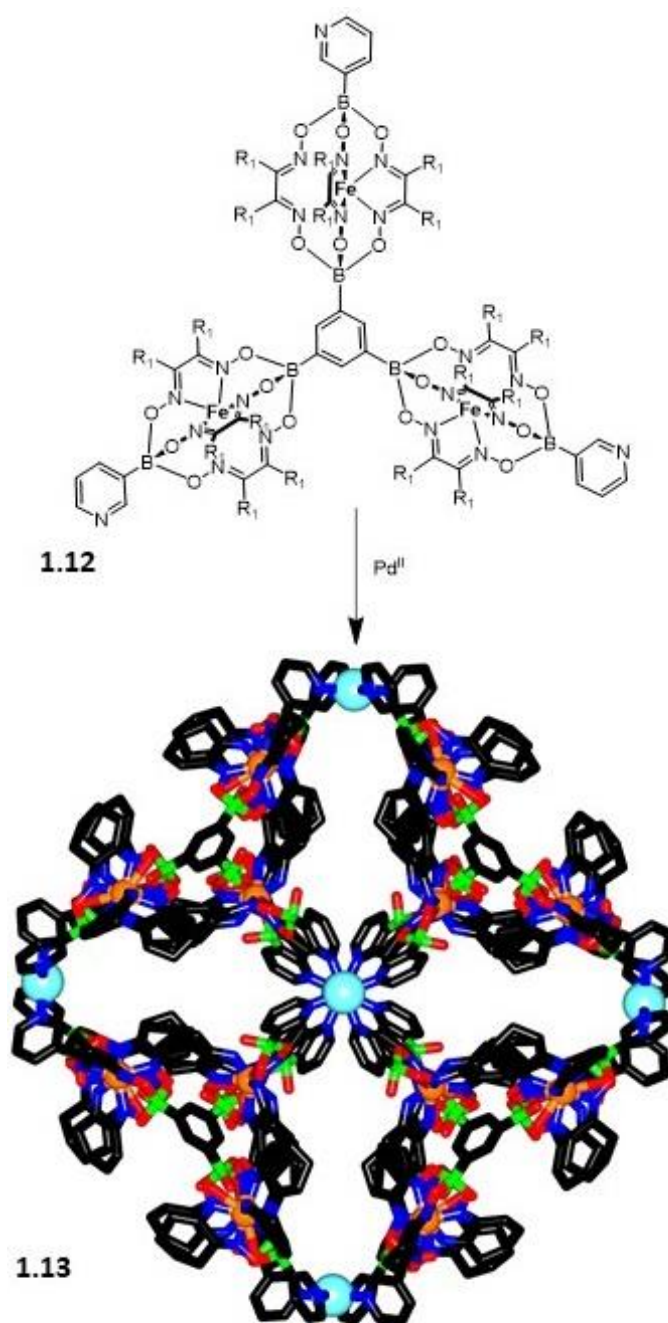


**Figure 1.6** - Demonstration of how the ligand aspect ratio is decisive factor for self-assembly of coordination cages. Reprinted with permission from reference <sup>[29]</sup>. Copyright 2016 American Chemical Society.

As mentioned in section 1.1, the robustness of the clathrochelates offers the opportunity to perform post-synthetic modifications on the lateral and apical positions. In fact, the use of halogen-substituted boronic acids paved the way for the synthesis of terminal tetrapyridyl clathrochelates. When they were combined with cis-blocked Pt<sup>II</sup> complexes, discrete supramolecular self-assemblies were formed. Depending on the lateral sizes of the metalloligands, a tetragonal or pentagonal barrels, or cages with unprecedented gyrobyofastigium or square orthobicupola-like structures were obtained.<sup>[30–32]</sup>

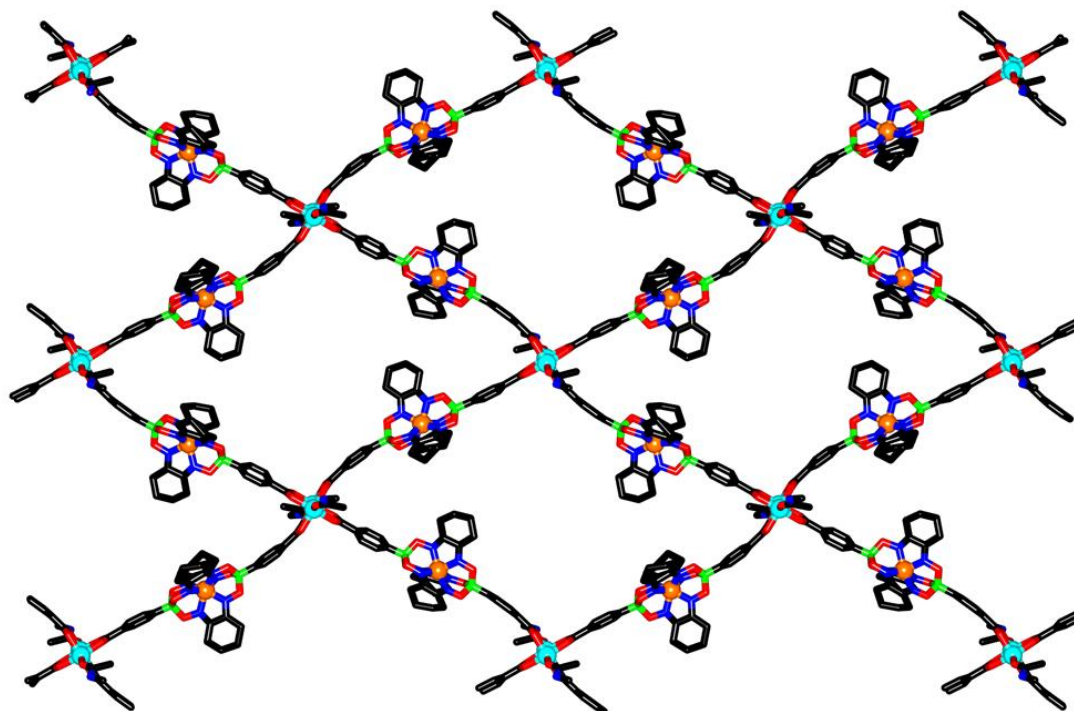
In 2013, Severin et al. demonstrated that, it is possible to obtain up to 5.4 nm long linear clathrochelate ligands.<sup>[3]</sup> Supramolecular assemblies with large molecular weights and long Pd-Pd were obtained by employing long di- and tritopic clathrochelate metalloligands synthesized via one-pot approach with apical pyridyl groups. It is worth noting that these complexes are among the largest palladium cage complexes described to date (a selected example is shown in Scheme 1.3).<sup>[29]</sup>



**Scheme 1.3** - Formation of triple clathrochelate-based molecular cage complexes with palladium salts. Color coding: C: black; B: green; Fe: orange; Pd: cyan; N: blue; O: red. Hydrogen atoms and solvent molecules have been omitted for clarity.

In addition to molecularly defined nanostructures, clathrochelate-based metalloligands have also been used to prepare Metal Organic Frameworks (MOFs): a class of crystalline materials consisting of coordination bonds between a transition metal cation and an organic ligand. For example, the combination of carboxylic acid-substituted clathrochelates with zinc salts resulted in 2D-layered coordination polymers, in which the clathrochelates bridge between  $\text{Zn}^{\text{II}}$  paddlewheel secondary building units (SBUs) (Figure 1.7). Removal of the guest solvent molecules led to collapse of the network structure, resulting in a nonporous material. Other mononuclear clathrochelate-based coordination polymers were obtained upon combination of 4-pyridyl

clathrochelates with 4,4-biphenyldicarboxylic in the presence of a zinc salt. The crystalline material revealed a pillared layer structure in which the clathrochelate interconnects 2D sheets of  $\text{Zn}^{\text{II}}$  SBUs.<sup>[3]</sup>



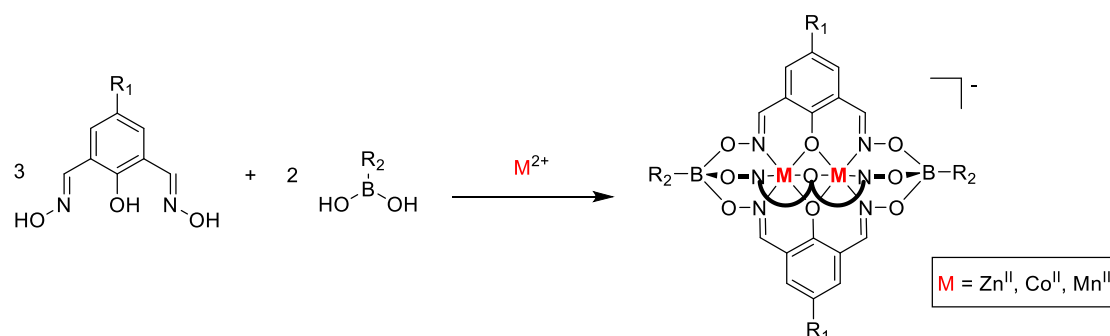
1.14

**Figure 1.7** - Part of the structure of the 2D  $\text{Fe}^{\text{II}}$ -based clathrochelate complex coordination polymer. Color coding: C: black; B: green; Zn: cyan; Ag: brown; N: blue; O: red. Hydrogen atoms and solvent molecules have been omitted for clarity.<sup>[3]</sup>

## 1.2 Dinuclear, boronate ester-capped clathrochelate complexes

Dinuclear clathrochelate complexes can be obtained by combining a divalent metal ion, a boronic acid, and a phenol dioxime ligand (Scheme 1.4).<sup>[4,11]</sup> The six-fold condensation reaction gives boronate ester-capped complexes with two hexa-coordinated  $\text{M}^{\text{II}}$  ions in the center. The macrobicyclic ligand has a formal charge of minus five, resulting in a net charge of minus one for the entire complex.<sup>[4,35,36]</sup>



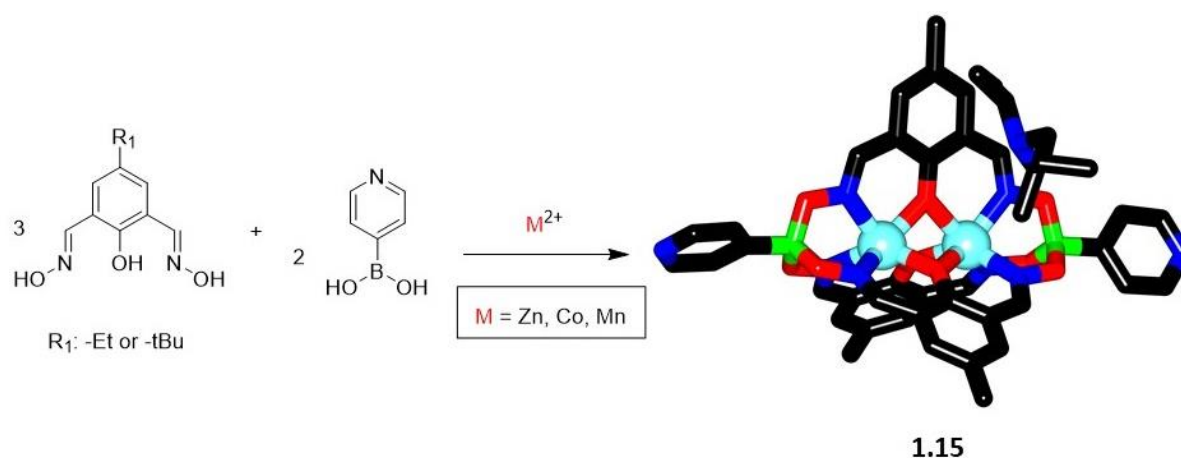


**Scheme 1.4** - Synthesis of dinuclear, boronate ester-capped clathrochelates. Cations have been omitted for clarity.

In 2006, Chaudhuri et al reported the first example of a *dinuclear* clathrochelate complex where 2,6-diformyl-4-methyl-phenol dioxime was combined with methylboronic acid and  $\text{Mn}(\text{ClO}_4)_2 \cdot \text{H}_2\text{O}$  in methanol. The X-ray structure of the resulting complex confirmed the encapsulation and coordination of manganese ions with a  $\text{MnN}_3\text{O}_3$  donor set.<sup>[35]</sup> Severin et al reported the synthesis of negatively charged boronate ester-capped Zn-, Co- and Mn-based clathrochelate complexes. It is worth noting that these complexes are robust and rigid. The lateral positions of the dinuclear clathrochelates can be modified by variation of the corresponding phenol dioxime ligand substituents. The capping boronic acids are often commercially available. A unique feature of clathrochelate metalloligands is their trigonal-bipyramidal geometry.<sup>[4]</sup> Such a geometry is difficult to access with purely organic scaffolds. The diamagnetic zinc-based clathrochelates are luminescent<sup>[37]</sup>, and the cobalt and manganese complexes are paramagnetic.<sup>[35,38]</sup> Such properties are encouraging for their use in supramolecular chemistry and materials science.

### 1.2.1 Applications in supramolecular chemistry and materials science

The group of Severin employed dinuclear clathrochelates as metalloligands for the preparation of discrete supramolecular self-assemblies. Dinuclear clathrochelates decorated with pyridyl groups at the apical positions were reported to have longer Py-Py distances and they are bulkier compared to their mononuclear analogs (Scheme 1.5).



**Scheme 1.5** - Synthesis of pyridyl- functionalized dinuclear clathrochelates. Color coding: C: black; B: green; M<sup>II</sup>: cyan; N: blue; O: red. Hydrogen atoms and solvent molecules have been omitted for clarity



When combined with cis-protected  $\text{Pt}^{\text{II}}$  corners, they form macrocycles and the negative charge brought by the clathrochelate complexes help with the stabilization of the assembly. Zinc-based clathrochelate complexes were used to prepare 2D and 3D MOFs with zinc and cadmium salts respectively.<sup>[37]</sup>

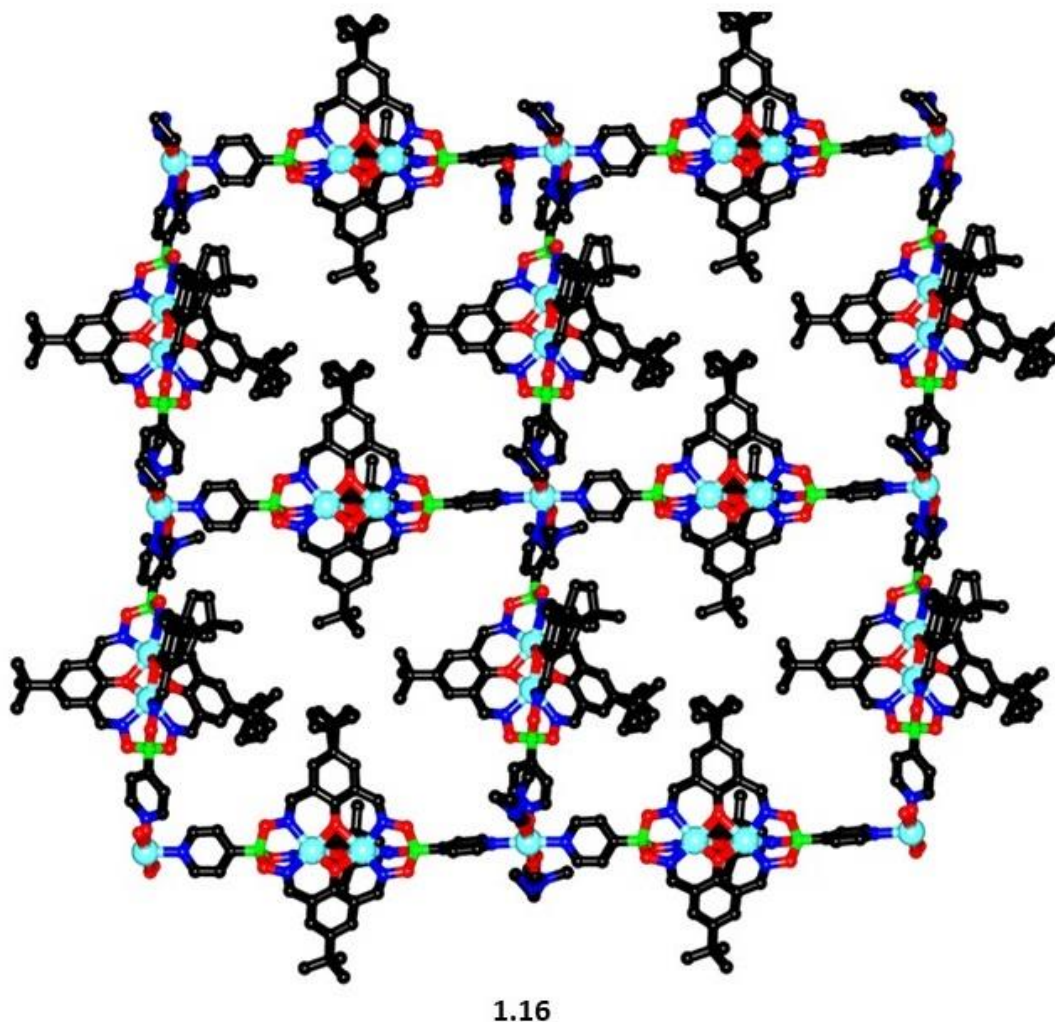


**Figure 1.8** - Part of the structure of the 2D  $\text{Zn}^{\text{II}}$ -based clathrochelate complex coordination polymer. Color coding: C: black; B: green; Co: cyan; Ag: brown; N: blue; O: red. Hydrogen atoms and solvent molecules have been omitted for clarity.<sup>[37]</sup>

The robustness of the dinuclear clathrochelates offered the possibility to perform post functionalization via Pd-catalyzed cross-coupling reactions. The poly-cross-coupling reactions are efficient and give the desired functionalized clathrochelates in high yields. The post-synthetic functionalization of the dinuclear clathrochelates with pyridyl moieties yields even longer and bulkier clathrochelate complexes. For instance, it is possible to synthesize penta- and heptatopic pyridyl-functionalized clathrochelate ligands which have hardly been studied in for the synthesis of supramolecular assemblies (Figure 1.9).<sup>[39]</sup>

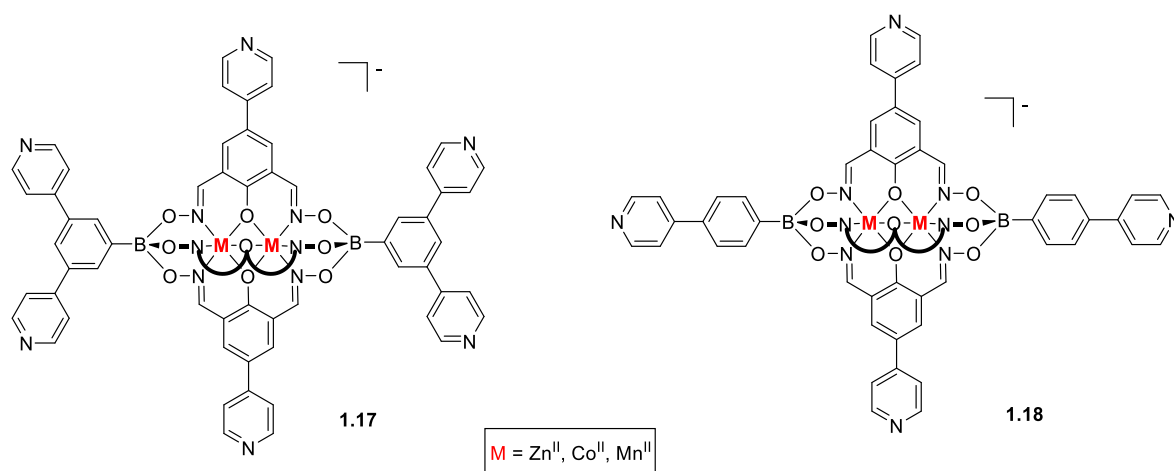
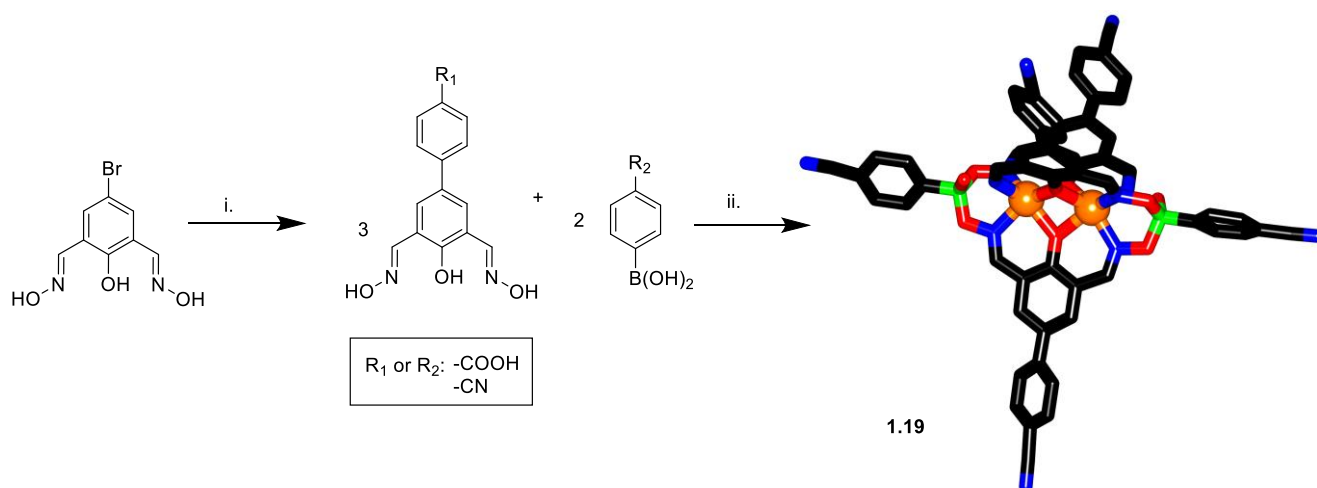


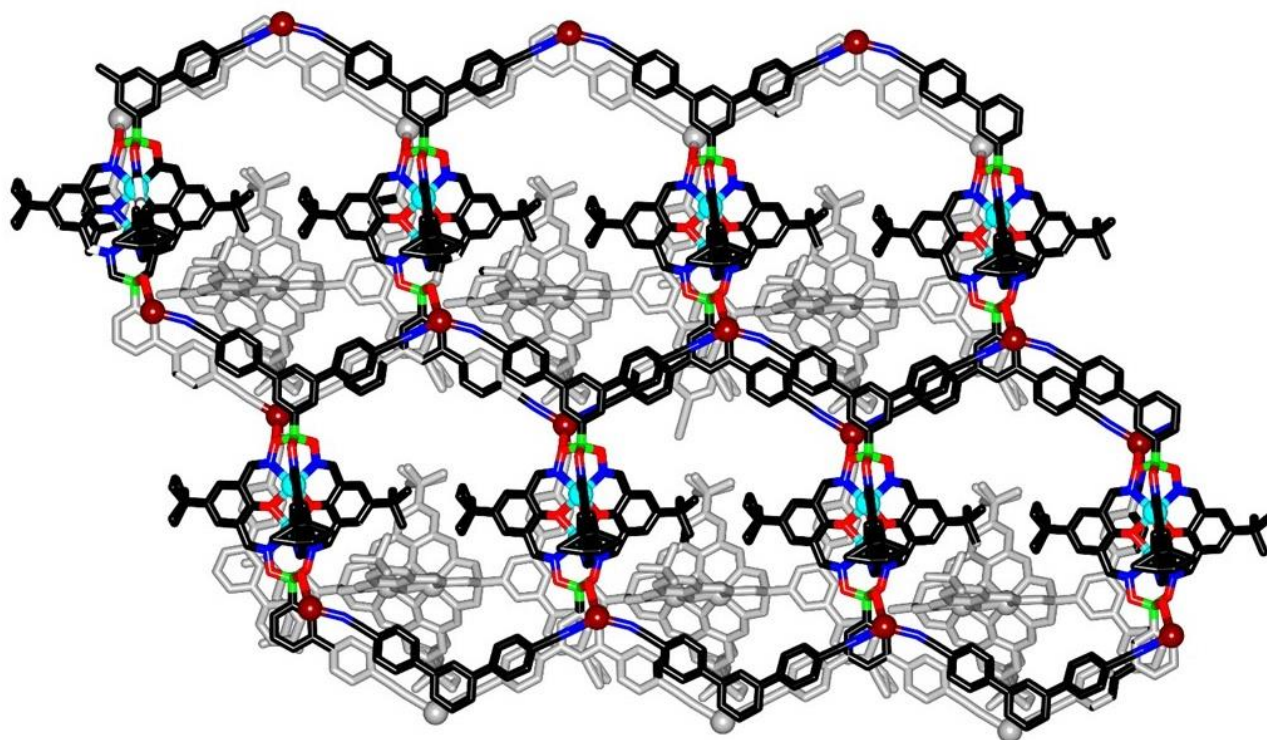
**Figure 1.9** – Polypyridyl-functionalized dinuclear, boronate ester-capped clathrochelate complexes.

Dinuclear clathrochelate complexes with two, three, four, or five cyano or carboxylic acid substituents in the ligand periphery can be prepared following two distinct synthetic strategies: *i*)  $\text{Zn}^{\text{II}}$  or  $\text{Co}^{\text{II}}$  templated polycondensation reactions of CN- or COOH-functionalized arylboronic acids and phenoldioximes, or *ii*) post synthetic cross-coupling reactions of polybrominated  $\text{Zn}^{\text{II}}$  clathrochelates with 4-cyanophenylboronic acid. (a selected example is shown in Scheme 1.6). These strategies were employed to prepare large di-, tri-, tetra-, and pentatopic carboxylic acid-based clathrochelate complexes.

Combining carboxylic acid-substituted polyfunctionalized clathrochelates with zinc and zirconium ions afforded 3D MOFs (Figure 1.10). The ditopic COOH-functionalized clathrochelates presented network interpenetration. Varying the steric bulk by using the clathrochelate metalloligands with less sterically demanding phenolatodioximato ligands (bromo instead of tert-butyl) had no influence. These MOFs presented low BET surface areas, suggesting that the MOFs collapse during the solvent exchange.<sup>[36]</sup>



**Scheme 1.6** - Synthesis of pentatopic cyano-functionalized dinuclear clathrochelates. Conditions: i) and ii) *n*BuOH/toluene (1:1),  $\text{Pd}_2(\text{dba})_3$ , SPhos and  $\text{K}_3\text{PO}_4$ , 96 h,  $\text{N}_2$  Color coding: C: black; B: green; Co: orange; N: blue; O: red. Hydrogen atoms and solvent molecules have been omitted for clarity.<sup>[38]</sup>



1.20

**Figure 1.10** - Part of the structure of the 3D Co<sup>II</sup>-based clathrochelate complex coordination polymer. Color coding: C: black; B: green; Co: cyan; Ag: brown; N: blue; O: red. Hydrogen atoms, solvent molecules and cations have been omitted for clarity. <sup>[38]</sup>

When the ditopic cyano-functionalized clathrochelate complexes were combined with Ag<sup>I</sup> salts they afforded a 1D coordination polymer. 2- and 3-D coordination polymers were generated from tetra- and pentatopic cyano-functionalized clathrochelate complexes with Ag<sup>I</sup> salts. The silver ions tend to form labile complexes with flexible coordination number and geometry hence reversible and malleable coordination polymers easier to crystallize can be formed ( a selected example is shown in Figure 1.10).<sup>[38]</sup>

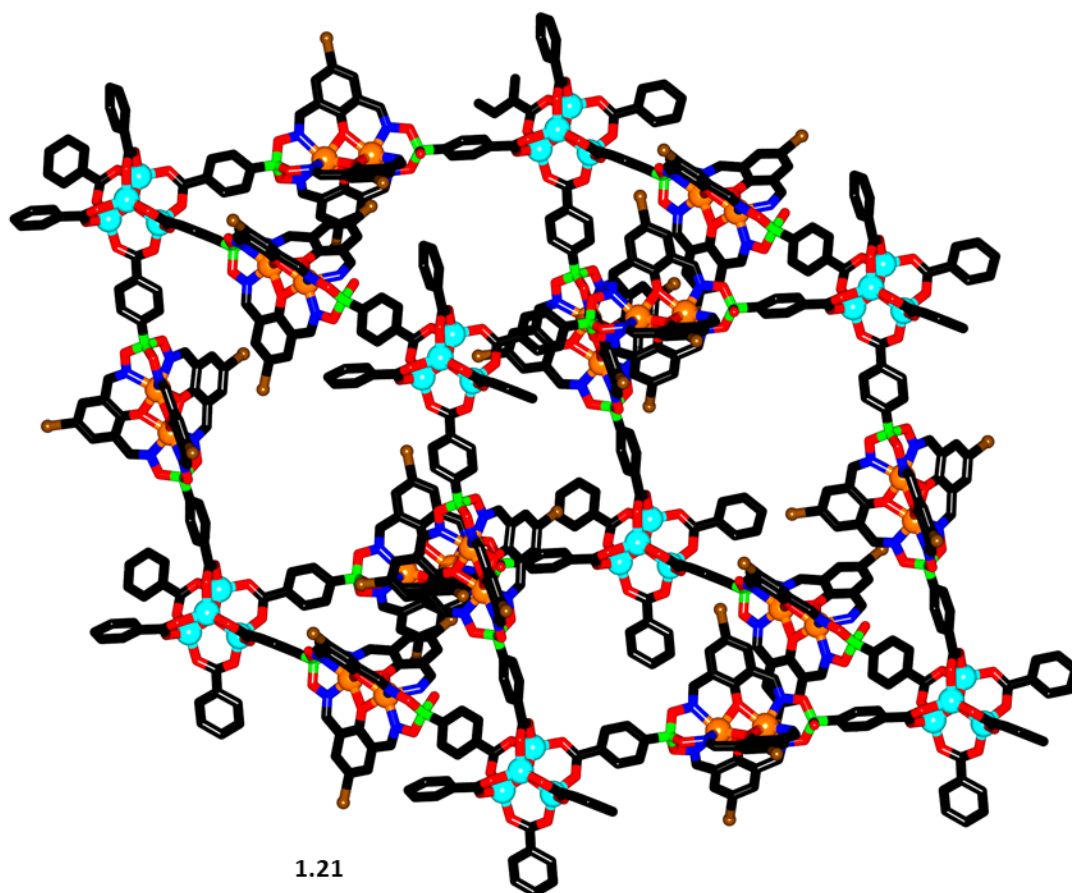
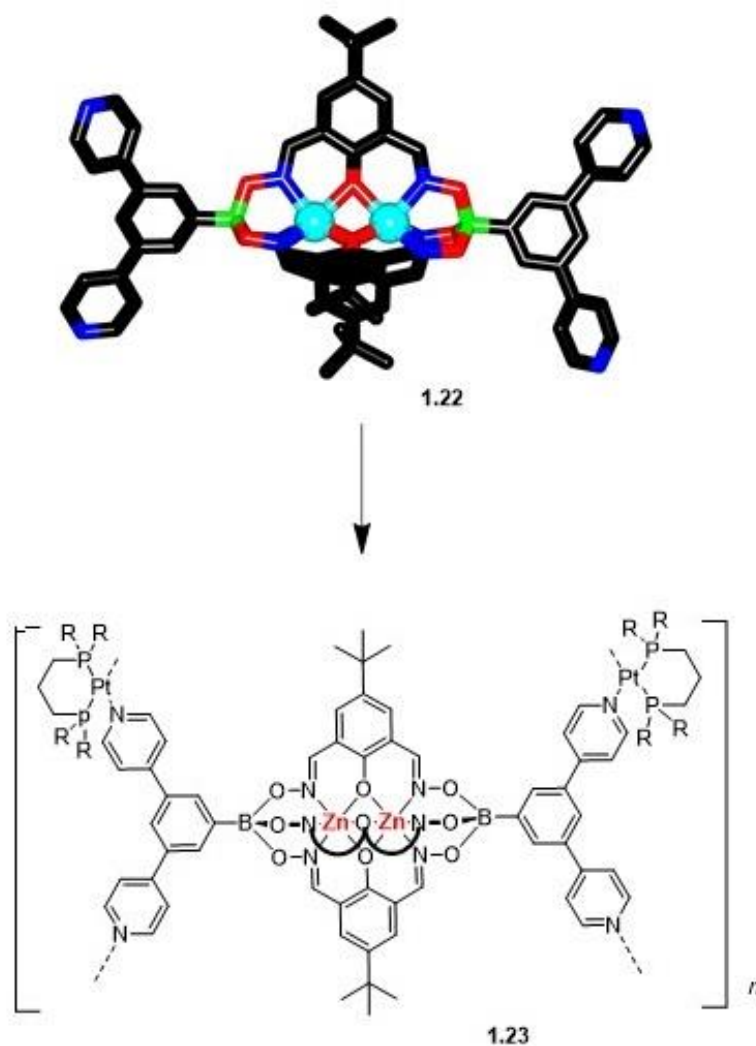


**Figure 1.11** - Part of the structure of the 3D Co<sup>II</sup>-based clathrochelate complex coordination polymer. Color coding: C: black; B: green; Co: orange; Zn: cyan; N: blue; O: red; Br: brown. Hydrogen atoms, solvent molecules, cations have been omitted for clarity.

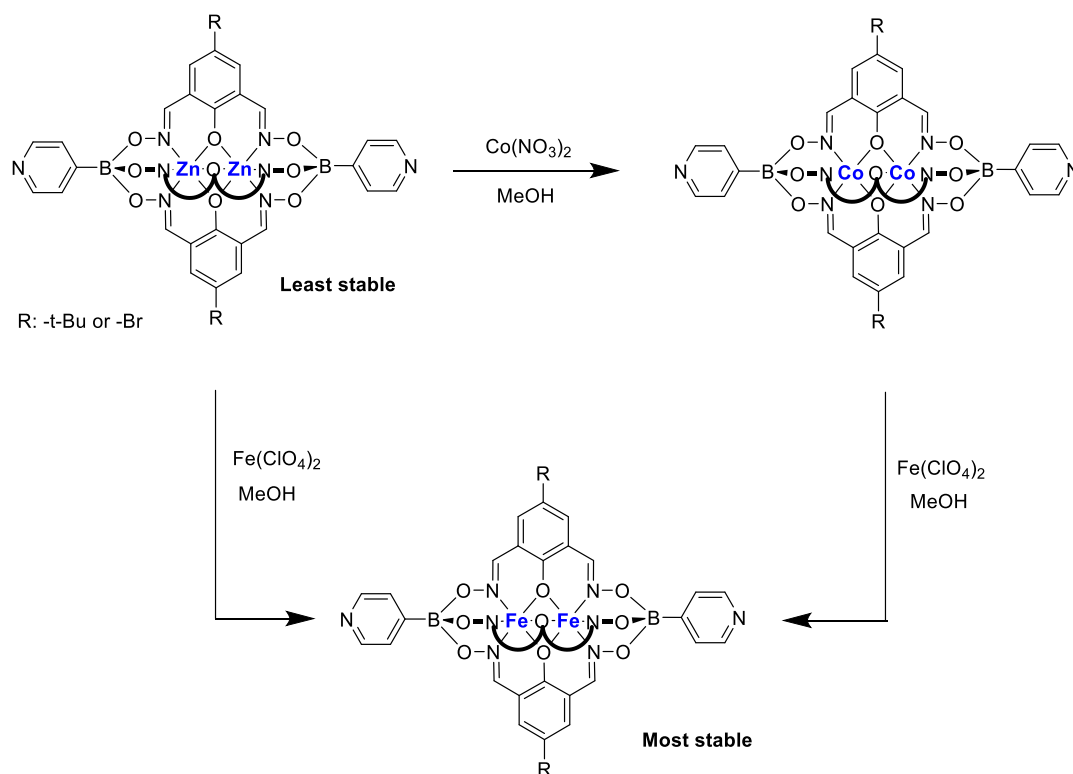
Anionic and zinc-based tetrapyridyl dinuclear clathrochelate complexes were obtained by employing polycross-coupling reactions. When such complexes are combined with *cis*-Pt<sup>II</sup> complexes they form pentagonal barrel structures (Scheme 1.7).<sup>[30]</sup>



**Scheme 1.7** - Formation of tetratopic clathrochelate-based coordination complexes with platinum salts. Color coding: C: black; B: green; Zn: cyan; N: blue; O: red. Hydrogen atoms, solvent molecules and cations have been omitted for clarity.<sup>[30]</sup>

### 1.3 Background and aims of the project

Clathrochelate complexes, boronate ester-capped in particular, have been studied for decades. It has been shown that their robustness, and easy synthesis paves the way for versatile functionalization along with a wide range of applications in supramolecular chemistry and material science. Preliminary investigations in our group by Dr. Mathieu Marmier had shown that it is possible to perform metal exchange reactions on dinuclear clathrochelates. When a solution of  $\text{Zn}^{\text{II}}$  clathrochelate in methanol was heated in the presence of an excess of  $[\text{Co}(\text{H}_2\text{O})_6](\text{NO}_3)_2$ , the MS data indicated a clean and complete metal ion exchange to the  $\text{Co}^{\text{II}}$  clathrochelate. When a solution of the  $\text{Co}^{\text{II}}$  clathrochelate was heated with an excess of  $\text{Zn}(\text{OTf})_2$ , no metal ion exchange was observed. These results showed that  $\text{Co}^{\text{II}}$  clathrochelates are more stable than  $\text{Zn}^{\text{II}}$  clathrochelates.



**Scheme 1.8** - Metal exchange investigations on clathrochelates.

Subsequent MS studies revealed that metal ion exchange reactions can also be performed with  $\text{Fe}^{\text{II}}$  salts, and the resulting complexes were found to be particularly stable. These initial MS studies prompted us to investigate the direct synthesis of dinuclear clathrochelate complexes containing iron ions. We were indeed able to develop synthetic procedures for several new complexes, and details are given in Chapter 2 of this thesis. In the course of our investigations, we realized that dinuclear Fe clathrochelates are unique compounds, with potential applications in materials science. Explorations along these lines are described in the subsequent chapters.



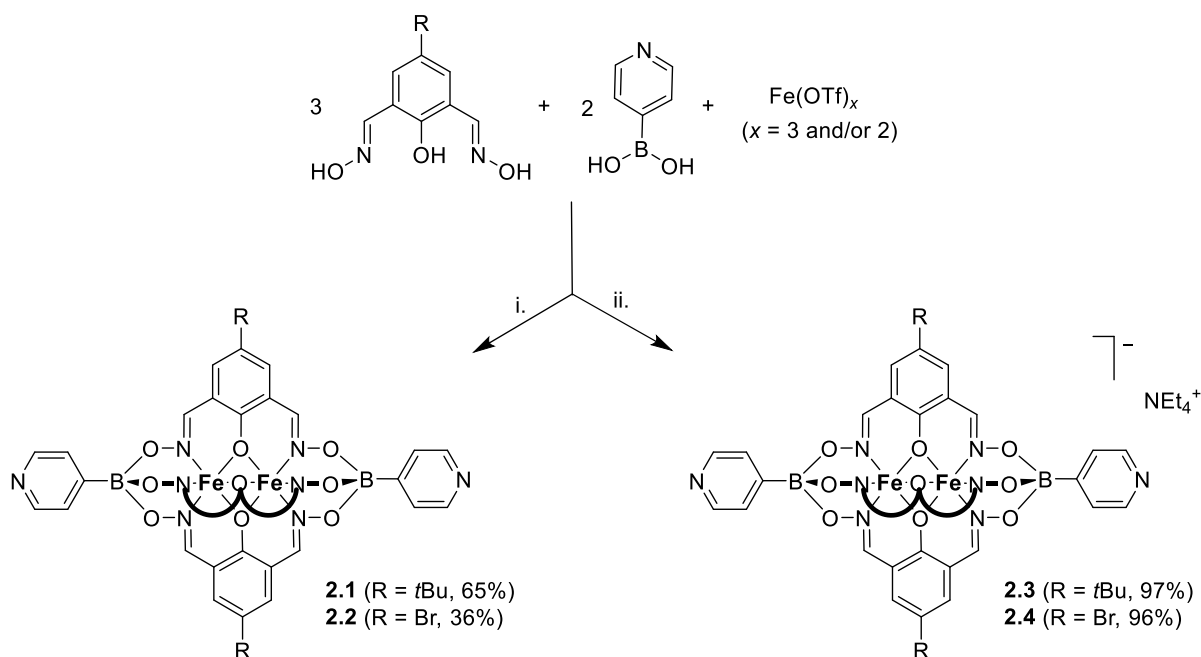
## Chapter 2 Homo- and heterodinuclear iron clathrochelate complexes

In this chapter, we will discuss the different strategies to synthesize dinuclear, boronate ester-capped clathrochelates. Part of this work was published in “Homo- and Heterodinuclear Iron Clathrochelate Complexes with Functional Groups in the Ligand Periphery”, José L. Bila, Mathieu Marmier, Konstantin O. Zhurov, Rosario Scopelliti, Ivica Živković, Henrik M. Rønnow, Elahi S. Noore, Andrzej Sienkiewicz, Cornel Fink, and Kay Severin, *European Journal of Inorganic Chemistry*, **2018**, 3118-3125. Dr. Mathieu Marmier, who is listed as a co-author, has investigated the metal ion exchange and ligand scrambling reactions mentioned in section 1.3. His work is not discussed in this chapter. The magnetic measurements and the EPR studies were performed by I. Živković, H. M. Rønnow, E. S. Noore, and A. Sienkiewicz.

### 2.1 Synthesis and characterization of dinuclear iron clathrochelate complexes containing terminal 4-pyridyl groups

Based on the results described in section 1.3, it was desirable to investigate the possibility to synthesize the dinuclear iron clathrochelates deliberately. When the condensation reaction was performed with  $\text{Fe}(\text{OTf})_2$  under strictly anaerobic conditions, we were able to isolate the  $\text{Fe}^{\text{II}}\text{-Fe}^{\text{II}}$  clathrochelate complexes **2.3** and **2.4** in good yields. However, when the reactions were performed in the presence of air, oxidation to the  $\text{Fe}^{\text{II}}\text{-Fe}^{\text{III}}$  complexes **2.1** and **2.2** were observed. The mixed-valence complexes can be prepared cleanly by using an equimolar mixture of  $\text{Fe}(\text{OTf})_3$  and  $\text{Fe}(\text{OTf})_2$  (Scheme 2.1). Notably, we were not able to prepare a  $\text{Fe}^{\text{III}}\text{-Fe}^{\text{III}}$  clathrochelate by exclusively using  $\text{Fe}(\text{OTf})_3$ .





**Scheme 2.1** - Synthesis of the Fe clathrochelate complexes. Conditions: i: MeOH, 60 °C, 2 h, then NEt<sub>4</sub>OH, room temp., 1 h; ii. MeOH/EtOH, 50 °C, 1–2 h, 1 h, then MeOH/EtOH, NEt<sub>4</sub>OH, room temp., 1 h.

The clathrochelate complexes **2.1** – **2.4** were analyzed by single-crystal X-ray diffraction (complex **2.1** as a double HOTf adduct). As expected, the Fe ions coordinate the oximate N-atoms and the bridging phenolato O-atoms (Figure 0.1). The coordination geometry around the iron centers can be described as trigonal prismatic for all complexes. A similar geometry is observed for dinuclear clathrochelates based on Zn<sup>II</sup>, Mn<sup>II</sup> or Co<sup>II</sup>, and for mononuclear Fe<sup>II</sup> Clathrochelate complexes.<sup>[4,8]</sup> The mixed-valence Fe<sup>II</sup>-Fe<sup>III</sup> complexes **2.1** and **2.2** feature shorter average Fe–O bonds compared to the Fe<sup>II</sup>-Fe<sup>II</sup> complexes **2.3** and **2.4** (Table 2.1). As result, the Fe···Fe distances are shorter for the oxidized complexes. The average Fe–N bond lengths, on the other hand, are similar for the all four complexes. It is worth noting that the two Fe centers in the mixed-valence complexes **2.1** and **2.2** cannot be distinguished crystallographically.

**Table 2.1** - Selected bond distances [Å] and angles [°] for the complexes **2.1** (HOTf)<sub>2</sub>, **2.2**, **2.3** and **2.4**.

Complex	Fe–O <sub>av.</sub>	Fe–N <sub>av</sub>	Fe···Fe	O–Fe–N <sub>av</sub>
<b>2.1</b> (HOTf) <sub>2</sub>	2.04	2.13	2.761(8)	81.8
<b>2.2</b>	2.04	2.13	2.766(4)	82.2
<b>2.3</b>	2.10	2.13	2.905(5)	81.8
<b>2.4</b>	2.11	2.13	2.925(7)	81.8

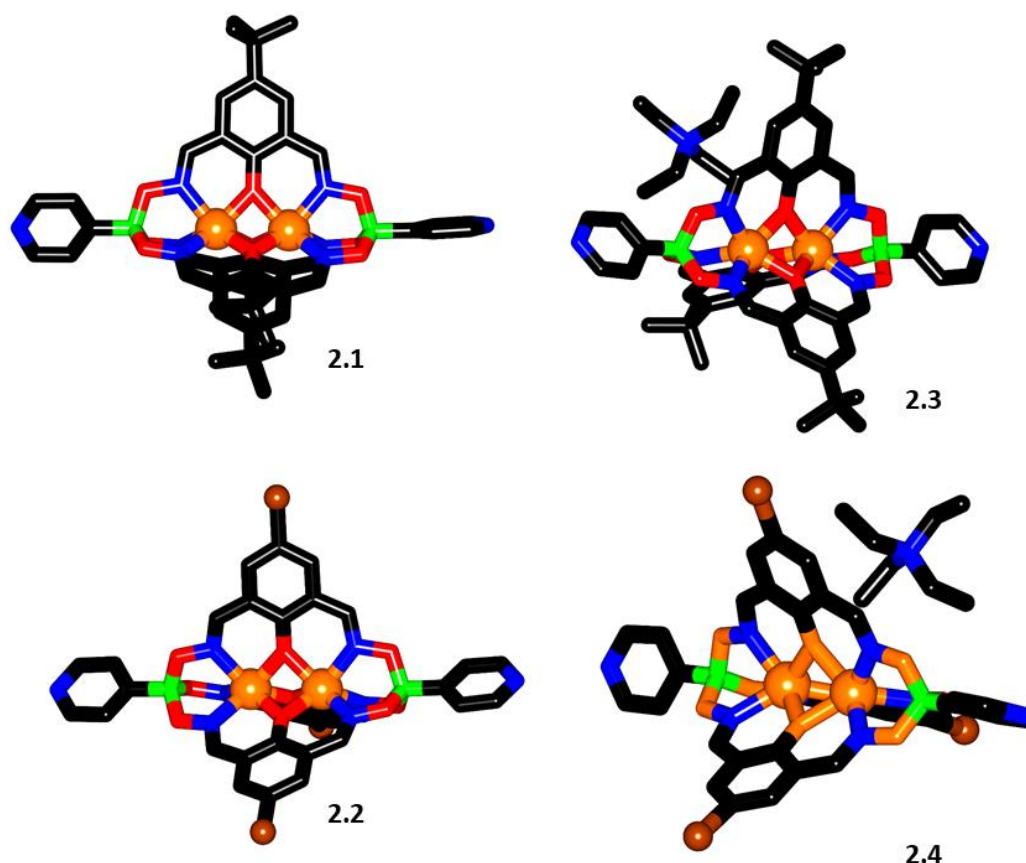


**Figure 2.1** - Molecular structures of the complexes **2.1** ( $\text{HOTf}$ )<sub>2</sub>, **2.2**, **2.3** and **2.4** in the crystal. Color-coding: C: black; Br: green; Fe: orange; N: blue; O: red; Br: brown. Hydrogen atoms, solvent molecules, and ( $\text{OTf}$ )<sup>-</sup> anions (**2.1**) have been omitted for clarity.

The redox behavior of the complexes **2.3** and **2.4** was investigated by means of cyclic voltammetry (CV) in DMF under inert atmosphere. Both compounds show a reversible one-electron oxidation at negative potential vs. a ferrocene/ferrocenium ( $\text{Fc}/\text{Fc}^+$ ) reference (Figure 2.2). The substituents in para-position to the phenolato group have a pronounced influence on the redox potential, with a difference of 253 mV between the bromo complex **2.4** ( $E_{1/2} = -0.158 \text{ V}$ ) and the tBu complex **2.3** ( $E_{1/2} = -0.411 \text{ V}$ ).

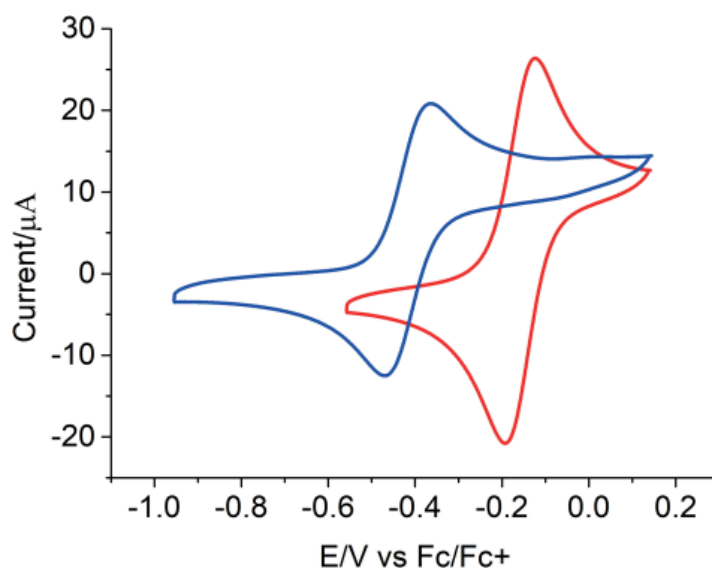
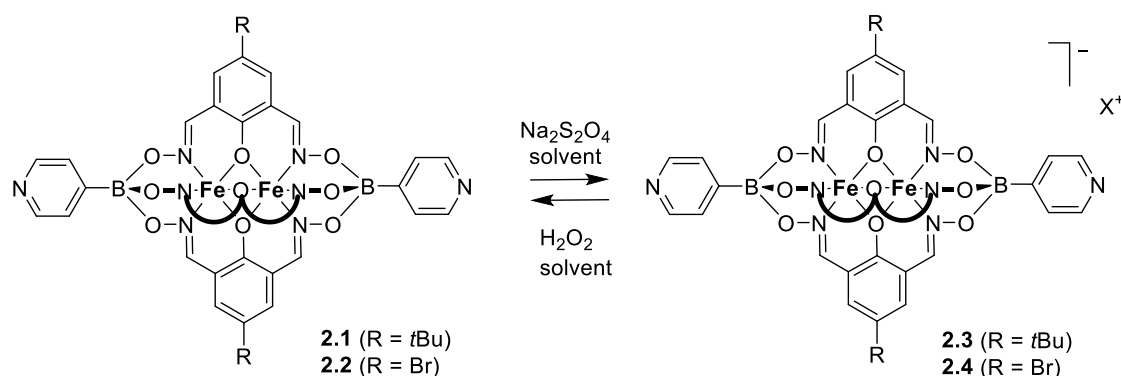


**Figure 2.2** - Cyclic voltammograms of solutions containing complex **2.3** (blue line) or **2.4** (red line). Conditions: solvent: DMF, electrolyte:  $\text{NBu}_4\text{PF}_6$ , scan rate:  $100 \text{ mV s}^{-1}$ . Working electrode (Carbon), Reference electrode (Ag, AgCl), and counter electrode (Pt wire).

The reversible redox chemistry observed by cyclic voltammetry prompted us to explore the chemical interconversion of the  $\text{Fe}^{\text{II}}\text{-Fe}^{\text{II}}$  complexes **2.3** and **2.4** and the mixed-valence  $\text{Fe}^{\text{II}}\text{-Fe}^{\text{III}}$  complexes **2.1** and **2.2**. We found that the  $\text{Fe}^{\text{II}}\text{-Fe}^{\text{II}}$  complexes can be oxidized by hydrogen peroxide, whereas the  $\text{Fe}^{\text{II}}\text{-Fe}^{\text{III}}$  complexes can be reduced by sodium dithionite (Scheme 2.2).



**Scheme 2.2** - Interconversion of the  $\text{Fe}^{\text{II}}\text{-Fe}^{\text{II}}$  complex **2.1** and **2.2** and the  $\text{Fe}^{\text{II}}\text{-Fe}^{\text{III}}$  complex **2.3** and **2.4** by chemical oxidation or reduction, respectively.

The mixed-valence  $\text{Fe}^{\text{II}}\text{-Fe}^{\text{III}}$  complexes **2.1** and **2.2** are black colored and the  $\text{Fe}^{\text{II}}\text{-Fe}^{\text{II}}$  complexes **2.3** and **2.4** are brown colored in solid state. The reactions can be followed by UV-Vis spectroscopy, because the oxidized complexes have characteristic absorption bands at 525 and 700 nm (Figure 2.3).

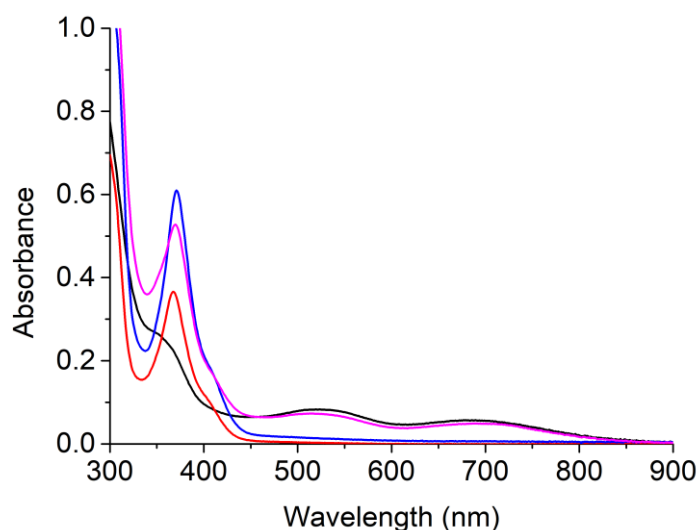


**Figure 2.3** - UV-vis absorbance of the iron complexes **2.1** (black), **2.2** (violet), **2.3** (red) and **2.4** (blue), and in DMSO (50  $\mu\text{M}$ ).

In addition, we used ESI mass spectrometry for reaction analysis, because the reduced complexes are detected in the negative mode (they have an overall charge of minus 1), whereas the oxidized complexes are detected in the positive mode (Figures 2.4 to 2.7).

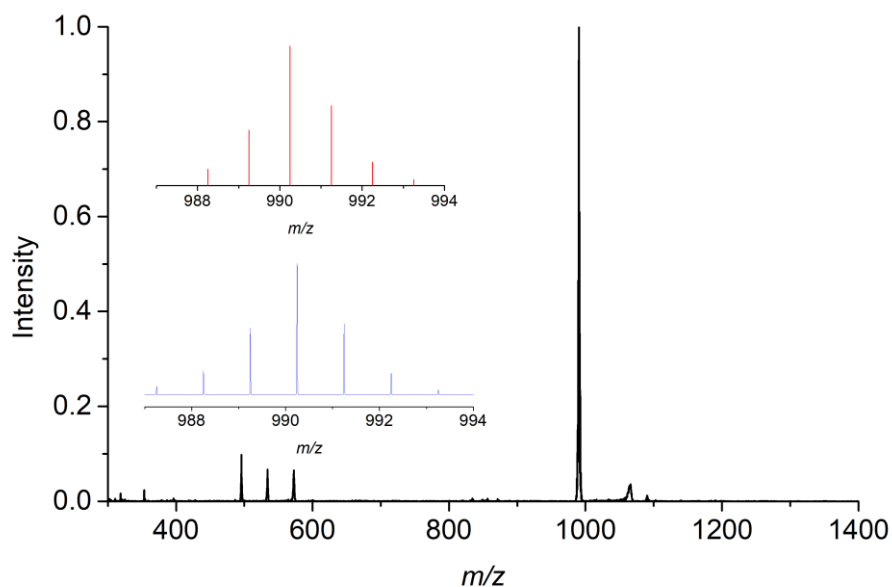


**Figure 2.4** - HRMS (positive mode) of complex **2.1** and zoom-in on the peak centered at  $m/z = 990.2458$  (red) and simulation (blue).

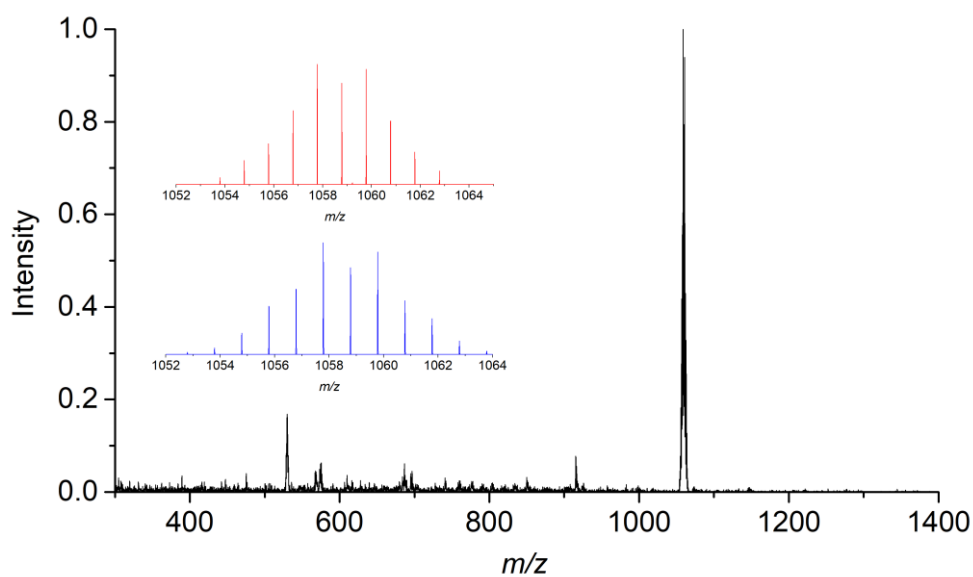


**Figure 2.5** - HRMS (positive mode) of complex **2.2** and zoom-in on the peak centered at  $m/z = 1055.7880$  (red) and simulation (blue).

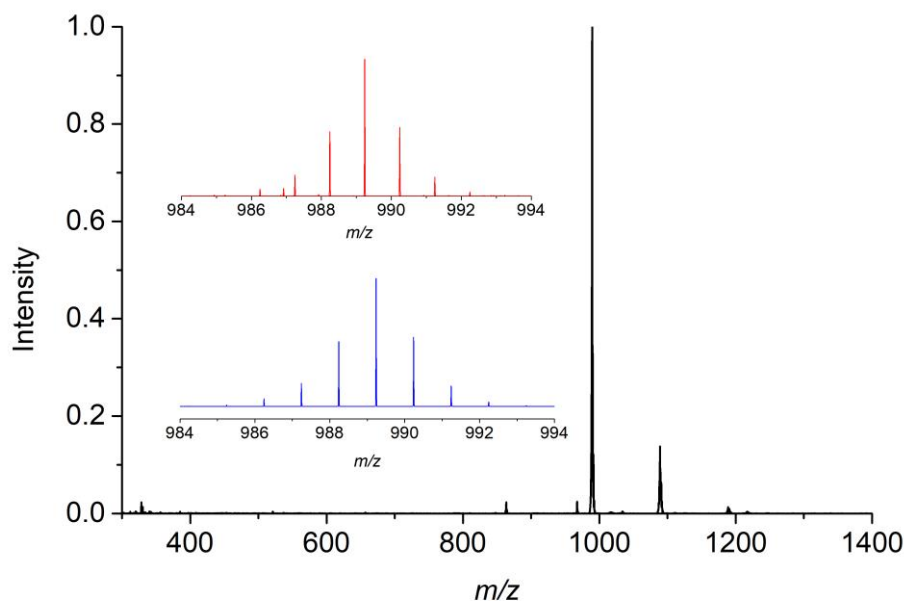


**Figure 2.6** - HRMS (negative mode) of complex **2.3** and zoom-in on the peak centered at  $m/z = 989.2377$  (red) and simulation (blue).

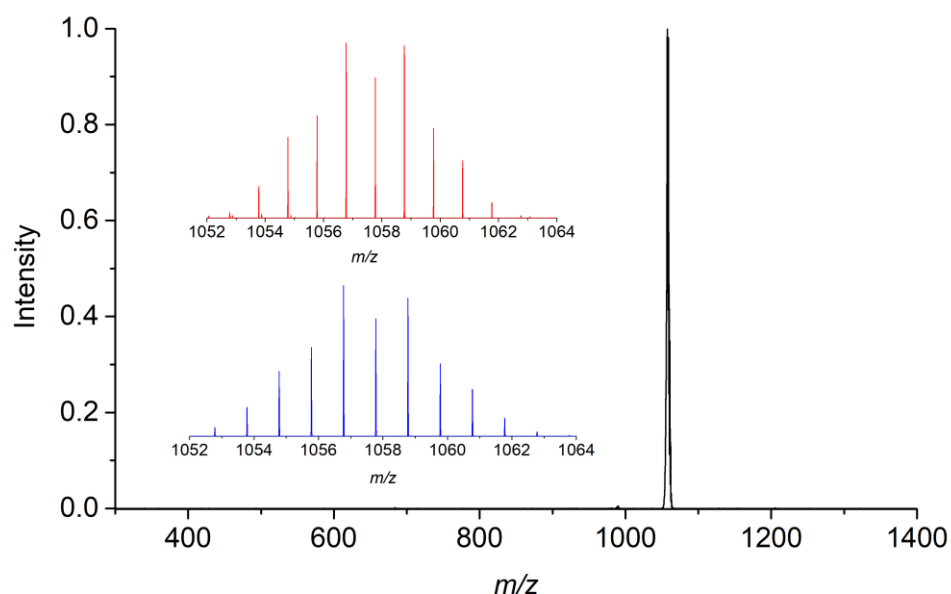


**Figure 2.7** - HRMS (negative mode) of complex **2.4** and zoom-in on the peak centered at  $m/z = 1054.7789$  (red) and simulation (blue).

The magnetic susceptibility of the iron clathrochelate complexes **2.2** and **2.4** was investigated in the temperature range of 5–350 K with an applied field of 1 T and zero field cooling (ZFC). The susceptibility of iron clathrochelates containing  $\text{Fe}^{\text{II}}\text{-Fe}^{\text{II}}$  shows a broad maximum around 40 K and decreases at higher temperatures (Figure 0.8). We modeled the behavior following a simple Hamiltonian  $H = J \cdot S_1 \cdot S_2$ , where  $J$  represents the exchange interaction between two  $\text{Fe}^{\text{II}}$  magnetic moments ( $S = 2$ ). Rather good agreement has been achieved with an antiferromagnetic coupling between the moments of  $J = 14$  K. If the high temperature part is fitted with a Curie–Weiss behavior [ $\chi_m = C/(T - T_c) + \chi_0$ ], one obtains a Curie constant of  $C = 3.18 \text{ emu K mol}^{-1}$  per  $\text{Fe}^{\text{II}}$ , which

is in good agreement with the theoretical value of  $C = 3.0 \text{ emu K mol}^{-1}$ . The inverse susceptibility of complexes containing  $\text{Fe}^{\text{II}}\text{-Fe}^{\text{III}}$  increases monotonically with temperature from 5 to 350 K with a slight upwards curvature. The low temperature slope corresponds to a Curie constant of  $12.6 \text{ emu K mol}^{-1}$ , which relates to a paramagnetic spin  $S = 9/2$  and a  $g$ -factor around 2. This implies that at low temperature, the  $\text{Fe}^{\text{II}}$   $S = 2$  and  $\text{Fe}^{\text{III}}$   $S = 5/2$  are coupled strongly ferromagnetically to a single  $S = 9/2$  moment.

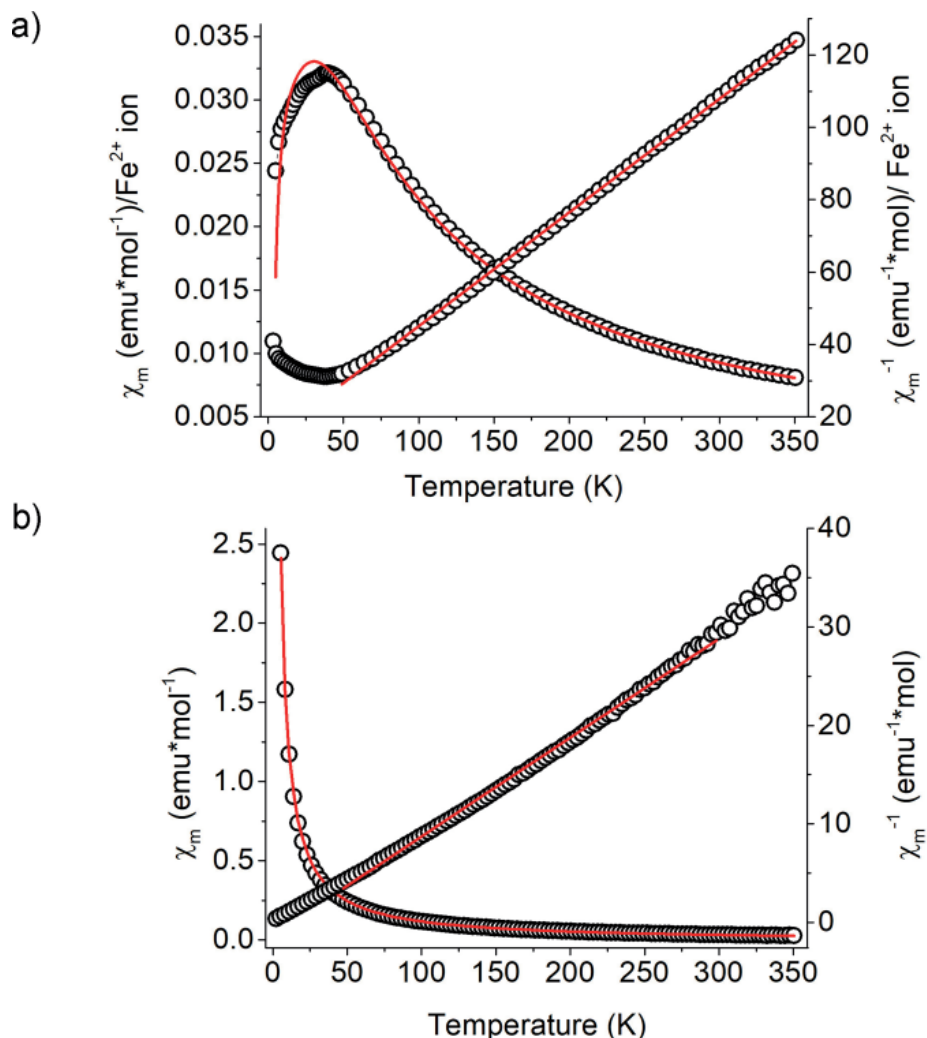


**Figure 2.8** - The magnetic susceptibility of the complexes (a) **2.4** and (b) **2.2**, as a function of temperature (the red curves indicate the fit).

However, the upwards curvature indicates that this ferromagnetic coupling is finite. We note that the values of JFM and  $\chi_0$  extracted from the fit correspond to a strong coupling. Given the similarity of the complexes we therefore fixed to the value obtained for complex **2.4**, which yielded JFM = 84(7) K. The observation of antiferromagnetic coupling between equal valence  $\text{Fe}^{\text{II}}$  ( $S = 2$ ) ions in complex **2.4** and ferromagnetic coupling between difference valence  $\text{Fe}^{\text{II}}$   $S = 2$  and  $\text{Fe}^{\text{III}}$   $S = 5/2$  in complex **2.2** agrees with what would be expected from respectively exchange and superexchange interactions (Figure 2.9)

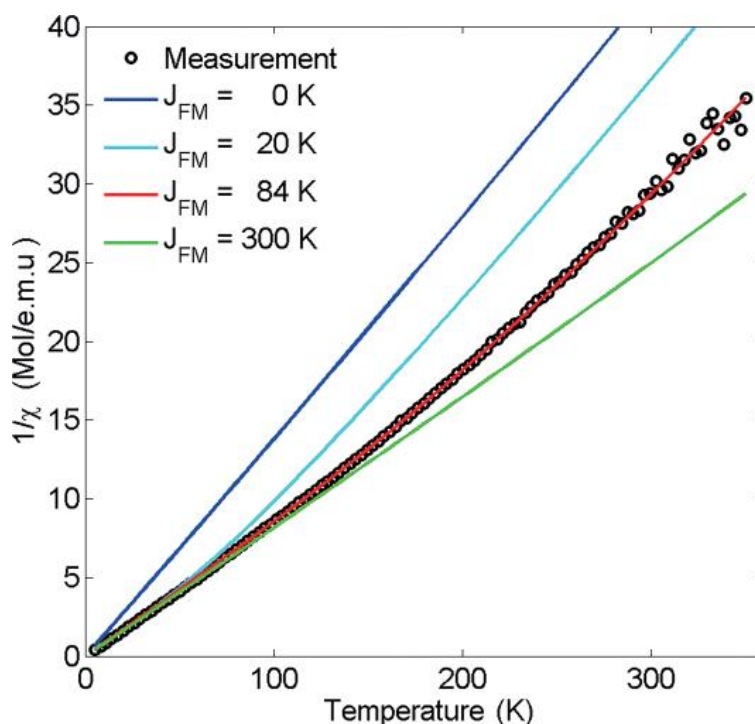
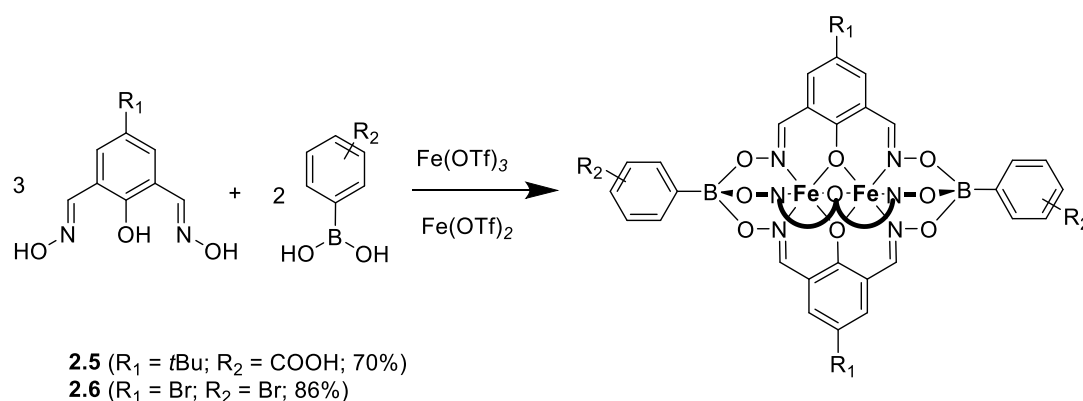


**Figure 2.9** - The magnetic susceptibility of complex **2.2** as a function of temperature. Lines indicate susceptibility calculated for a coupled system of  $S = 2$  and a  $S = 5/2$  with various values of ferromagnetic coupling  $J_{FM}$ .

## 2.2 Synthesis and characterization of dinuclear iron clathrochelate complexes containing different functional groups in the ligand periphery

As described in chapter 1, the structural diversity of clathrochelate complexes through ligand functionalization can bring versatility with respect to potential applications. Negatively charged  $\text{Fe}^{\text{II}}\text{-Fe}^{\text{II}}$  clathrochelate complexes are only stable under inert conditions. Their purification is achieved by filtration followed by washing with methanol and diethyl ether a solvent. The neutral mixed-valence  $\text{Fe}^{\text{II}}\text{-Fe}^{\text{III}}$  clathrochelate complexes can be purified by silica gel column chromatography.



**Scheme 2.3** - Synthesis of dinuclear Fe clathrochelate complexes with bromo and carboxylate groups. Conditions: MeOH, 60 °C, 2 h,  $\text{NEt}_4\text{OH}$ , room temperature.

Following the established procedure for the synthesis of neutral clathrochelate complexes with 4-pyridyl-groups (**2.1** – **2.4**), we investigated the synthesis of clathrochelate complex **2.5** using a tert-butyl-substituted dioxime and 4-carboxyphenylboronic acid (Scheme 2.3). The resulting complex **2.5** was characterized by single

crystal X-ray diffraction (Figure 2.10). Despite all efforts, we were not able to obtain a mass spectrum for complex **2.5**.

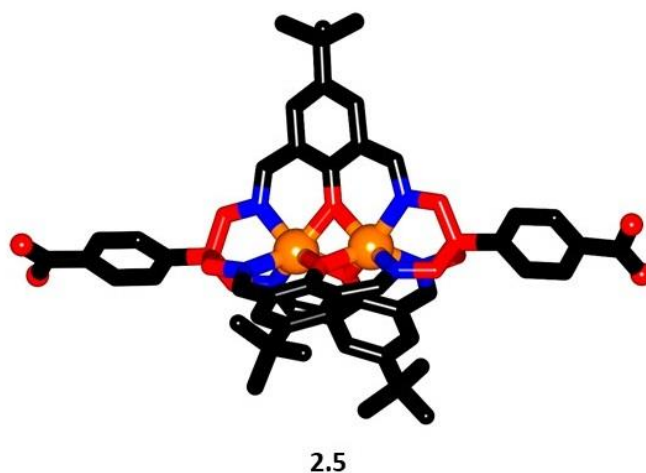


**Figure 2.10** - Molecular structure of complex **2.5** in the crystal. Color-coding: C: black; B: green; Fe: orange; N: blue; O: red; Hydrogen atoms and solvent molecules have been omitted for clarity.

We also synthesized the pentabrominated  $\text{Fe}^{\text{II}}\text{-Fe}^{\text{III}}$  clathrochelate complex **2.6** in 86% yield using a brominated phenol dioxime along with 4-bromophenylboronic acid. Clathrochelate complex **2.6** was characterized by MS (Figure 2.12), single crystal X-ray diffraction (Figures 2.11). The five bromo functions of **2.6** are arranged in a trigonal bipyramidal fashion, as evidenced by the crystallographic analysis.

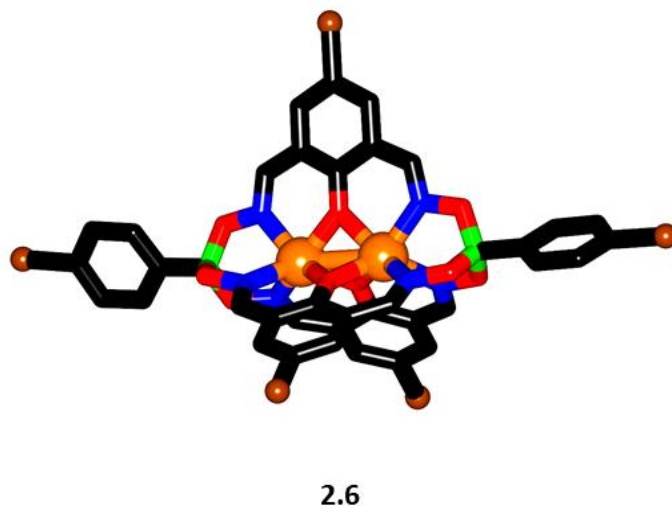


**Figure 2.11** - Molecular structure of complex **2.6** in the crystal. Color-coding: C: black; B: green; Fe: orange; N: blue; O: red; Br: brown. Hydrogen atoms and solvent molecules have been omitted for clarity.



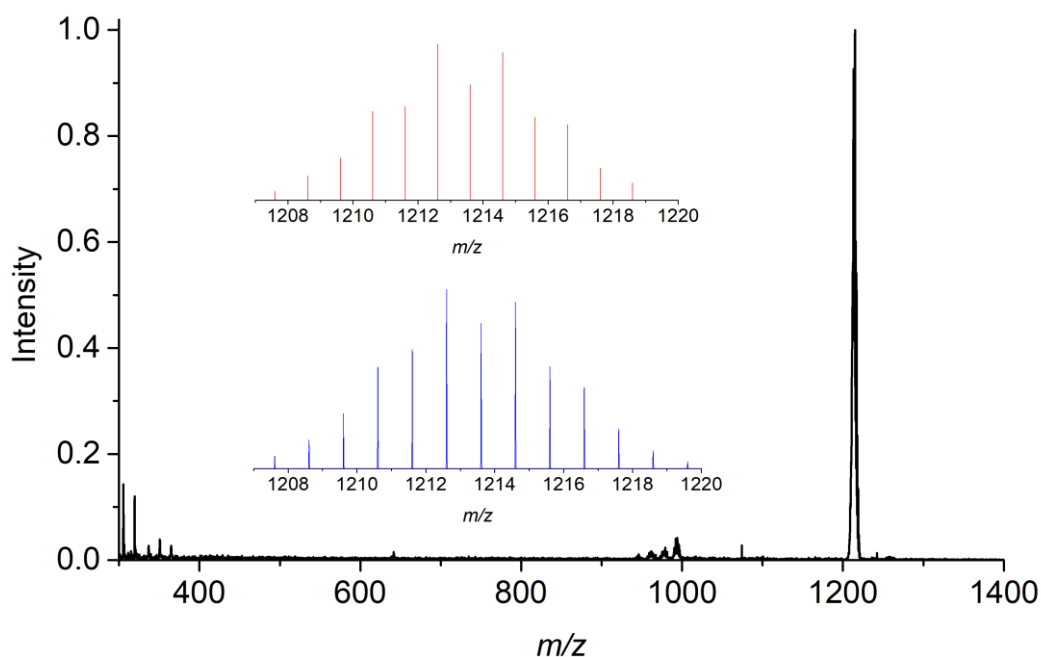
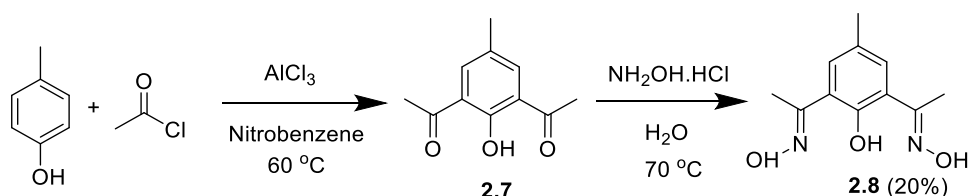


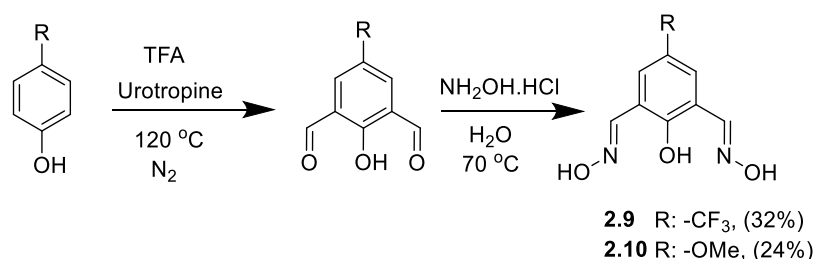
**Figure 2.12** - HRMS (positive mode) of complex **2.6** and zoom-in on the peak centered at  $m/z = 1212.6074$  (red) and simulation (blue).

Next, we investigated the synthesis of other dioxime derivatives. First, we employed a Friedel-Crafts acylation of 4-methylphenol to synthesize 1,3-diacetyl-2-hydroxy-5-methylbenzene as described by Reedijk et al.<sup>[40]</sup> The reaction was performed in nitrobenzene at 60 °C overnight, and the crude diketone compound **2.7** was subsequently reacted with hydroxylamine hydrochloride in water to give the desired dioxime compound **2.8** in 60% yield. Compound **2.8** was characterized by  $^1\text{H}$ -NMR and  $^{13}\text{C}$ -NMR spectroscopy.



**Scheme 2.4** - Synthesis of dioxime **2.8**.

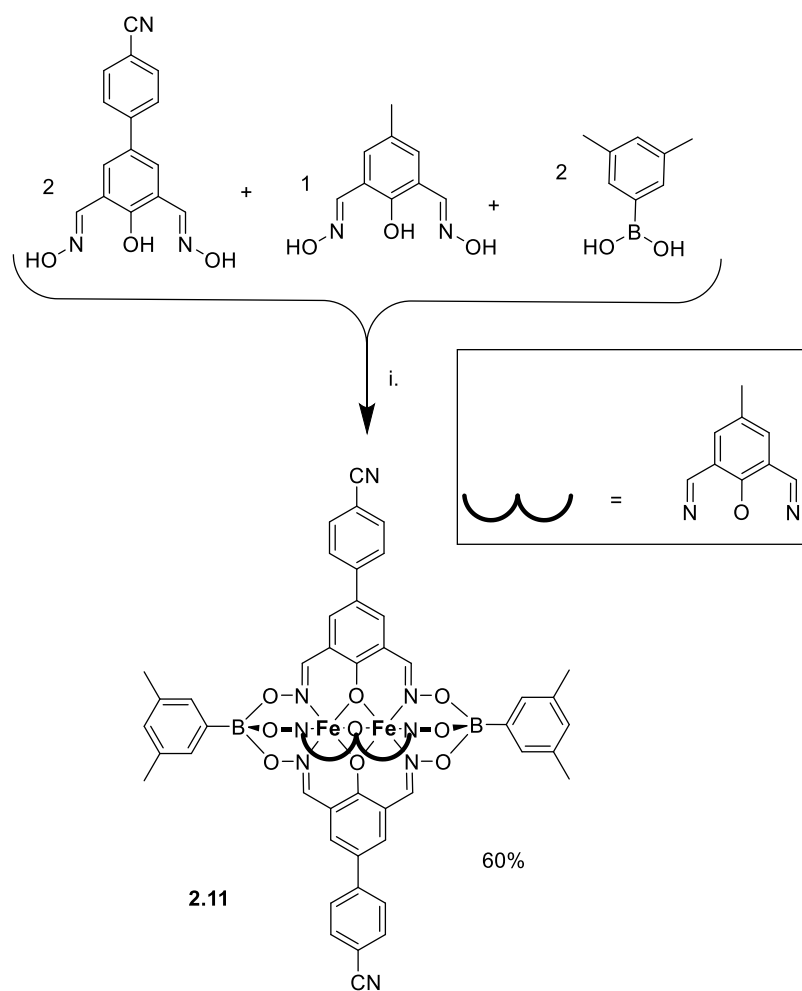
In addition, we investigated the dioxime substitution in the *para* position with respect to the hydroxyl group. For this purpose, 4-methoxyphenol or 4-(trifluoromethyl)phenol was combined with urotropine in the presence of trifluoroacetic acid under nitrogen. The resulting emulsion-like mixture was treated with 4.0 M hydrochloric acid solution, followed by extraction and flash column chromatography purification in DCM. The dioximes **2.9** and **2.10** were obtained with yields of 35 % and 53 %, respectively. The compounds were characterized by  $^1\text{H}$ -NMR and  $^{13}\text{C}$ -NMR.



**Scheme 2.5** - Synthesis of dioximes **2.9** and **2.10**.

Subsequently, we combined the dioxime **2.8** with 4-tertbutyl-benzeneboronic acid in an attempt to synthesize Fe<sup>II</sup>-Fe<sup>II</sup> and Fe<sup>II</sup>-Fe<sup>III</sup> clathrochelate complexes. For this purpose, the optimized conditions given in Scheme 2.1 were employed. Surprisingly, no product was observed, as evidenced by mass spectrometry measurements. Changing the capping groups from 4-tertbutyl-benzeneboronic acid to pyridineboronic acid did not yield the desired complexes. Similar results were obtained when dioximes **2.9** and **2.10** were employed. This could be due to electronic effects. Therefore, no further experiments were undertaken.

Cyano-functionalized dinuclear Co-based clathrochelate complexes were employed as metalloligands for the preparation of Ag-based MOFs.<sup>[41]</sup> Here we present preliminary data of the preparation of a neutral and asymmetric (different lateral group) cyano-functionalized clathrochelate complexes. 3,5-Dimethylphenylboronic acid was mixed with a cyanophenyl- and a methyl-functionalized phenol dioxime in MeOH with Et<sub>4</sub>NOH as base (Scheme 2.6). The resulting clathrochelates were separated by silica gel flash column chromatography. Complex **2.11** was the major product and was analyzed by single crystal X-ray diffraction (Figure 2.13). Further investigations were not undertaken.



**Scheme 2.6** - Synthesis of an asymmetric, cyano-functionalized clathrochelate complex. Conditions: i: MeOH, NEt<sub>4</sub>OH 70 °C, 2 h.

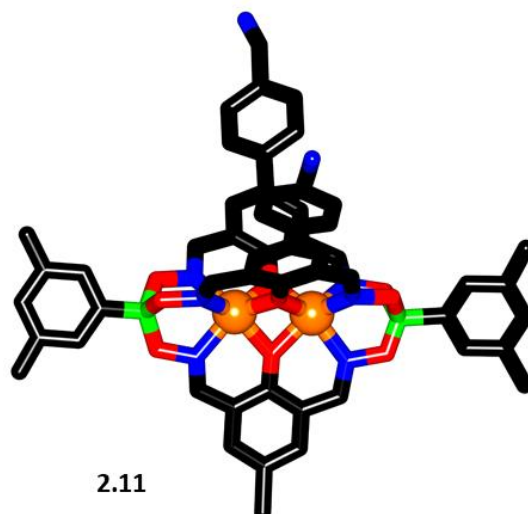
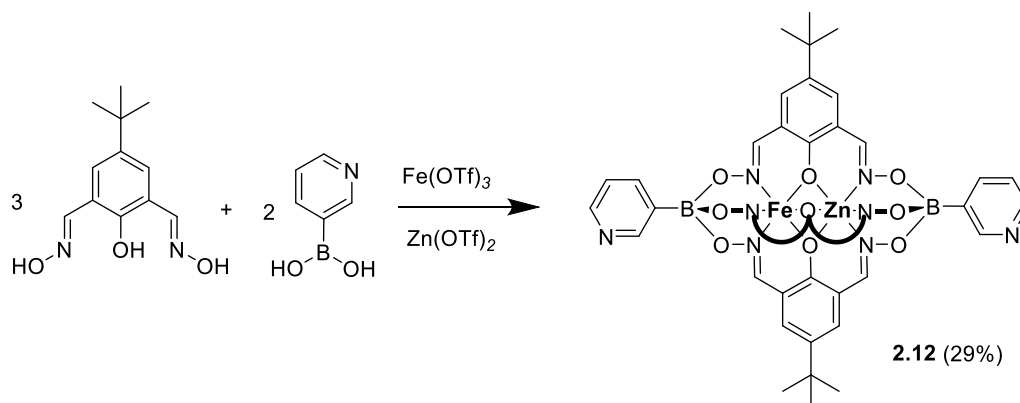


**Figure 2.13** - Molecular structure of complex **2.11** in the crystal. Color-coding: C: black; B: green; Fe: orange; Mn: cyan; N: blue; O: red. Hydrogen atoms and solvent molecules have been omitted for clarity.

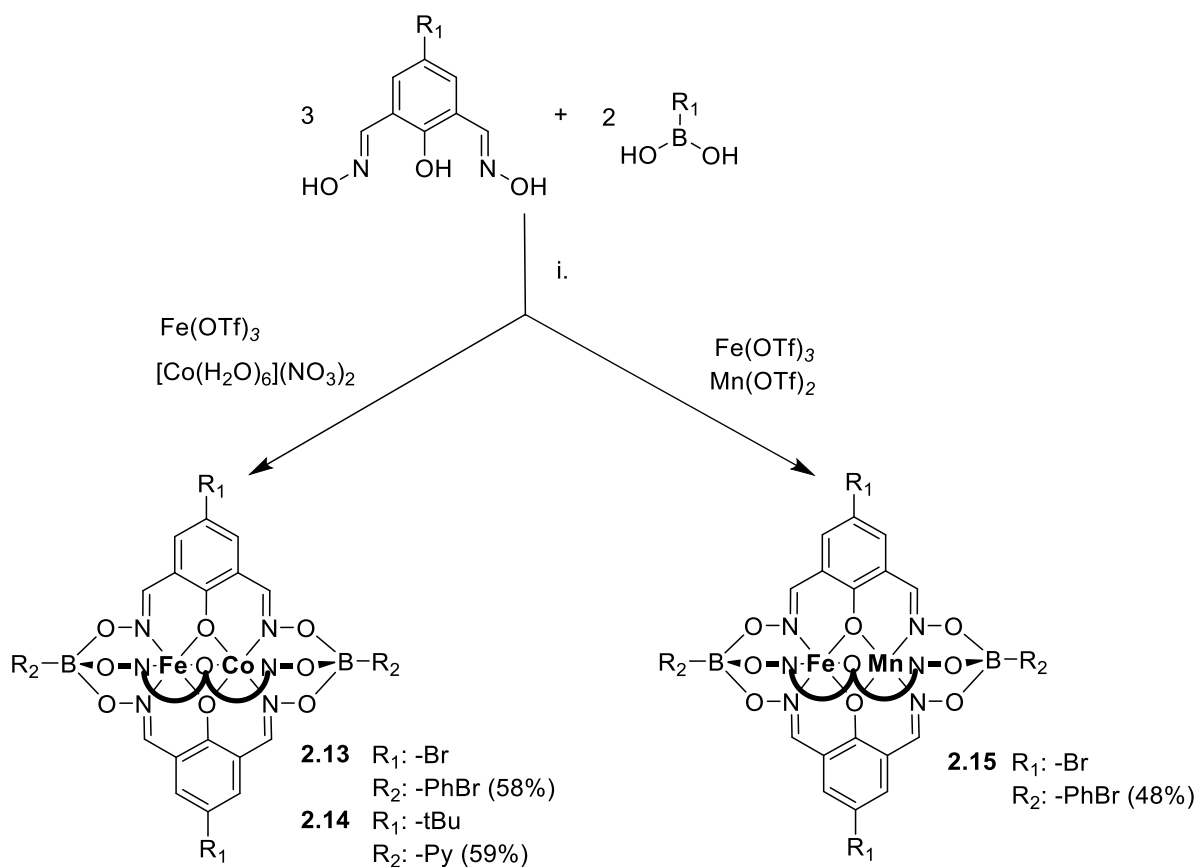
### 2.3 Heterometallic clathrochelate complexes

The possibility to synthesize heterobimetallic clathrochelate complexes was first investigated by Dr. Mathieu Marmier. For this purpose, the typical condensation reaction was performed with an equimolar mixture of  $\text{Zn}(\text{OTf})_2$  and  $\text{Fe}(\text{OTf})_3$ . As ligand precursors, a *t*-Bu-substituted phenol dioxime and 3-pyridylboronic acid were used. The reaction with two different metal salts was expected to give the homobimetallic  $\text{Zn}^{\text{II}}$  clathrochelate along with the desired  $\text{Zn}^{\text{II}}$ - $\text{Fe}^{\text{III}}$  complex (Scheme 2.7). The formation of a  $\text{Fe}^{\text{III}}$ - $\text{Fe}^{\text{III}}$  complex as a side product was not expected, because such a complex could not be obtained from  $\text{Fe}^{\text{III}}$  salts. The resulting clathrochelates are neutral. Hence, purification by silica gel column chromatography is possible.



**Scheme 2.7** - Synthesis of the heterobimetallic  $\text{Zn}^{\text{II}}$ - $\text{Fe}^{\text{III}}$  clathrochelate **2.12**. Conditions: i: MeOH:DCM (1:1) 70 °C, 2 h; then  $\text{NEt}_4\text{OH}$ , 1 h.

These results prompted us to investigate if other heterobimetallic clathrochelate complexes could be obtained. Condensation reactions were carried out with equimolar mixtures of  $[\text{Co}(\text{H}_2\text{O})_6](\text{NO}_3)_2$  or  $\text{Mn}(\text{OTf})_2$  and  $\text{Fe}(\text{OTf})_3$ . 4-Bromophenylboronic acid/4-pyridylboronic acid and Br- or *t*-Bu-substituted phenol dioxime were used as ligand precursors (Scheme 2.8). The resulting clathrochelate complexes **2.13**, **2.14** and **2.15** were characterized by HRMS and single crystal X-ray diffraction (Figures 2.14 to 2.16). The neutral clathrochelate complexes were purified by silica gel column chromatography.



**Scheme 2.8** - Synthesis of the heterobimetallic Co<sup>II</sup>-Fe<sup>III</sup> and Mn<sup>II</sup>-Fe<sup>III</sup> clathrochelates **2.13**, **2.14** and **2.15** respectively. Conditions: i: MeOH, NEt<sub>4</sub>OH, 70 °C, 2 h.

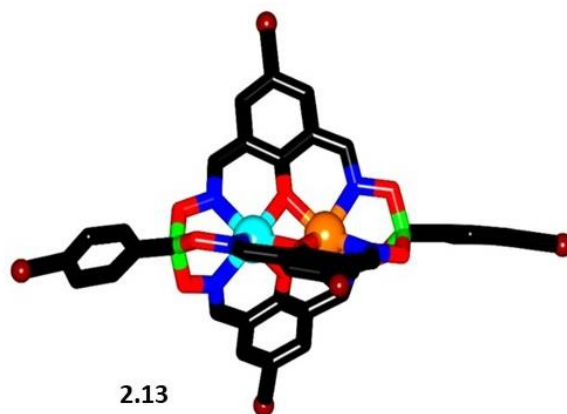


**Figure 2.14** - Molecular structure of complex **2.13** in the crystal. Color-coding: C: black; B: green; Fe: orange; Co: cyan; N: blue; O: red; Br: brown. Hydrogen atoms and solvent molecules have been omitted for clarity.

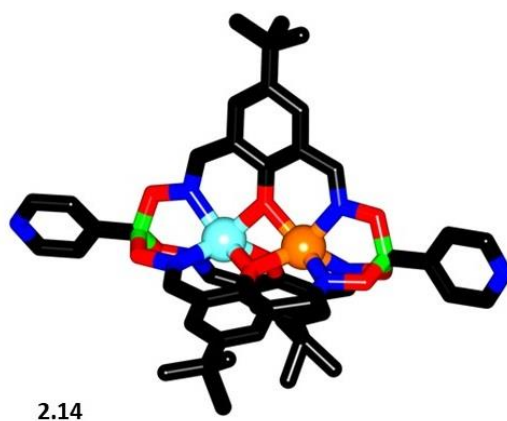


**Figure 2.15** - Molecular structure of complex **2.14** in the crystal. Color-coding: C: black; B: green; Fe: orange; Co: cyan; N: blue; O: red. Hydrogen atoms and solvent molecules have been omitted for clarity.

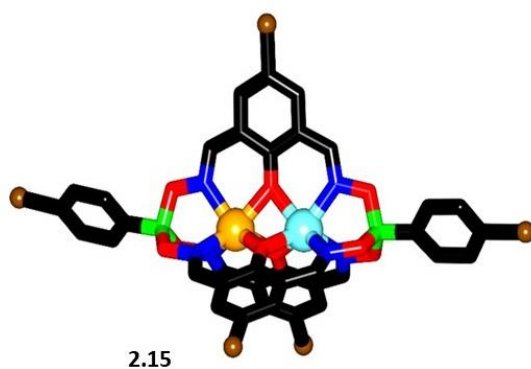


**Figure 2.16** - Molecular structure of complex **2.15** in the crystal. Color-coding: C: black; B: green; Fe: orange; Mn: cyan; N: blue; O: red; Br: brown. Hydrogen atoms and solvent molecules have been omitted for clarity.



# Chapter 3 Dinuclear iron clathrochelates as redox-active compounds for redox flow batteries

In this chapter, we discuss the synthesis and characterization of dinuclear iron clathrochelates and their applications as redox-redox active complexes for redox flow batteries (RFB). The cyclic voltammetry experiments were performed with the help of Ophelie Marie Planes. The RFB measurements were performed in collaboration with the group of Guihua Yu at the University of Texas at Austin.

## 3.1 Introduction

The concerns brought by greenhouse gas emissions and the lack of energy security have forced a rapid transition from carbon-based sources to renewable energy.<sup>[42,43]</sup> Indeed, a large number of solar and wind power plants were built over the last decade and a major expansion is expected in the next years.<sup>[44,45]</sup> Nevertheless, renewable energy sources such as solar and wind suffer from high intermittence; the energy demand diverges from the energy production.<sup>[46]</sup> A solution for this problem is the installation of intelligent energy storage systems such as pumped hydro, compressed air, thermal, flywheel, superconducting magnetic, electric double layer and electrochemical energy storage. The latter is more advantageous because it can be installed anywhere without geographical and geological restrictions.<sup>[47]</sup> Lithium-ion batteries dominate the electrochemical energy sector due to their superior performance and significant price regression. In addition, lithium-ion batteries present high energy densities with potential for higher capacities and relatively low self-discharge. However, lithium-ion batteries suffer from relatively low lifetime and scalability.<sup>[48]</sup> Lithium-ion batteries are not easily scalable because they are small self-contained units and for them to adopt a grid scale storage one would require large quantities. Moreover, they are subject to ageing even when not in use along with low number of charge/discharge cycles; typically around 1200 – 1500.<sup>[48]</sup>

Redox Flow Batteries (RFBs) (Figure 3.1) present an alternative to lithium-ion batteries in the electrochemical energy storage sector. A typical RFB is composed of an electrochemical cell (with two electrodes and a separator), and two tanks (containing the redox active cathode and anode in electrolyte solutions known as catholyte and anolyte).<sup>[49]</sup> The catholyte and anolyte solutions are circulated between these components with the help of pumps. The separator allows the selective migration of the supporting electrolytes in a similar fashion to fuel cells. Therefore, RFBs can be scaled independently from each other economically and safely without



incurring losses of power density. In order to scale-up power, one simply needs to increase the electrode active surface area, the number of electrodes in a cell stack, and the number of stacks in a system. In addition, the storage capacity can be increased by increasing the volume of electrolytes and/or concentrations of the active species.<sup>[50,51]</sup> Therefore, a high solubility of the redox-active material is needed in order to maintain a high current density while minimizing mass transport losses. The cost of a RFB is highly dependent on its components but mainly on corresponding redox-active species.<sup>[48]</sup>

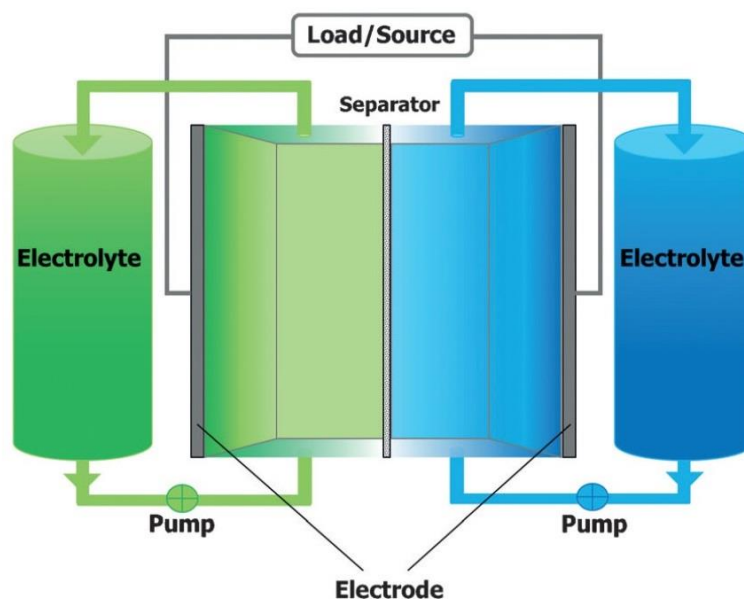


**Figure 3.1** - Schematic representation of a redox flow battery. Reprinted with permission from reference <sup>[47]</sup>. Copyright 2017 Angewandte Chemie International Edition.

Metal-based redox flow batteries have received significant attention and vanadium-based systems have been commercialized. Currently, vanadium-based RFBs are the most developed systems given their high charge/discharge cycles up to 20.000, high reversibility and relative large power outputs.<sup>[49–52]</sup>

In order to ensure that the energy storage systems are economically viable, the US Department of energy (DoE) has set a cost target of USD 150 kWh<sup>-1</sup> by 2023. Although vanadium-based RFBs incur a capital cost of USD 80 kWh<sup>-1</sup>, they still display low energy densities < 40 WhL<sup>-1</sup> compared to lithium-ion batteries with >200 WhL<sup>-1</sup>.<sup>[46]</sup> In addition, vanadium is expensive with limited resources and their RFBs often employ corrosive and hazardous electrolytes. Alternatively, zinc-halogen RFBs have been developed. However; such systems suffer from low current performances, electrolyte crossovers and employ highly expensive membranes.<sup>[53–57]</sup>

Organic redox-active materials (Figure 3.2) offer the potential to overcome metal-related problems. For instance, organic compounds consist of earth-abundant elements, which can be synthetically tuned to yield higher chemical and electrochemical stabilities as well as higher solubilities. The latter would result in high energy densities.<sup>[58]</sup> Unlike metal-based RFBs, the use of organic materials paves the way for the use of organic solvents. In fact, organic aprotic solvents show a better electrochemical stability in a wider window than protic

solvents like water. Hence, the batteries in aprotic solvents have higher energy densities as redox couples with elevated voltage can be used.<sup>[59]</sup> It is worth noting that ion conductivity decreases in organic solvents, limiting their applicable current density due to the limited number of soluble electrolytes.<sup>[47]</sup> However, organic materials soluble in water can also be employed to increase current densities although still restricted by the redox couples.<sup>[60,61]</sup> The use of organic redox-active materials can be envisioned in two forms; *i.* in combination with inorganic materials (single flow RFB) or *ii.* in combination with other organic materials (all-organic RFB). Polymeric materials can also be used in combination with metallic or halogen anode/cathodes to prepare flow batteries with high energy densities and coulombic efficiencies however not directly related to this thesis therefore, we will not discuss it further.<sup>[46–48]</sup>

Several benchmarks can be used to judge the electrical performance of a redox flow battery. For instance, the **volumetric capacity** of the electrolyte indicates the amount of charge that can be stored in a certain amount of electrolyte. Hence, it is highly dependent on the amount of redox-active material and the number of electrons that participate in the redox process. Another parameter is the **energy density**, which is directly proportional to the product of the volumetric capacity and the voltage between the utilized redox couples. The **Coulombic efficiency** and **voltage efficiencies** indicate the electrical quality of the battery. For instance, Coulombic efficiencies <99% are an indication of crossover of redox-active material through the membrane into the opposite half-cell or irreversible side reactions of the redox-active material or the electrolyte. Voltage efficiency is the ratio between the mean discharging and charging voltage at constant current. The product of the Coulombic and voltage efficiencies yields the **energy efficiencies**, which is the measure of the applied and retained energy. Typical RFBs have 50 – 90% energy efficiencies. **Current densities** are related to the membrane areas of the electrochemical cells and directly impact the charging/discharging times.<sup>[47]</sup>

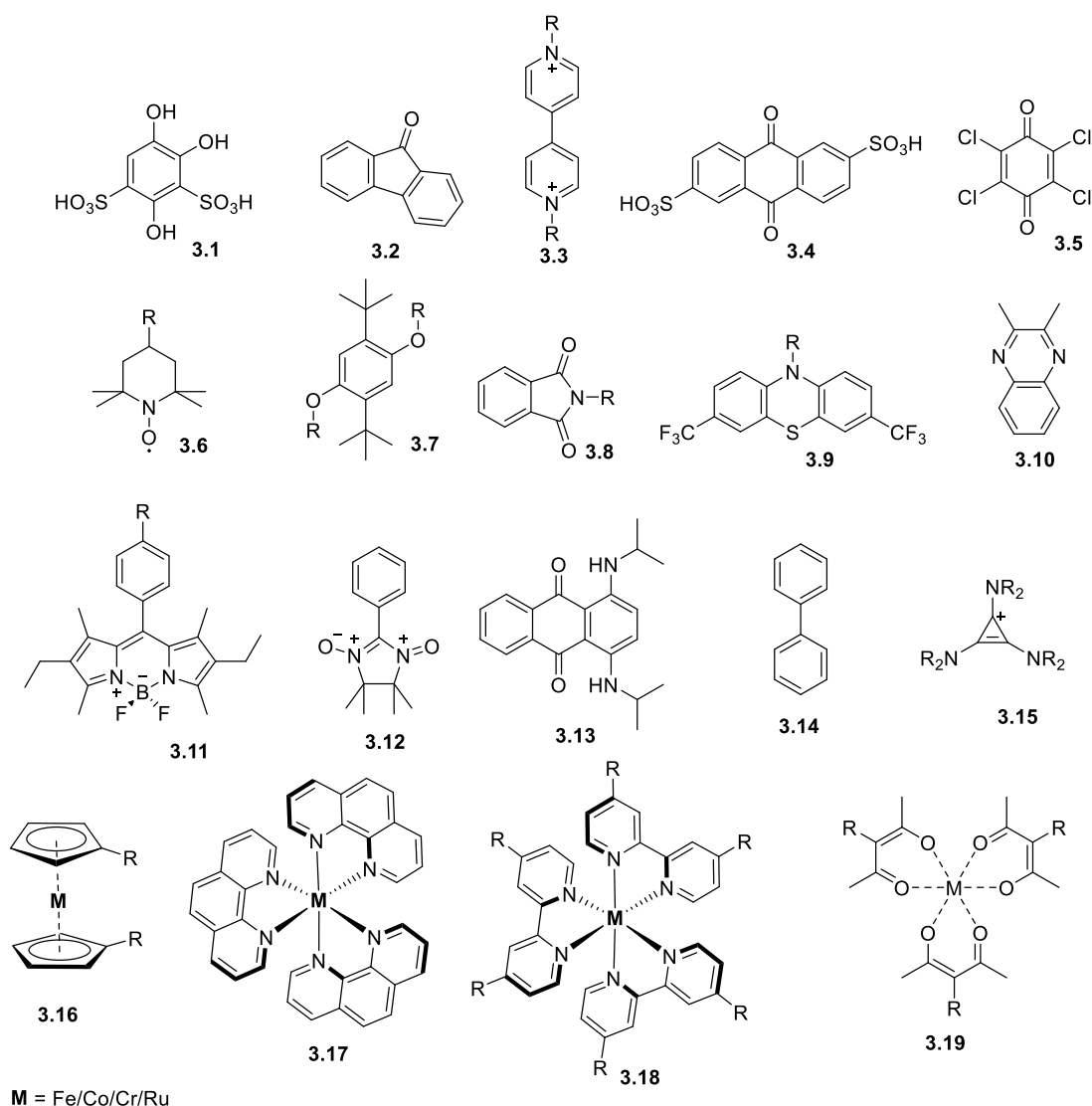


**Figure 3.2** - Representative structures of redox-active organic and organometallic compounds used for redox flow battery applications.

The first organic/inorganic RFB was reported in 2009 by the group of Xu where cadmium was used as the anode and tetrachloro-*p*-benzoquinone (**3.5**) was utilized as the organic cathode. This battery revealed a charge voltage of 1.18 V and a discharge voltage of 0.97 V and high current density of 10 mAcm<sup>-2</sup>. The Coulombic efficiency was 99% with an energy efficiency of 82% over the first 100 charge/discharge cycles. Being a single flow battery, the advantage is being membrane-free. However, the use of a strongly acidic electrolyte (sulfuric acid) is a drawback.<sup>[62]</sup> The same research group later reported a lead/4,5-dibenzoquinone-1,3-benzenedisulfonate (**3.1**) battery, where Nafion 115 was used as a membrane. The battery revealed an average Coulombic efficiency of 93% and an average energy efficiency of 82% with a current density of 10 mAcm<sup>-2</sup>.<sup>[63]</sup>

Wang et al. reported a RFB based on compound **3.4** with methoxytriethyleneglycol substituents as cathode material and lithium as the anode. The ethylene glycol moieties were used to promote solubility. The static test cell demonstrated an energy efficiency of 82% and a theoretical specific density of 25 WhL<sup>-1</sup> over 9 cycles with a current density of 10 mA cm<sup>-2</sup>. However, a decline in the discharge capacity was observed. It is worth noting that

anthraquinones are well known organic cathode materials for lithium-ion batteries.<sup>[64]</sup> The combination of lithium as anode and 2,2,6,6-tetramethylpiperidine-1-oxyl (TEMPO, **(3.6)**) as the organic active material is also possible. In fact, TEMPO is stable and has been reported as a redox active compound.<sup>[65–67]</sup> The static test cell with TEMPO concentrations of 0.1 M gave an energy efficiency of 86%, a Coulombic efficiency of 99%, a voltage efficiency of 87% and an average capacity retention of 99.8% per cycle with a current density of 10 mA cm<sup>-2</sup>. In addition, this system yields an average voltage of 3.5 V. The advantage of TEMPO is the high attainable concentrations in ethylene carbonate/propylene carbonate/ethylmethylcarbonate mixtures, which leads to high energy densities.<sup>[68]</sup>

It is also possible to combine organic compounds with different redox potentials to prepare all-organic RFBs by employing either protic or aprotic solvents. For instance, Li *et al.* reported the first RFB where TEMPO and N-methylphthalimide were used as redox-active materials. The combination resulted in a cell voltage of 1.6 V however, with a low current density of 0.35 mA cm<sup>-2</sup>. The Coulombic efficiencies exceeded 90% and the energy density was reported as 1.7 WhL<sup>-1</sup> over 20 charge/discharge cycles.<sup>[69]</sup> Combining the phenothiazine derivative 3,7-bis(trifluoromethyl)-N-ethylphenothiazine (**(3.9)**) as an organic cathode material and 2,3,6-trimethylquinoxaline (**(3.10)**) as an anode material resulted in Coulombic efficiencies of 92% with low energy densities of 0.84 WhL<sup>-1</sup> after 100 charge/discharge cycles. Nevertheless, it was observed that compound **(3.9)** undergoes a second irreversible oxidation that decreases the overall capacity of the system.<sup>[70]</sup>

Several 1,4-dimethoxybenzene derivatives of **(3.7)** were investigated as redox-active materials for non-aqueous RFBs. For example, dimethoxy-ditert-butylbenzene was found to have high chemical and electrochemical stability. An introduction of oligoethylene oxide chains moderately increases the solubility and yield to higher energy densities. For instance, 2,3-dimethyl-1,4-dimethoxybenzene (23DDB) and 2,5-dimethyl-1,4-dimethoxybenzene (25DDB) were also tested as cathode materials for lithium-ion batteries. However, the calculated energy densities of 0.05 WhL<sup>-1</sup> were attained. Another drawback of these derivatives is up to 50% of the starting materials turn to non-rechargeable species after 15 cycles.<sup>[71,72]</sup> On the other hand, Coulombic efficiencies up to 90% were achieved. Other 1,4-dimethoxybenzene derivatives of **(3.7)**, namely ANL-8, ANL-9, and ANL-10 were investigated in carbonate solvents by cyclic voltammetry and were found to maintain an electrochemical redox behaviour with redox potentials of 4.0 V versus Li/Li<sup>+</sup>. Hence, they are good candidates for high density RFBs.<sup>[73]</sup> ANL-8 and 9-flourenone (**(3.2)**) were used as cathode and anode, respectively, resulting in a cell voltage of less than 2 V, a current density of 15 mA cm<sup>-2</sup> with Coulombic efficiencies of 83% and theoretical energy efficiencies of 15 WhL<sup>-1</sup> over 100 charge/discharge cycles. In addition, the redox active materials displayed high solubilities in organic solvents at room temperatures and presented well-defined electrochemical properties. However, this system does not retain the charge/discharge capacity. Hence not yet suitable for practical applications.<sup>[74]</sup>

The utilization of nonflammable water as solvent is advantageous from the safety point of view.<sup>[75]</sup> Organic redox-active materials can be tuned to improve their solubility in water. For instance, Yang *et al.* reported the

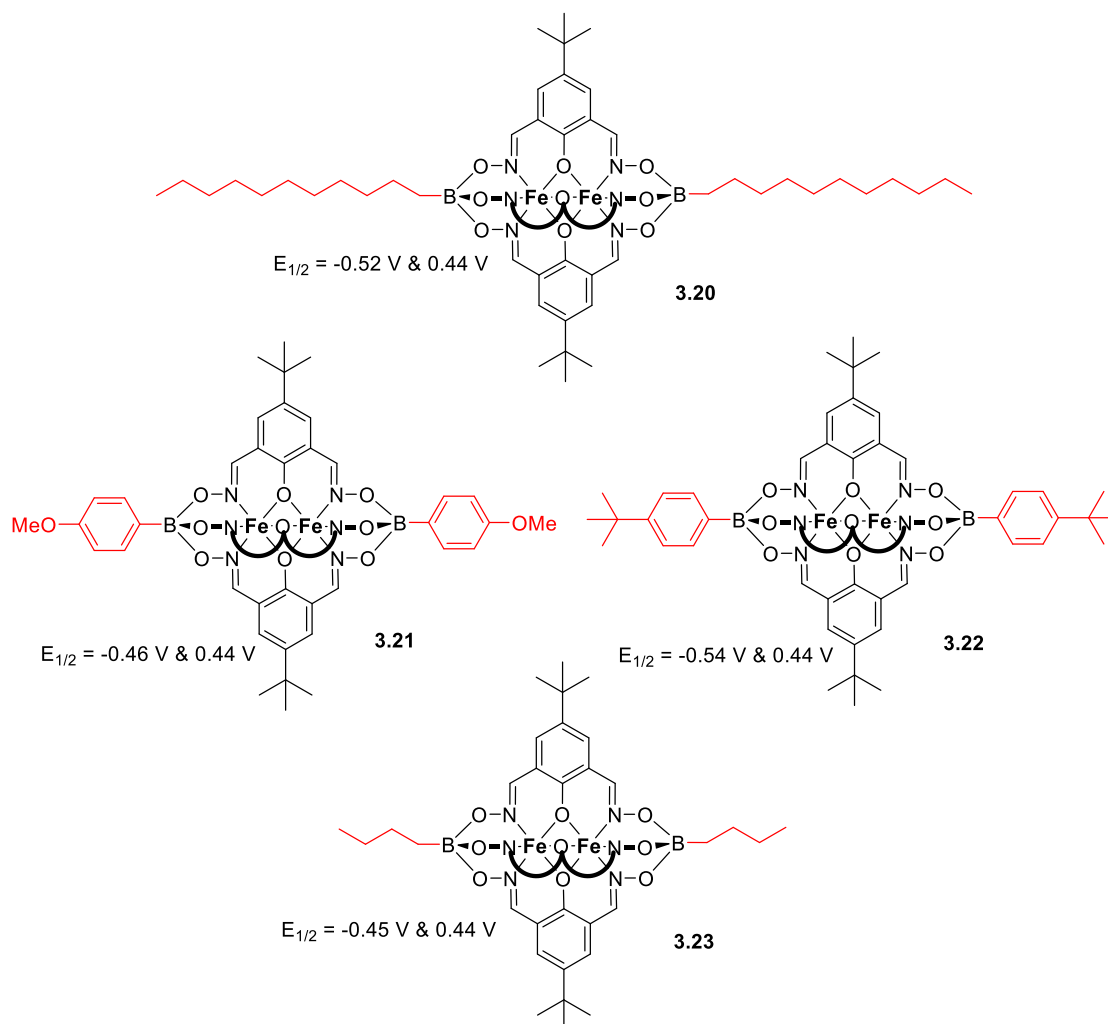
synthesis of water-soluble 1,2-benzoquinone-3,5-disulfonic acid (**3.1**) as the organic cathode active material and anthraquinone-2-sulfonic acid as well as anthraquinone-2,6-disulfonic acid as the organic anode active material. The resulting cell was tested for 12 charge/discharge cycles at current densities of  $10 \text{ mA cm}^{-2}$  and had a calculated energy density of  $1.25 \text{ WhL}^{-1}$ .<sup>[61]</sup> In another report, Zhang et al, demonstrated the use of water-soluble 1,2-benzoquinone-3,5-disulfonic acid (**3.1**) as the catholyte and an inexpensive anthraquinone derivative, 3,4-dihydroxy-9,10-anthraquinone-2-sulfonic acid, as the anolyte and a calculated discharge capacity retention of around 98%, as well as a columbic efficiency of 99% were achieved.<sup>[76]</sup> Liu et al. demonstrated that an aqueous RFB with 4-hydroxy-2,2,6,6-tetramethylpiperidine-1-oxyl (4-HOTEMPO) and methylviologen derivatives of **3.3** as the organic redox-active catholyte and anolyte, respectively, could reach high current densities up to  $100 \text{ mA cm}^{-2}$ , voltage efficiency of 62% with Coulombic efficiencies above 99% over 100 charge/discharge cycles. The calculated energy density of the system was  $8.4 \text{ WhL}^{-1}$ .<sup>[77]</sup>

Metal complexes (Figure 3.2) are alternative compounds for redox flow battery applications. For instance, ferrocene is well known for its high chemical, electrochemical and thermal stability. In addition, its derivatives have been employed in various applications over decades. Ferrocene can be functionalized with hydrophilic groups resulting in water soluble ferrocene compounds suitable for RFBs. In fact, water-soluble ferrocene compounds were synthesized from an hydrophobic ferrocene precursor and combined with viologen-based anolytes. The batteries demonstrated high theoretical energy densities of  $45.5 \text{ WhL}^{-1}$  and excellent current densities up to  $100 \text{ mA cm}^{-2}$  over 700 cycles.<sup>[75,78–80]</sup> The pairing of ferrocene as catholyte with lithium as anode was also reported to reach voltages of 3.2 V with energy conversions over 70%.<sup>[81]</sup> In addition, ferrocene can be modified to improve solubility and display multi-electron behaviour. Such properties are known to increase the operating current densities and capacities of the battery.<sup>[82]</sup> N-Ferrocenenylophthalimide was prepared by replacing the hydrogen atom on the N-site of phthalimide with ferrocene moiety. The resulting product displays two redox waves corresponding to each moiety with fast charge transfer kinetics.<sup>[83]</sup> Cobaltocene and ferrocene derivatives were also studied as redox active materials in redox flow batteries as anode and cathode, respectively. The compounds were shown to display relatively good solubilities and the cell exhibited stable capacity retention and discharge potentials.<sup>[84]</sup> Iron complexes bearing redox "non-innocent" diiminepyridine ligands were reported as suitable anolytes for redox flow battery applications.<sup>[85]</sup> Fe- and Co-based tris(1,10-phenanthroline) complexes were investigated as redox couples for RFB applications. They displayed a potential difference of 2.1 V with coulombic, voltage and energy efficiencies up to 80%, 40% and 39%, respectively.<sup>[86]</sup>

## 3.2 Clathrochelate complexes

As described in chapter 2, clathrochelate complexes **2.1** to **2.4** with pyridyl boronic acids as capping groups showed a reversible one-electron oxidation at negative potentials vs. a ferrocene/ferrocenium ( $\text{Fc}/\text{Fc}^+$ ) reference (Figure 2.2). Therefore, we were interested in understanding the effect of different boronic acid substitutions on the redox activity of clathrochelate complexes. For this purpose, we synthesized several neutral  $\text{Fe}^{\text{II}}\text{-Fe}^{\text{III}}$

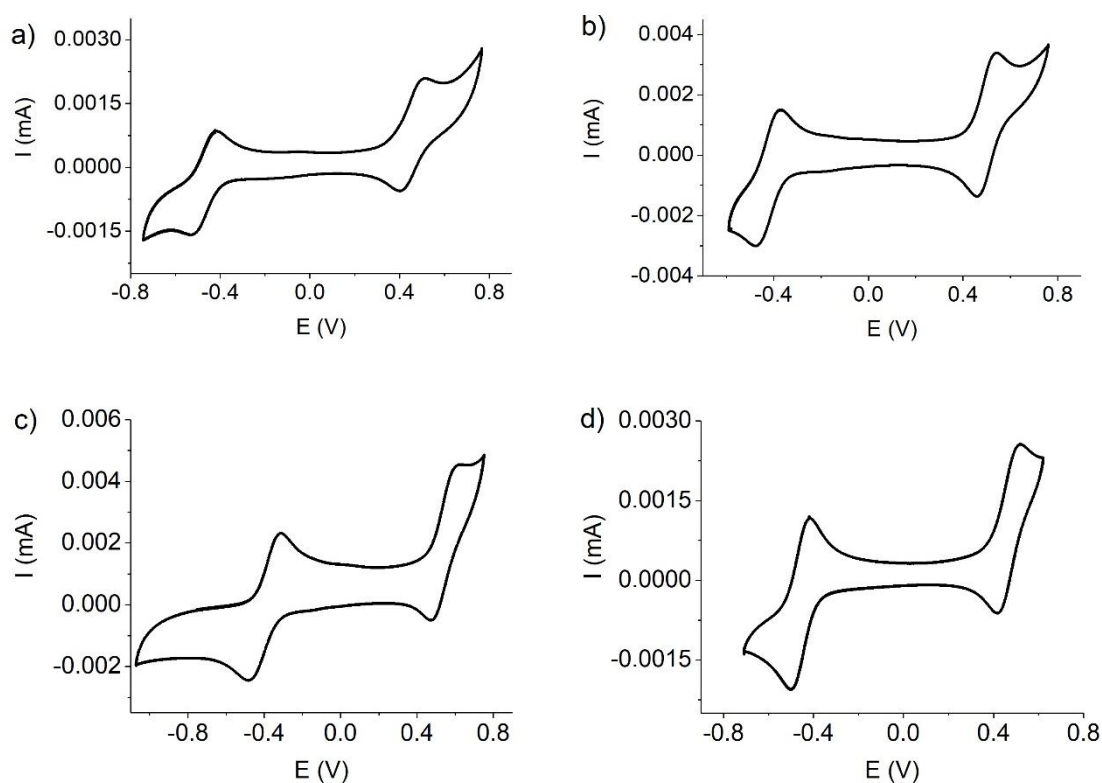
clathrochelate complexes (**3.20** – **3.27**) and investigated their redox properties with the help of cyclic voltammetry.



**Figure 3.3** - Clathrochelate complexes **3.20** to **3.23**.

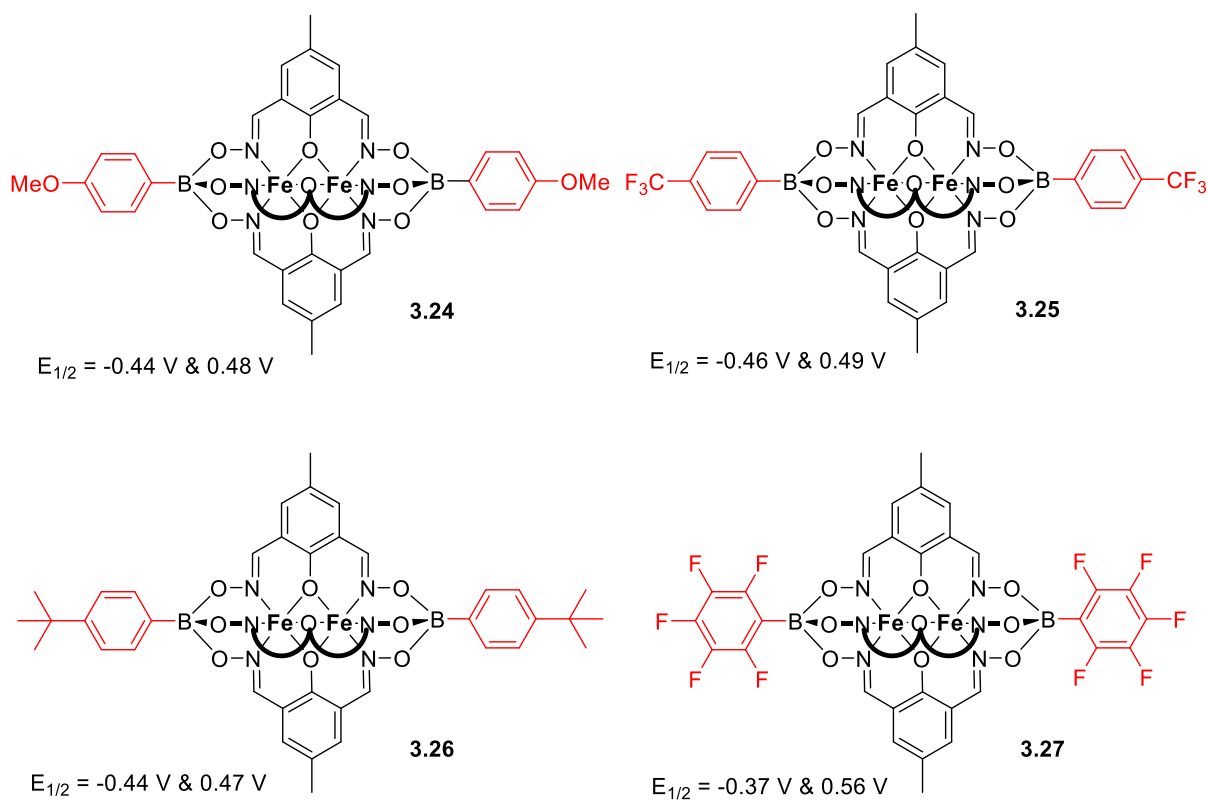
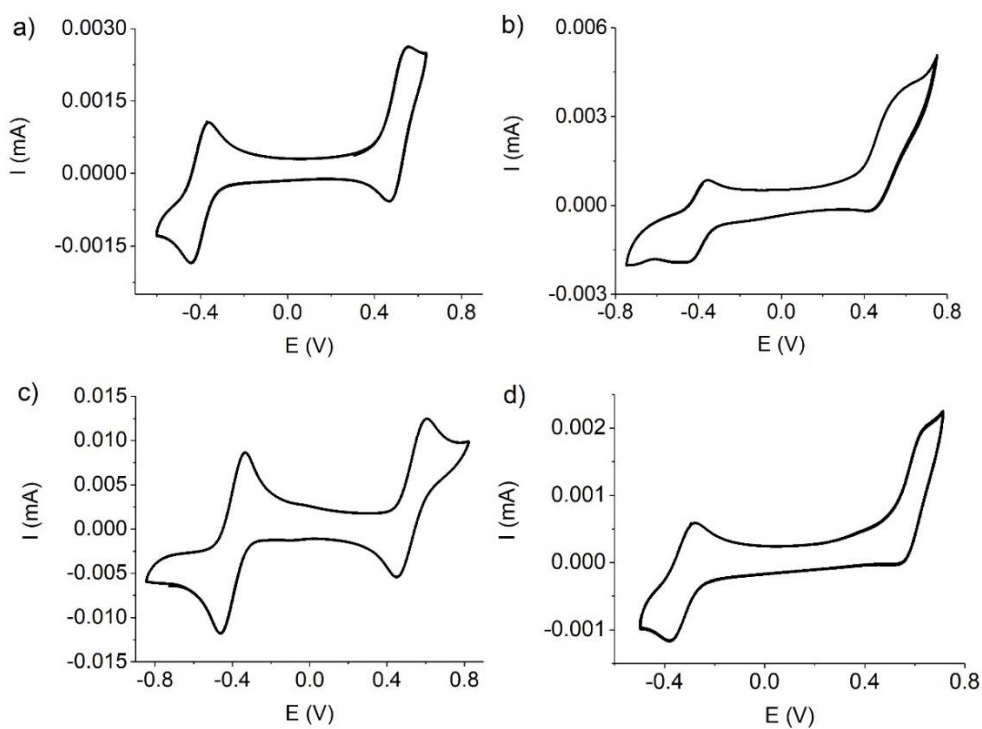
The complexes **3.20** – **3.23** displayed a reversible one-electron oxidation at negative potentials vs.  $\text{Fc}/\text{Fc}^+$ . In the positive region, we observed either reversible or quasi-reversible peaks depending on the boronic acid employed. For instance, the use of n-decyl-substituted boronic acid resulted in complex **3.20**, which gave two reversible peaks of  $E_{1/2} = -0.52 \text{ V}$  and  $E_{1/2} = 0.44 \text{ V}$  at negative and positive redox potentials, respectively. Similarly, complex **3.21** also gave two reversible peaks of  $E_{1/2} = -0.46 \text{ V}$  and  $E_{1/2} = 0.44 \text{ V}$  at negative and positive redox potentials, respectively. On the other hand, complexes **3.22** and **3.23** resulted in reversible peaks at negative potentials ( $E_{1/2} = -0.54 \text{ V}$  for **3.22** and  $E_{1/2} = -0.45 \text{ V}$  for **3.23**), and quasi-reversible peaks at positive potentials ( $E_{1/2} = 0.44 \text{ V}$  for both **3.22** and **3.23**). The reason for this such behaviour is not yet known. However, we can hypothesize that increasing the electron donor strength of the boronate ester capping groups can result in the stabilization of  $\text{Fe}^{\text{III}}\text{-Fe}^{\text{III}}$  clathrochelate complexes. It is worth noting that this effect was only observed electrochemically. Attempts to synthesize  $\text{Fe}^{\text{III}}\text{-Fe}^{\text{III}}$  clathrochelate complexes using exclusively  $\text{Fe}^{\text{III}}$  salts failed

(see section 2.1). As evident from the results depicted in Figure 3.3, varying the boronic acid substitutions results in minor shifts (<100 mV) of the redox potentials. In fact, clathrochelate complexes **3.20**, **3.21**, **3.22** and **3.23** displayed redox potentials of  $E_{1/2} = -0.52$  V,  $E_{1/2} = -0.54$  V,  $E_{1/2} = -0.46$  V and  $E_{1/2} = -0.46$  V respectively at negative potentials.



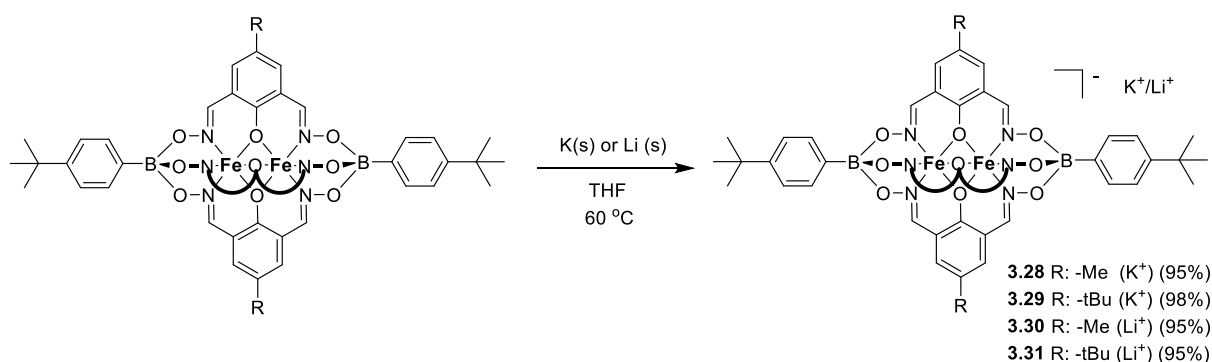
**Figure 3.4** - CV curves of clathrochelate complexes (a) **3.20**, (b) **3.21**, (c) **3.22** and (d) **3.23** vs FC/Fc<sup>+</sup> at 50 mV s<sup>-1</sup> scan rate in DMF solvent, 0.1 M TBAPF<sub>6</sub> as supporting electrolyte. Working electrode (Carbon), Reference electrode (Ag, AgCl), and counter electrode (Pt wire).

A similar effect was observed with clathrochelate complexes **3.24** and **3.26** containing electron-donating boronate ester capping groups. Indeed, complexes **3.24** and **3.26** gave two reversible peaks at negative ( $E_{1/2} = -0.44$  V for both **3.24** and **3.26**) and positive potentials ( $E_{1/2} = 0.48$  V for **3.24** and  $E_{1/2} = 0.48$  V for **3.26**). The pronounced effect of boronate ester capping groups bearing electron-withdrawing groups can be seen from clathrochelate complexes **3.25** and **3.27**, which show a reversible peak at negative potential ( $E_{1/2} = -0.46$  V for both **3.25** and  $E_{1/2} = -0.37$  V **3.27**), and an irreversible peak at positive potentials ( $E_{1/2} = 0.49$  V for **3.25** and  $E_{1/2} = 0.56$  V for **3.27**). These results corroborate the hypothesis that electron-donating capping groups can help stabilize the formation of Fe<sup>III</sup>-Fe<sup>III</sup> clathrochelate complexes, while a reverse effect is observed for capping groups with electron-withdrawing substituents. However, further investigations are required to fully understand the redox behaviour of these complexes.


 Figure 3.5 - Clathrochelate complexes **3.24** to **3.27**.

 Figure 3.6 - CV curves of clathrochelate complexes (a) **3.24**, (b) **3.25**, (c) **3.26** and (d) **3.27** vs FC/Fc<sup>+</sup> at  $50 \text{ mV s}^{-1}$  scan rate in DMF solvent,  $0.1 \text{ M}$  TBAPF<sub>6</sub> as supporting electrolyte. Working electrode (Carbon), Reference electrode (Ag, AgCl), and counter electrode (Pt wire).



As described in chapter 2, the reduction of neutral  $\text{Fe}^{\text{II}}\text{-Fe}^{\text{III}}$  clathrochelates can be achieved by using sodium dithionite. This reduction can be monitored by UV-vis and/or HRMS. In fact, solutions of  $\text{Fe}^{\text{II}}\text{-Fe}^{\text{III}}$  complexes are black/dark purple, whereas solutions of  $\text{Fe}^{\text{II}}\text{-Fe}^{\text{II}}$  complexes are brown. For applications of clathrochelate complexes in RFBs, it would be important that they are compatible with strongly reducing alkali metals. Therefore, we attempted to reduce the clathrochelate complexes with Li and K metals. Solutions of the complexes **3.22** and **3.26** in THF were mixed with Li or K, and the suspension were heated to 60 °C overnight. The resulting brown solutions indicated the formation of reduced  $\text{Fe}^{\text{II}}\text{-Fe}^{\text{II}}$  clathrochelates, which was confirmed by HRMS and UV-vis. The products were isolated by filtration (to remove any remaining Li or K metals), followed by removal of the solvent.



**Scheme 3.1** - Chemical reduction of clathrochelate **3.22** and **3.26** with Li(s) or K(s) in THF.

Single crystals were obtained for clathrochelate complexes **3.28** (through slow evaporation of solvent from a solution of complex **3.28** in THF) and **3.29** (through slow diffusion of  $\text{Et}_2\text{O}$  into a solution of complex **3.29** in THF). The products were analyzed by single-crystal X-ray diffraction. Complex **3.28** forms a macrocyclic structure in the solid state. The potassium cations interact with two THF molecules, four oxygen atoms and engages in a weak cation- $\pi$  interaction with the phenyl group from an adjacent clathrochelate complex. Complex **3.29** displays a linear polymeric structure, where the potassium cations interact with one solvent molecule, two oxygen atoms from each clathrochelate, and engaging in a weak cation- $\pi$  interaction with the phenyl ring of the capping boronate ester. All attempts to crystallize complexes **3.30** and **3.31** failed. The  $\text{K}^+\cdots\text{O}$  interactions distances vary between 2.692(2) - 3.065(2) Å for both **3.28** and **3.29**. Weak interactions in similar ranges were reported before.<sup>[87,88]</sup>

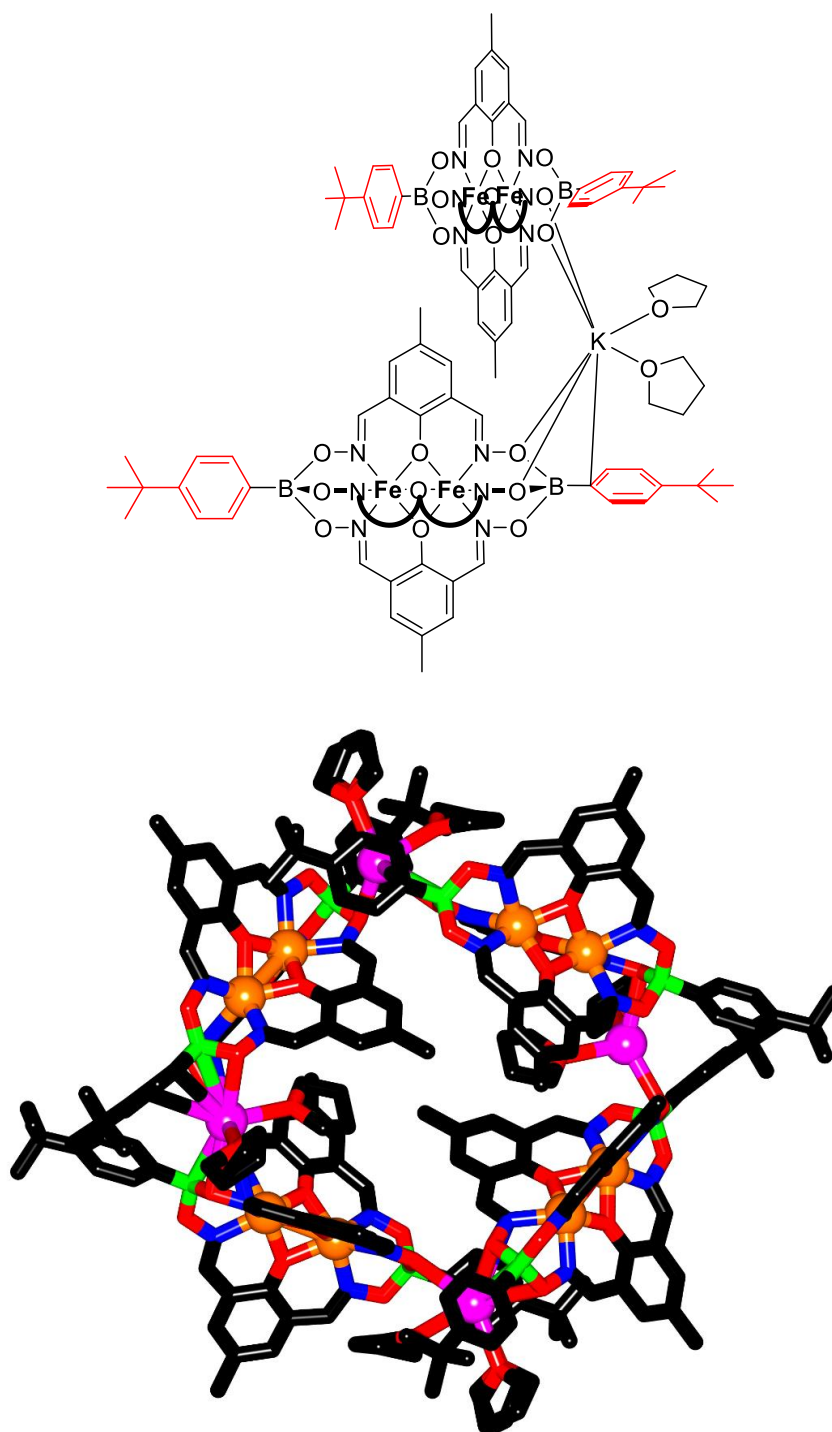


**Figure 3.7** - Molecular structure of complexes **3.28** in the crystal. Color-coding: C: black; B: green; Fe: orange; N: blue; O: red; K: (purple). Hydrogen atoms and solvent molecules have been omitted for clarity.

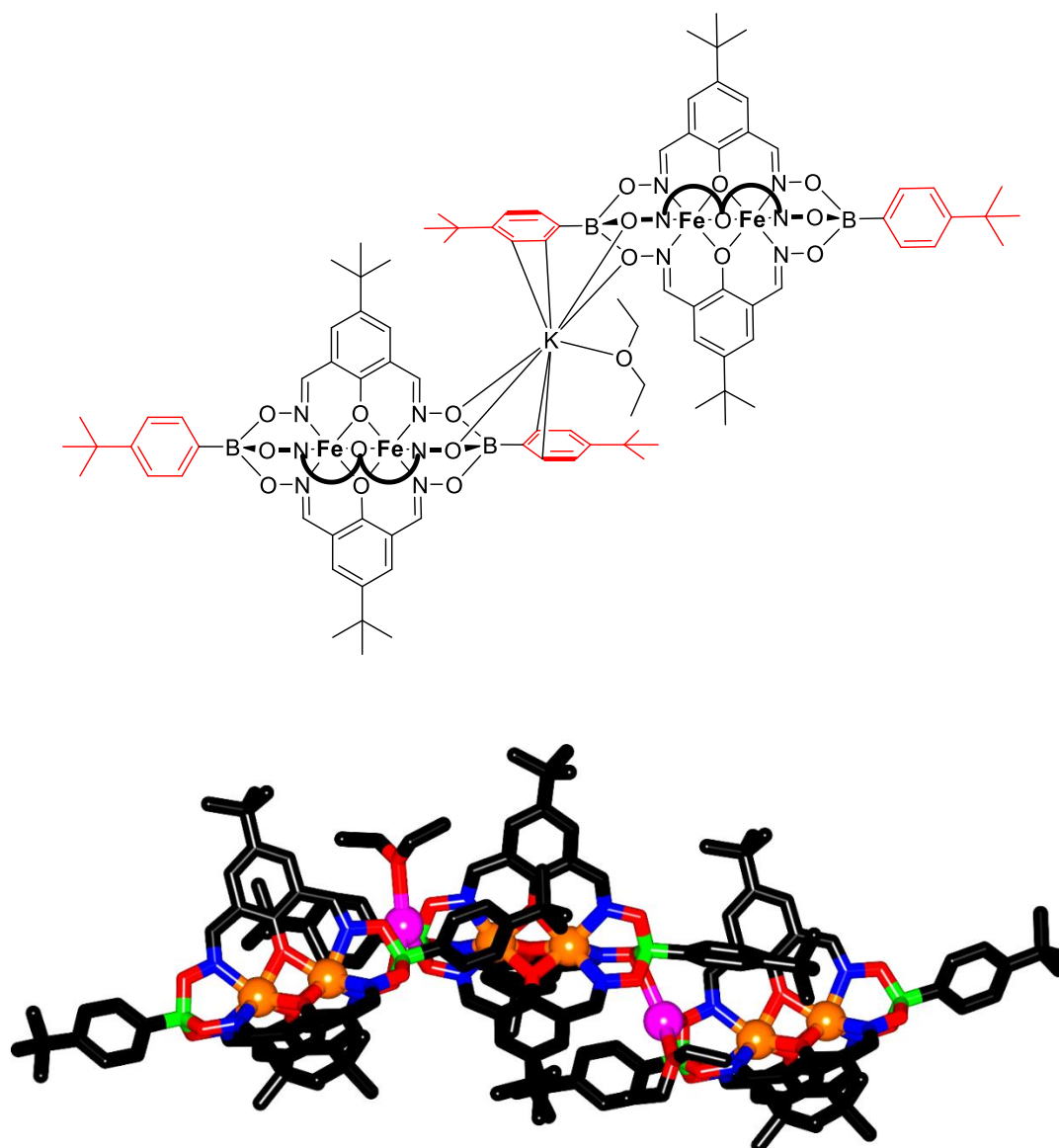


**Figure 3.8** - Molecular structure of complexes **3.29** in the crystal. Color-coding: C: black; B: green; Fe: orange; N: blue; O: red; K: (purple). Hydrogen atoms and solvent molecules have been omitted for clarity.

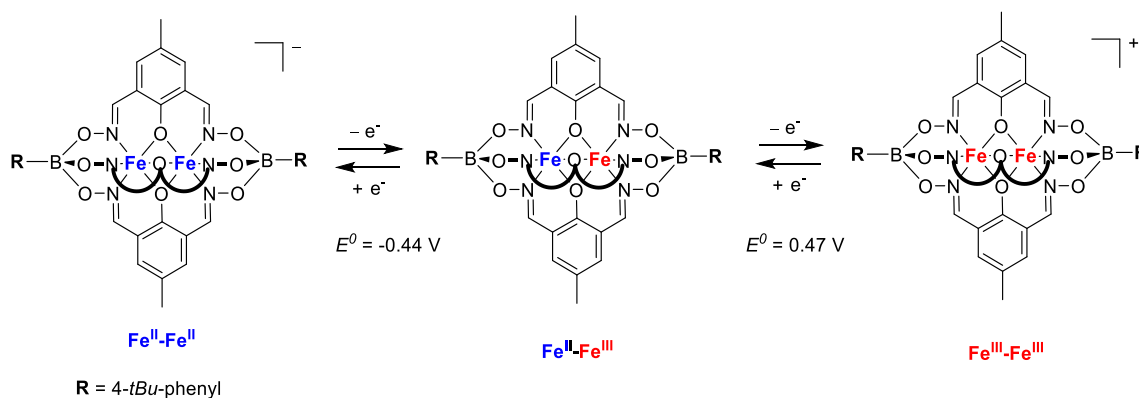
### 3.3 Clathrochelate-based redox flow batteries

As discussed in section 3.1, the RFB research field has seen several advances in the past decade. The adoption of organic chemistry has expanded the possibilities over the selection of materials. Despite all advantages offered by the employment of organic chemistry, most materials still suffer from low solubilities and low efficiencies. In addition, the cost is an important factor when considering market penetration. In fact, most of the reported organic redox-active materials do not meet the cost requirements. Therefore, the investigation of new redox-active materials is still need. Iron clathrochelate complexes are easy to synthesize and display redox activities. In addition, they can be functionalized to increase the solubility.

We hypothesized that Fe-based clathrochelate complexes could be used as redox-active material for redox flow battery applications. To test our hypothesis, clathrochelate complex **3.26** was used as the catholyte and Li metal

as the anode. Complex **3.26** was found to maintain a solubility of 10 mM in 0.1 M lithium bistriflimide (LiTFSI) co-electrolyte solution in DMF at room temperature.

*Positive electrolyte (cathode):*



*Negative electrolyte (anode):*



Preliminary results of the Li/clathrochelate cell (Figure 3.9) gave about 3.5 V and showed good stabilities after 45 cycles. The active material utilization was high (about 94%), with Coulombic efficiencies at 100%, but low current densities of 0.02 mAcm<sup>-2</sup> (Figure 3.10 and 3.11). The results show that clathrochelate complexes are promising compounds for RFBs. However, further structural variations are needed in order to increase the solubilities, which would allow to achieve higher current and energy densities.

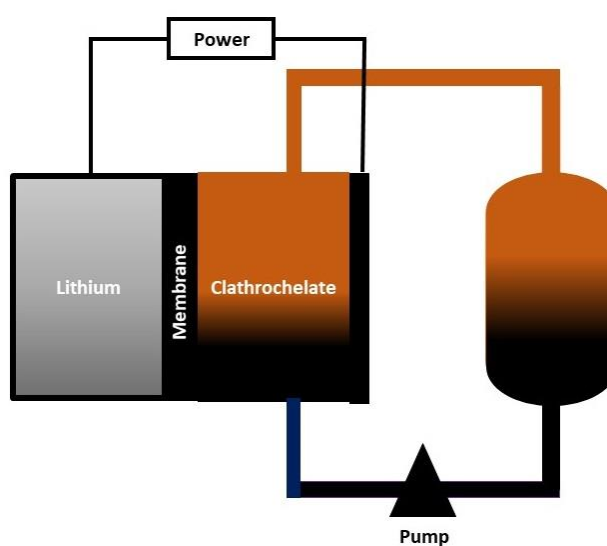


**Figure 3.9** - Schematic view of the Li/clathrochelate RFB system.

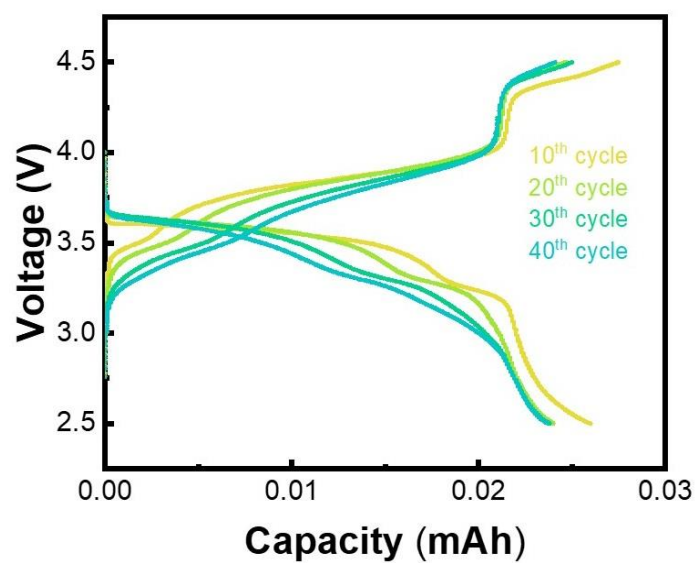


Figure 3.10 - Voltage vs capacity plot of clathrochelate/Li cell.

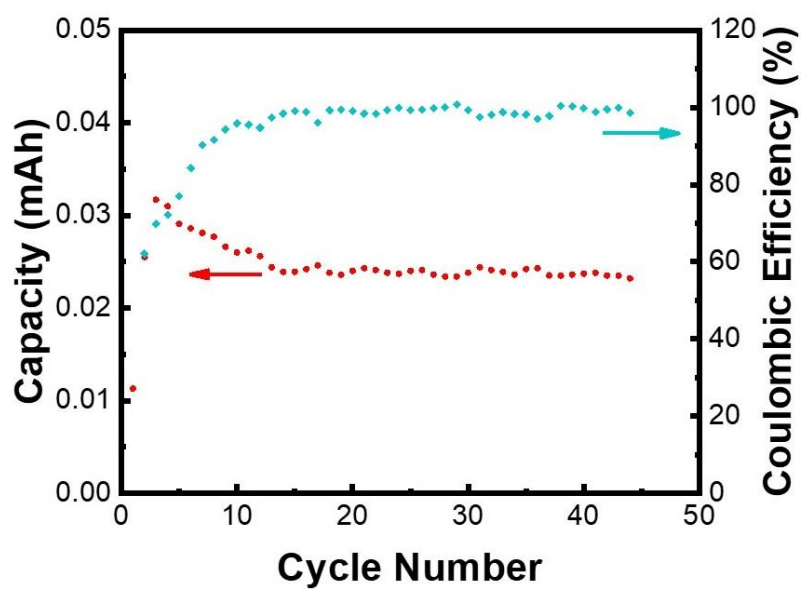


Figure 3.11 - Capacity and Coulombic efficiencies of clathrochelate/Li cell.



## Chapter 4 Porous networks based on iron clathrochelate complexes

In this chapter, we will discuss the use of Fe-based clathrochelate complexes as monomers for the preparation of porous networks. Part of this work was published in “Porous networks based on iron (ii) clathrochelate complexes”, José L. Bila, Joffrey Pijeat, Andrea Ramorini, Farzaneh Fadaei-Tirani, Rosario Scopelliti, Emilie Baudat and Kay Severin, *Dalton Transactions*, **2019**, 48, 4582-4588; and “Homo- and Heterodinuclear Iron Clathrochelate Complexes with Functional Groups in the Ligand Periphery”, José L. Bila, Mathieu Marmier, Konstantin O. Zhurov, Rosario Scopelliti, Ivica Živković, Henrik M. Rønnow, Elahi S. Noore, Andrzej Sienkiewicz, Cornel Fink, and Kay Severin, *European Journal of Inorganic Chemistry*, **2018**, 3118-3125.

### 4.1 Introduction

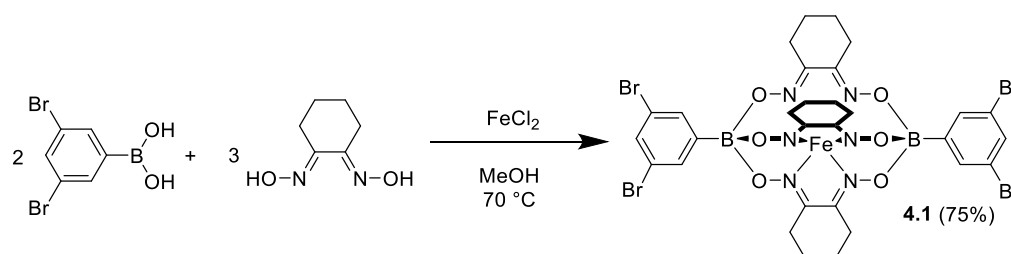
The use of rigid polyfunctional monomers in metal-catalyzed carbon-carbon coupling reactions can give rise to a vast range of microporous polymers known as porous aromatic frameworks (PAFs) or conjugated microporous polymers (CMPs).<sup>[89–93]</sup> Several types of coupling reactions have been employed for this purpose including Yamamoto coupling of polybrominated monomers, the Pd<sup>II</sup>/Cu<sup>I</sup>-catalyzed homo-coupling of polyethynylbenzenes, the Suzuki-Miyaura cross-coupling of polyhalogenated compounds with polyarylboronic acids, and the Sonogashira-Hagihara cross-coupling of polyhalogenated compounds with monomers featuring two or more terminal alkyne groups. PAFs and CMPs are non-crystalline, hence bearing a disadvantage over other materials with permanent porosity such as porous molecular crystals, covalent organic frameworks (COFs) or metal-organic frameworks (MOFs).<sup>[94,95,104,105,96–103]</sup> However, PAFs and CMPs present higher chemical and thermal stability, which is necessary for various applications.

The nature of the polyfunctional monomers defines the properties of the resulting polymer. Although most studies in this area have focused on organic monomers, the utilization of inorganic monomers represents an interesting alternative. A prerequisite of using inorganic monomers for the synthesis of PAFs or CMPs is their stability under polymerization conditions. It is worth noting that transition metal-catalyzed C-C coupling reaction are often performed under rather harsh reaction conditions.<sup>[102]</sup> In addition, the synthesis of functional inorganic monomers can be challenging, costly and time-consuming.

In this chapter, we discuss the use of Fe-based clathrochelate complexes as polyfunctionalized monomers for porous materials.

## 4.2 Clathrochelate complexes as building blocks for porous networks

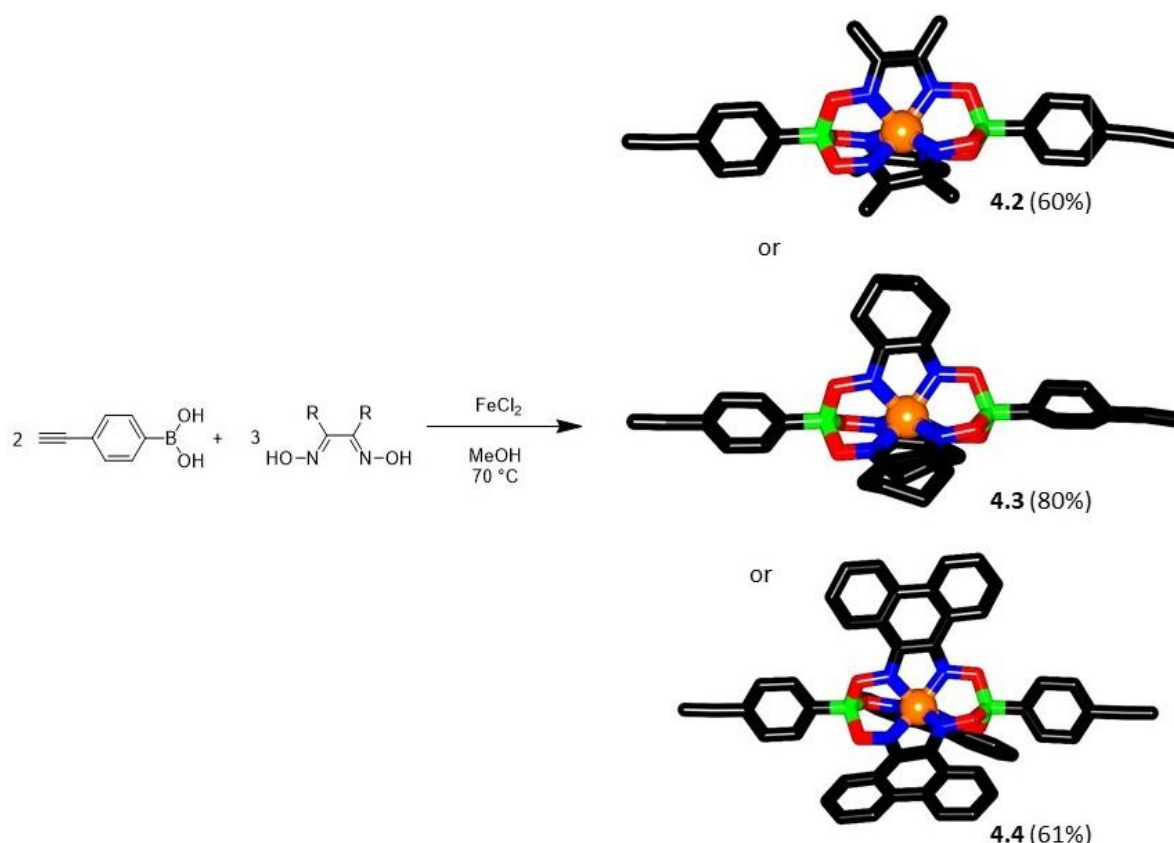
As mentioned in chapter 1, clathrochelate complexes can be prepared by a one-pot reaction from commercially available materials. They can be easily functionalized and display high stability under harsh metal-catalyzed reactions.<sup>[4]</sup> Hence, clathrochelates appear to be excellent building blocks for porous networks. To test this hypothesis, we have synthesized complexes **4.1** – **4.5** as monomers for metal-catalyzed reactions (Scheme 4.1 – 4.3). Combining (3,5-dibromophenyl)boronic acid, nioxime, and iron chloride results in clathrochelates with bromo substituents arranged in a divergent fashion<sup>[30,31,39]</sup> (scheme 4.1). Suzuki-Miyaura-type cross-coupling reactions are possible, as evidenced by the successful coupling of **4.1** with pyridylboronic acid.<sup>[31,41]</sup>



**Scheme 4.1** - Synthesis of the clathrochelate complexes **4.1**.

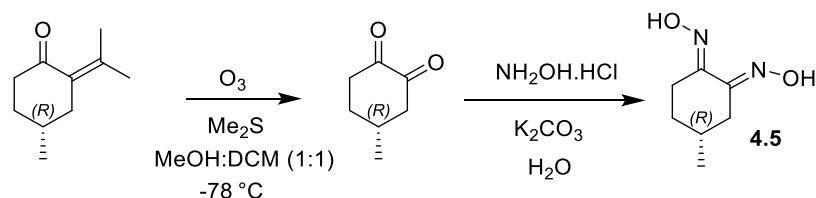
Sonogashira-Hagihara polycross-coupling reactions are also frequently employed in materials science.<sup>[10,94,98]</sup> In order to examine if this coupling chemistry is compatible with clathrochelate complexes, we have synthesized the monomers **4.2**, **4.3** and **4.4** featuring terminal alkyne functions in 60%, 80% and 76% yields respectively. The complexes **4.2** and **4.4** were characterized by X-ray crystallography (Scheme 4.2).





**Scheme 4.2** - Synthesis of the clathrocholate complexes **4.2**, **4.3** and **4.4**. The graphic representations of the structures of **4.2** – **4.4** are based on crystallographic analyses. Color coding: C (black), Fe (orange), N (blue), O (red), and B (green). Hydrogens are not shown for clarity.

One interesting feature of clathrocholate complexes is the fact that the lateral side chains can easily be varied by using a different dioxime during the synthesis. We wanted to explore if we could use a dioxime with a stereogenic center in order to prepare chiral clathrocholate complexes. The latter could then be used for the synthesis of chiral networks. (R)-Pulegone is a commercially available compound, which can be converted into the corresponding diketone by ozonolysis.<sup>[106,107]</sup> Subsequent reaction with hydroxylamine hydrochloride in water gave the dioxime **4.5** in 64% yield (Scheme 4.3).

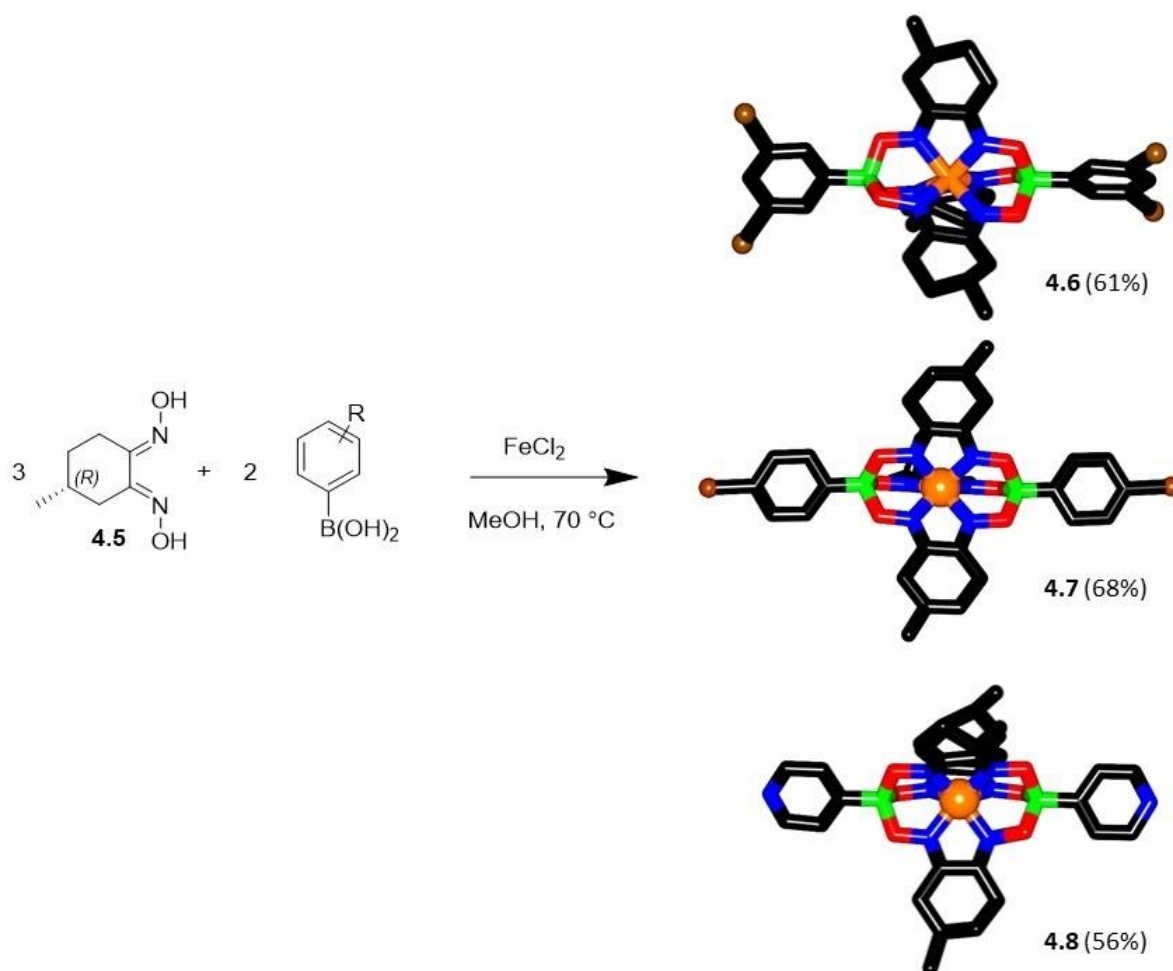


**Scheme 4.3** - Synthesis of dioxime **4.5**.

The reaction between **4.5**,  $\text{FeCl}_2$ , and functionalized phenylboronic acids in MeOH at  $70^\circ\text{C}$  under  $\text{N}_2$  atmosphere provided the chiral clathrochelates **4.6** to **4.8** in high yields up to 80%.

Complexes **4.6** to **4.8** were obtained as a mixture of two isomers, which differ by the relative orientation of the chiral methyl groups with respect to the  $\text{B}\cdots\text{Fe}\cdots\text{B}$  axis.<sup>[12]</sup> These isomers cannot be distinguished by NMR spectroscopy, but they co-crystallize, and one can observe disorder for the position of the

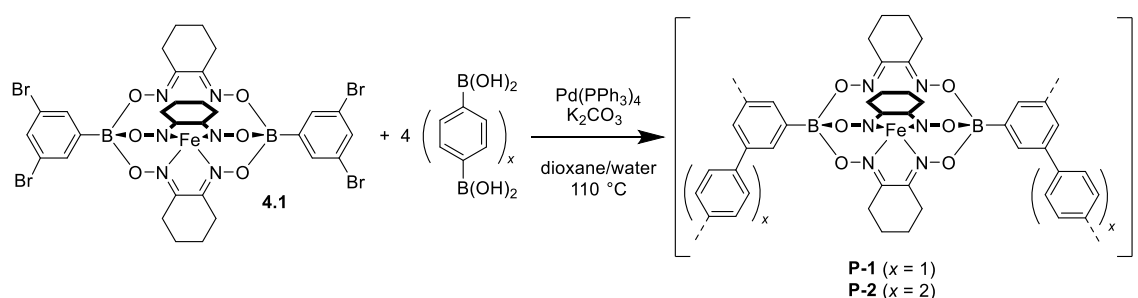
methyl groups on the dioximato ligand. TLC tests revealed very similar  $R_f$  values for the two isomers, and a chromatographic separation was not attempted.



**Scheme 4.4** - Synthesis of the clathrocholate complexes **4.6**, **4.7** and **4.8**. The graphic representations of the structures of **4.6** – **4.8** are based on crystallographic analyses. Color coding: C (black), Fe (orange), N (blue), O (red), Br (brown) and B (green). Hydrogens are not shown for clarity.

### 4.3 Porous networks based on mononuclear iron clathrocholate complexes

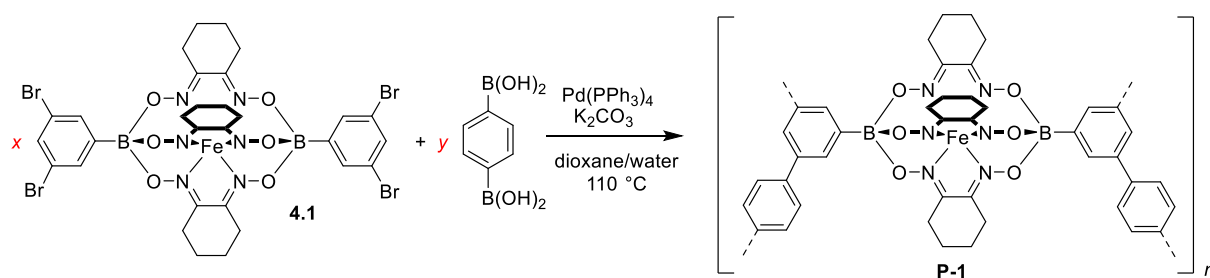
In order to prepare polymeric networks, we have investigated polycross-coupling reactions of **4.1** with 1,4-benzenediboronic acid or 4,4'-biphenyldiboronic acid, respectively.



**Scheme 4.5** - Synthesis of the clathrocholate networks **P-1** and **P-2**.

We prepared the porous clathrochelate polymers **P-1** and **P-2** by heating the reaction mixtures at 110 °C for 24 h (Scheme 4.6). As catalyst precursor, we have employed  $\text{Pd}(\text{PPh}_3)_4$  (7.5 mol% with respect to the boronic acid) in combination with  $\text{K}_2\text{CO}_3$  as base. The covalent linkage of the clathrochelates via phenylene and diphenylene spacers is expected to give large macrocyclic structures if fully connected 2D networks are formed. However, the formation of 3-dimensional network structures is conceivable as well.

It is worth noting that the reaction conditions depicted in Scheme 4.5 were optimized using the porosity of the final polymer as main criteria. First, the ratio between clathrochelate **4.1** (**x**) and 1,4-benzene diboronic acid (**y**) was varied. The apparent BET surface areas were determined by 11 point  $\text{N}_2$  isotherms at 77 K, and the resulting values are reported in Table 4.1. A molar ratio of 4:1 between the diboronic acid and the brominated clathrochelate was found to give polymers with the highest porosity. Most likely, the excess of boronic acid is needed to compensate for protodeboronation reactions.<sup>[108,109]</sup>



**Scheme 4.6** - Synthesis of **P-1** using different ratios of starting materials.

**Table 4.1** - Influence of the ratio of the starting materials on the porosity of the final polymer.

	<b>A</b>	<b>B</b>	<b>C</b>	<b>D</b>	<b>E</b>
<b>x</b>	1	1	1	1	1
<b>y</b>	1	2	3	4	5
<b>SA<sub>BET</sub> [m<sup>2</sup> g<sup>-1</sup>]</b>	28	126	481	550	432

Subsequently, we have examined the influence of the base (Table 4.2) and the solvent (Table 4.3). The utilization of dioxane/water (6:1) as solvent and  $\text{K}_2\text{CO}_3$  as base was found to be advantageous giving higher BET surface areas.

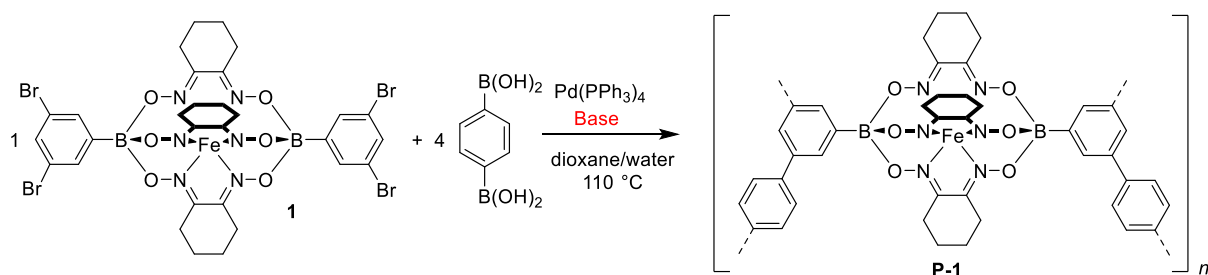

 Scheme 4.7 - Synthesis of **P-1** with different bases.

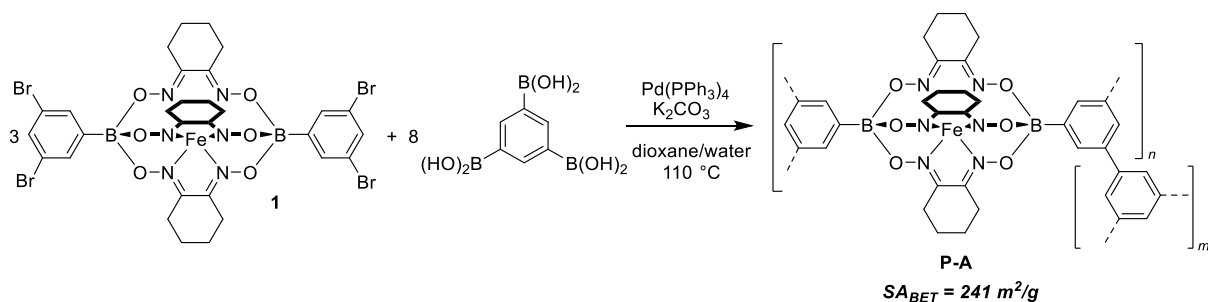
Table 4.2 - Influence of the base on the porosity of the final polymer.

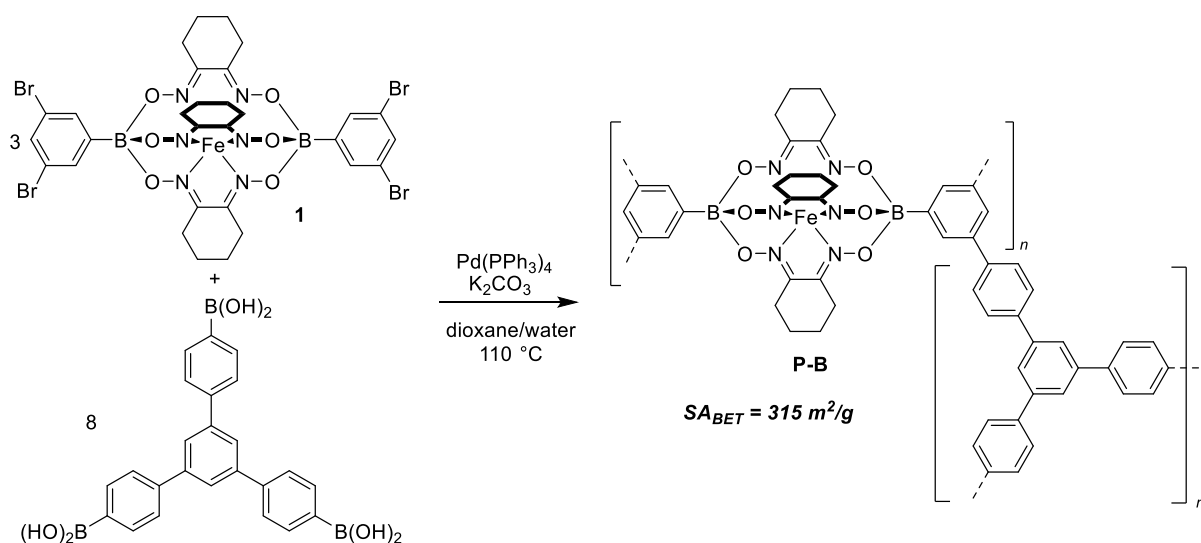
	A	B	C	D
<b>Base</b>	K <sub>2</sub> CO <sub>3</sub>	Na <sub>2</sub> CO <sub>3</sub>	CS <sub>2</sub> CO <sub>3</sub>	KOtBu
<b>SA<sub>BET</sub> [m<sup>2</sup> g<sup>-1</sup>]</b>	550	461	5	7

Table 4.3 - Influence of the solvent on the porosity of the final polymer.

	A	B	C	D
<b>Solvent</b>	Dioxane:H <sub>2</sub> O (6:1)	THF:H <sub>2</sub> O (6:1)	DMF:H <sub>2</sub> O (6:1)	DMF:THF:H <sub>2</sub> O (3:3:1)
<b>SA<sub>BET</sub> [m<sup>2</sup> g<sup>-1</sup>]</b>	550	381	501	456

The optimized reactions conditions were used to perform polycross-coupling reactions between clathrocholate **4.1** and triboronic acids. The resulting polymers **P-A** and **P-B** did show a lower apparent surface area compared to the polymers based on diboronic acids (**P-1** and **P-2**), and more detailed investigations were not undertaken.


 Scheme 4.8 - Synthesis of polymer **P-A**.

Scheme 4.9 - Synthesis of polymer **P-B**.

The  $\text{N}_2$  physisorption measurements of **P-1** and **P-2** were performed at 77 K and the pore size distribution was calculated from nonlocal density functional theory (Figure 4.1 and Table 4.4). The sorption measurements revealed an apparent Brunauer-Emmett-Teller (BET) surface area of  $SA_{\text{BET}} = 550 \text{ m}^2 \text{ g}^{-1}$  for **P-1**. The BET surface of **P-2** is only slightly higher ( $593 \text{ m}^2 \text{ g}^{-1}$ ), despite the fact that clathrochelates are connected by significantly longer diphenylene spacers. The micropores of both polymers have a diameter of around 1.4 nm.  $\text{CO}_2$ , and  $\text{H}_2$  uptakes were measured up to 1 bar at 273 K and 77 K, respectively. The corresponding values ( $\text{CO}_2$ :  $58 \text{ cm}^3 \text{ g}^{-1}$  (**P-1**),  $48 \text{ cm}^3 \text{ g}^{-1}$  (**P-2**);  $\text{H}_2$ :  $101 \text{ cm}^3 \text{ g}^{-1}$  (**P-1**),  $90 \text{ cm}^3 \text{ g}^{-1}$  (**P-2**)) are within the expected range for microporous polymers of the given porosity (Figure 4.1).

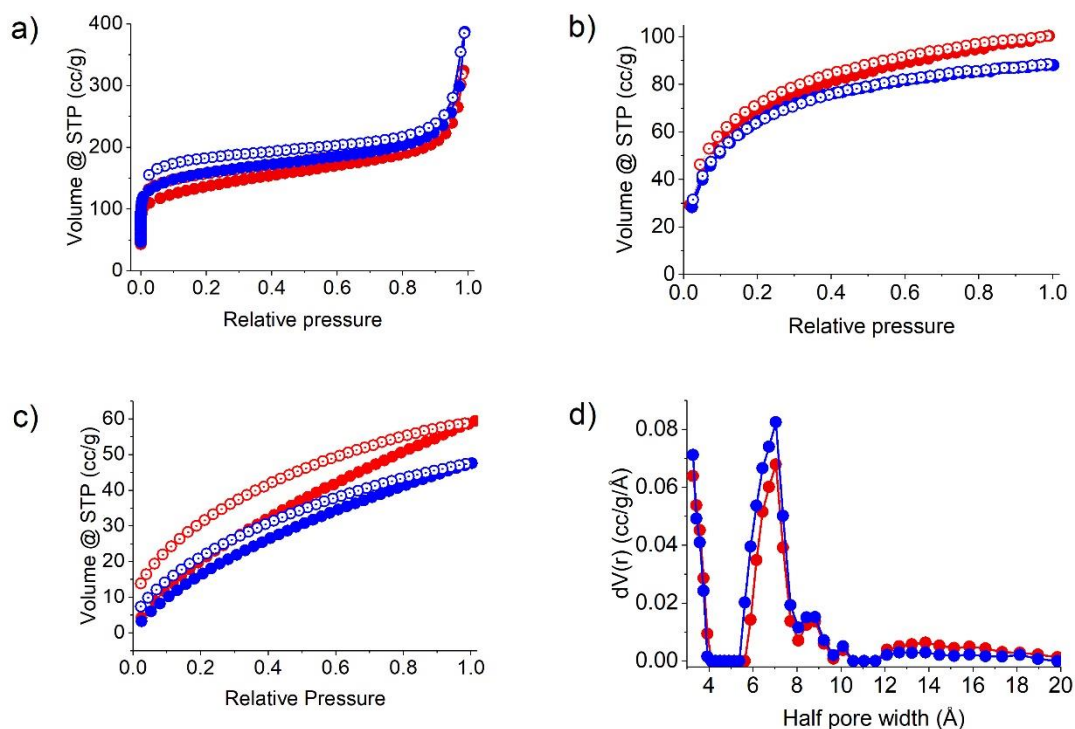


**Figure 4.1** - Characterization of **P-1** (red symbols) and **P-2** (blue symbols) by sorption measurements and SEM. a) N<sub>2</sub> adsorption (filled symbols) and desorption (open symbols) isotherms at 77 K; b) H<sub>2</sub> adsorption (filled symbols) and desorption (open symbols) isotherms at 77 K; c) CO<sub>2</sub> adsorption (filled symbols) and desorption (open symbols) isotherms at 273 K and d) Pore size distribution.

**Table 4.4** - Results of N<sub>2</sub> sorption measurements at 77 K of **P-1** (P-Po<sup>-1</sup> range: 0.08-0.15) and **P-2** (P-Po<sup>-1</sup> range: 0.10-0.21).

polymer	$SA_{\text{BET}}$ [m <sup>2</sup> g <sup>-1</sup> ]	$SA_{\text{Lang}}$ [m <sup>2</sup> g <sup>-1</sup> ]	pore vol. [cm <sup>3</sup> g <sup>-1</sup> ]	av. pore diam. [nm]
<b>P-1</b>	550	691	0.38	1.40
<b>P-2</b>	593	670	0.25	1.39

**P-1** and **P-2** were analyzed by scanning electron microscopy (SEM) and energy-dispersive X-ray (EDX) spectroscopy. EDX revealed only minor amounts of residual bromine (~1.15% of the initial amount), indicating efficient conversion of the bromo functions during the cross-coupling process. We were also able to detect Pd, the concentration of which varied depending on the precise location of the measurement on the polymer sample (0.31–0.47 Pd per Fe). Most likely, Pd nanoparticles are formed from the catalyst precursor Pd(PPh<sub>3</sub>)<sub>4</sub> during the polymerization process. The presence of Pd has been observed for other polymers, which were obtained by Suzuki-Miyaura polycross-coupling reactions.<sup>[110]</sup> The SEM image of **P-1** (Figure 4.2) shows agglomerates of irregular spherical nanoparticles, which are typical for porous cross-linked polymers.

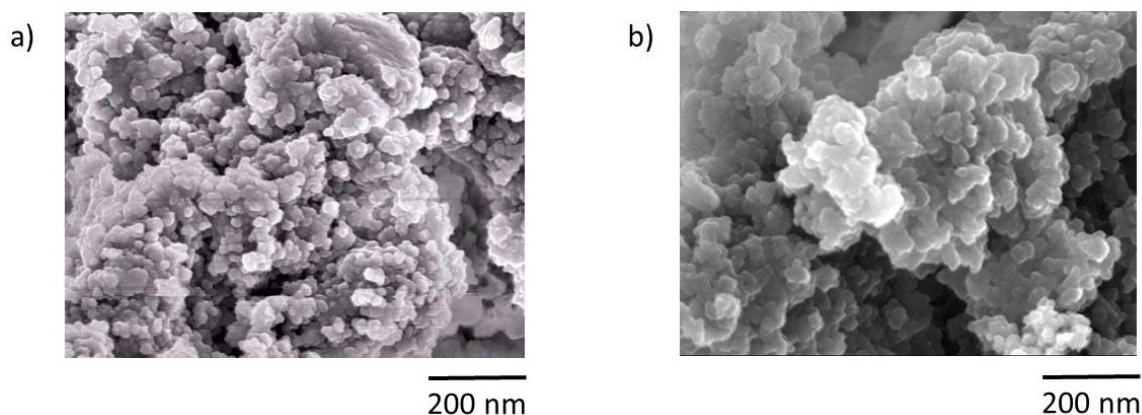
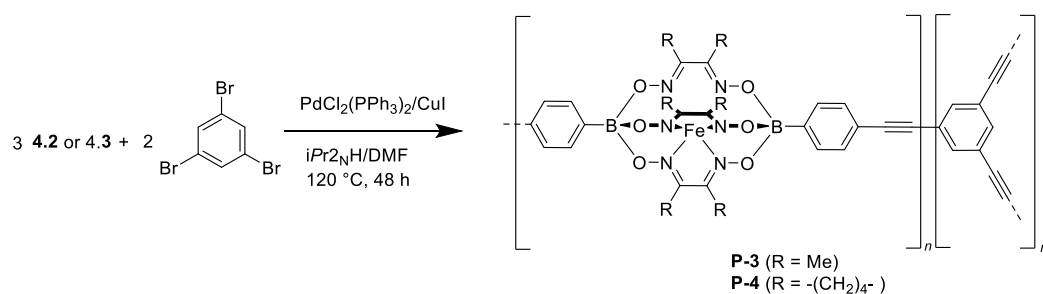


Figure 4.2 - SEM images of (a) **P-1** and (b) **P-2**.

Next we explored the cross-coupling reaction of clathrochelate complexes **4.2** and **4.3** by Pd-catalyzed reactions with 1,3,5-tribromobenzene (Scheme 4.4). As catalyst precursor, we used  $\text{PdCl}_2(\text{PPh}_3)_2$  (3.5 mol% with respect to the **4.2/4.3**) and CuI, and the reactions were carried out at 120 °C for 48 h in DMF/*i*Pr<sub>2</sub>NH (1:1).



Scheme 4.10 - Synthesis of the clathrochelate networks **P-3** and **P-4**.

The polymers **P-3** and **P-4** were characterized by the same analytical techniques used for **P-1** and **P-2**. N<sub>2</sub> sorption measurements at 77 K gave apparent BET surface areas of 205 and 360 m<sup>2</sup> g<sup>-1</sup>, respectively (Table 4.5). The micropores of both polymers have a diameter of around 1.3 nm. CO<sub>2</sub>, and H<sub>2</sub> uptakes were measured up to 1 bar at 273 K and 77 K, respectively. The corresponding values (CO<sub>2</sub>: 58 cm<sup>3</sup> g<sup>-1</sup> for **P-3**, 48 cm<sup>3</sup> g<sup>-1</sup> for **P-4**; H<sub>2</sub>: 101 cm<sup>3</sup> g<sup>-1</sup> for **P-3**, 90 cm<sup>3</sup> g<sup>-1</sup> for **P-4**) (Figure 4.3).

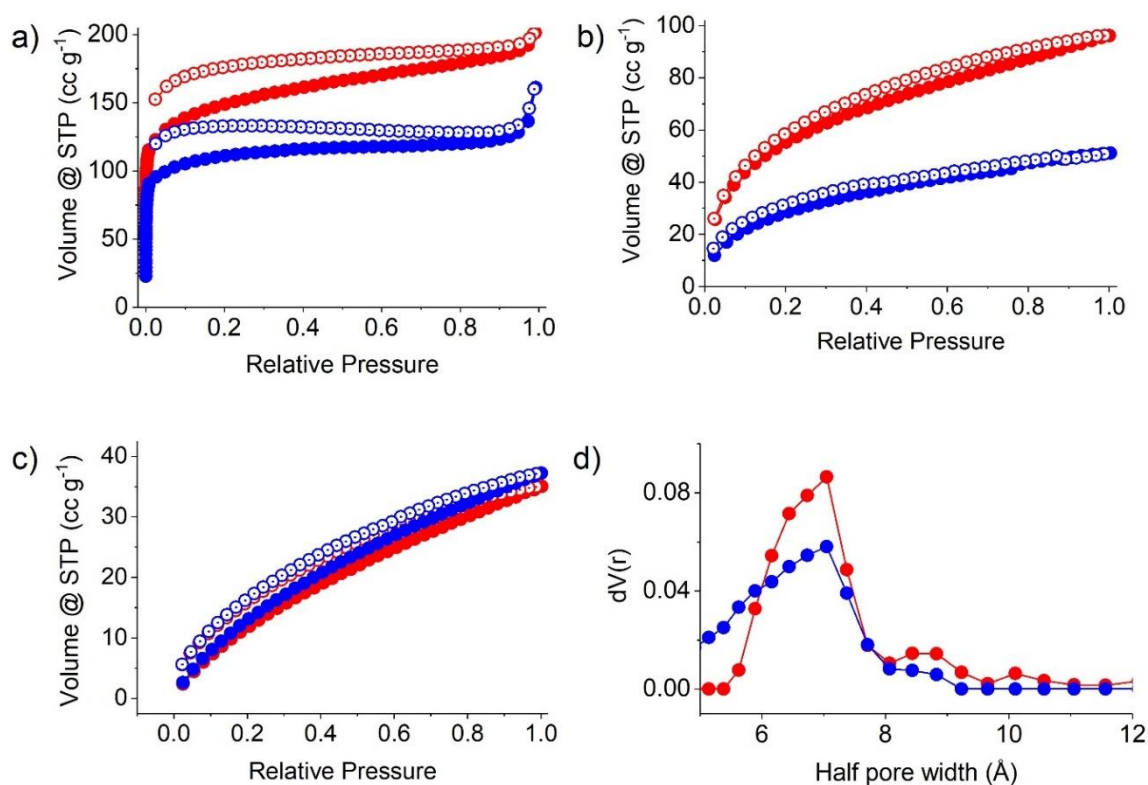


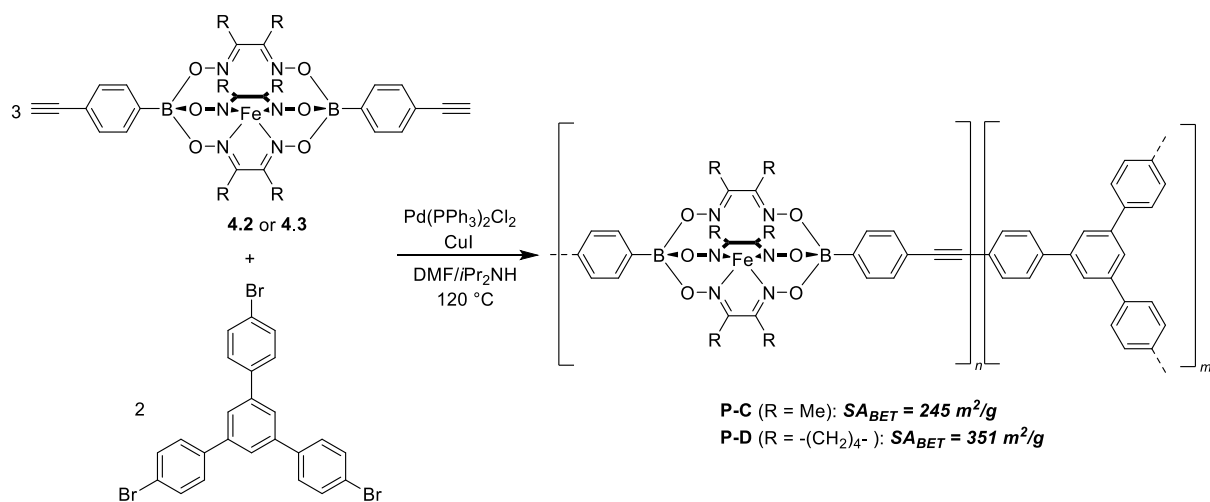
**Figure 4.3** - Characterization of **P-3** (red symbols) and **P-4** (blue symbols) by sorption measurements and SEM. a) N<sub>2</sub> adsorption (filled symbols) and desorption (open symbols) isotherms at 77 K; b) H<sub>2</sub> adsorption (filled symbols) and desorption (open symbols) isotherms at 77 K; c) CO<sub>2</sub> adsorption (filled symbols) and desorption (open symbols) isotherms at 273 K and d) Pore size distribution.

**Table 4.5** - Results of N<sub>2</sub> sorption measurements at 77 K of **P-3** (P-Po<sup>-1</sup> range: 0.05-0.09) and **P-4** (P-Po<sup>-1</sup> range: 0.05-0.09).

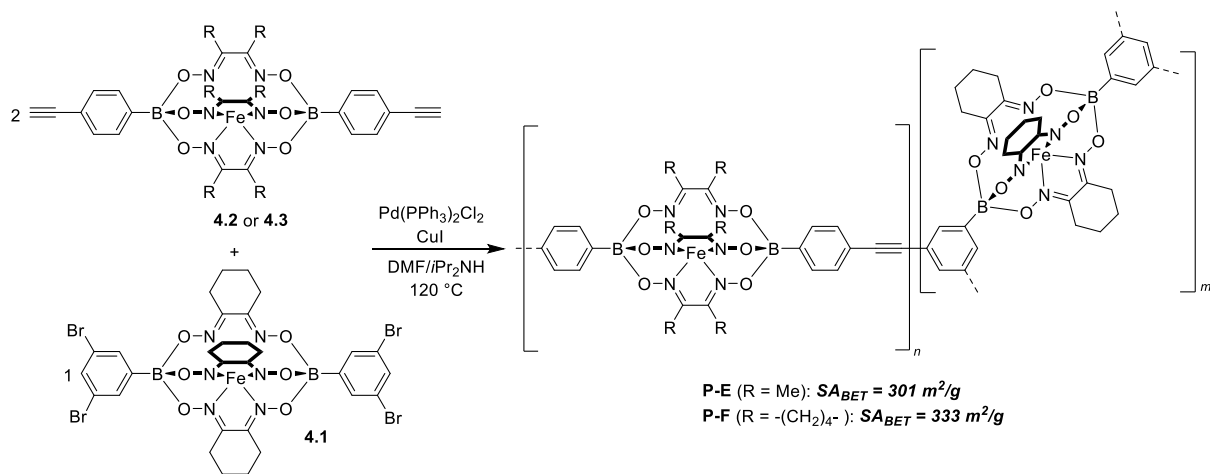
polymer	$S_{\text{BET}}$ [m <sup>2</sup> g <sup>-1</sup> ]	$S_{\text{Lang}}$ [m <sup>2</sup> g <sup>-1</sup> ]	pore vol. [cm <sup>3</sup> g <sup>-1</sup> ]	av. pore diam. [nm]
<b>P-3</b>	235	318	0.30	1.35
<b>P-4</b>	360	525	0.28	1.33

The reaction conditions for the synthesis of **P-3** and **P-4** were used to perform polycross-coupling of clathrocholate **4.2** or **4.3** with 1,3,5-tris (4-bromophenyl) benzene or the bromo substituted clathrocholate **4.1**. The resulting polymers did not show a significant change in apparent *BET* surface areas compared to **P-3** and **P-4**. Hence further investigations were not performed.





Scheme 4.11 - Synthesis of the polymers P-C and P-D.



Scheme 4.12 - Synthesis of the polymers P-E and P-F.

The SEM image of **P-1** (Figure 4.4) shows agglomerates of irregular spherical nanoparticles similar to **P-1** and **P-2**.

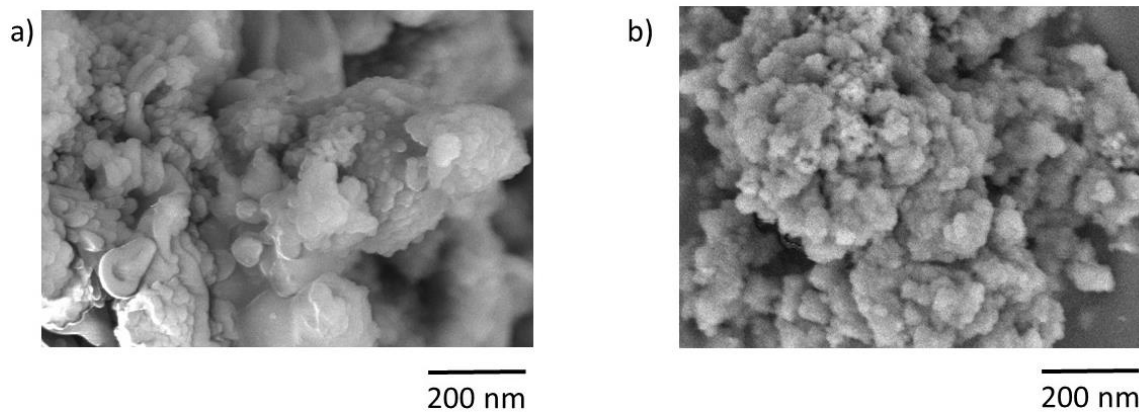
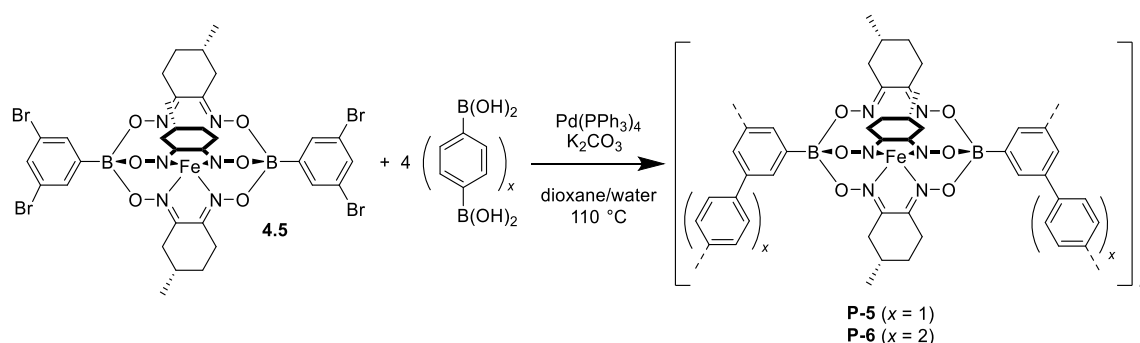


Figure 4.4 - SEM images of (a) P-3 (b) P-4.

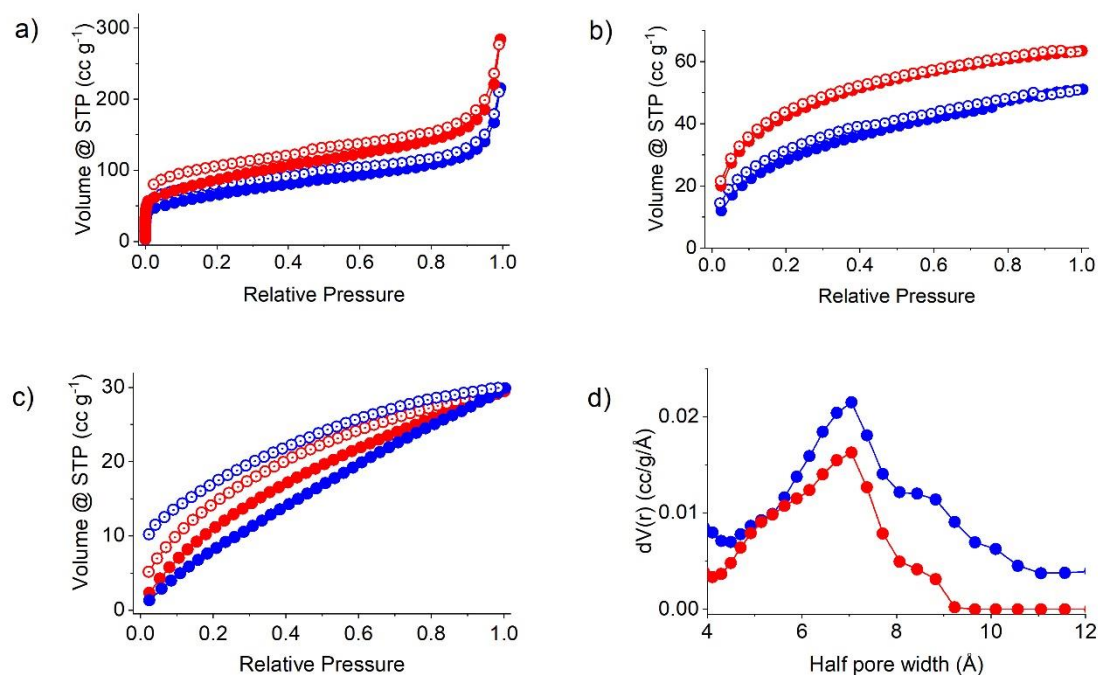
Homochiral materials with permanent porosity and high thermal stabilities are of interest for applications in enantiomeric separation and catalysis.<sup>[110–115]</sup> Therefore, complex **4.5** was used for polycross-coupling reactions with 1,4-benzenediboronic acid or 4,4'-biphenyldiboronic acid, respectively (Scheme 4.13) to yield the chiral polymers **P-5** and **P-6**. The reaction conditions were analogous to what was used for the networks **P-1** and **P-2**.



**Scheme 4.13** - Synthesis of the clathrochelate networks **P-5** and **P-6**.

Sorption measurements for the homochiral networks **P-5** and **P-6** gave apparent BET surface areas of 548 and 417 m<sup>2</sup> g<sup>-1</sup> respectively (Table 4.6). H<sub>2</sub> and CO<sub>2</sub> uptakes gave the corresponding values CO<sub>2</sub>: 30 cm<sup>3</sup> g<sup>-1</sup> for **P-4**, 29 cm<sup>3</sup> g<sup>-1</sup> for **P-5**; H<sub>2</sub>: 60 cm<sup>3</sup> g<sup>-1</sup> for **P-4**, 48 cm<sup>3</sup> g<sup>-1</sup> for **P-5** (Figure 4.5).

As in the case of **P-1** and **P-2**, the polymers are thermally robust and not susceptible to hydrolytic degradation.

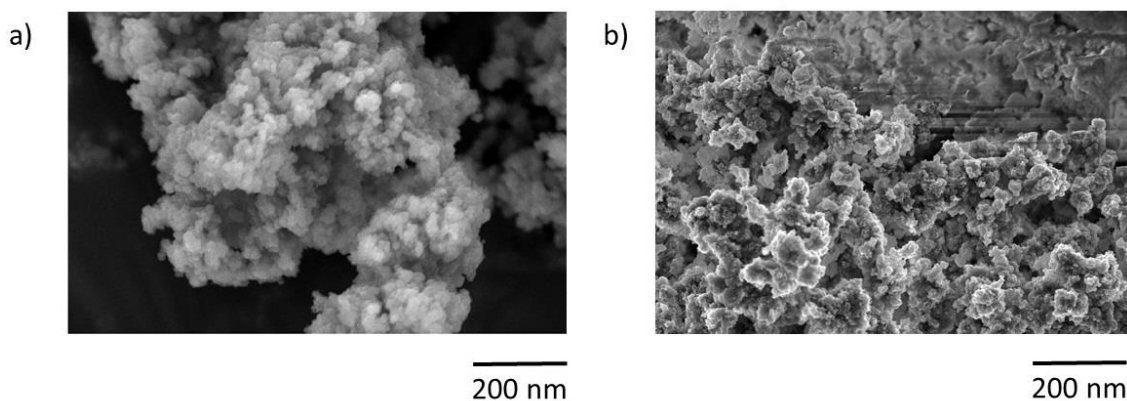


**Figure 4.5** - Characterization of **P-5** (red symbols) and **P-6** (blue symbols) by sorption measurements and SEM. a) N<sub>2</sub> adsorption (filled symbols) and desorption (open symbols) isotherms at 77 K; b) H<sub>2</sub> adsorption (filled symbols) and desorption (open symbols) isotherms at 77 K; c) CO<sub>2</sub> adsorption (filled symbols) and desorption (open symbols) isotherms at 273 K and d) Pore size distribution.

**Table 4.6** - Results of N<sub>2</sub> sorption measurements at 77 K of **P-5** (P<sub>Po</sub><sup>-1</sup> range: 0.06-0.10) and **P-6** (P<sub>Po</sub><sup>-1</sup> range: 0.05-0.09).

polymer	$SA_{\text{BET}}$ [m <sup>2</sup> g <sup>-1</sup> ]	$SA_{\text{Lang}}$ [m <sup>2</sup> g <sup>-1</sup> ]	<i>pore vol.</i> [cm <sup>3</sup> g <sup>-1</sup> ]	<i>av. pore diam.</i> [nm]
<b>P-5</b>	548	634	0.24	1.38
<b>P-6</b>	417	493	0.31	1.41

The SEM image of **P-5** and **P-6** (Figure 4.6) shows agglomerates of irregular spherical nanoparticles similar to **P-1** and **P-2**.

**Figure 4.6** - SEM images of (a) **P-4** and (b) **P-5**.

All mononuclear iron clathrochelate complexes are chemically and physically very stable. Accordingly, we expected a high stability for the networks **P-1** to **P-6**. Indeed, TGA measurements revealed a good thermal stability, with decomposition occurring between 250 and 300 °C (Figure 4.7). Heating suspensions of **P-1** in water at 80 °C for 6 h resulted in no significant loss of porosity.

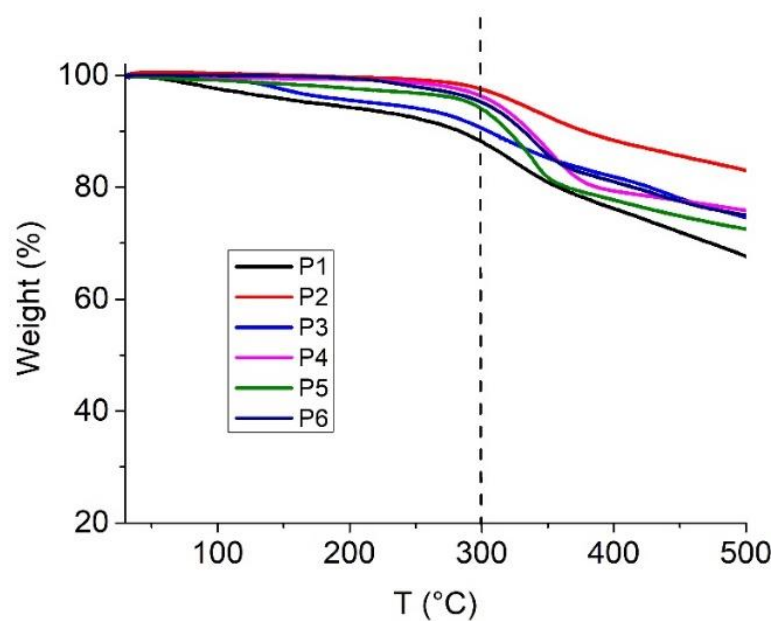


**Figure 4.7** - Thermogravimetric analysis of **P-1** to **P-6** under  $N_2$  atmosphere with  $20\text{ mL min}^{-1}$  flowrate and  $10\text{ }^\circ\text{C min}^{-1}$ .

The structural integrity of polymers **P-1** to **P-6** was verified by CP-MAS  $^{13}\text{C}$  NMR (Figure 4.8 to 4.13). The broad chemical shifts appearing in the region between 120 and 160 ppm belong to the aromatic carbons and the peaks located between 10 and 40 ppm can be attributed to the aliphatic carbons of the networks.

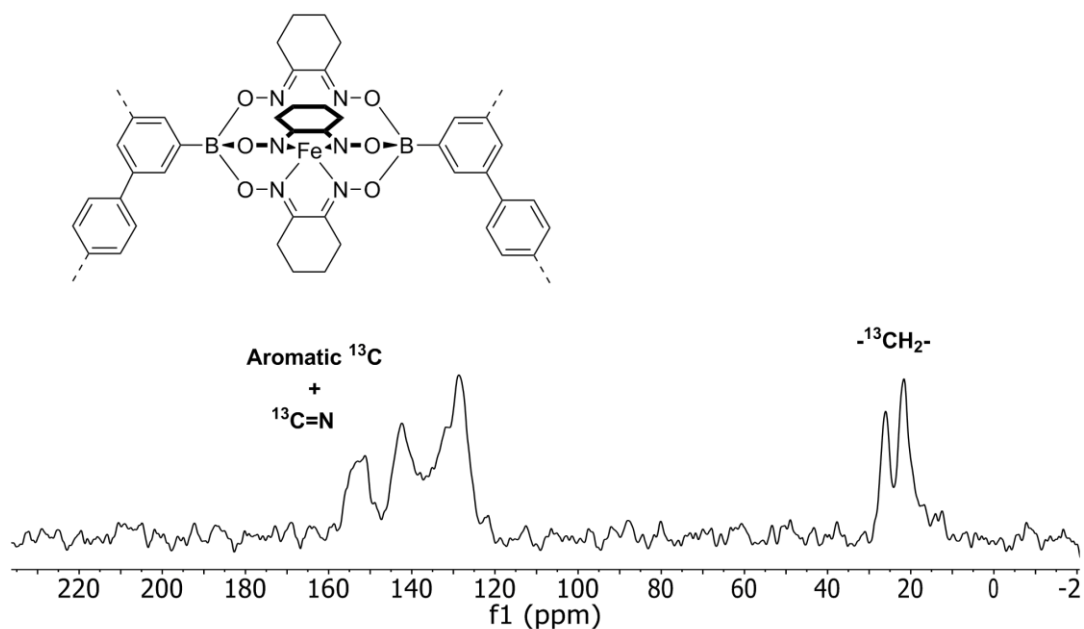


**Figure 4.8** -  $^{13}\text{C}$  Solid-state MAS NMR of **P-1**.

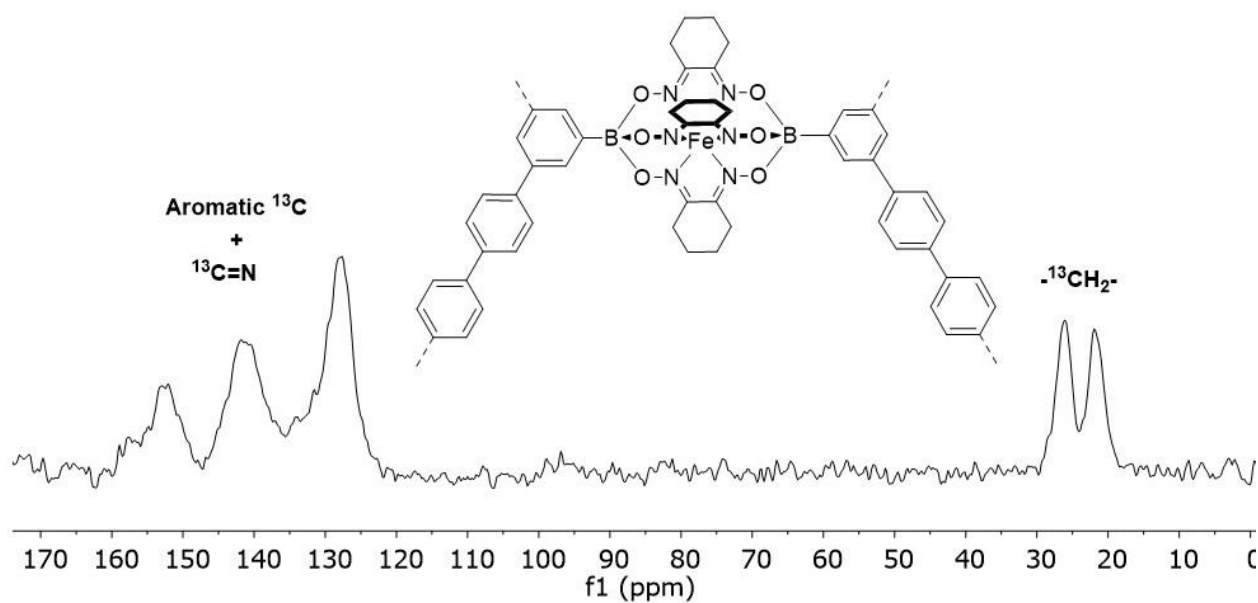


Figure 4.9 -  $^{13}\text{C}$  Solid-state MAS NMR of P-2.

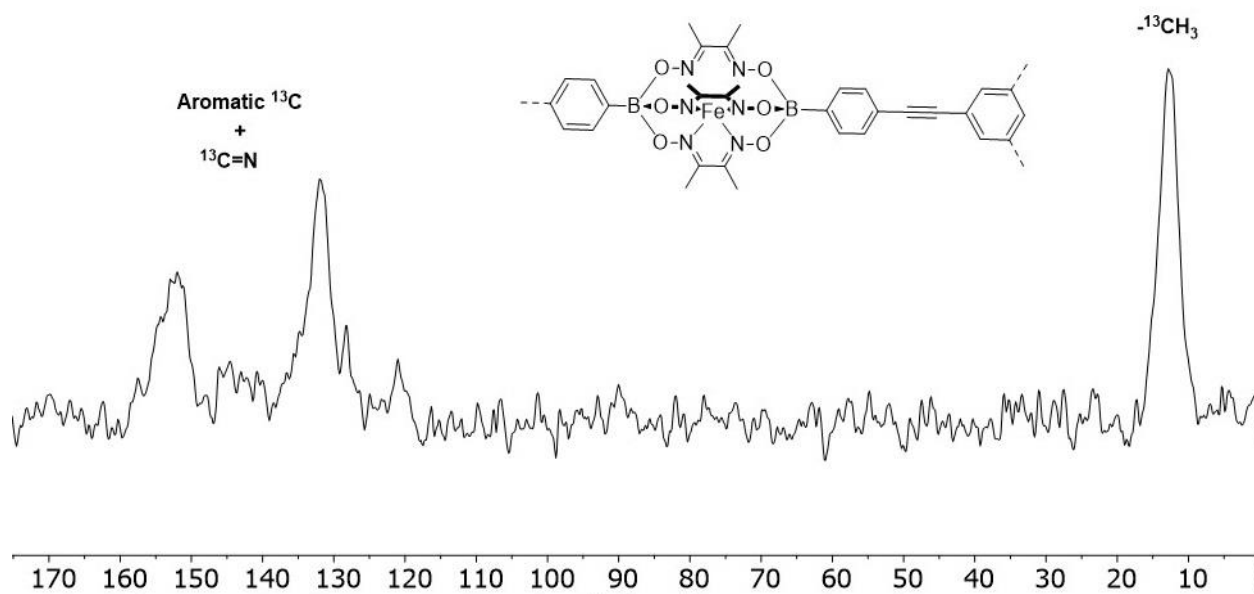
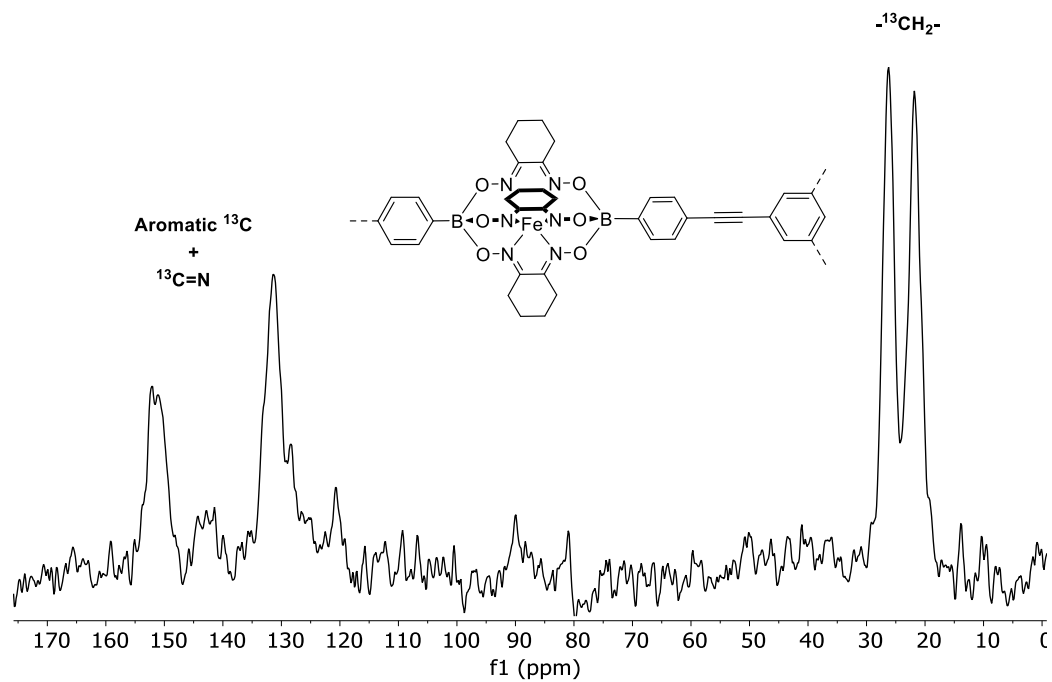
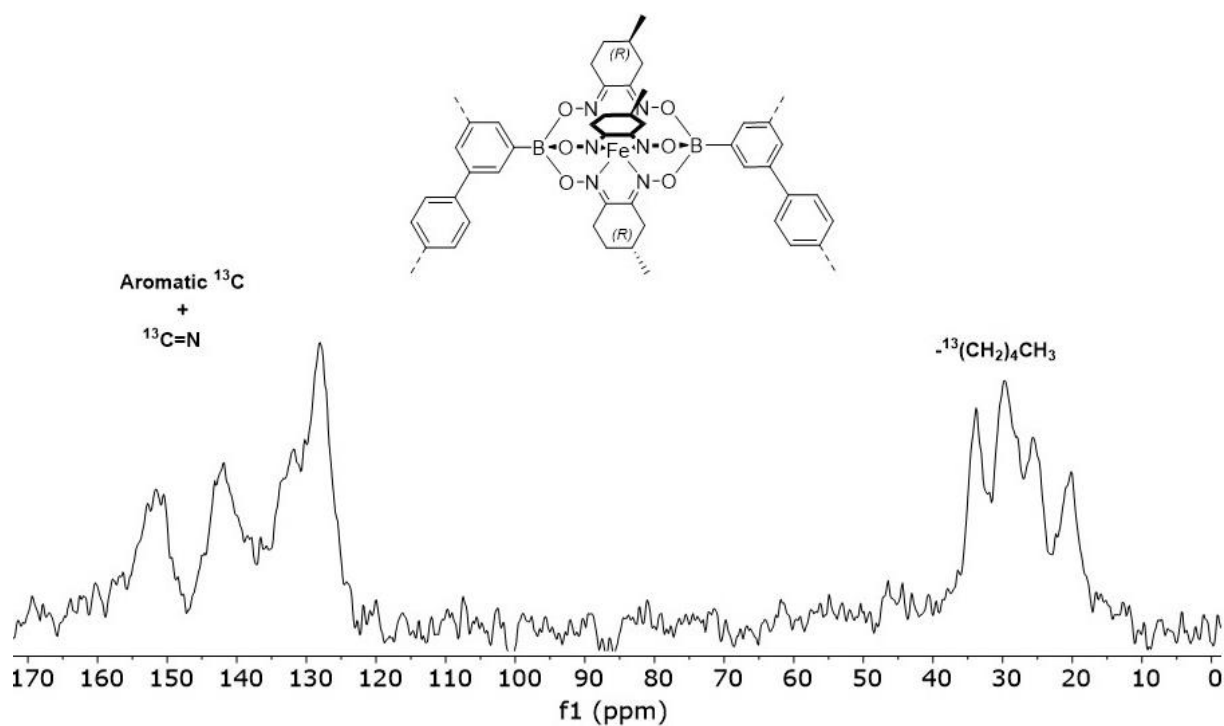


Figure 4.10 -  $^{13}\text{C}$  Solid-state MAS NMR of P-3.


 Figure 4.11 -  $^{13}\text{C}$  Solid-state MAS NMR of P-4.

 Figure 4.12 -  $^{13}\text{C}$  Solid-state MAS NMR of P-5.

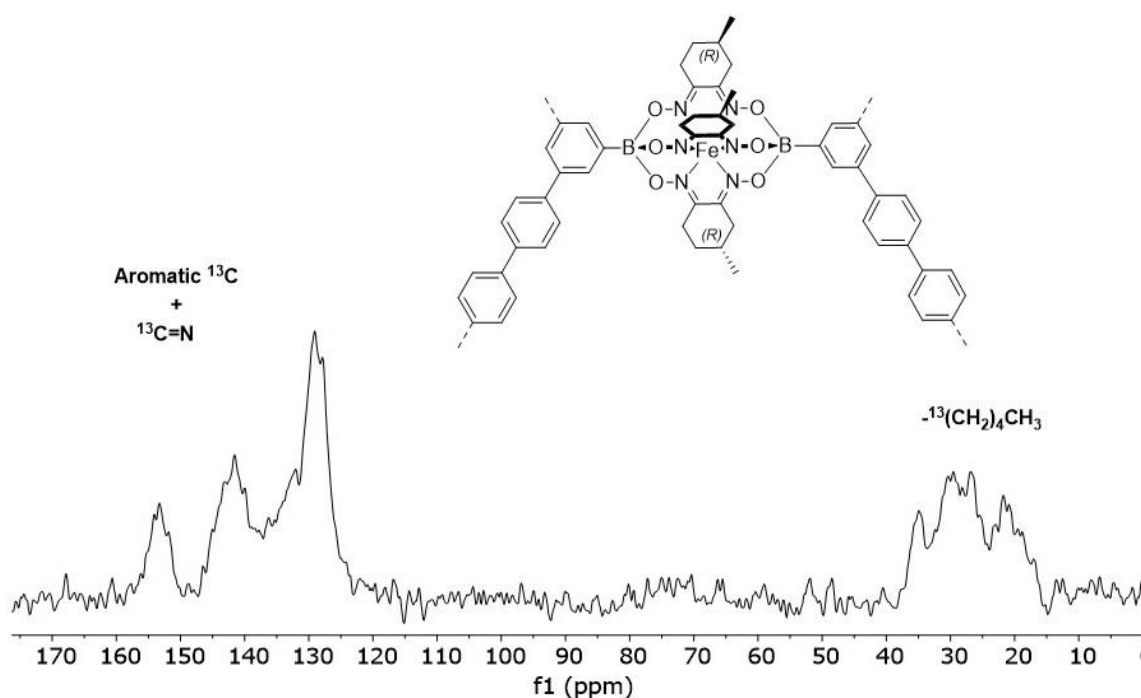


Figure 4.13 -  $^{13}\text{C}$  Solid-state MAS NMR of P-6.

Inspired by a study by Hosseini,<sup>[116]</sup> we have then studied the adsorption of L- and D- tryptophan by using the homochiral porous networks **P-5** and **P-6**. Before the measurements, the polymers were dried for 10 hours at 120 °C under vacuum. The activated polymers (4 mg) were suspended in a solution of either L- or D- tryptophan (2 mL, 120  $\mu\text{M}$ ). The mixtures were sonicated for 30 s, mixed with a vortex mixer for 1 min, and then stirred at room temperature. The concentration of the amino acid in solution was determined by measuring the absorption at 280 nm as a function of time. All measurements were performed in triplicates. For polymer **P-5**, the adsorption kinetics for L- and D-tryptophan were very similar (Figure 4.14). Polymer **P-6**, on the other hand, preferentially absorbed D-Tryptophan: after 100 minutes, the concentration of D-tryptophan was reduced to 57  $\mu\text{M}$ , whereas the L-tryptophan concentration was still at 91  $\mu\text{M}$ .

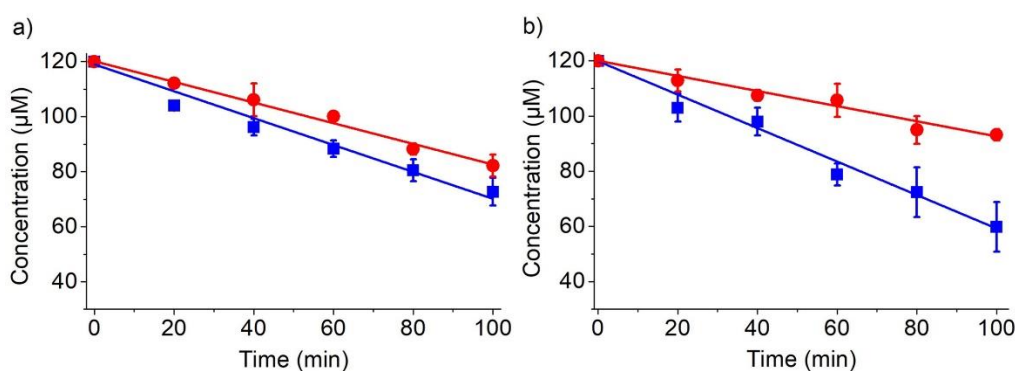


Figure 4.14 - D-Tryptophan (blue symbols) and L-tryptophan (red symbols) concentration as a function of time in the presence of the polymers P-5 (a) or P-6 (b).

#### 4.4 Porous materials based on dinuclear iron clathrochelate complexes

N<sub>2</sub> sorption measurements of polymers **P-7** and **P-8** at 77 K gave apparent BET surface areas of 510 and 473 m<sup>2</sup> g<sup>-1</sup>, respectively (Table 4.7). The micropores of both polymers have a diameter of around 1.2 nm. CO<sub>2</sub>, and H<sub>2</sub> uptakes were measured up to 1 bar at 273 K and 77 K, respectively. The



corresponding values ( $\text{CO}_2$ :  $61 \text{ cm}^3 \text{ g}^{-1}$  for **P-7**,  $35 \text{ cm}^3 \text{ g}^{-1}$  for **P-8**;  $\text{H}_2$ :  $98 \text{ cm}^3 \text{ g}^{-1}$  for **P-7**,  $62 \text{ cm}^3 \text{ g}^{-1}$  for **P-8** (Figure 4.3).

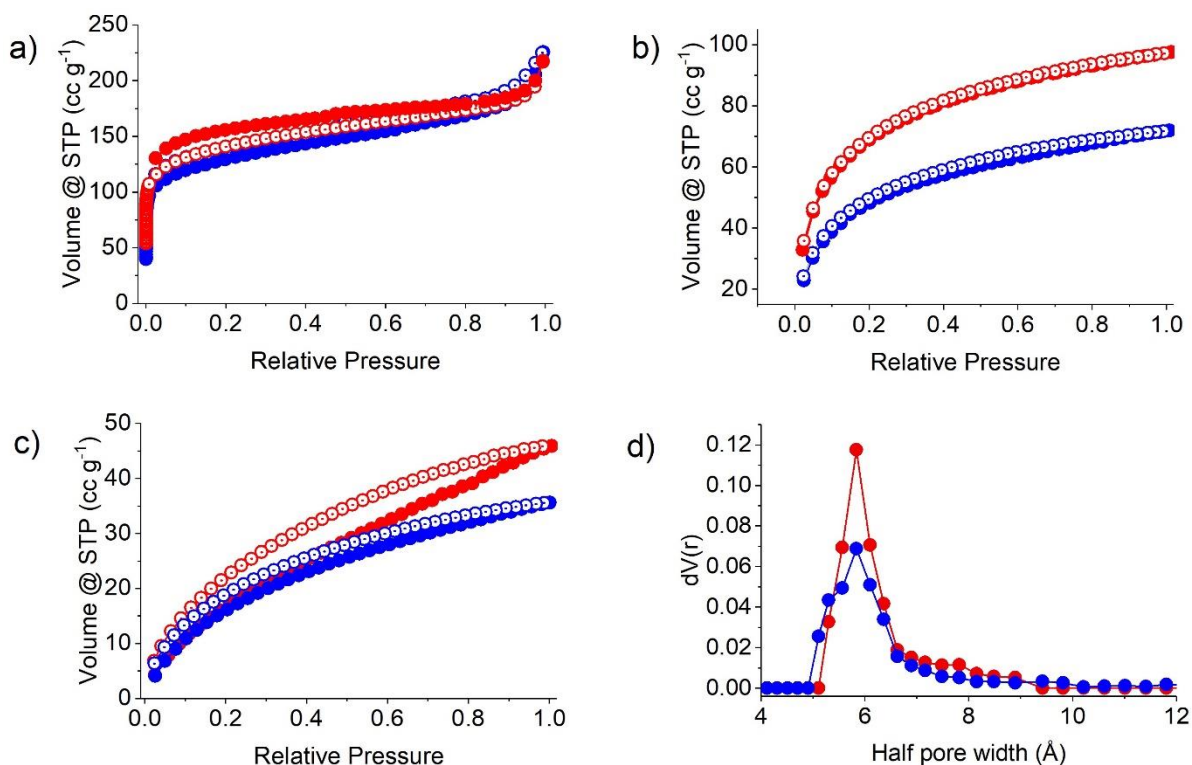


**Figure 4.15** - Characterization of **P-7** (red symbols) and **P-8** (blue symbols) by sorption measurements and SEM. a)  $\text{N}_2$  adsorption (filled symbols) and desorption (open symbols) isotherms at 77 K; b)  $\text{H}_2$  adsorption (filled symbols) and desorption (open symbols) isotherms at 77 K; c)  $\text{CO}_2$  adsorption (filled symbols) and desorption (open symbols) isotherms at 273 K and d) Pore size distribution.

**Table 4.7** - Results of  $\text{N}_2$  sorption measurements at 77 K of **P-7** ( $\text{P-Po}^{-1}$  range: 0.08-0.15) and **P-8** ( $\text{P-Po}^{-1}$  range: 0.08-0.20).

polymer	$SA_{\text{BET}}$ [ $\text{m}^2 \text{ g}^{-1}$ ]	$SA_{\text{Lang}}$ [ $\text{m}^2 \text{ g}^{-1}$ ]	pore vol. [ $\text{cm}^3 \text{ g}^{-1}$ ]	av. pore diam. [nm]
<b>P-7</b>	510	635	0.24	1.2
<b>P-8</b>	473	680	0.28	1.2

The SEM image of **P-7** and **P-8** (Figure 4.6) shows agglomerates of irregular spherical nanoparticles (Figure 4.16)

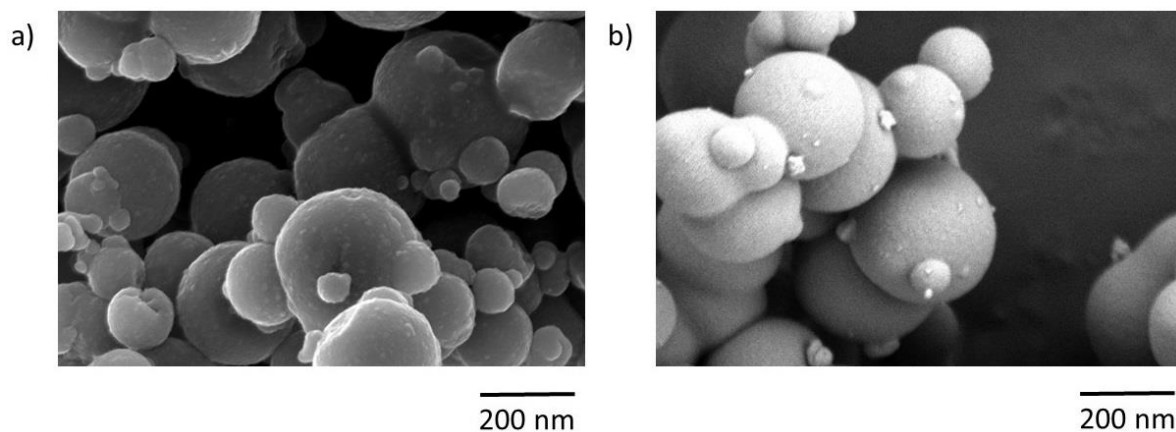


Figure 4.16 - SEM images of (a) P-7 (b) P-8.

TGA measurements of P-7 and P-8 (Figure 4.17) revealed good thermal stabilities up to 250 °C, and no loss in porosity was observed when a suspension of P-7 and P-8 was heated at 80 °C for 6 h in H<sub>2</sub>O.

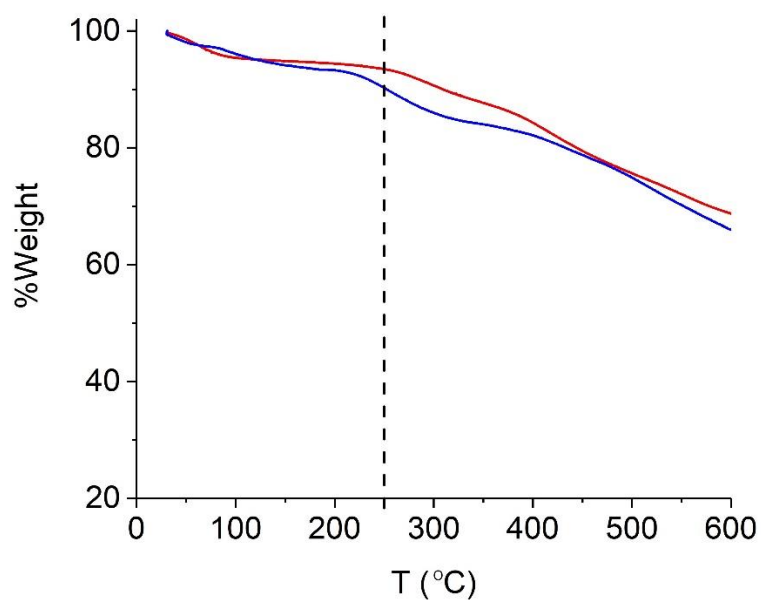


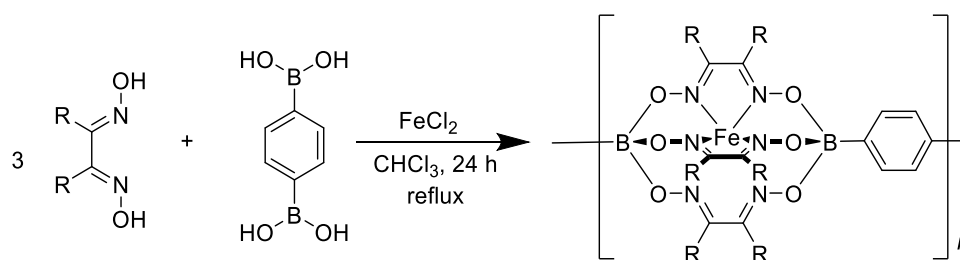
Figure 4.17 - Thermogravimetric analysis of P-7 (red line) and P-8 (blue line) under N<sub>2</sub> atmosphere with 20 mL min<sup>-1</sup> flowrate and 10 °C min<sup>-1</sup>.

## Chapter 5 Porous materials based on Fe-templated polycondensation reactions

In this chapter, we will discuss the synthesis, characterization and potential application of new porous polymer networks based on Fe-templated polycondensation reactions. Dr. Suzanne Janze contributed with the synthesis of triboronic acids.<sup>[34]</sup>

### 5.1 Introduction

Polycondensation reactions can be employed for the synthesis of a wide range of porous materials, which are of interest for energy storage, catalysis, gas storage and/or separation.<sup>[117–121]</sup> A prerequisite for their application is a good physical and chemical stability.<sup>[117]</sup> Clathrochelate complexes are very robust, and thus of interest for applications in materials science.<sup>[4]</sup> Bassam et al. reported the synthesis and characterization of the first polymer containing boronate ester-capped clathrochelate complexes obtained from Fe-templated polycondensation reactions. The polymers were prepared by reaction of benzene-1,4-diboronic acid was reacted with different vicinal dioximes in the presence of  $\text{FeCl}_2$  (Scheme 5.1). Some of the polymers displayed intrinsic microporosity with BET surface areas up to  $412 \text{ m}^2/\text{g}$  and average pore volume of  $0.36 \text{ cm}^3/\text{g}$ .<sup>[119]</sup> The Fe-templated condensation reaction of 9,9-dialkyl fluorene-2,7-diboronic acid with highly soluble vicinal dioxime moieties resulted in highly soluble metal-organic polymers, which showed gelation upon sonication.<sup>[122]</sup>

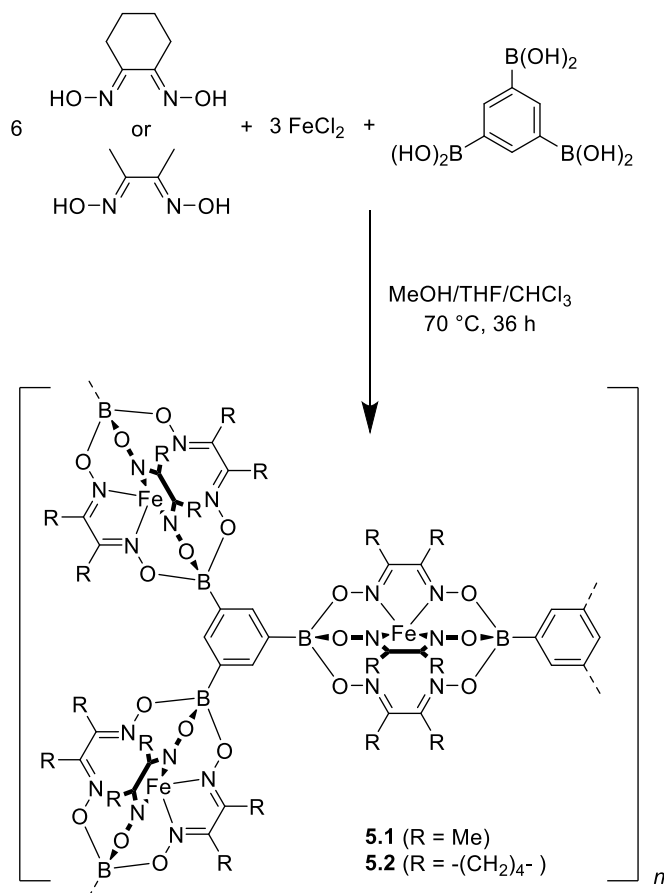


**Scheme 5.1** - Synthesis of linear polymers by Fe-templated condensation reactions.<sup>[119]</sup>

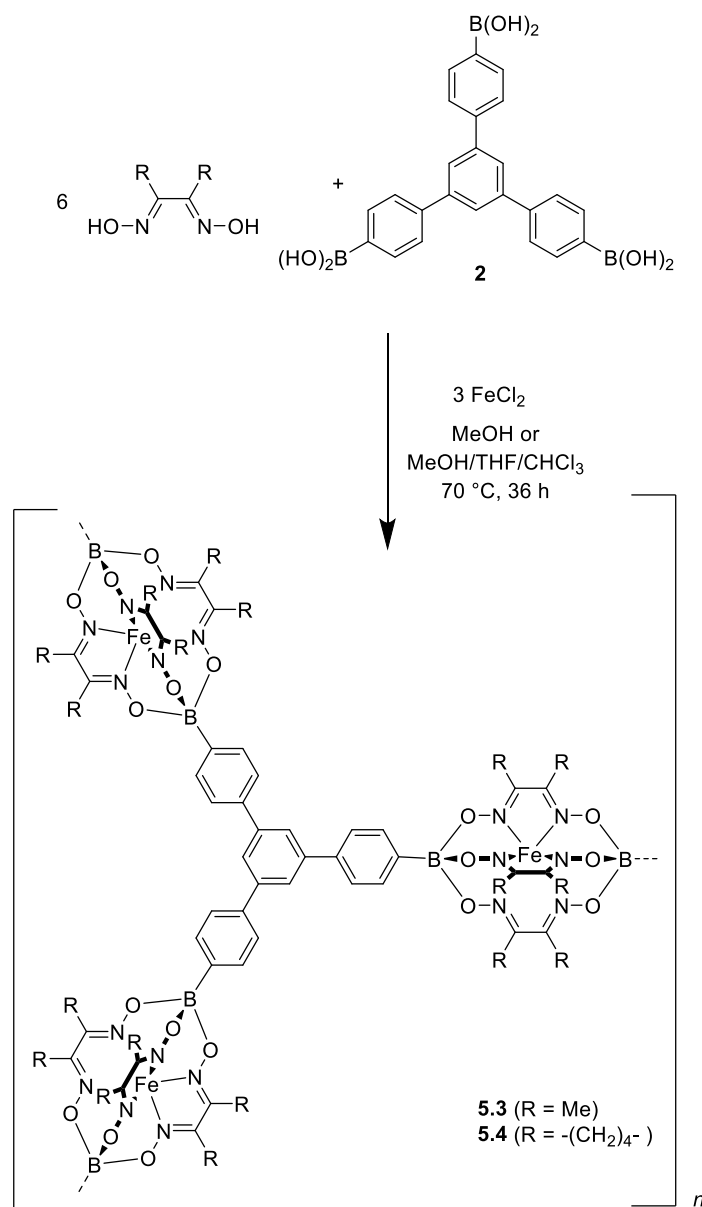
We hypothesized that it should be possible to obtain polymer networks (instead of linear polymers) by using triboronic acids. In the following, we discuss the synthesis, the characterization, and potential application of these polymer networks.

## 5.2 Synthesis and characterization of porous networks containing Fe clathrochelate complexes

In order to prepare polymer networks, we have investigated the Fe<sup>II</sup>-templated condensation reaction of 1,3,5-benzenetriboric acid with nioxime or dimethylglyoxime (Scheme 5.2). The reactions were carried out at 70 °C in a mixture of methanol, tetrahydrofuran, and chloroform (1:2:2), resulting in the formation of the polymers **5.1** and **5.2**. Employing similar conditions, we have prepared the polymers **5.3** and **5.4** with an extended triboronic acid (Scheme 5.2).



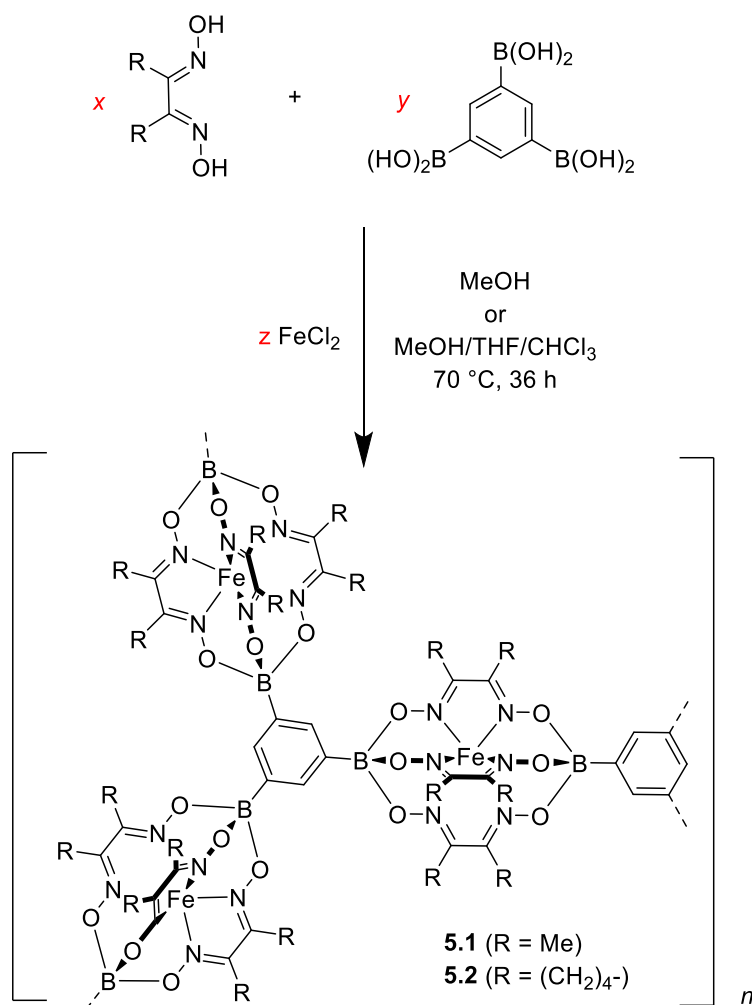
**Scheme 5.2** - Synthesis of the clathrochelate networks **5.1** and **5.2**.



**Scheme 5.3** - Synthesis of the clathrochelate networks **5.3** and **5.4**.

The preparation of polymers **5.1-5.4** resembles a standard MOF synthesis, because metal-ligand interactions mediate network formation. However, it is worth noting a crucial difference: clathrochelate complexes are kinetically and thermodynamically very stable. Hence, they resemble more a normal organic link than a coordination complex. One should also note that the cleavage of a clathrochelate link would require breaking a covalent bond, whereas MOFs can be cleaved by rupture of metal-ligand interactions.

It is worth noting that the boronic acid, the dioxime and  $\text{FeCl}_2$  were used in a ratio of 1:3:6 respectively, because a screening revealed that the resulting polymers have a higher porosity than those prepared with the ‘ideal’ stoichiometry of 1:1.5:4.5 (Table 5.3).


 Scheme 5.4 - Synthesis of **5.1** and **5.2** under different conditions.

**Table 5.1** - Influence of the solvent and of the stoichiometry of the reactants on the porosity of the final polymer.

R	$x$	$y$	$z$	Solvent	$SA_{\text{BET}} (\text{m}^2 \text{g}^{-1})$
Me	4.5	1	1.5	MeOH	n.d. <sup>a</sup>
Me	6	1	3	MeOH	550
Me	6	1	3	MeOH/THF/ $\text{CHCl}_3$	557
$(\text{CH}_2)_4^-$	4.5	1	1.5	MeOH/THF/ $\text{CHCl}_3$	405
$(\text{CH}_2)_4^-$	4.5	1	1.5	MeOH/THF/ $\text{CHCl}_3$ <sup>b</sup>	457
$(\text{CH}_2)_4^-$	4.5	1	3	MeOH/THF/ $\text{CHCl}_3$	n.d. <sup>a</sup>
$(\text{CH}_2)_4^-$	6	1	1.5	MeOH/THF/ $\text{CHCl}_3$	267
$(\text{CH}_2)_4^-$	6	1	3	MeOH/THF/ $\text{CHCl}_3$	637
$(\text{CH}_2)_4^-$	9	1	3	MeOH/THF/ $\text{CHCl}_3$	55

<sup>a</sup> BET surface area not determined due to low yields.

<sup>b</sup> MeOH/THF/ $\text{CHCl}_3$  ratio = 1:4:4.

Dinitrogen sorption measurements of polymers **5.1** – **5.4** at 77 K gave apparent Brunauer-Emmett-Teller surface areas between 448 and 927  $\text{m}^2 \text{g}^{-1}$  (Table 5.1). It is interesting to note that the polymers containing clathrochelates with methyl side chains are less porous compared to the polymers containing clathrochelates with cyclohexyl side chains (**5.1** vs **5.2** and **5.3** vs **5.4**). The opposite trend would be

expected based on steric considerations. However, one should point out that these polymers are obtained by kinetically controlled polymerization reactions. Changing the monomers (e.g. nioxime vs. dimethylglyoxime) can have a pronounced effect on the polymerization process. For example, intermediates such as short oligomers could have a very different solubility.

Polymer networks **5.1**–**5.2** exhibit pore volumes ranging from 0.26 to 0.55 cm<sup>3</sup> g<sup>-1</sup> (Table 5.1). Although two different triboronic acids were used for the syntheses, the pore radii are approximately the same for all polymers (ca. 1.4 nm).

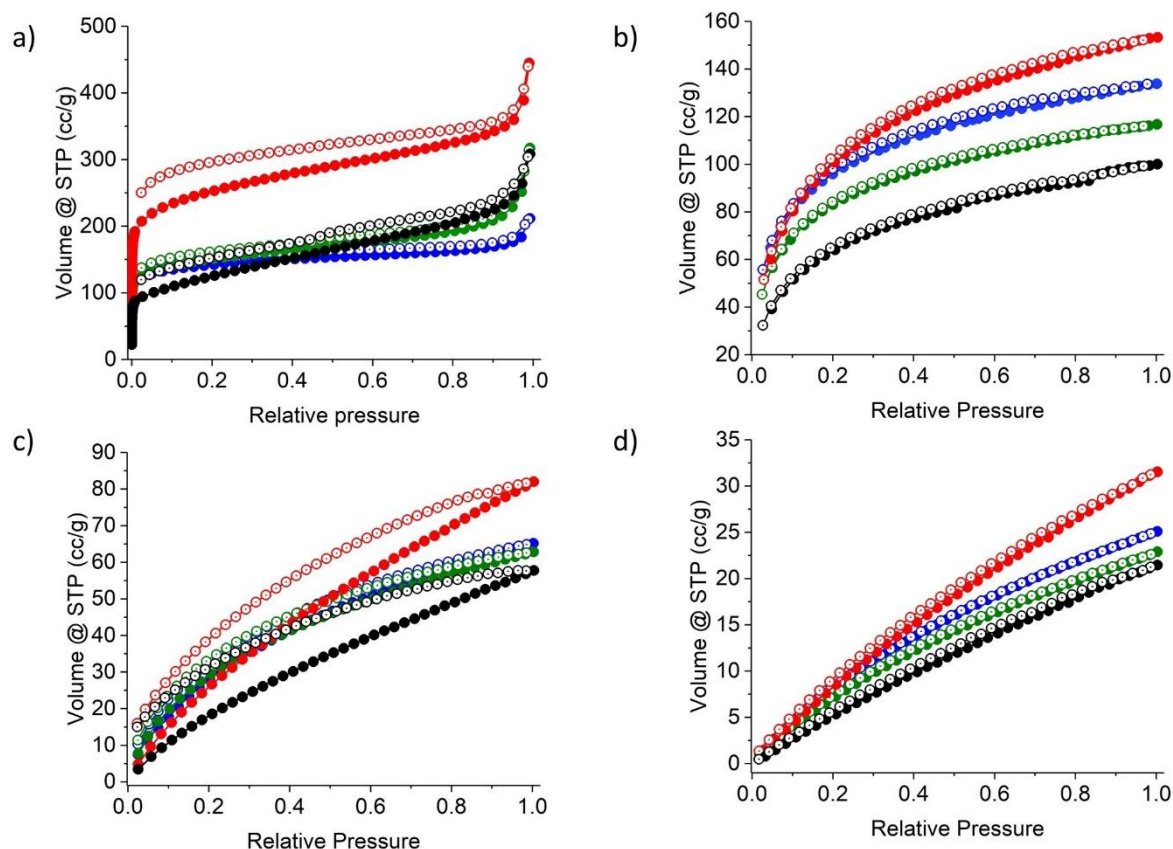


**Figure 5.1** - Characterization of **5.1** (green symbols), **5.2** (blue symbols), **5.3** (black symbols) and **5.4** (red symbols), a) N<sub>2</sub> adsorption (filled symbols) and desorption (open symbols) isotherms at 77 K; b) H<sub>2</sub> adsorption (filled symbols) and desorption (open symbols) isotherms at 77 K; c) CO<sub>2</sub> adsorption (filled symbols) and desorption (open symbols) isotherms at 273 K; d) CH<sub>4</sub> adsorption (filled symbols) and desorption (open symbols) isotherms at 273 K;

**Table 5.2** - Results of N<sub>2</sub> sorption measurements at 77 K **5.1** (P-Po<sup>-1</sup> range: 0.05-0.10), **5.2** (P-Po<sup>-1</sup> range: 0.05-0.10), **5.3** (P-Po<sup>-1</sup> range: 0.06-0.12) and **5.4** (P-Po<sup>-1</sup> range: 0.05-0.08).

polymer	$SA_{\text{BET}}$ [m <sup>2</sup> g <sup>-1</sup> ]	$SA_{\text{Lang}}$ [m <sup>2</sup> g <sup>-1</sup> ]	pore vol. [cm <sup>3</sup> g <sup>-1</sup> ]	av. pore diam. [nm]
<b>5.1</b>	557	568	0.36	1.36
<b>5.2</b>	637	783	0.26	1.38
<b>5.3</b>	448	621	0.39	1.37
<b>5.4</b>	927	1193	0.55	1.41

All porous polymers (**5.1** - **5.4**) are amorphous solids as shown by scanning electron microscope (SEM) analysis (Figure 5.2). Moreover, the stability of the polymers in water was investigated by suspending the polymers in water in a pyrex vial. The suspension was heated to 50 °C or 80 °C for several hours and then filtered, washed with water, methanol and diethyl ether. It was found that the polymers are stable in water at 50 °C for 24 to 30 h, whereas at 80 °C for only 6 to 8 h. Their stabilities were investigated by surface area measurements.

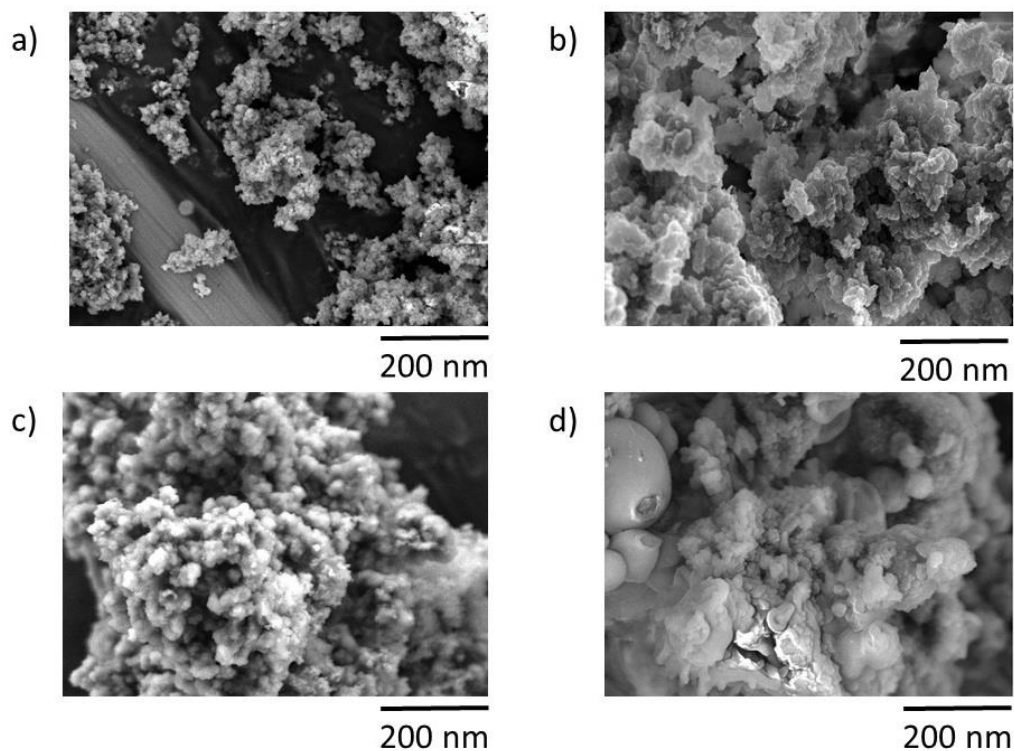


**Figure 5.2** - SEM images of (a) **5.1** (b) **5.2** (c) **5.3** (d) **5.4**.

The thermogravimetric analysis (TGA) of **5.1–5.4** reveal high thermal stability up to ca. 300 °C (Figure 5.3).



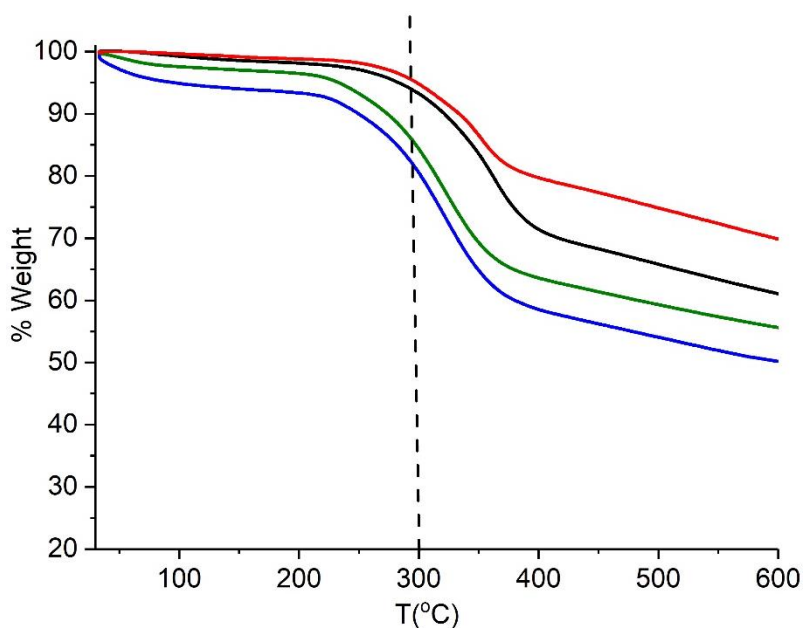


**Figure 5.3** - Thermogravimetric analysis of polymers **5.1** (green line), **5.2** (blue line), **5.3** (black line) and **5.4** (red line) under N<sub>2</sub> atmosphere with 20 mL min<sup>-1</sup> flowrate and 10 °C min<sup>-1</sup>.

The structural integrity of polymers **5.1** – **5.4** was verified by CP-MAS <sup>13</sup>C NMR (Figure 5.4 to 5.7). The broad chemical shifts appearing in the region between 120 and 160 ppm belong to the aromatic carbons and the peaks located between 10 and 30 ppm can be attributed to the aliphatic carbons of the networks.

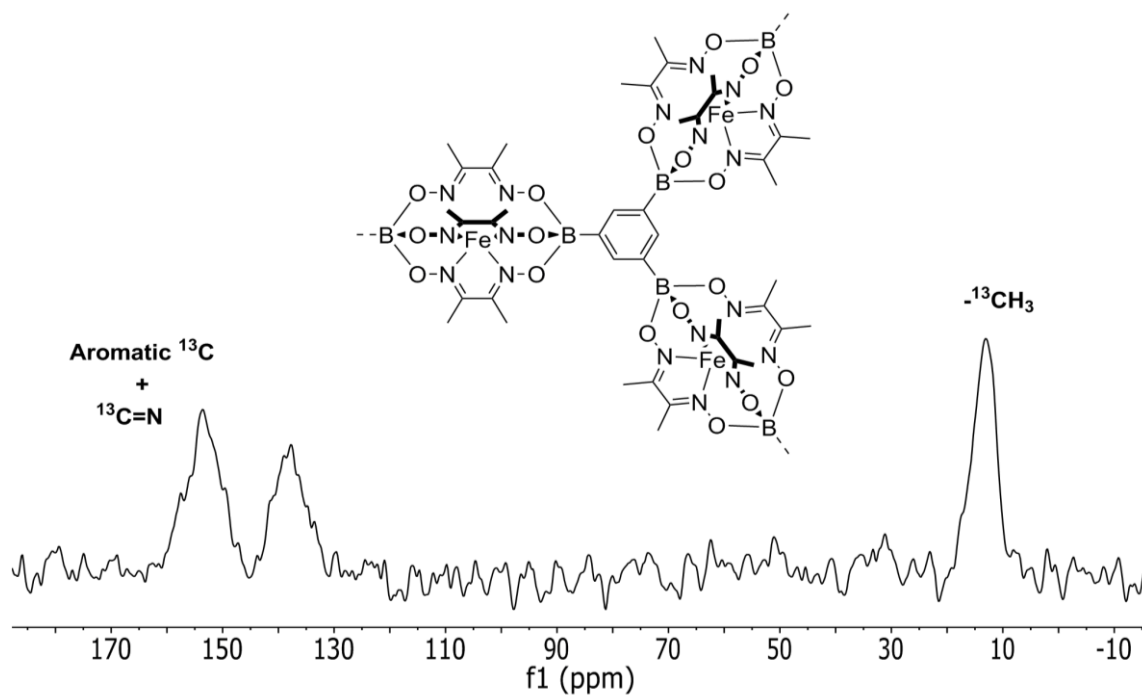


**Figure 5.4** - <sup>13</sup>C Solid-state MAS NMR of polymer **5.1**.

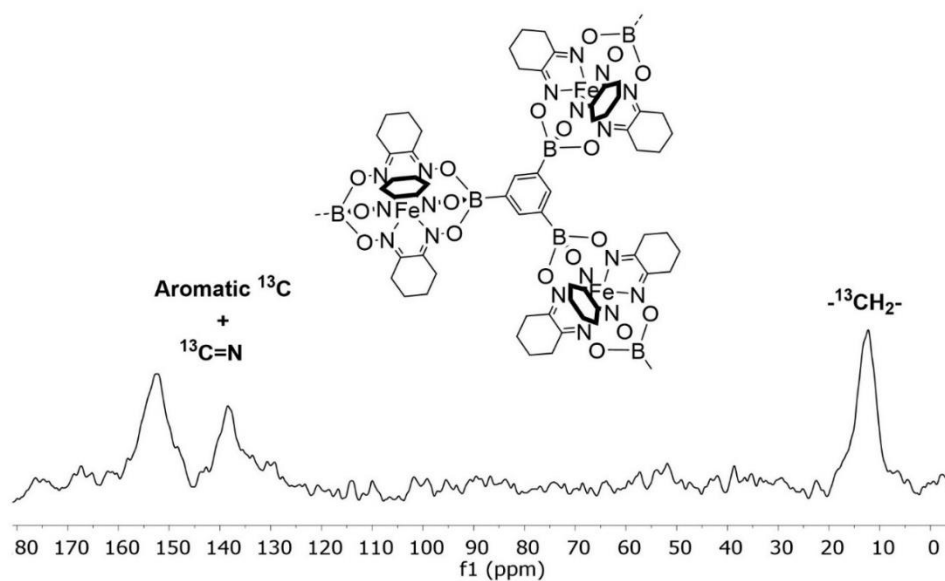


Figure 5.5 -  $^{13}\text{C}$  Solid-state MAS NMR of polymer 5.2.

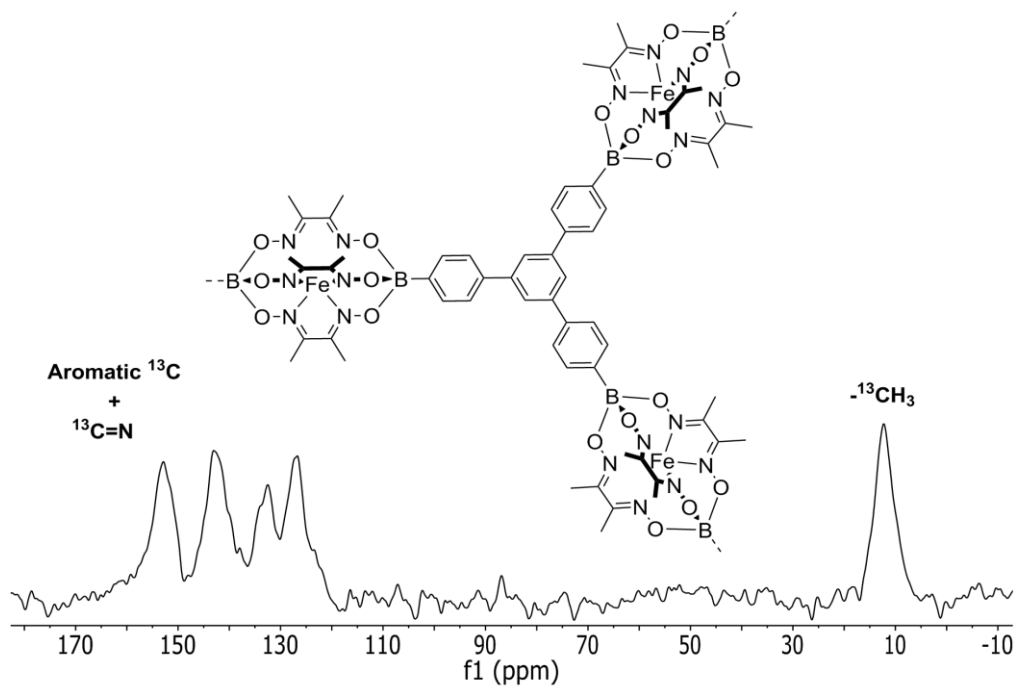


Figure 5.6 -  $^{13}\text{C}$  Solid-state MAS NMR of polymer 5.3.

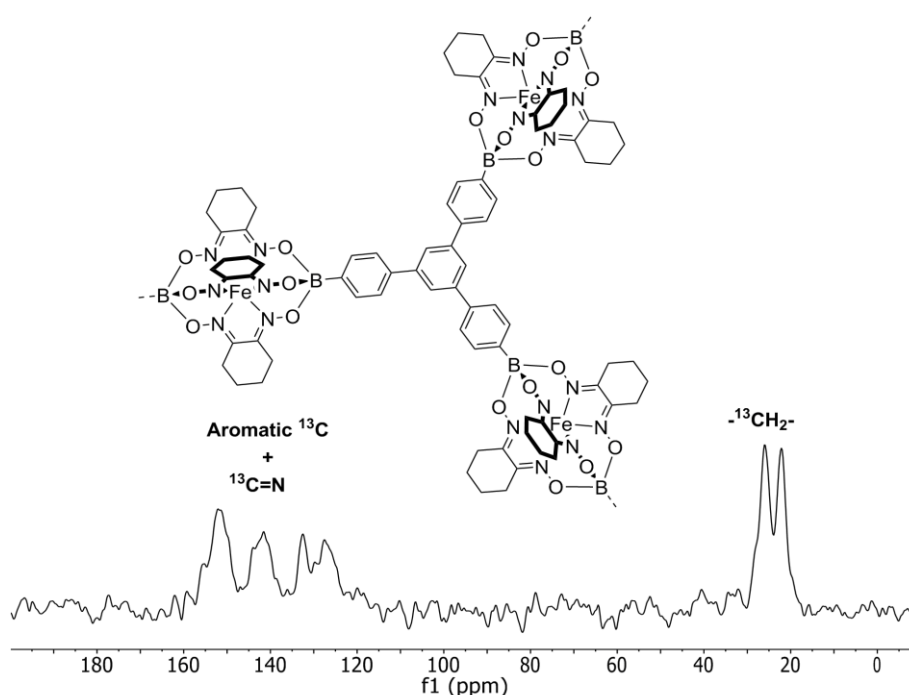


Figure 5.7 -  $^{13}\text{C}$  Solid-state MAS NMR of polymer **5.4**.

### 5.3 Removal of Cr (VI) from water

Cr(VI) is known as a potential carcinogen with a permissible upper limit of 0.05 mg/L according to the World Health Organization.<sup>[123]</sup> The pollution with Cr(VI) originates mainly from industrial tannery, electroplating and dying effluents. Among the different water treatment processes for Cr (VI) polluted water, adsorption technology is the most convenient and energy saving.<sup>[124]</sup> For instance, low-cost activated carbon, lignocellulose, wheat residue derived black carbon, seaweed, sawdust, agricultural biowaste, and polyfunctionalized nanoporous materials are known for the solid phase extraction of chromium from water.<sup>[125,126,135,127–134]</sup> However, such materials suffer from low adsorption capacities and poor selectivity. Therefore, the investigation of new adsorbents is still attractive. We investigated ability to remove Cr(VI) from aqueous solutions using porous clathrochelate polymers derived from Fe-templated polycondensation reactions.

### 5.4 Batch adsorption experiments

An aqueous solution of Cr(VI) was prepared by dissolving  $\text{K}_2\text{Cr}_2\text{O}_7$  with milli-Q water at room temperature and the pH values were adjusted by adding HCl or NaOH. A solution of Cr(VI) mixed with the adequate amount of polymer **5.4** was first sonicated for 30 s then stirred with the vortex mixer for 1-2 min. Adsorption kinetics were measured using equally prepared mixtures, where each was stirred for the required amount of time. The adsorbent was separated from the liquid with a syringe filter (0.22  $\mu\text{m}$ ). The concentration of Cr(VI) was monitored by measuring the absorption at 350 nm and inductively coupled plasma mass spectrometry (ICP-MS) as function of time. All measurements were performed in triplicates.

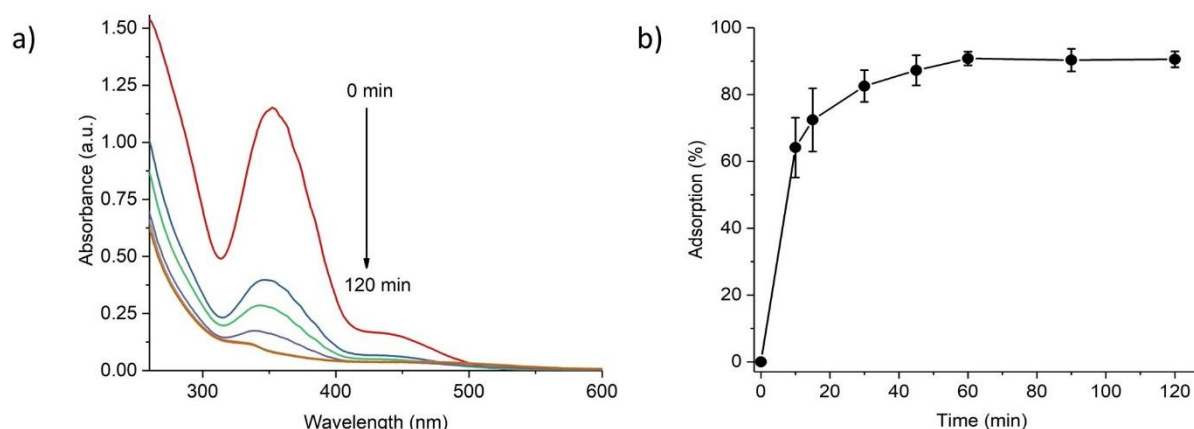


**Figure 5.8** - Cr(VI) adsorption studies for polymer **5.4**; (a) UV-vis. Adsorption and (b) calculated percent adsorption at 350 nm as function of time at pH = 6.5.

The adsorption percentage and adsorption capacity were calculated from equation 1 and 2, where  $C_0$  is the initial concentration (mg/L),  $C_e$  is the equilibrium concentration (mg/L),  $m$  (g) is the mass of the adsorbent, and  $V$  (mL) is the volume of the suspension and  $Q_e$  (mg/g) is the equilibrium adsorption capacity.

$$\text{Adsorption (\%)} = \frac{C_0 - C_e}{C_0} \times 100 \% \quad (1)$$

$$Q_e = (C_0 - C_e) \times \frac{V}{m} \quad (2)$$

The adsorption studies reveal up to 90% adsorption of Cr (VI) from water after 120 min at pH = 6.5 for polymer **5.4** (Figure 5.8). The effect of polymer **5.4** dosage (m/V) on aqueous solutions of Cr(VI) was investigated at pH 6.5 and room temperature. The initial Cr(VI) concentration was 200 ppm and the adsorbent's dosage was varied from 3 to 6 g/L. The results reveal an increase in uptake as function of dosage (Figure 5.9).

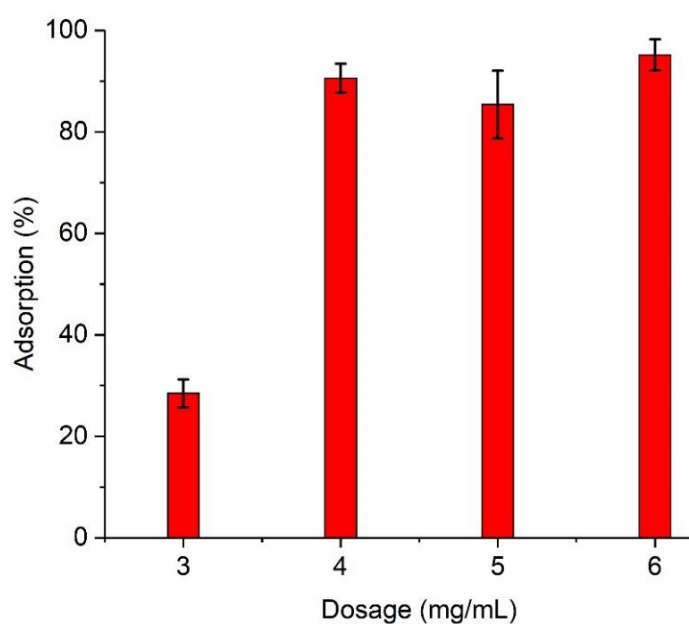


**Figure 5.9** - The effect of dosage increase on Cr(VI) uptake of polymer **5.4**.

Subsequently, we tested the adsorption capacity of polymer **5.4** at pH values between 2 and 10. The highest adsorption capacity of Cr(VI) was obtained at pH = 6, with a value of  $120 \text{ mg g}^{-1}$ . An increased pH resulted in a decrease of the uptake.

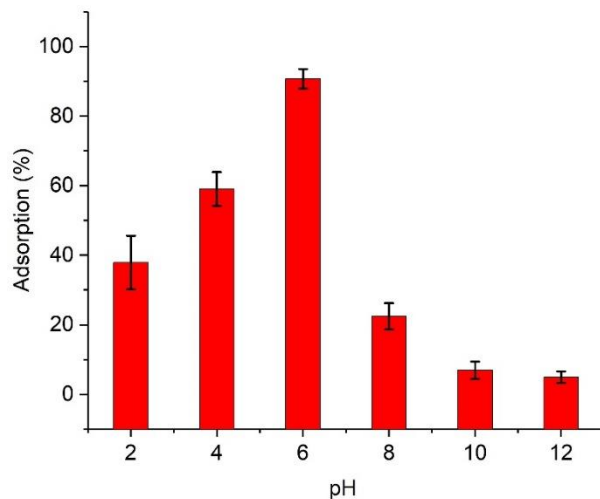


**Figure 5.10** - The effect of pH on Cr(VI) adsorption of polymer **5.4**.

Lastly, the recyclability of polymer **5.4** was investigated by soaking and washing the polymer after each adsorption and re-used. The ability of polymer **5.4** to remove Cr(VI) decreases significantly with the number of runs. This could be attributed to the saturation and the lower desorption rate of the polymer.

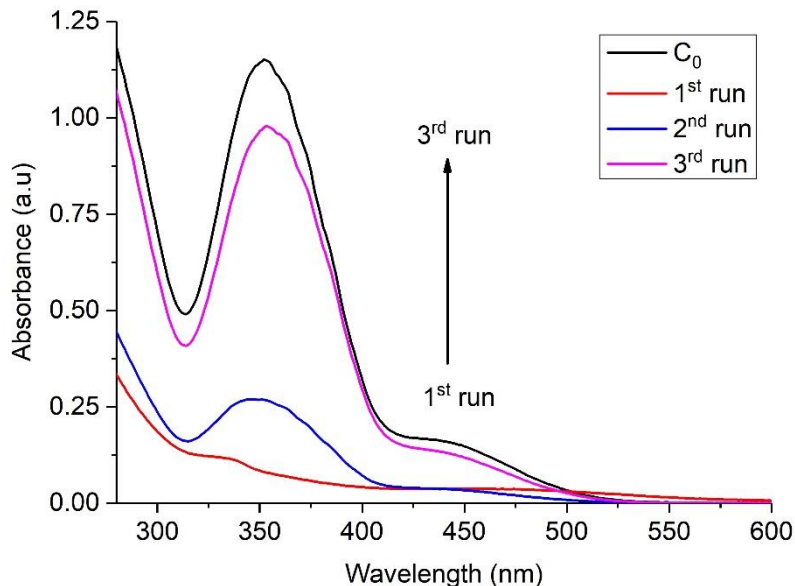


**Figure 5.11** - Recyclability of polymer **5.4**. The measurements were performed with a stock solution at 100 ppm, pH = 6.5 and polymer loading of 4 mg/mL.

It is worth noting that the adsorption mechanism of the clathrochelate polymer is not known and further investigations are required.



## Chapter 6 Conclusion and outlook

This thesis focuses on the synthesis, characterization and applications of iron clathrochelate complexes in materials science. Clathrochelates are easy to synthesize, and they are stable under harsh conditions. In addition, some clathrochelate complexes are redox-active, paramagnetic, or luminescent, depending on the metal ion employed.

Dinuclear iron clathrochelate complexes can be accessed in two distinct oxidation states. The preparation of clathrochelates with exclusively  $\text{Fe}^{\text{II}}$  salts under inert atmosphere results in negatively charged  $\text{Fe}^{\text{II}}\text{-Fe}^{\text{II}}$  clathrochelates. On the other hand, the use of equimolar  $\text{Fe}^{\text{II}}$  and  $\text{Fe}^{\text{III}}$  salts affords neutral  $\text{Fe}^{\text{II}}\text{-Fe}^{\text{III}}$  clathrochelate complexes. The  $\text{Fe}^{\text{II}}\text{-Fe}^{\text{II}}$  complexes are antiferromagnetic and the  $\text{Fe}^{\text{II}}\text{-Fe}^{\text{III}}$  complexes are paramagnetic. The redox potentials are affected by the substituents on the dioxime periphery. However, a similar effect is not observed with the capping boronic acid groups. Upon varying the boronic acid capping groups, the redox potentials change by less than 100 mV.

It is worth noting that the deliberate synthesis and isolation of  $\text{Fe}^{\text{III}}\text{-Fe}^{\text{III}}$  clathrochelate complexes was not achieved. However,  $\text{Fe}^{\text{III}}\text{-Fe}^{\text{III}}$  complexes can be observed electrochemically. In addition, the introduction of electron-donating moieties to the capping boronic acid groups was found to stabilize the  $\text{Fe}^{\text{III}}\text{-Fe}^{\text{III}}$  oxidation states of the clathrochelates as evidenced electrochemically. In fact, dinuclear iron clathrochelate complexes decorated with electron-donating moieties on the boronic acid display two reversible/quasi-reversible peaks. On the other hand, complexes decorated with electron-withdrawing groups show one reversible and one irreversible peak in the cyclic voltammogram. The dinuclear iron clathrochelates are stable during the electrochemical measurements (reduction and oxidation). Therefore, these complexes can be employed as redox-active compounds for redox flow batteries. Indeed, their combination with lithium as anode results in high battery voltages of 3.5 V and Coulombic efficiencies >99%.

The fact that clathrochelate complexes are stable under the harsh conditions of metal-catalyzed coupling reactions makes them interesting for applications in materials science. Mono- and dinuclear iron clathrochelate complexes can be used as coupling partners for Suzuki and Sonogashira reactions, resulting in the formation of polymer networks with permanent porosity and apparent BET surface areas of up to  $593 \text{ m}^2\text{g}^{-1}$ . The easy functionalization of mononuclear clathrochelates facilitates the introduction of chiral groups in the ligand

periphery. As a result, homochiral porous networks can be prepared. The latter are able to preferentially adsorb D-tryptophan from water.

It is also possible to prepare porous networks based on Fe-templated polycondensation reactions. These networks display high chemical stability in water and apparent BET surface areas up to  $927 \text{ m}^2\text{g}^{-1}$ . The strategy to use condensation reactions resembles a standard MOF synthesis, given that the metal-ligand interactions mediate the network formation. However, clathrochelates are kinetically and thermodynamically stable. Hence, they resemble more a normal organic link than a coordination complex. The porous networks based on Fe-templated polycondensation reactions were found to effectively adsorb chromium (VI) from water.

In summary, our results show that iron clathrochelate complexes are versatile building blocks for applications in materials science. Both mononuclear and dinuclear clathrochelate complexes are suitable monomers for the preparation of porous networks. Preliminary studies show that dinuclear iron clathrochelate complexes can be employed as redox-active compounds for redox flow batteries. In combination with lithium as anode, high voltages and Coulombic efficiencies were observed. These first results show that clathrochelate complexes are very promising compounds for this type of application. However, further efforts are needed to increase the solubility of these compounds. Given that clathrochelates are synthesized in a highly modular fashion, I believe that complexes with the desired properties (stability and solubility) can be obtained in the near future.



## Chapter 7 Experimental details

### 7.1 General

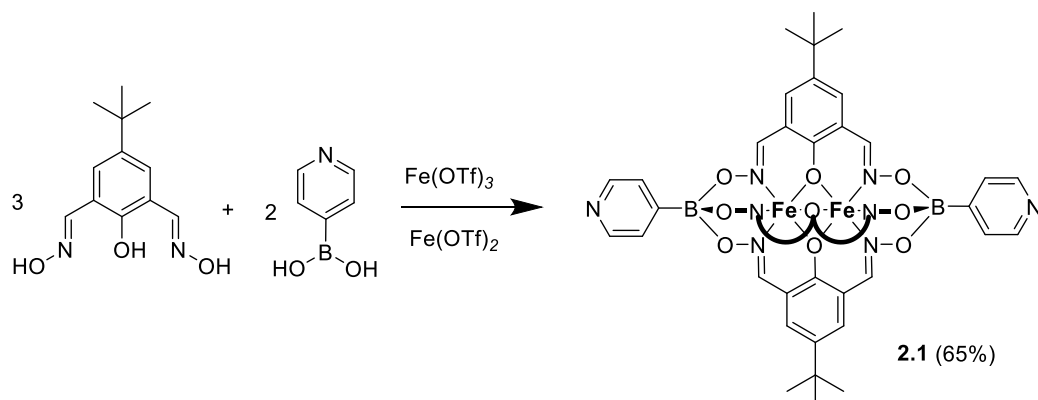
All reagents were obtained from commercial sources and used without further purification unless stated otherwise. Solid state MAS NMR were measured on a Bruker AVIIIHD spectrometers (400 MHz and 800 MHz) equipped with a 2.5 mm H/X/Y CP-MAS (solid) and 1.3 mm  $^1\text{H}/^{13}\text{C}/^{79}\text{Br}/^{15}\text{N}$  CP-MAS (solid) probes respectively. Liquid state  $^1\text{H}$  NMR and  $^{13}\text{C}$  NMR spectra were obtained on a Bruker Avance III spectrometer ( $^1\text{H}$ : 400 MHz) equipped with a 5 mm BBFO-Plus<sub>z</sub> probe and a Bruker Avance III HD spectrometer ( $^1\text{H}$ : 600MHz) equipped with 5 mm CPTCl<sub>z</sub> probe. The chemical shifts are reported in parts per million  $\delta$  (ppm) referenced to an internal solvent. All spectra were recorded at 298 K. The NMR data was analyzed with the help of MestreNova software. Cyclic voltammetry (CV) experiments were performed using a CHI760E electrochemical workstation (CH Instruments, Inc.) potentiostat. The measurements of the cyclic voltammetry were conducted under  $\text{N}_2$  atmosphere with a computer controlled voltammetry analyzer connected to three electrodes. Working electrode (Carbon), Reference electrode (Ag, AgCl), and counter electrode (Pt wire). The electrodes were immersed in a DMF solution containing  $\approx 5$  mg/mL of sample. Tetrabutylammonium hexafluorophosphate (0.1 M) was used as electrolyte. The susceptibility measurements were carried out on a Quantum Design MPMS-XL 5T Superconducting Quantum Interference Device (SQUID) magnetometer. The samples were placed in a plastic capsule which was incorporated into two plastic straws as sample holder. The measurements were done with an applied field of 1 T and temperatures ranging from 5 to 350 K using the Zero Field Cooled method (ZFC). Electrospray-ionisation MS data were acquired on a Q-ToF Ultima mass spectrometer (Waters) operated in the positive and negative ionization modes using the ZSpray™ dual-orthogonal multimode ESI/APCI/ESCI® source and processed using the MassLynx 4.1 software. IR spectra were recorded on a Perkin Elmer Spectrum One Golden Gate FT/IR spectrometer. UV-vis spectra were recorded on an Agilent technologies, Cary-60 spectrophotometer. Nitrogen (77 K), carbon dioxide (273 K), and hydrogen (77 K) sorption measurements were performed on a Quantachrome Autosorb iQ analyzer. Polymers were dried at 100 °C (5-8 h) and 120 °C (5 h) before measurements. The surface area was calculated with BET assistant (built-in software) and a Rouquerol plot within the valid BET relative pressure range (0.05-0.30). Density functional theory (DFT) was used with  $\text{N}_2$  adsorption isotherms to calculate the pore size distribution and the cumulative pore volume. SEM measurements were performed on a Zeiss Merlin SEM. The thermogravimetric

analyses were performed with a Perkin Elmer 4000 TGA between 30 °C and 700 °C with a nitrogen atmosphere at 20 mL min<sup>-1</sup> flowrate. The data were analyzed with Perkin Elmer Pyris software. In the cell assembly, a cylinder cell was made by sealing two cylindrical quartz shells (inner/outer diameters are 8/10 mm) sandwiching the LATP ( $\text{Li}_{1+x+3z}\text{Al}_x(\text{Ti,Ge})_{2-x}\text{Si}_{3z}\text{P}_{3-z}\text{O}_{12}$ ) membrane using sealant (heating Surlyn<sup>®</sup> resin sealant at 120 °C for 5 hours). Subsequently, current collector was made for cathode and anode respectively. In the cathode part, Ti foil was coated with Super P/PVDF thin layer by doctor blading, and one hole was drilled on Ti foil to inject catholyte. Super P carbon and PVDF were mixed in NMP solvent (mass ratio of 90:10), and the as-prepared current collector was dried at 120 °C for 12 hours to evaporate NMP solvent. The loading of super P/PVDF is about 1 mg/cm<sup>2</sup>. In the anode part, copper mesh was welded to copper foil as current collector and the cell transferred to glovebox to add electrolytes. In the anode, Li metal was pressed on copper mesh as anode, and A6 electrolyte (BASF<sup>®</sup>) was injected into the quartz shell of the anode part and then covered by the copper foil in the glovebox. In the cathode, the as-prepared catholyte was injected into the cylindrical quartz shell through the hole drilled on Ti in advance and then the hole was sealed by tape. In the last step, the cell was taken out of glovebox and the anode was sealed hermetically using epoxy.

## 7.2 Experimental procedures

### 7.1.1 Experimental procedures for chapter 2

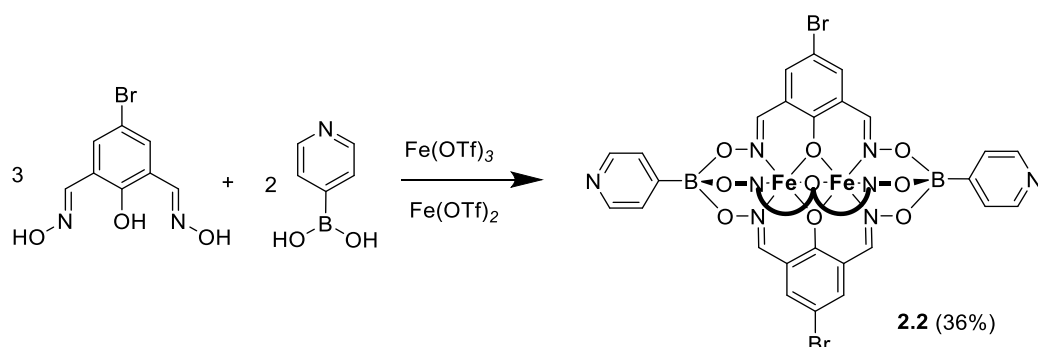
#### Synthesis of complex 2.1:



A solution of  $\text{Fe}(\text{OTf})_2$  (57 mg, 160  $\mu\text{mol}$ ) and  $\text{Fe}(\text{OTf})_3$  (80 mg, 160  $\mu\text{mol}$ ) in MeOH (10 mL) was added to a solution of 2,6-diformyl-4-tert-butylphenol dioxime (100 mg, 423  $\mu\text{mol}$ ) and 4-pyridylboronic acid (39.5 mg, 321  $\mu\text{mol}$ ) in MeOH (10 mL) and heated to reflux for 2 h. The solution was cooled to RT and  $\text{NEt}_4\text{OH}$  solution (100  $\mu\text{L}$ , 1.5 M in MeOH) was added and stirred for 1 h. The solvent was evaporated to dryness and the product was purified by a silica gel column chromatography (EtOAc) to obtain a black powder. *Yield*: 82 mg (65%). **HRMS-ESI** (positive mode):  $m/z$  calculated for  $\text{C}_{46}\text{H}_{48}\text{B}_2\text{Fe}_2\text{N}_8\text{O}_9$   $[\text{M}+\text{H}]^+$  990.2446; found: 990.2458. **IR**: 1724, 1673, 1605,

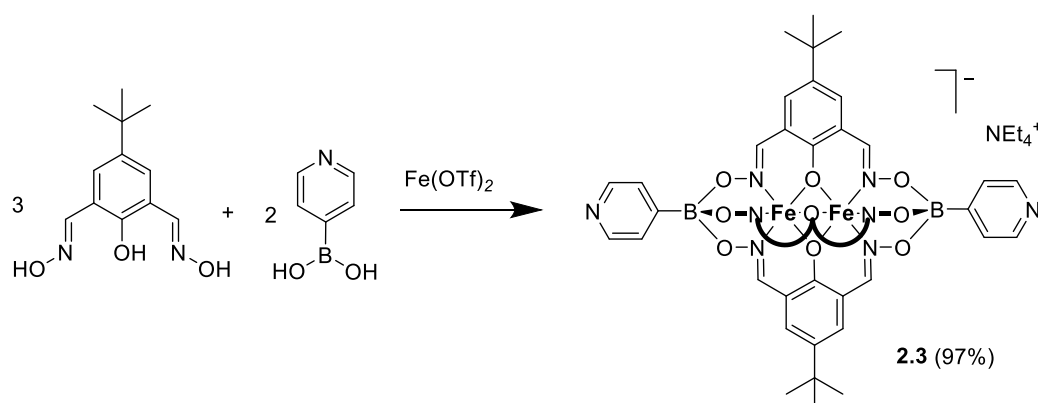
1577, 1452, 1308, 1259, 1230, 1210, 1179, 1099, 1037, 927, 844, 792, 762, 697, 644, 582, 563. Single crystals were obtained by slow diffusion of diisopropyl ether to a solution of complex **2.1** in THF.

### Synthesis of complex **2.2**:



A solution of  $\text{Fe}(\text{OTf})_2$  (45 mg, 127  $\mu\text{mol}$ ) and  $\text{Fe}(\text{OTf})_3$  (64.7 mg, 127  $\mu\text{mol}$ ) in MeOH (10 mL) was added to a solution of 2,6-diformyl-4-bromo-phenol dioxime (100 mg, 386  $\mu\text{mol}$ ) and 4-pyridylboronic acid (36 mg, 257  $\mu\text{mol}$ ) in MeOH (10 mL) and heated to reflux for 2 h. The solution was cooled to RT and  $\text{NEt}_4\text{OH}$  solution (100  $\mu\text{L}$ , 1.5 M in MeOH) was added and stirred for 1 h. The solvent was evaporated to dryness and the product was purified by a silica gel column chromatography (EtOAc:MeOH, 25:1) to obtain a black powder. *Yield*: 49.5 mg (36%) **HRMS-ESI** (positive mode):  $m/z$  calculated for  $\text{C}_{34}\text{H}_{21}\text{B}_2\text{Br}_3\text{Fe}_2\text{N}_8\text{O}_9$   $[\text{M}+\text{H}]^+$ : 1055.7870; found: 1055.7880. **IR**: 1708, 1598, 1547, 1491, 1424, 1323, 1214, 1167, 1028, 986, 896, 780, 703, 637, 539. Single crystals were obtained by slow evaporation of its dissolution in THF and acetonitrile.

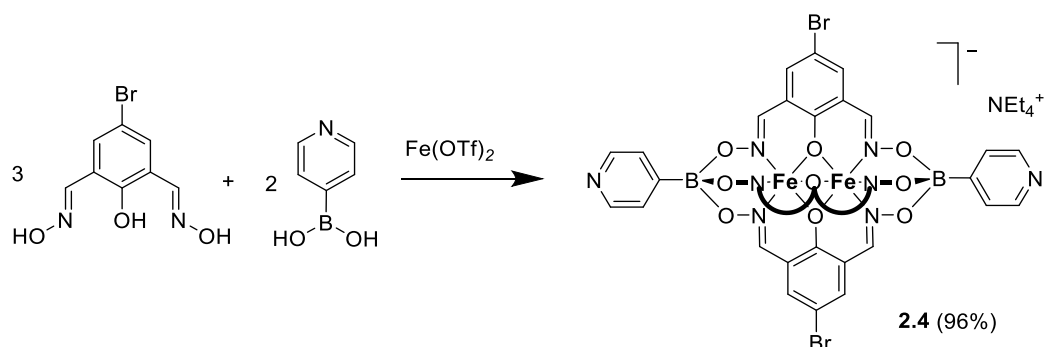
### Synthesis of complex **2.3**:



$\text{Fe}(\text{OTf})_2$  (113.6 mg, 321  $\mu\text{mol}$ ) was added to a solution of 2,6-diformyl-4-tert-butyl-phenol dioxime (100 mg, 423  $\mu\text{mol}$ ) and 4-pyridylboronic acid (39.5 mg, 321  $\mu\text{mol}$ ) in MeOH (20 mL) in the glovebox. The reaction mixture was stirred at 50  $^\circ\text{C}$  for 1 h and then cooled to RT. The precipitates were isolated by filtration under air and washed with EtOH and diethyl ether. The product was suspended in EtOH (20 mL) and  $\text{NEt}_4\text{OH}$  (190  $\mu\text{L}$ , 1.5 M in

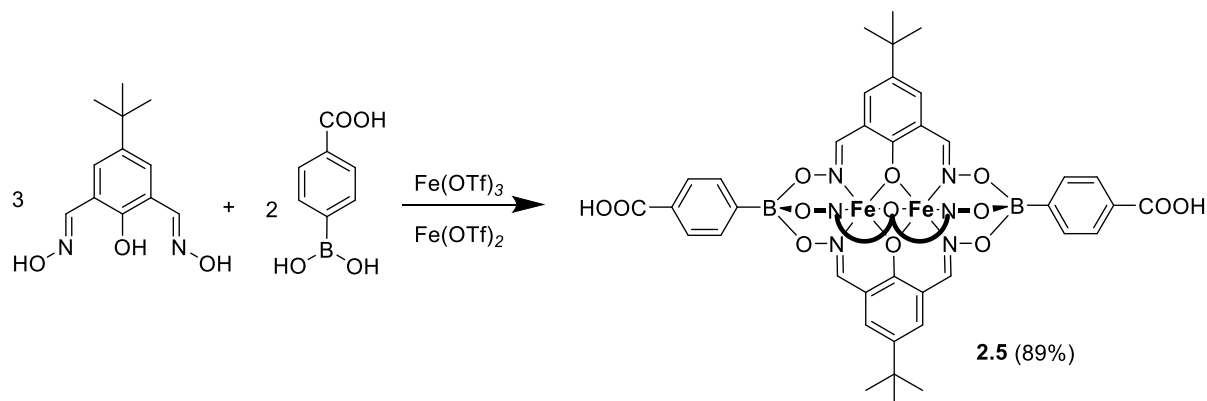
MeOH) was added and stirred for 1 h at RT. The solution was concentrated under reduced pressure, filtered and washed with ethanol and diethyl ether to afford a brown powder. *Yield*: 135 mg (97%). **HRMS-ESI** (negative mode): *m/z* calculated for  $C_{46}H_{47}B_2Fe_2N_8O_9 [M]^-$ : 989.2350; found: 989.2377. **IR**: 1663, 1605, 1550, 1444, 1406, 1333, 1223, 1201, 1081, 1034, 980, 924, 839, 782, 696, 651, 622, 549. Single crystals were obtained by slow diffusion of pentane to a solution of complex **2.3** in  $CHCl_3$ .

#### Synthesis of complex **2.4**:



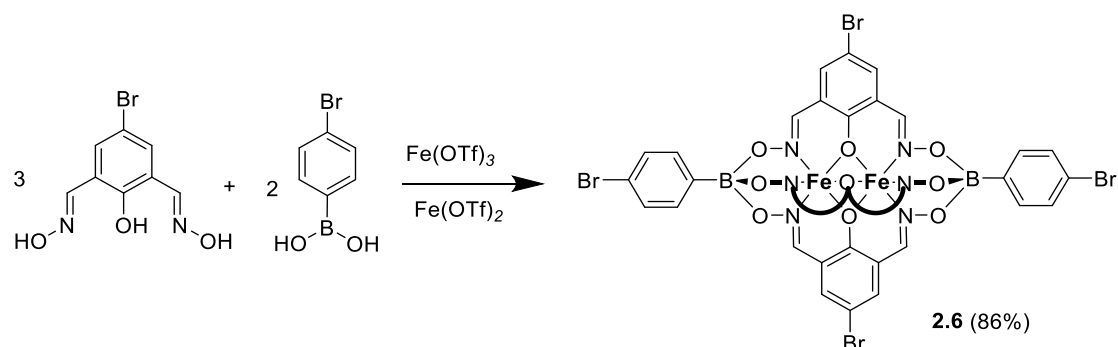
$Fe(OTf)_2$  (113.6 mg, 321  $\mu$ mol) was added to a solution of 2,6-diformyl-4-bromo-phenol dioxime (100 mg, 386  $\mu$ mol) and 4-pyridylboronic acid (36 mg, 257  $\mu$ mol) in MeOH (20 mL) in the glovebox. The reaction mixture was stirred at 50  $^{\circ}C$  for 1 h and then cooled to RT. The precipitates were isolated by filtration under air and washed with EtOH and diethyl ether. The product was suspended in EtOH (20 mL) and  $NEt_4OH$  (100  $\mu$ L, 1.5 M in MeOH) was added and stirred for 1 h at RT. The product was concentrated under reduced pressure, filtered and washed with ethanol and diethyl ether to afford a brown powder. *Yield*: 130 mg (96%). **HRMS-ESI** (negative mode): *m/z* calculated for  $C_{34}H_{20}B_2Br_3Fe_2N_8O_9 [M]^-$ : 1054.7790; found: 1054.7789. **IR**: 1595, 1546, 1480, 1426, 1321, 1202, 1073, 1036, 979, 948, 888, 815, 780, 751, 685, 649. Single crystals were obtained by slow diffusion of pentane to a solution of complex **2.4** in THF.

#### Synthesis of complex **2.5**:



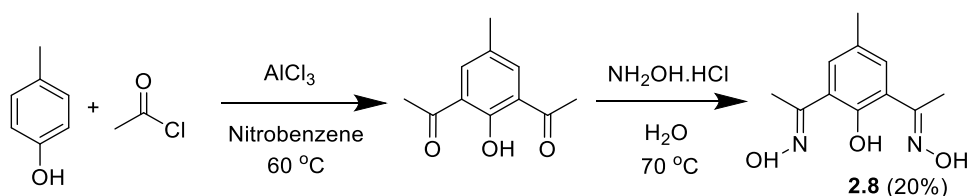
$\text{Fe}(\text{ClO}_4)_2$  (36 mg, 140  $\mu\text{mol}$ ) was added to a solution of 2,6-diformyl-4-tert-butyl-phenol dioxime (50 mg, 211  $\mu\text{mol}$ ) and 4-carboxybenzeneboronic acid (23.1 mg, 140  $\mu\text{mol}$ ) in MeOH (15 mL). Subsequently,  $\text{NEt}_4\text{OH}$  solution (200  $\mu\text{L}$ , 1.5 M in MeOH) was added and the mixture was heated to reflux for 2 h and then cooled to RT. The precipitates were isolated by filtration and washed with EtOH and diethyl ether to afford a black powder. *Yield*: 49 mg (89.5%). Despite all efforts, we were not able to obtain an MS spectrum for complex **2.5**. Single crystals were obtained by slow diffusion of pentane to a solution of complex **2.5** in THF.

#### Synthesis of complex **2.6**:



A solution of  $\text{Fe}(\text{OTf})_2$  (226 mg, 640  $\mu\text{mol}$ ) and  $\text{Fe}(\text{OTf})_3$  (321 mg, 640  $\mu\text{mol}$ ) in MeOH (10 mL) was added to a solution of 2,6-diformyl-4-bromo-phenol dioxime (500 mg, 1930  $\mu\text{mol}$ ) and 4-bromophenylboronic acid (258 mg, 1280  $\mu\text{mol}$ ) in MeOH (10 mL). Subsequently,  $\text{NEt}_4\text{OH}$  solution (400  $\mu\text{L}$ , 1.5 M in MeOH) was added and the mixture was heated to reflux for 2 h. After cooling to RT, the solvent was evaporated to dryness and the product was purified by a silica gel column chromatography (DCM) to obtain a black powder. *Yield*: 667 mg (86%) **HRMS-ESI** (positive mode):  $m/z$  calculated for  $\text{C}_{36}\text{H}_{20}\text{B}_2\text{Br}_5\text{Fe}_2\text{N}_6\text{O}_9$  [M]: 1212.6065; found: 1212.6074. **IR**: 1708, 1598, 1547, 1491, 1424, 1323, 1214, 1167, 1028, 986, 896, 780, 703, 637, 539. Single crystals were obtained by slow diffusion of  $\text{Et}_2\text{O}$  to a solution of complex **2.6** in DMF.

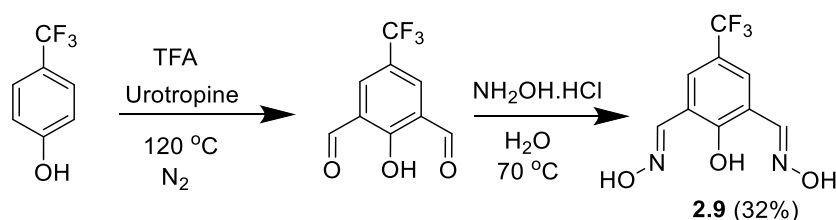
#### Synthesis of dioxime **2.8**:



4-Methylphenol (1 g, 9.5 mmol) was added to a solution of  $\text{AlCl}_3$  (1.9 g, 14.2 mmol) dissolved in nitrobenzene (30 mL). The resulting solution was cooled with an ice bath and acetyl chloride (1.5 g, 19 mmol) was added dropwise. Subsequently the temperature of the reaction mixture was raised to 60  $^\circ\text{C}$  and left to stir overnight. After completion, the reaction mixture was cooled with an ice bath and an ice cooled 6M HCl solution (40 mL) was added slowly, filtered and washed with toluene. The solvent was removed under reduced pressure and the

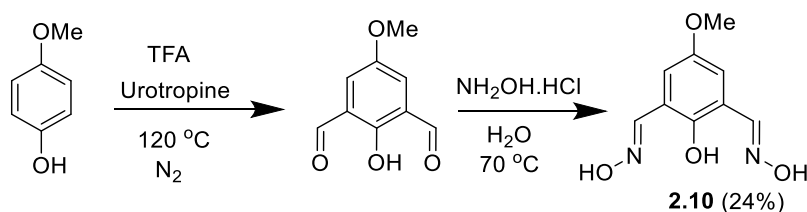
remaining brown solution was used without further purification. Hydroxylamine hydrochloride in large excess was added to a solution of crude compound 3.20 in water (30 mL) and left to stir at 70 for 3 h. The product was filtered and washed with water and dried over 2 days under vacuum to afford a white powder. Yield: 400 mg (20 %).  $^1\text{H NMR}$  (400 MHz, Chloroform-*d*)  $\delta$  2.25 (s, 3H,  $\text{CH}_3$ ), 2.60 (s, 6H,  $\text{CH}_3$ ), 7.70 (s, 2H, Ar-CH), 13.05 (s, 2H, OH);  $^{13}\text{C NMR}$  (DMSO-*d*<sub>6</sub>, 101 MHz, TMS)  $\delta$  13.39 ( $\text{CH}_3$ ), 20.55 ( $\text{CH}_3$ ), 122.93 (Ar-C), 127.30 (CCH<sub>3</sub>), 129.88 (Ar-CH), 153.72 (C-NOH), 156.53 (C-OH).

#### Synthesis of dioxime 2.9:



4-(Trifluoromethyl) phenol (1 g, 6.2 mmol) was added to a solution of urotropine (3.5 g, 24.8 mmol) in TFA (30 mL) and degassed. The reaction mixture was stirred at 120 °C under inert atmosphere for 48 h. the reaction was then cooled to room temperature and a H<sub>2</sub>SO<sub>4</sub> 50% (40 mL) was added. The solution was poured into H<sub>2</sub>O (200 mL) and the precipitates were isolated by filtration and washed with water (100 mL). The yellow precipitates were then dissolved in DCM and dried over MgSO<sub>4</sub>. Purification by column chromatography (DCM) afforded a yellow compound. Subsequently, the compound was suspended in water and a large excess of hydroxylamine hydrochloride was added and left to stir at 70 °C for 3 h. The product was filtered and washed with water and dried over 2 days under vacuum to afford a white powder. Yield: 500 mg (32%).  $^1\text{H NMR}$  (400 MHz, DMSO-*d*<sub>6</sub>)  $\delta$  8.4 (s, 2H, Ar-CH), 11.46 (s, H, OH), 11.67 (s, 2H, CHO), 12.90 (s, 2H, NOH);  $^{13}\text{C NMR}$  (DMSO-*d*<sub>6</sub>, 101 MHz, TMS)  $\delta$  119.93 (Ar-C), 122.81 (Ar-C(CF<sub>3</sub>)), 130.35 (CF<sub>3</sub>), 146.98 (Ar-CH), 158.18 (C-NOH), 166.80 (C-OH).

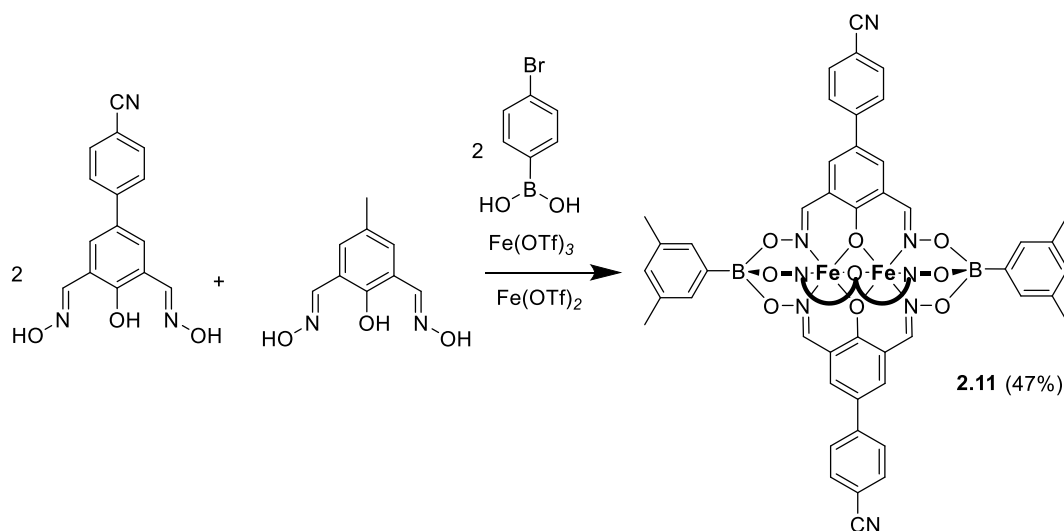
#### Synthesis of dioxime 2.10:



4-Methoxyphenol (1 g, 8.1 mmol) was added to a solution of urotropine (4.6 g, 32.4 mmol) in TFA (30 mL) and degassed. The reaction mixture was stirred at 120 °C under inert atmosphere for 48 h. the reaction was then cooled to room temperature and a H<sub>2</sub>SO<sub>4</sub> 50% (40 mL) was added. The solution was poured into H<sub>2</sub>O (200 mL) and the precipitates were isolated by filtration and washed with water (100 mL). The yellow precipitates were then dissolved in DCM and dried over MgSO<sub>4</sub>. Purification by column chromatography (DCM) afforded a yellow

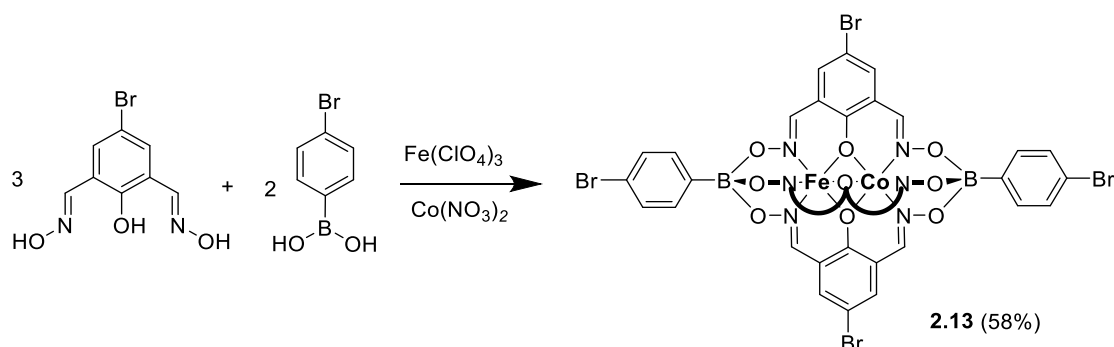
compound. Subsequently, the compound was suspended in water and a large excess of hydroxylamine hydrochloride was added and left to stir at 70 °C for 3 h. The product was filtered and washed with water and dried over 2 days under vacuum to afford a white powder. *Yield*: 400 mg (24%).  $^1\text{H NMR}$  (400 MHz, DMSO- $d_6$ )  $\delta$  3.77 (s, 3H,  $\text{CH}_3$ ), 7.19 (s, 2H, Ar-CH), 8.40 (s, 2H, CHO), 10.32 (s, H, OH), 11.57 (s, 2H, NOH);  $^{13}\text{C NMR}$  (DMSO- $d_6$ , 101 MHz, TMS)  $\delta$  55.92 ( $\text{CH}_3$ ), 114.10 (Ar-CH), 120.18 (Ar-C), 147.14 (-CH), 149.03 (C-OH), 152.46 (C-OMe).

#### Synthesis of complex **2.11**:



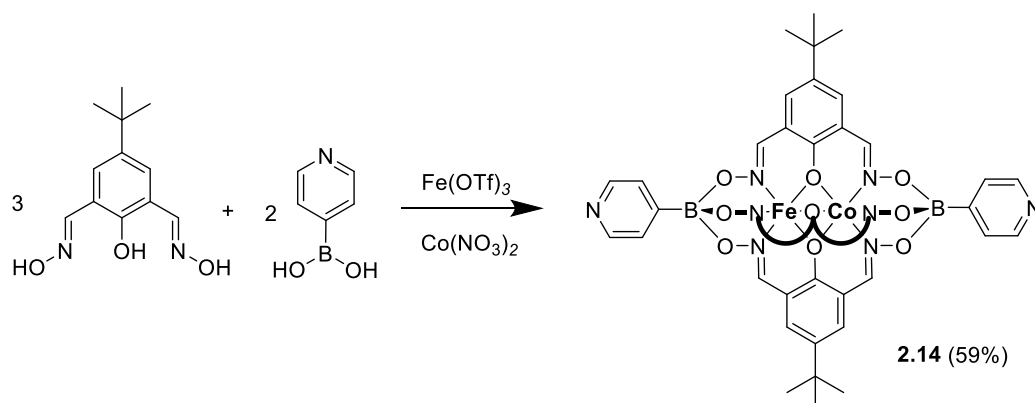
A solution of  $\text{Fe}(\text{OTf})_2$  (31.5 mg, 89  $\mu\text{mol}$ ) and  $\text{Fe}(\text{OTf})_3$  (44.8 mg, 89  $\mu\text{mol}$ ) in MeOH (10 mL) was added to a solution of 2,6-diformyl-4-methyl-phenol dioxime (17.3 mg, 89  $\mu\text{mol}$ ), 2,6-diformyl-4-cyanophenyl-phenol dioxime (50 mg, 178  $\mu\text{mol}$ ) and 3,5-dimethylphenylboronic acid (26.2 mg, 178  $\mu\text{mol}$ ) in MeOH (10 mL). Subsequently,  $\text{NEt}_4\text{OH}$  solution (400  $\mu\text{L}$ , 1.5 M in MeOH) was added and the mixture was heated to reflux for 2 h and then cooled to RT. The solvent was evaporated to dryness and the product was purified by a silica gel column chromatography (DCM) to obtain a black powder. *Yield*: 49.5 mg (47%) Despite all efforts, we were not able to obtain an MS spectrum for complex **2.11**. Single crystals were obtained by slow diffusion of pentane to a solution of complex **2.11** in DCM.

#### Synthesis of complex **2.13**:



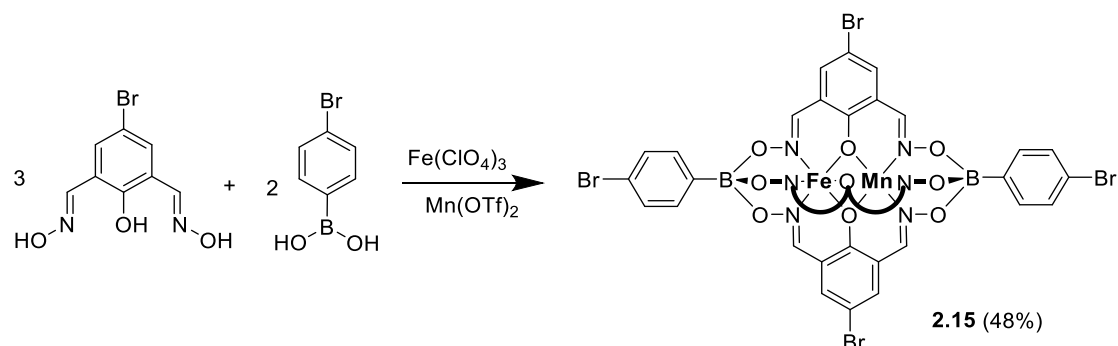
$\text{Fe}(\text{ClO}_4)_3$  (45.3 mg, 128  $\mu\text{mol}$ ) and  $\text{Co}(\text{NO}_3)_2 \cdot 6\text{H}_2\text{O}$  (37.4 mg, 128  $\mu\text{mol}$ ) were added to a solution of 2,6-diformyl-4-bromo-phenol dioxime (100 mg, 386  $\mu\text{mol}$ ) and 4-bromophenylboronic acid (51.5 mg, 257  $\mu\text{mol}$ ) in MeOH (20 mL). Subsequently,  $\text{NEt}_4\text{OH}$  solution (400  $\mu\text{L}$ , 1.5 M in MeOH) was added and the mixture was heated to reflux for 2 h and then cooled to RT. The product was concentrated under reduced pressure and purified by flash column chromatography with DCM as eluent to afford a brown product. *Yield*: 58 mg (58%). **HRMS-ESI** (negative mode):  $m/z$  calculated for  $\text{C}_{36}\text{H}_{20}\text{B}_2\text{Br}_5\text{FeCoN}_6\text{O}_9$   $[\text{M}]^-$ : 1211.6076; found: 1211.611. **IR**: 1587.1, 1553.4, 1480.5, 1436, 1381.7, 1293.3, 1204.8, 1093, 1048.8, 1009.3, 973, 934, 887.59, 786.7, 759.3, 702.96, 671.17, 559.9, 536.5, 510.5. Single crystals were obtained by slow diffusion of pentane to a solution of complex **2.13** in DCM.

#### Synthesis of complex **2.14**:

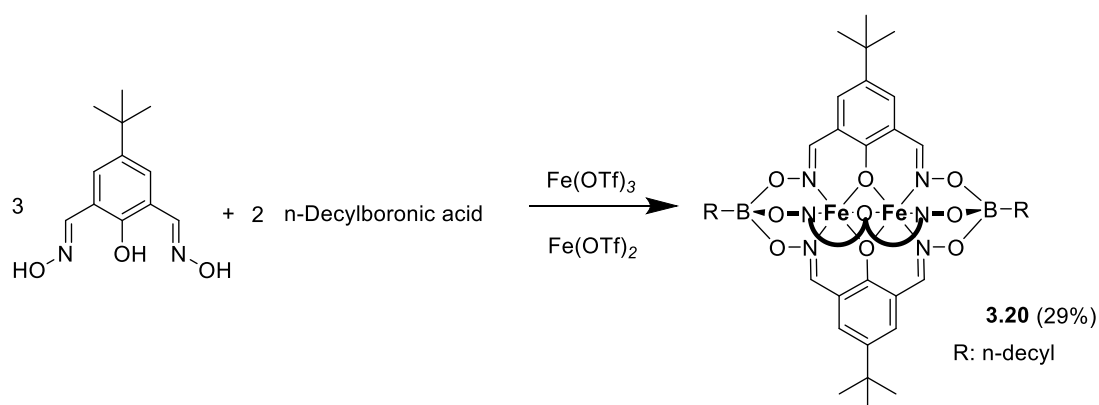


$\text{Fe}(\text{OTf})_3$  (14 mg, 28  $\mu\text{mol}$ ) and  $\text{Co}(\text{NO}_3)_2 \cdot 6\text{H}_2\text{O}$  (8.2 mg, 28  $\mu\text{mol}$ ) were added to a solution of 2,6-diformyl-4-tert-butyl-phenol dioxime (20 mg, 85  $\mu\text{mol}$ ) and 4-pyridylboronic acid (6.9 mg, 56  $\mu\text{mol}$ ) in MeOH (20 mL). Subsequently,  $\text{NEt}_4\text{OH}$  solution (400  $\mu\text{L}$ , 1.5 M in MeOH) was added and the mixture was heated to reflux for 2 h and then cooled to RT. The product was concentrated under reduced pressure and purified by flash column chromatography with DCM:MeOH (95:5) as eluent to afford a brown product. *Yield*: 12.5 mg (59%). **HRMS-ESI** (negative mode):  $m/z$  calculated for  $\text{C}_{46}\text{H}_{47}\text{B}_2\text{FeCoN}_8\text{O}_9$   $[\text{M}]^-$ : 992.2333; found: 992.2678. **IR**: 1592.3, 1553.6, 1436, 1379, 1298.5, 1204.8, 1093, 1046.2, 1009.9, 970.8, 937, 890.2, 786.2, 759.9, 760.2, 700.35, 671.8, 567.73, 536.5, 507.9. Single crystals were obtained by slow diffusion of pentane to a solution of complex **2.14** in DMF: $\text{CHCl}_3$  (1:1).



**Synthesis of complex 2.15:**

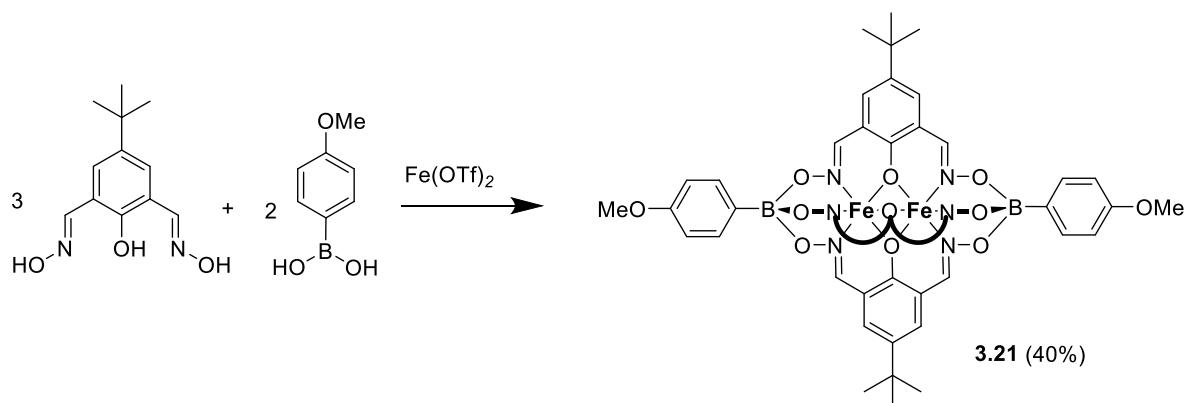
$\text{Fe}(\text{ClO}_4)_3$  (45.3 mg, 128  $\mu\text{mol}$ ) and  $\text{Mn}(\text{OTf})_2$  (45 mg, 128  $\mu\text{mol}$ ) were added to a solution of 2,6-diformyl-4-bromo-phenol dioxime (100 mg, 386  $\mu\text{mol}$ ) and 4-bromophenylboronic acid (51.5 mg, 257  $\mu\text{mol}$ ) in MeOH (20 mL). Subsequently,  $\text{NEt}_4\text{OH}$  solution (400  $\mu\text{L}$ , 1.5 M in MeOH) was added and the mixture was heated to reflux for 2 h and then cooled to RT. The product was concentrated under reduced pressure and purified by flash column chromatography with DCM as eluent to afford a black product. *Yield*: 48 mg (48%). **HRMS-ESI** (negative mode):  $m/z$  calculated for  $\text{C}_{36}\text{H}_{20}\text{B}_2\text{Br}_5\text{FeMnN}_6\text{O}_9$   $[\text{M}]^-$ : 1207.6125; found: 1207.9224 **IR**: 1595, 1561.1, 1441.5, 1376.5, 1301, 1202.2, 1095.6, 1048.8, 1009.7, 976, 932.2, 892.8, 791.4, 759.3, 702.9, 671.8, 539.1, 507.9. Single crystals were obtained by slow diffusion of pentane to a solution of complex **2.15** in DCM.

**7.1.2 Experimental procedures for chapter 3****Synthesis of complex 3.20:**

$\text{Fe}(\text{OTf})_2$  (99.6 mg, 280  $\mu\text{mol}$ ) and  $\text{Fe}(\text{OTf})_3$  (140 mg, 280  $\mu\text{mol}$ ) was added to a solution of 2,6-di-tert-butyl-phenol dioxime (200 mg, 840  $\mu\text{mol}$ ) and n-decylboronic acid (119 mg, 555  $\mu\text{mol}$ ) in MeOH (20 mL). The reaction mixture was stirred at 50  $^\circ\text{C}$  for 1 h and then cooled to RT. The product was concentrated under reduced pressure and subjected to a flash column chromatography with DCM:MeOH (95:5) as eluent to afford a black product. *Yield*: 76 mg (29%). **HRMS-APPI** (negative mode):  $m/z$  calculated for  $\text{C}_{56}\text{H}_{81}\text{B}_2\text{Fe}_2\text{N}_6\text{O}_9$   $[\text{M}]^-$ : 1115.4950;

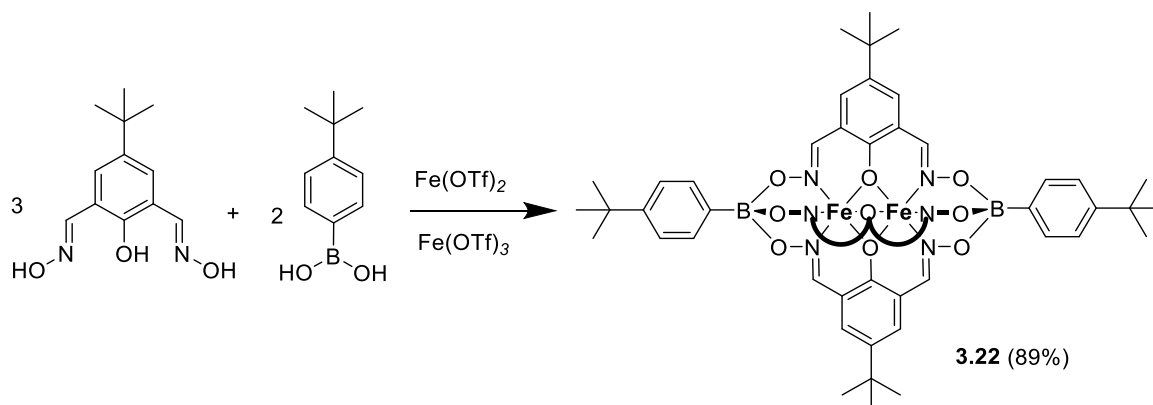
found: 1115.4995. IR: 2921, 2849.3, 1606.5, 1455.3, 1308.7, 1254.4, 1226, 1176, 1072.3, 1034.5, 1003.8, 916.31, 843.03, 791.02, 762.65, 715.74, 700.12635.34, 515.72, 455.1.

### Synthesis of complex 3.21:



$\text{Fe}(\text{OTf})_2$  (24.7 mg, 70  $\mu\text{mol}$ ) and  $\text{Fe}(\text{OTf})_3$  (35.2 mg, 70  $\mu\text{mol}$ ) was added to a solution of 2,6-diformyl-4-tertbutylphenol dioxime (50 mg, 210  $\mu\text{mol}$ ) and 4-methoxyphenylboronic acid (25 mg, 140  $\mu\text{mol}$ ) in MeOH (20 mL). The reaction mixture was stirred at 50 °C for 1 h and then cooled to RT. The product was concentrated under reduced pressure and subjected to a flash column chromatography with DCM:MeOH (95:5) as eluent to afford a black product. Yield: 31.6 mg (40%). HRMS-APPI (negative mode):  $m/z$  calculated for  $\text{C}_{50}\text{H}_{56}\text{B}_2\text{Fe}_2\text{N}_6\text{O}_{11}$  [ $\text{M}+3\text{H}$ ] $^-$ : 1050.2892; found: 1050.2459. IR: 2957, 1604.7, 1592.3, 1577.4, 1506.5, 1451.9, 1394.7, 1368.7, 1311.5, 1282.9, 1223, 1207.3, 1172, 1100.8, 1043.6, 1000.3, 981.2, 939.6, 921.4, 845.9, 825.2, 793.97, 761.2, 695.1, 648.3, 585.9, 544.3, 528.7, 463.7.

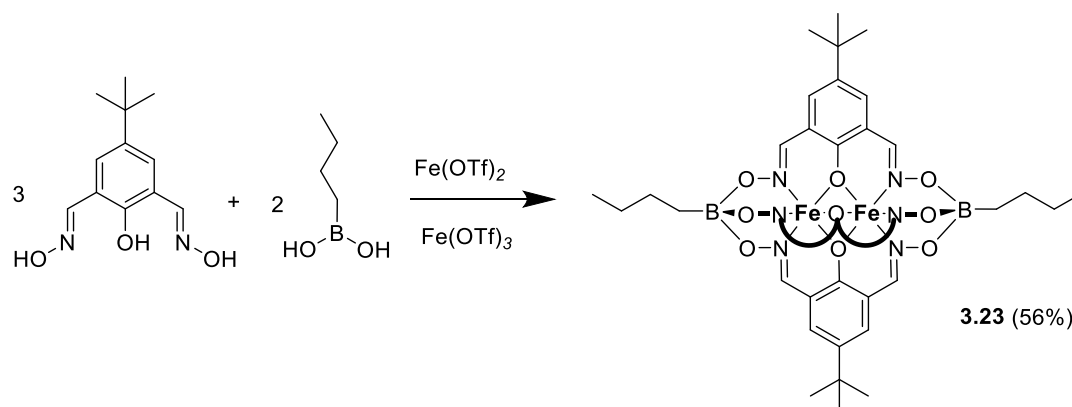
### Synthesis of complex 3.22:



$\text{Fe}(\text{OTf})_2$  (24.7 mg, 70  $\mu\text{mol}$ ) and  $\text{Fe}(\text{OTf})_3$  (35.2 mg, 70  $\mu\text{mol}$ ) was added to a solution of 2,6-diformyl-4-tertbutylphenol dioxime (50 mg, 210  $\mu\text{mol}$ ) and 4-tertbutylphenylboronic acid (24.9 mg, 140  $\mu\text{mol}$ ) in MeOH (20 mL). The reaction mixture was stirred at 50 °C for 1 h and then cooled to RT. The product was concentrated

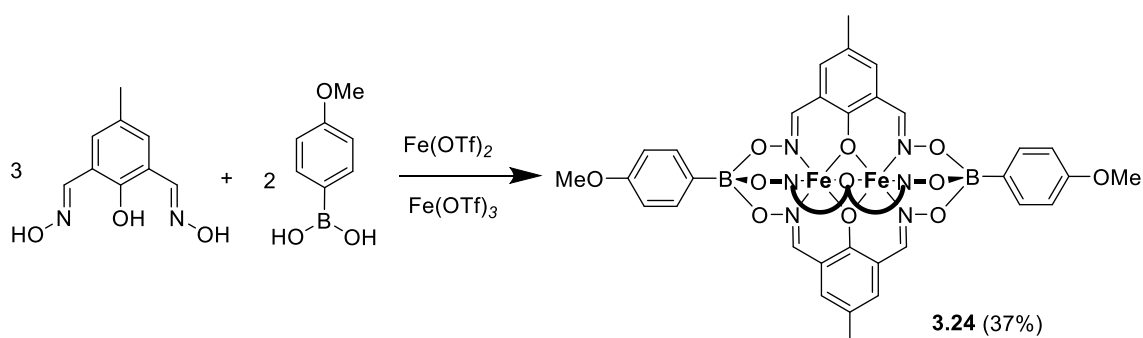
under reduced pressure and subjected to a flash column chromatography with DCM:MeOH (95:5) as eluent to afford a black product. *Yield*: 68 mg (85%). **HRMS-APPI** (negative mode): *m/z* calculated for  $C_{56}H_{65}B_2Fe_2N_6O_9 [M]^-$ : 1099.3698; found: 1099.3672. **IR**: 1607.7, 1576.7, 1454.5, 1394.6, 1309.5, 12779.3, 1230.9, 1215.2, 1100.4, 1048.8, 1007.2, 983.8, 937, 845.98, 796.57, 760, 723.76, 567.89, 531.32, 474.11.

#### Synthesis of complex 3.23:



$Fe(OTf)_2$  (248.9 mg, 705  $\mu$ mol) and  $Fe(OTf)_3$  (354.6 mg, 70  $\mu$ mol) was added to a solution of 2,6-diformyl-4-tertbutylphenol dioxime (500 mg, 2.12 mmol) and n-butylboronic acid (144 mg, 1.4 mmol) in MeOH (50 mL). The reaction mixture was stirred at 50 °C for 1 h and then cooled to RT. The product was concentrated under reduced pressure and subjected to a flash column chromatography with DCM:MeOH (95:5) as eluent to afford a black product. *Yield*: 404 mg (56%). **HRMS-APPI** (negative mode): *m/z* calculated for  $C_{44}H_{57}B_2Fe_2N_6O_9 [M]^-$ : 947.3072; found: 947.3389. **IR**: 1610.5, 1579.3, 1449.3, 1393.7, 1306, 1259.5, 1228.3, 1173.6, 1106, 1030.6, 939.6, 832.87, 767.97, 721.16, 630.14, 515.7

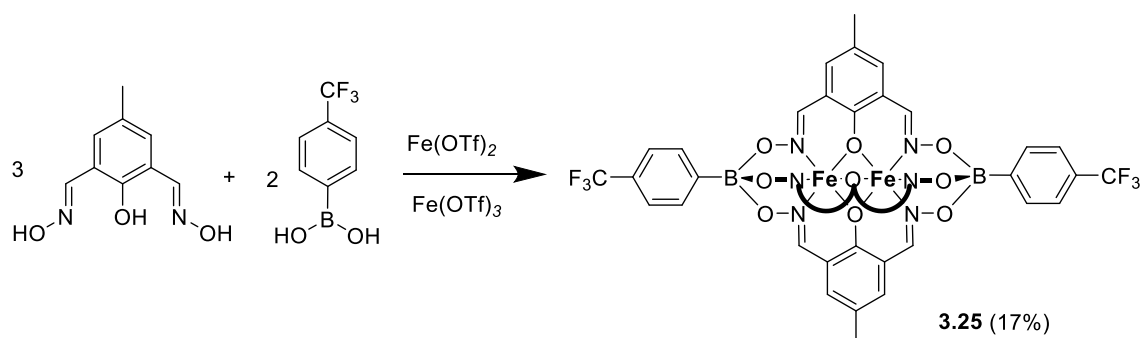
#### Synthesis of complex 3.24:



$Fe(OTf)_2$  (30.3 mg, 86  $\mu$ mol) and  $Fe(OTf)_3$  (43 mg, 86  $\mu$ mol) was added to a solution of 2,6-diformyl-4-methylphenol dioxime (50 mg, 257  $\mu$ mol) and 4-methoxyphenylboronic acid (30.6 mg, 172  $\mu$ mol) in MeOH (20 mL). The reaction mixture was stirred at 50 °C for 1 h and then cooled to RT. The product was concentrated under reduced pressure and subjected to a flash column chromatography with DCM:MeOH (95:5) as eluent to afford a black

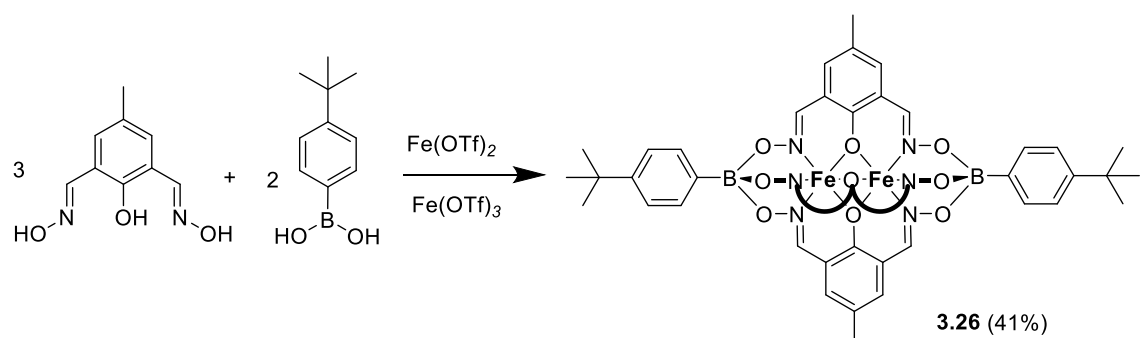
product. *Yield*: 35.6 mg (37%). **HRMS-APPI** (negative mode):  $m/z$  calculated for  $C_{41}H_{34}B_2Br_3Fe_2N_6O_{11}$   $[M]^-$ : 920.1170; found: 920.1133. **IR**: 1595, 1579.2, 1506.5, 1449.3, 1306.3, 1280.3, 1207.4, 1174.1, 1103.4, 1046.2, 1007.2, 944.8, 937, 832.98, 765.4, 684.75, 588.3, 549.53, 513.1.

#### Synthesis of complex 3.25:



$Fe(OTf)_2$  (30.3 mg, 86  $\mu$ mol) and  $Fe(OTf)_3$  (43 mg, 86  $\mu$ mol) was added to a solution of 2,6-diformyl-4-methylphenol dioxime (50 mg, 257  $\mu$ mol) and 4-(Trifluoromethyl)phenylboronic acid (32.7 mg, 172  $\mu$ mol) in MeOH (20 mL). The reaction mixture was stirred at 50 °C for 1 h and then cooled to RT. The product was concentrated under reduced pressure and subjected to a flash column chromatography with DCM:MeOH (95:5) as eluent to afford a black product. *Yield*: 16.3 mg (17%). **HRMS-ESI** (positive mode):  $m/z$  calculated for  $C_{42}H_{29}B_2F_6Fe_2N_6O_9$   $[M+H]^+$ : 998.0863; found: 998.0857. **IR**: 1613.1, 1594.6, 1582, 1451.9, 1321.9, 1306.3, 1262, 1233.5, 1202.2, 1176.2, 1113.8, 1048.8, 1010, 950, 929.2, 832.9, 762.8, 640.6, 541.7, 518.3, 430.13.

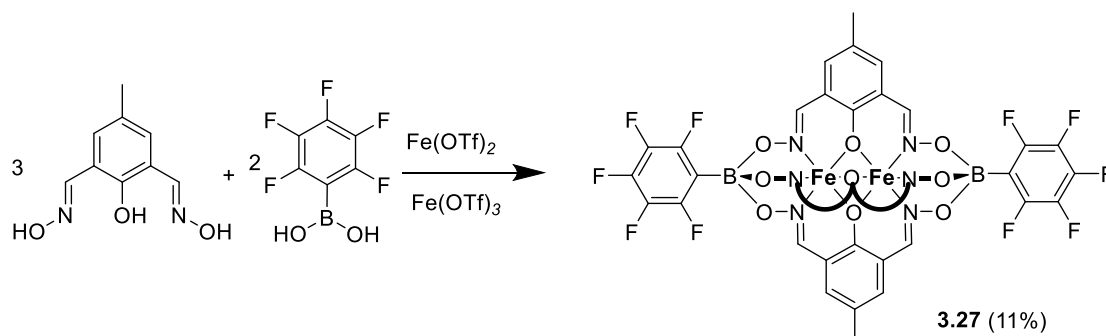
#### Synthesis of complex 3.26:



$Fe(OTf)_2$  (30.3 mg, 86  $\mu$ mol) and  $Fe(OTf)_3$  (43 mg, 86  $\mu$ mol) was added to a solution of 2,6-diformyl-4-methylphenol dioxime (50 mg, 257  $\mu$ mol) and 4-tertbutylphenylboronic acid (30.6 mg, 172  $\mu$ mol) in MeOH (20 mL). The reaction mixture was stirred at 50 °C for 1 h and then cooled to RT. The product was concentrated under reduced pressure and subjected to a flash column chromatography with DCM:MeOH (95:5) as eluent to afford a black product. *Yield*: 39.6 mg (41%). **HRMS-APPI** (negative mode):  $m/z$  calculated for  $C_{47}H_{46}B_2Fe_2N_6O_9$   $[M]^-$ : 972.2211;

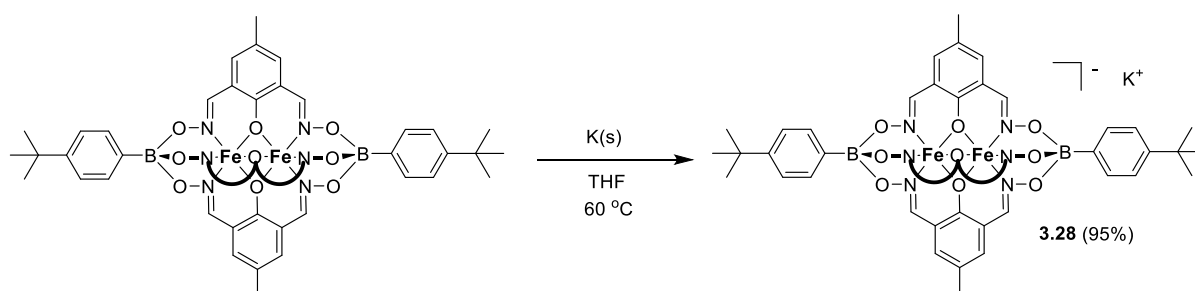
found: 972.2196. **IR:** 1610.5, 1579.3, 1449.3, 1393.7, 1306, 1259.5, 1228.3, 1173.6, 1106, 1030.6, 939.6, 832.87, 767.97, 721.16, 630.14, 515.7.

### Synthesis of complex 3.27:

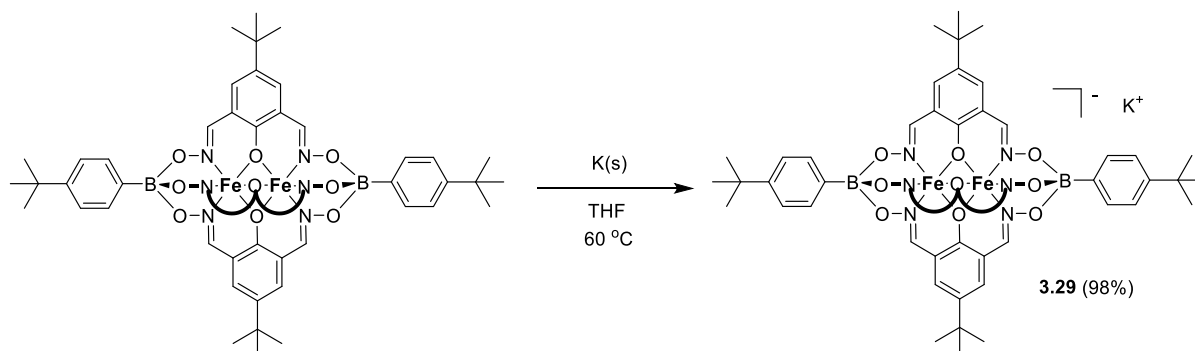


$\text{Fe}(\text{OTf})_2$  (30.3 mg, 86  $\mu\text{mol}$ ) and  $\text{Fe}(\text{OTf})_3$  (43 mg, 86  $\mu\text{mol}$ ) was added to a solution of 2,6-diformyl-4-methylphenol dioxime (50 mg, 257  $\mu\text{mol}$ ) and 4-pentafluorophenylboronic acid (36.4 mg, 172  $\mu\text{mol}$ ) in MeOH (20 mL). The reaction mixture was stirred at 50 °C for 1 h and then cooled to RT. The product was concentrated under reduced pressure and subjected to a flash column chromatography with DCM:MeOH (95:5) as eluent to afford a black product. *Yield:* 9.6 mg (11%). **HRMS-ESI** (negative mode):  $m/z$  calculated for  $\text{C}_{39}\text{H}_{21}\text{B}_2\text{F}_{10}\text{Fe}_2\text{N}_6\text{O}_9$   $[\text{M}]^-$ : 1041.0095; found: 1041.0392. **IR:** 1641.2, 1613, 1595.7, 1584.5, 1515.3, 1464.9, 1381.7, 1308.9, 1288, 1230.9, 1186.6, 1103.4, 1054, 1015, 955, 869.4, 864.2, 835.6, 767.9, 732.4, 536.6, 515.7.

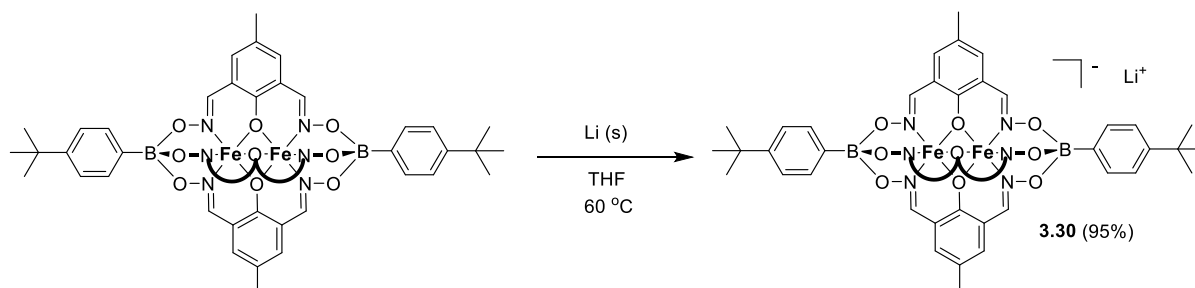
### Synthesis of complex 3.28:



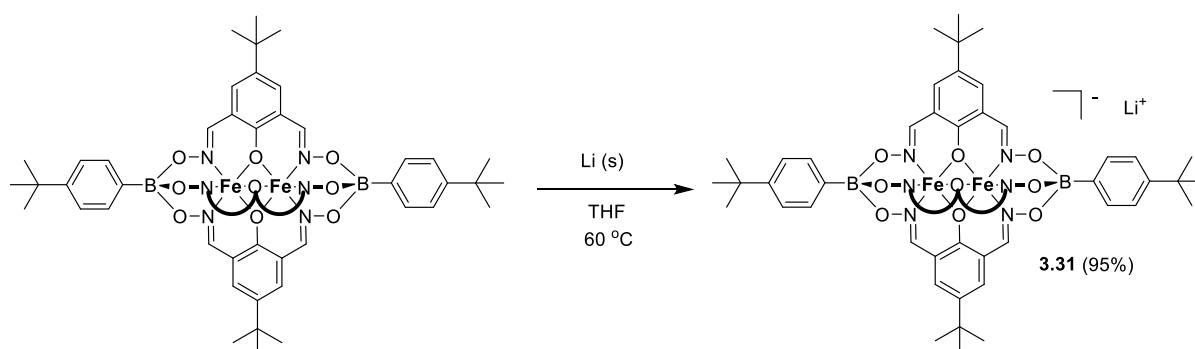
Potassium (4 mg, 102  $\mu\text{mol}$ ) was added to a solution of complex **3.26** (100 mg, 102  $\mu\text{mol}$ ) in THF in the glovebox. The reaction mixture was left to stir for overnight at 50 °C then cooled to RT. The resulting brown solution was filtered and the solvent was removed under reduced pressure to yield a brown powder. *Yield:* 99 mg (95%). **HRMS-ESI** (positive mode):  $m/z$  calculated for  $\text{C}_{47}\text{H}_{47}\text{B}_2\text{Fe}_2\text{N}_6\text{O}_9$   $[\text{M}]^+$ : 973.2289; found: 973.2330.

**Synthesis of complex 3.29:**

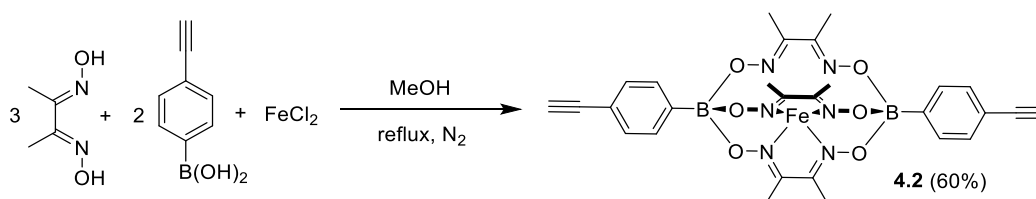
Potassium (3.56 mg, 90  $\mu$ mol) was added to a solution of complex **3.22** (100 mg, 90  $\mu$ mol) in THF in the glovebox. The reaction mixture was left to stir for overnight at 50 °C then cooled to RT. The resulting brown solution was filtered and the solvent was removed under reduced pressure to yield a brown powder. *Yield*: 102 mg (98%). **HRMS-ESI** (negative mode): *m/z* calculated for  $C_{56}H_{65}B_2Fe_2N_6O_9$  [M] $^-$ : 1099.3703; found: 1099.3750.

**Synthesis of complex 3.30:**

Lithium (1.43 mg, 205  $\mu$ mol) was added to a solution of complex **3.26** (100 mg, 102  $\mu$ mol) in THF in the glovebox. The reaction mixture was left to stir for overnight at 50 °C then cooled to RT. The resulting brown solution was filtered and the solvent was removed under reduced pressure to yield a brown powder. *Yield*: 96 mg (95%). **HRMS-ESI** (positive mode): *m/z* calculated for  $C_{47}H_{47}B_2Fe_2N_6O_9$  [M] $^+$ : 973.2289; found: 973.2330.

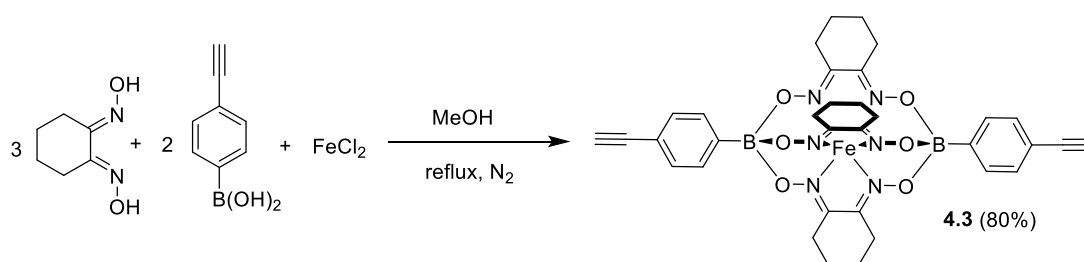
**Synthesis of complex 3.31:**

Lithium (1.26 mg, 181  $\mu\text{mol}$ ) was added to a solution of complex **3.22** (100 mg, 90  $\mu\text{mol}$ ) in THF in the glovebox. The reaction mixture was left to stir for overnight at 50  $^{\circ}\text{C}$  then cooled to RT. The resulting brown solution was filtered and the solvent was removed under reduced pressure to yield a brown powder. *Yield*: 96 mg (95%). **HRMS-ESI** (positive mode):  $m/z$  calculated for  $\text{C}_{56}\text{H}_{65}\text{B}_2\text{Fe}_2\text{N}_6\text{O}_9$   $[\text{M}+2\text{H}]^+$ : 1101.3849; found: 1101.3844.

**7.1.3 Experimental procedures for chapter 4****Synthesis of complex 4.2:**

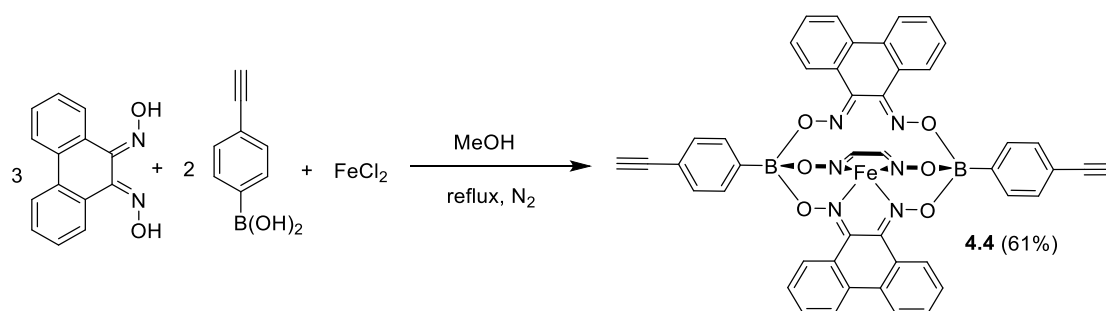
Dimethylglyoxime (59.6 mg, 0.51 mmol), 4-ethynylphenylboronic acid (50 mg, 0.34 mmol), and anhydrous  $\text{FeCl}_2$  (21.7 mg, 0.17 mmol) were dissolved in MeOH (15 mL) and heated under reflux under an inert atmosphere for 3 h. The reaction mixture was allowed to cool to RT, and the resulting precipitates were isolated by filtration, washed with MeOH and diethyl ether, and dried under vacuum to yield a brown powder (63 mg, 60%).  **$^1\text{H}$  NMR** ( $\text{CDCl}_3$ , 400 MHz, TMS)  $\delta$  2.35 (s, 18H,  $\text{CH}_3$ ), 2.99 (s, 2H,  $\text{CH}$ ), 7.43 (d,  $J = 8.0$  Hz, 4H, Ar-CH), 7.63 (d,  $J = 8.0$  Hz, 4H, Ar-CH);  **$^{13}\text{C}$  NMR** ( $\text{CDCl}_3$ , 101 MHz, TMS)  $\delta$  13.4 ( $\text{CH}_3$ ), 76.5 ( $\text{C}\equiv\text{CH}$ ), 84.7 ( $\text{C}\equiv\text{CH}$ ), 121.3 ( $\text{C}(\text{C}\equiv\text{CH})$ ), 131.2 (Ar-CH), 131.6 (Ar-CH), 152.2 (N-C), (C-B not detected); **HRMS-ESI** (positive mode):  $m/z$  calculated for  $\text{C}_{28}\text{H}_{28}\text{B}_2\text{FeN}_6\text{O}_6$   $[\text{M}+\text{H}]^+$  622.1605; found: 622.1662.

**Synthesis of complex 4.3:**



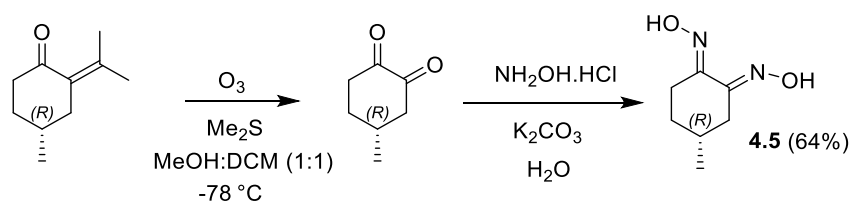
Nioxime (73 mg, 0.51 mmol), 4-ethynylphenylboronic acid (50 mg, 0.34 mmol), and anhydrous  $\text{FeCl}_2$  (21.7 mg, 0.17 mmol) were dissolved in MeOH (15 mL) and heated under reflux under an inert atmosphere for 3 h. The reaction mixture was allowed to cool to RT, and the resulting precipitates were isolated by filtration, washed with MeOH and diethyl ether, and dried under vacuum to yield a brown powder (96 mg, 80%).  $^1\text{H NMR}$  ( $\text{CDCl}_3$ , 400 MHz, TMS)  $\delta$  1.73 (s, 12H,  $\text{CH}_2$ ), 2.86 (s, 12H,  $\text{CH}_2$ ), 2.98 (s, 2H,  $\text{CH}$ ), 7.41 (d,  $J = 8.0$  Hz, 4H, Ar-CH), 7.59 (d,  $J = 8.0$  Hz, 4H, Ar-CH);  $^{13}\text{C NMR}$  ( $\text{CDCl}_3$ , 101 MHz, TMS)  $\delta$  21.6 ( $\text{CH}_2$ ), 26.3 ( $\text{CH}_2$ ), 76.4 ( $\text{CH}$ ), 84.7 ( $\text{C}\equiv\text{CH}$ ), 121.2 ( $\text{C}(\text{C}\equiv\text{CH})$ ), 131.1 (Ar-CH), 131.6 (Ar-CH), 151 (N-C), (C-B not detected); **HRMS-APPI** (positive mode):  $m/z$  calculated for  $\text{C}_{34}\text{H}_{35}\text{B}_2\text{FeN}_6\text{O}_6$   $[\text{M}+\text{H}]^+$  701.2148; found: 701.2118.

#### Synthesis of complex 4.4:



Phenanthrenequinone dioxime (122 mg, 0.51 mmol), 4-ethynylphenylboronic acid (50 mg, 0.34 mmol), and anhydrous  $\text{FeCl}_2$  (21.7 mg, 0.17 mmol) were dissolved in MeOH (15 mL) and heated under reflux under an inert atmosphere for 3 h. The reaction mixture was allowed to cool to RT, and the resulting precipitates were isolated by filtration, washed with MeOH and diethyl ether, and dried under vacuum to yield a purple powder (89 mg, 61%).  $^1\text{H NMR}$  ( $\text{CDCl}_3$ , 400 MHz, TMS)  $\delta$  3.30 (s, 2H,  $\text{CH}$ ), 7.51 – 9.73 (m, 32 H, Ar-CH); Despite all efforts, we were not able to obtain an MS spectrum for complex **4.4**.

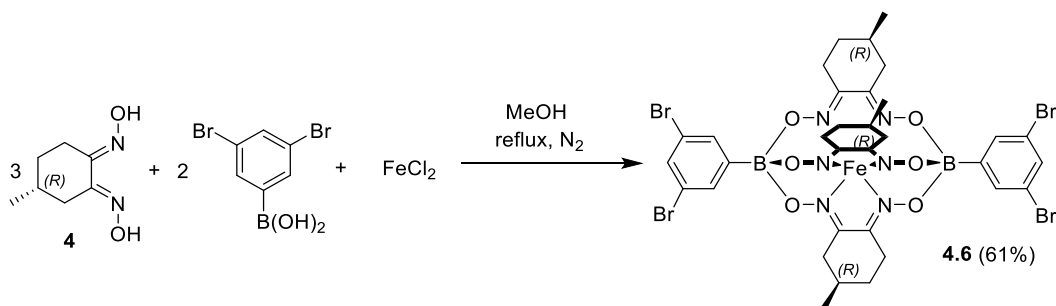
#### Synthesis of dioxime 4.5:





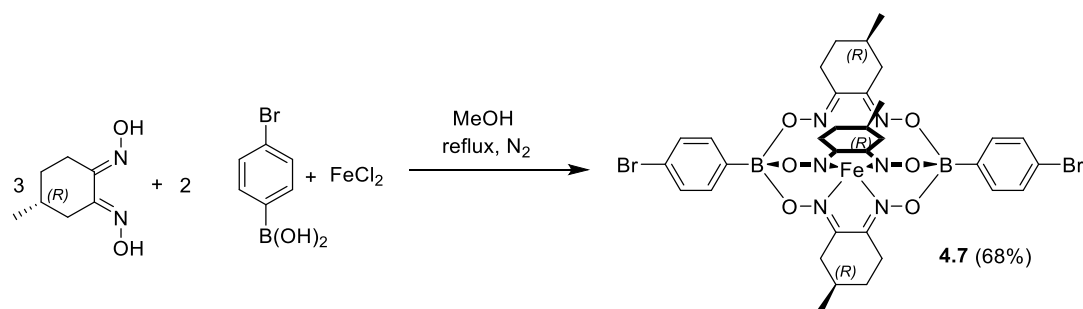
(R)-(+)- Pulegone (2.0 g, 0.013 mol) was dissolved in a mixture of MeOH and DCM (1:1, 20 mL) and cooled to  $-78^{\circ}\text{C}$ . Ozone was added, and the mixture was stirred until the solution became blue. The system was purged with  $\text{N}_2$  for 5 min until the blue color disappeared. Subsequently,  $\text{Me}_2\text{S}$  (5 mL) was added slowly at  $-78^{\circ}\text{C}$ . The reaction mixture was left to warm to RT, followed by stirring for additional 3 h. The solvent was removed to dryness, and the product was filtered through a silica pad and the pad was washed with a mixture of hexane and  $\text{Et}_2\text{O}$  (1:1, 50 mL). The solvent was removed under vacuum and the product was used without further purification. A mixture of  $[\text{NH}_3\text{OH}]\text{Cl}$  (18.2 g, 0.26 mol) and  $\text{K}_2\text{CO}_3$  (26.9 g, 0.19 mol) in distilled water (50 mL) was added to the crude diketone, and the mixture was stirred overnight at RT. The solution was placed in a fridge ( $4^{\circ}\text{C}$ ). After 12 h, the resulting precipitates were isolated by filtration, washed with water (300 mL), and dried under vacuum overnight to give a light pink powder (1.31 g, 64 %).  $^1\text{H NMR}$  ( $\text{DMSO}-d_6$ , 400 MHz, TMS)  $\delta$  1.01 (d,  $J = 6.5$  Hz, 3H,  $\text{CH}_3$ ), 1.28 – 1.13 (m, 1H, CH), 1.80 – 1.62 (m, 2H,  $\text{CCH}_2\text{CH}_2$ ), 1.92 (dd,  $J = 17.1, 11.0$  Hz, 1H,  $\text{CCH}_2\text{CH}_2$ ), 2.29 (ddd,  $J = 17.8, 11.9, 6.2$  Hz, 1H,  $-\text{CCH}_2\text{CH}_2$ ), 2.85 (dddd,  $J = 23.6, 17.6, 5.3, 2.7$  Hz, 2H,  $\text{CCH}_2$ ), 11.21 (s, 2H, OH);  $^{13}\text{C NMR}$  ( $\text{DMSO}-d_6$ , 101 MHz, TMS)  $\delta$  21.8 ( $\text{CH}_3$ ), 24.2 ( $\text{CCH}_2\text{CH}_2$ ), 28.9 ( $\text{CCH}_2\text{CH}_2$ ), 30.3 (CH), 33.3 ( $\text{CCH}_2$ ), 152.2 (N-C); HRMS (ESI TOF)  $m/z$  calcd for  $\text{C}_7\text{H}_{13}\text{N}_2\text{O}_2$   $[\text{M}-\text{H}]^+$  157.0972, found 157.0977.

#### Synthesis of complex 4.6:



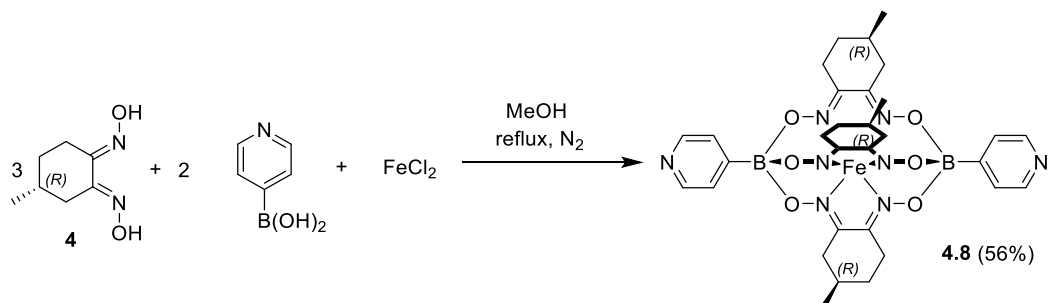
Compound 4.5 (50 mg, 0.32 mmol), 3,5-dibromobenzenboronic acid (61.5 mg, 0.22 mmol), and anhydrous  $\text{FeCl}_2$  (13.4 mg, 0.11 mmol) were dissolved in MeOH (15 mL) and heated under reflux under an inert atmosphere for 3 h. The reaction mixture was allowed to cool to RT, and the resulting precipitates were isolated by filtration, washed with MeOH and diethyl ether, and dried under vacuum to yield a brown powder (107 mg, 61%).  $^1\text{H NMR}$  (400 MHz,  $\text{Chloroform}-d$ )  $\delta$  1.04 (d,  $J = 6.4$  Hz, 9H,  $\text{CH}_3$ ), 1.37 (tq,  $J = 12.5, 5.4$  Hz, 3H, CH), 1.84 (s, 6H,  $\text{CCH}_2\text{CH}_2$ ), 2.27 (dd,  $J = 18.8, 10.7$  Hz, 3H,  $\text{CCH}_2\text{CH}_2$ ), 2.66 (ddd,  $J = 18.7, 11.6, 6.1$  Hz, 3H,  $-\text{CCH}_2\text{CH}_2$ ), 3.18 – 3.04 (m, 4H,  $\text{CCH}_2$ ), 7.54 (q,  $J = 1.9$  Hz, 2H, Ar-CH), 7.63 (p,  $J = 1.7$  Hz, 4H, Ar-CH);  $^{13}\text{C NMR}$  ( $\text{CDCl}_3$ , 101 MHz, TMS)  $\delta$  21.1 ( $\text{CH}_3$ ), 25.5 (CH), 28.5 ( $\text{CCH}_2\text{CH}_2$ ), 29.6 ( $\text{CCH}_2\text{CH}_2$ ), 34.1 ( $\text{CCH}_2$ ), 122.6 (C-Br), 133.2 (Ar-CH), 152.2 (N-C), 152.5 (N-C), (C-B not detected). All attempts to record a HRMS failed.

#### Synthesis of complex 4.7:



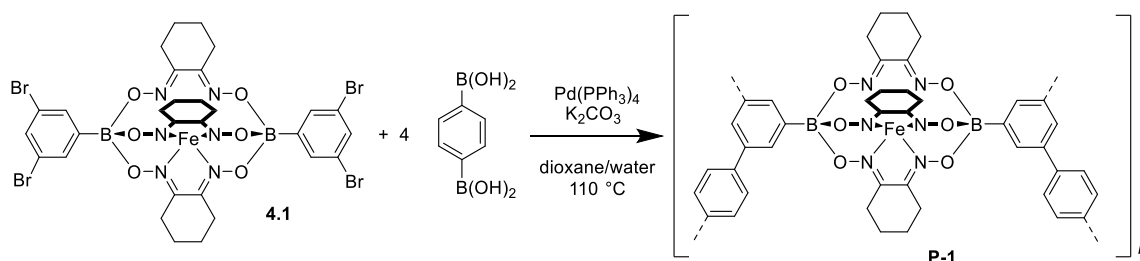
Compound **4.5** (50 mg, 0.32 mmol), 4-bromophenylboronic acid (44.2 mg, 0.22 mmol), and anhydrous  $\text{FeCl}_2$  (13.4 mg, 0.11 mmol) were dissolved in MeOH (15 mL) and heated under reflux under an inert atmosphere for 3 h. The reaction mixture was allowed to cool to RT, and the resulting precipitates were isolated by filtration, washed with MeOH and diethyl ether, and dried under vacuum to yield a brown powder (62 mg, 68%).  $^1\text{H NMR}$  (400 MHz,  $\text{CDCl}_3$ )  $\delta$  1.02 (d,  $J = 6.4$  Hz, 9H,  $\text{CH}_3$ ), 1.37 (tq,  $J = 12.5, 5.4$  Hz, 3H,  $\text{CH}$ ), 1.46 (s, 6H,  $\text{CCH}_2\text{CH}_2$ ), 2.26 (dd,  $J = 18.8, 10.7$  Hz, 3H,  $\text{CCH}_2\text{CH}_2$ ), 2.66 (ddd,  $J = 18.7, 11.6, 6.1$  Hz, 3H,  $-\text{CCH}_2\text{CH}_2$ ), 3.16 – 3.06 (m, 4H,  $\text{CCH}_2$ ), 7.40 (q,  $J = 1.9$  Hz, 2H, Ar-CH), 7.50 (p,  $J = 1.7$  Hz, 4H, Ar-CH);  $^{13}\text{C NMR}$  ( $\text{CDCl}_3$ , 101 MHz, TMS)  $\delta$  21.1 ( $\text{CH}_3$ ), 25.4 ( $\text{CH}$ ), 28.6 ( $\text{CCH}_2\text{CH}_2$ ), 29.7 ( $\text{CCH}_2\text{CH}_2$ ), 34.0 ( $\text{CCH}_2$ ), 122.4 (C-Br), 133.4 (Ar-CH), 151.8 (N-C), 152.1 (N-C), (C-B not detected). All attempts to record a HRMS failed.

#### Synthesis of complex 4.8:



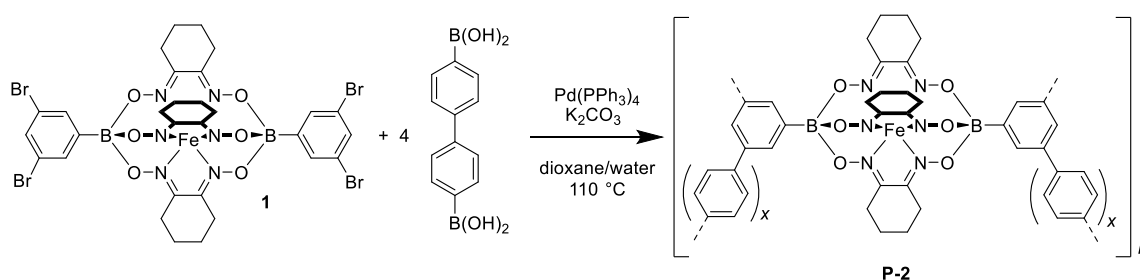
Compound **4.5** (100 mg, 0.64 mmol), pyridylphenylboronic acid (51.6 mg, 0.42 mmol), and anhydrous  $\text{FeCl}_2$  (27 mg, 0.22 mmol) were dissolved in MeOH (15 mL) and heated under reflux under an inert atmosphere for 3 h. The reaction mixture was allowed to cool to RT, and the resulting precipitates were isolated by filtration, washed with MeOH and diethyl ether, and dried under vacuum to yield a brown powder (84 mg, 56%).  $^1\text{H NMR}$  (400 MHz,  $\text{CDCl}_3$ )  $\delta$  1.10 (d,  $J = 6.4$  Hz, 9H,  $\text{CH}_3$ ), 1.5 (tq,  $J = 12.5, 5.4$  Hz, 3H,  $\text{CH}$ ), 1.46 (s, 6H,  $\text{CCH}_2\text{CH}_2$ ), 2.43 (dd,  $J = 18.8, 10.7$  Hz, 3H,  $\text{CCH}_2\text{CH}_2$ ), 2.79 (ddd,  $J = 18.7, 11.6, 6.1$  Hz, 3H,  $-\text{CCH}_2\text{CH}_2$ ), 3.23 – 3.08 (m, 4H,  $\text{CCH}_2$ ), 8.04 (q,  $J = 1.9$  Hz, 2H, Ar-CH), 8.83 (p,  $J = 1.7$  Hz, 4H, Ar-CH);  $^{13}\text{C NMR}$  ( $\text{CDCl}_3$ , 101 MHz, TMS)  $\delta$  20.82 ( $\text{CH}_3$ ), 25.34 ( $\text{CH}$ ), 28.36 ( $\text{CCH}_2\text{CH}_2$ ), 29.42 ( $\text{CCH}_2\text{CH}_2$ ), 33.87 ( $\text{CCH}_2$ ), 126.9 ( $\text{CH-CB}$ ), 146.9 ( $\text{CH-N}$ ), 152.28 (C-NO). (C-B not detected). **HRMS (ESI TOF)**  $m/z$  calcd for  $\text{C}_{31}\text{H}_{40}\text{B}_2\text{FeN}_8\text{O}_6$   $[\text{M}-2\text{H}]^{2+}$  349.1303, found 349.1320.

#### Synthesis of polymer P-1:



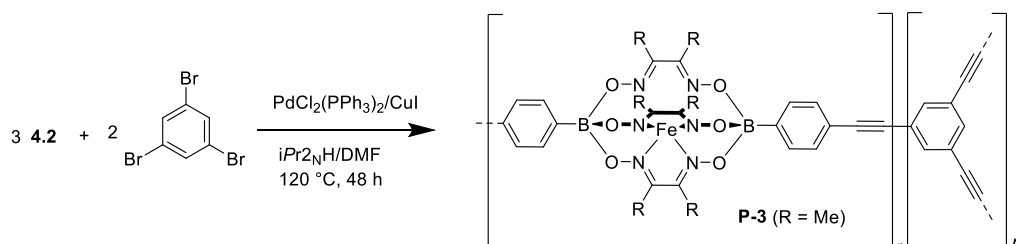
1,4-Dioxane (15 mL) was purged with  $\text{N}_2$  for 30 min in a Pyrex microwave vial. Subsequently, clathrochelate **4.1** (50 mg, 0.052 mmol) and 1,4-benzenediboronic acid (34.5 mg, 0.208 mmol) were added, and the mixture was purged again with  $\text{N}_2$  for 10 min. A solution of  $\text{K}_2\text{CO}_3$  (100 mg, 0.723 mmol) in water (2.5 mL) was added, and the solution was purged with  $\text{N}_2$  for another 15 min.  $\text{Pd(PPh}_3)_4$  (19.4 mg, 0.016 mmol) was added, the vial was sealed, and the solution was stirred overnight at 110 °C. The precipitates were isolated by filtration and washed with hot solvents (50 mL DMF, 60 mL water, and 60 mL diethyl ether) to yield a brown powder (65 mg).

#### Synthesis of polymer P-2:



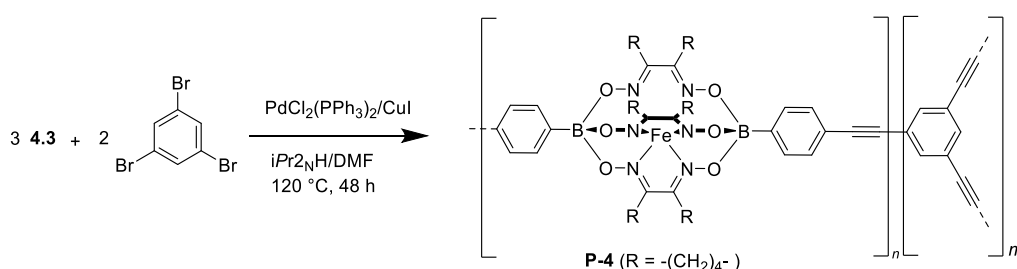
1,4-Dioxane (15 mL) was purged with nitrogen for 30 min in a Pyrex microwave vial. Subsequently, clathrochelate **1** (50 mg, 0.052 mmol) and 4,4'-biphenyldiboronic acid (50.3 mg, 0.208 mmol) were added, and the mixture was purged with  $\text{N}_2$  for 10 min. A solution of  $\text{K}_2\text{CO}_3$  (100 mg, 0.723 mmol) in water (2.5 mL) was added, and the solution was purged with  $\text{N}_2$  for another 15 min.  $\text{Pd(PPh}_3)_4$  (19.4 mg, 0.016 mmol) was added, the vial was sealed, and the solution was stirred overnight at 110 °C. The precipitates were isolated by filtration and washed with hot solvents (50 mL DMF, 60 mL water, and 60 mL diethyl ether) to yield a brown powder (106 mg).

#### Synthesis of polymer P-3:



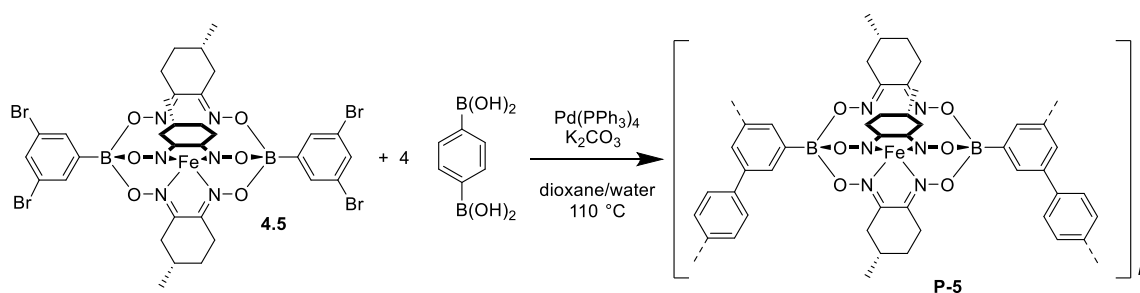
A mixture of DMF and *i*PrNH<sub>2</sub> (1:1, 10 mL) was purged with N<sub>2</sub> for 30 min in a Pyrex microwave vial. Subsequently, 1,3,5-tribromobenzene (16.8 mg, 0.053 mmol) and complex **4.2** (50 mg, 0.080 mmol) were added, and the mixture was purged with N<sub>2</sub> for 10 min. CuI (0.5 mg, 0.004 mmol) and Pd(PPh<sub>3</sub>)<sub>2</sub>Cl<sub>2</sub> (2.1 mg, 0.004 mmol) were added under N<sub>2</sub>, the reaction mixture was sealed and stirred for 48 h at 120 °C. The precipitates were isolated by filtration while hot and washed with DMF (50 mL), water (50 mL), THF (50 mL), and diethyl ether (50 mL) to yield a brown product (60 mg).

#### Synthesis of polymer P-4:



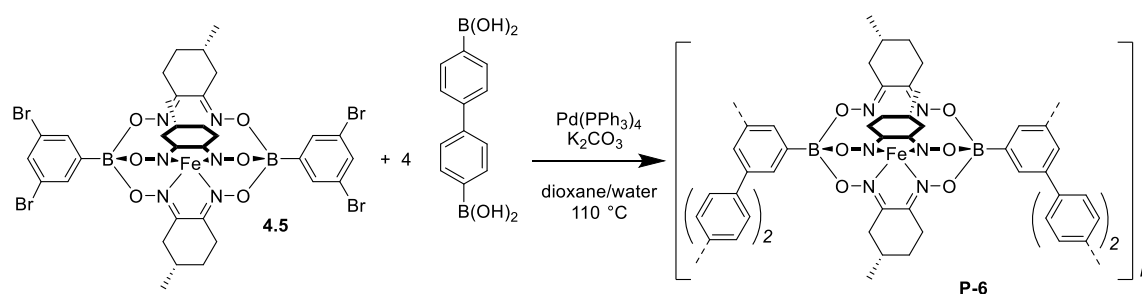
A mixture of DMF and *i*Pr<sub>2</sub>NH (1:1, 10 mL) was purged with nitrogen for 30 min in a Pyrex microwave vial. Subsequently, the 1,3,5-tribromobenzene (14.9 mg, 0.048 mmol) and complex **4.3** (50 mg, 0.071 mmol) were added, and the mixture was purged with N<sub>2</sub> for 10 min. CuI (0.7 mg, 0.004 mmol) and Pd(PPh<sub>3</sub>)<sub>2</sub>Cl<sub>2</sub> (2.8 mg, 0.004 mmol) were added under N<sub>2</sub>, the reaction mixture was sealed and stirred for 48 h at 120 °C. The precipitates were isolated by filtration while hot and washed with DMF (50 mL), water (50 mL), THF (50 mL), and diethyl ether (50 mL) to yield a brown product (58 mg).

#### Synthesis of polymer P-5:



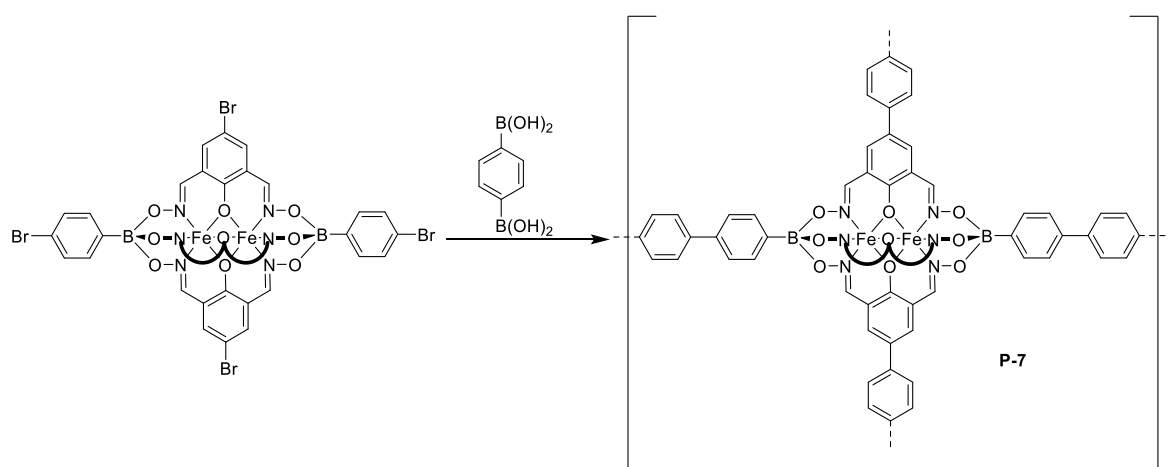
1,4-Dioxane (10 mL) was purged with N<sub>2</sub> for 30 min in a Pyrex microwave vial. Subsequently, complex **4.5** (50 mg, 0.05 mmol) and 1,4-benzenediboronic acid (32.5 mg, 0.20 mmol) were added, and the mixture was purged again with N<sub>2</sub> for 10 min. A solution of K<sub>2</sub>CO<sub>3</sub> (135 mg, 0.98 mmol) in water (2.5 mL) was added, and the solution was purged with N<sub>2</sub> for another 15 min. Pd(PPh<sub>3</sub>)<sub>4</sub> (17 mg, 0.015 mmol) was added, the vial was sealed, and the solution was stirred overnight at 110 °C. The precipitates were isolated by filtration and washed with hot solvents (50 mL DMF, 60 mL water, and 60 mL diethyl ether) to yield a brown powder (51 mg).

#### Synthesis of polymer P-6:



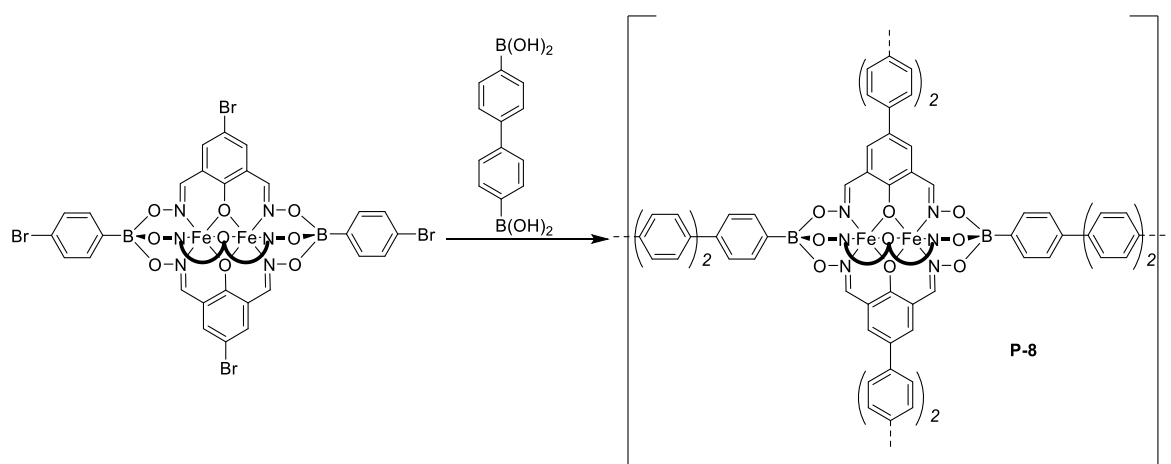
1,4-Dioxane (10 mL) was purged with  $\text{N}_2$  for 30 min in a Pyrex microwave vial. Subsequently, complex **4.5** (50 mg, 0.05 mmol) and 4,4'-biphenyldiboric acid (48.4 mg, 0.20 mmol) were added, and the mixture was purged with  $\text{N}_2$  for 10 min. A solution of  $\text{K}_2\text{CO}_3$  (135 mg, 0.98 mmol) in water (2.5 mL) was added, and the solution was purged with  $\text{N}_2$  for another 15 min.  $\text{Pd(PPh}_3)_4$  (17 mg, 0.015 mmol) was added, the vial was sealed, and the solution was stirred overnight at  $110^\circ\text{C}$ . The precipitates were isolated by filtration and washed with hot solvents (50 mL DMF, 60 mL water, and 60 mL diethyl ether) to yield a brown powder (85 mg).

#### Synthesis of polymer P-7:



$\text{Pd(PPh}_3)_4$  (13.9 mg, 12  $\mu\text{mol}$ ) was added a solution of complex **2.6** (50 mg, 40  $\mu\text{mol}$ ), 1,4-phenyldiboric acid (18 mg, 120  $\mu\text{mol}$ ) and  $\text{K}_2\text{CO}_3$  (66 mg, 480  $\mu\text{mol}$ ) in 1,4-dioxane: $\text{H}_2\text{O}$  (4:1) (15 mL) under  $\text{N}_2$ . The solution was sealed and stirred at  $110^\circ\text{C}$  for 12 h, and then cooled to RT. The product was isolated by filtration, washed with 1,4-dioxane, DMF, water, and diethyl ether to yield a greyish polymer. *Yield*: 45 mg. **IR**: 1593, 1559, 1481, 1438, 1378, 1296, 1201, 1091, 1045, 1006, 969, 929, 889, 787, 757, 701, 670, 535.

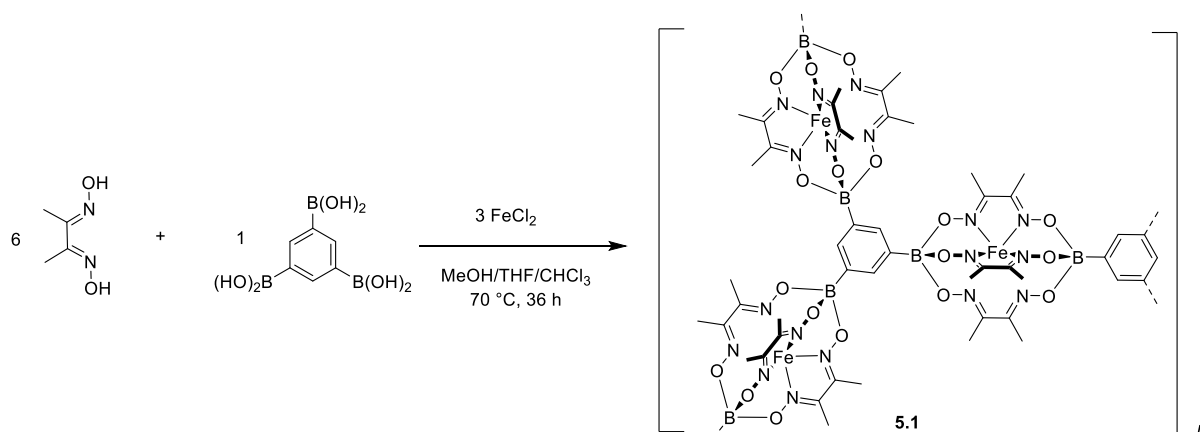
#### Synthesis of polymer P-8:



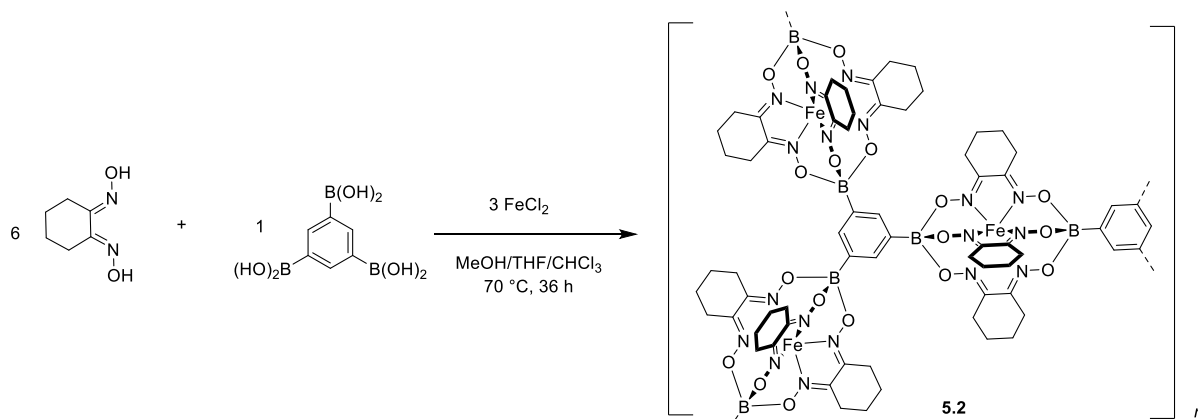
$\text{Pd}(\text{PPh}_3)_4$  (28 mg, 24  $\mu\text{mol}$ ) was added a solution of complex **2.6** (100 mg, 80  $\mu\text{mol}$ ), 1,4-biphenyldiboronic acid (58 mg, 240  $\mu\text{mol}$ ) and  $\text{K}_2\text{CO}_3$  (112 mg, 960  $\mu\text{mol}$ ) in 1,4-dioxane:H<sub>2</sub>O (4:1) (15 mL) under  $\text{N}_2$ . The solution was sealed and stirred at 110 °C for 12 h, and then cooled to RT. The product was isolated by filtration, washed with 1,4-dioxane, DMF, water, and diethyl ether to yield a greyish polymer. *Yield*: 184 mg. **IR**: 1699., 1608.9, 1530, 1402.5, 1319.3, 1288.1217.8, 1111.2, 1041, 1020.2, 976, 939.6, 856.38, 786.2, 713.9, 661.5, 596.66, 502.7.

#### 7.1.4 Experimental procedures for chapter 5

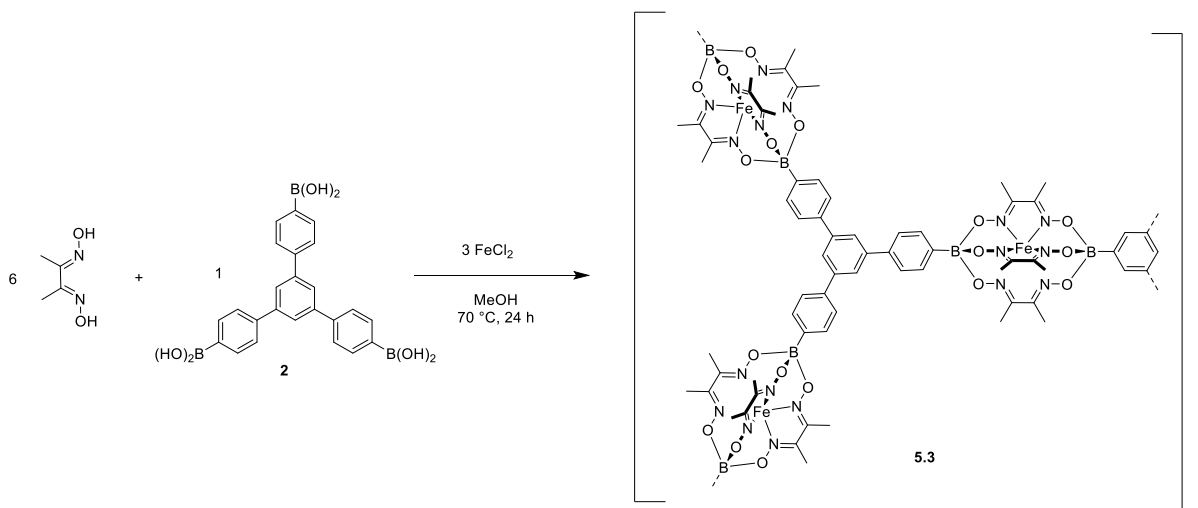
##### Synthesis of polymer 5.1:



1,3,5-Benzenetriboronic acid (50 mg, 0.238 mmol) and dimethyl glyoxime (166 mg, 1.43 mmol) were dissolved in MeOH/ $\text{CHCl}_3$ /THF (60 mL, 1:2:2) and degassed with  $\text{N}_2$ .  $\text{FeCl}_2$  (90.5 mg, 0.714 mmol) was added under  $\text{N}_2$  and the reaction mixture was left to stir under reflux and  $\text{N}_2$  for 36 h. The precipitates were isolated by filtration and washed with  $\text{CHCl}_3$  (50 mL), MeOH (50 mL), THF (50 mL) and diethyl ether (50 mL). The product was dried under vacuum to afford a brown colored compound (132 mg). **IR**: 1585, 1362, 1182, 1055, 997, 924, 793, 707, 594, and 497.

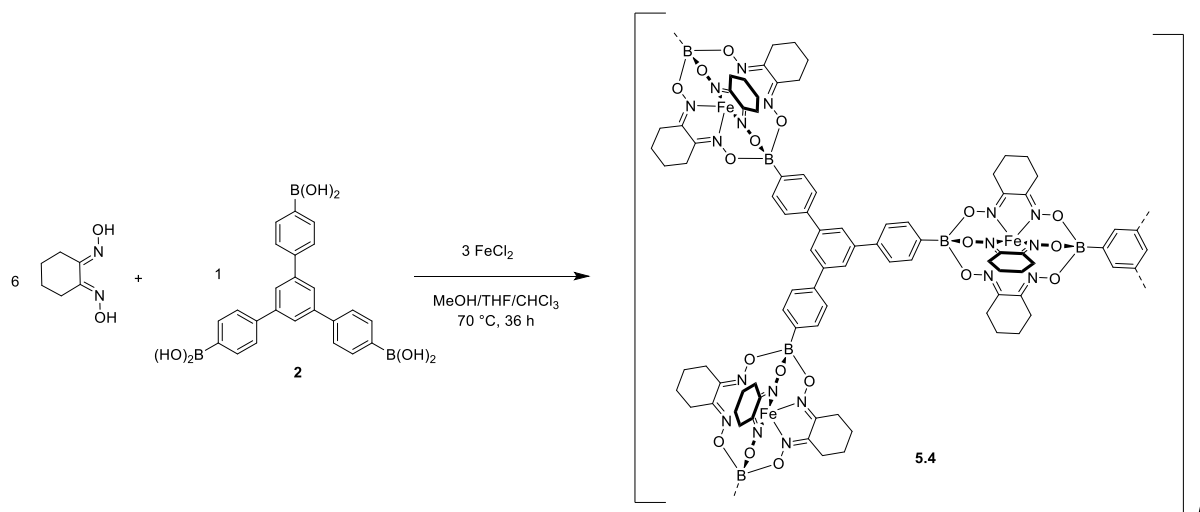
**Synthesis of polymer 5.2:**

1,3,5-Benzenetriboronic acid (50 mg, 0.238 mmol) and nioxime (203 mg, 1.43 mmol) were dissolved in MeOH/CHCl<sub>3</sub>/THF (60 mL, 1:2:2) and degassed with N<sub>2</sub>. FeCl<sub>2</sub> (90.5 mg, 0.714 mmol) was added under N<sub>2</sub> and the reaction mixture was left to stir under reflux and N<sub>2</sub> for 36 h. Then the precipitates were filtered and washed with hot solvents: CHCl<sub>3</sub> (50 mL), MeOH (50 mL), THF (50 mL) and diethyl ether (50 mL). The product was dried under vacuum to afford a brown colored compound (138 mg) **IR**: 1582, 1360, 1184, 1056, 999, 917, 799, 704, 592, and 500.

**Synthesis of polymer 5.3:**

The triboronic acid **2** (20 mg, 0.046 mmol) and dimethylglyoxime (31.8 mg, 0.28 mmol) were dissolved in MeOH (30 mL) and degassed with N<sub>2</sub>. FeCl<sub>2</sub> (43.3 mg, 0.342 mmol) was added under N<sub>2</sub> and the reaction mixture was left to stir under reflux for 24 h. Then the precipitates were filtered and washed with CHCl<sub>3</sub> (50 mL), MeOH (50 mL), THF (50 mL) and diethyl ether (50 mL). The product was dried under vacuum to afford a brown colored compound (32 mg) **IR**: 1584, 1383, 1185, 1055, 996, 970, 940, 828, 720, 596, 508.

## Synthesis of polymer 5.4:



The triboronic acid **2** (50 mg, 0.114 mmol) and nioxime (97.1 mg, 0.684 mmol) were dissolved in MeOH/CHCl<sub>3</sub>/THF (60 mL, 1:2:2) and the solution was degassed with N<sub>2</sub>. FeCl<sub>2</sub> (43.3 mg, 0.342 mmol) was added under N<sub>2</sub> and the reaction mixture was left to stir under reflux for 36 h. The precipitates were isolated by filtration and washed with CHCl<sub>3</sub> (50 mL), MeOH (50 mL), THF (50 mL) and diethyl ether (50 mL). The product was dried under vacuum to afford a brown colored compound (97 mg). **IR:** 1596, 1493, 1435, 1393, 1201, 1062, 962, 820, 574, and 597.





## Chapter 8 Appendix

### 8.1 Crystallographic tables

The X-ray crystal structures of complexes, **2.5**, **2.11**, **2.13**, **2.14**, **2.15**, **4.4**, **4.7** and **4.8** were not finalized. Therefore, their crystallographic tables were not provided in this thesis.

**Table 8.1** – Crystallographic data of clathrochelates **2.1**, **2.2** and **2.3**.

Compound	2.1	2.2	2.3
Formula	C <sub>46</sub> H <sub>48</sub> B <sub>2</sub> Fe <sub>2</sub> N <sub>8</sub> O <sub>9</sub>	C <sub>34</sub> H <sub>21</sub> B <sub>2</sub> Br <sub>3</sub> Fe <sub>2</sub> N <sub>8</sub> O <sub>9</sub>	
$D_{calc}/\text{g cm}^{-3}$	1.294	1.779	1.443
$\mu/\text{mm}^{-1}$	4.299	8.913	6.884
Formula Weight	990.24	1055.78	
Size/mm <sup>3</sup>	0.241×0.187×0.143	0.268 x 0.094 x 0.034	0.484 x 0.309 x 0.056
$T/\text{K}$	140.00(10)	140.00(10)	140.00(10)
Crystal System	triclinic	monoclinic	monoclinic
Space Group	<i>P</i> -1	<i>C</i> 2/ <i>c</i>	<i>P</i> 2 <sub>1</sub> / <i>c</i>
$a/\text{\AA}$	19.1124(7)	21.57161(18)	11.8807(3)
$b/\text{\AA}$	20.1642(6)	11.37072(9)	31.6735(6)
$c/\text{\AA}$	21.5640(8)	18.30024(15)	17.5962(4)
$\alpha/^\circ$	69.941(3)	90	90
$\beta/^\circ$	75.382(3)	90.7604(7)	99.79
$\gamma/^\circ$	84.800(3)	90	90
$V/\text{\AA}^3$	7553.6(5)	4488.37(6)	6524.9(2)
$Z$	4	4	4
Wavelength/ $\text{\AA}$	1.54184	1.54184	1.54184
$\theta_{min}/^\circ$	3.646	4.099	3.776
$\theta_{max}/^\circ$	76.129	73.643	75.591
Measured Refl.	32020	15027	50097
Independent Refl.	32020	4465	13314
$R_{int}$	0	0.0164	0.0434
Parameters	1837	310	834
Restraints	575	0	84
Largest Peak/e $\text{\AA}^{-3}$	1.44	0.494	1.335
Deepest Hole/e $\text{\AA}^{-3}$	-1.09	-0.324	-1.198
GooF	0.969	1.062	1.044
$wR_2$ (all data)	0.2055	0.0478	0.1332
$wR_2$	0.2261	0.0483	0.1411
$R_1$ (all data)	0.0735	0.0193	0.0600
$R_1$	0.1032	0.0200	0.0512

**Table 8.2** - Crystallographic data of clathrochelates **2.4** and **2.6**.

Compound	2.4	2.6
Formula	C <sub>48</sub> H <sub>53</sub> B <sub>2</sub> Br <sub>3</sub> Fe <sub>2</sub> N <sub>9</sub> O <sub>11</sub>	
$D_{calc}/\text{g cm}^{-3}$	1.651	1.844
$\mu/\text{mm}^{-1}$	2.904	4.503
Formula Weight		
Size/mm <sup>3</sup>	0.690 x 0.470 x 0.307	0.529 x 0.158 x 0.066
$T/\text{K}$	120.00(2)	140.00(10) K
Crystal System	orthorhombic	triclinic
Space Group	$C222_1$	$P-1$
$a/\text{\AA}$	15.322(3)	13.6247(5)
$b/\text{\AA}$	25.459(5)	14.0739(3)
$c/\text{\AA}$	26.917(5)	15.2323(5)
$\alpha/^\circ$	90	87.441(2)
$\beta/^\circ$	90	68.569(3)
$\gamma/^\circ$	90	72.159(3)
$V/\text{\AA}^3$	10500(4)	2580.65(15)
$Z$	8	2
Wavelength/ $\text{\AA}$	0.71073	0.71073
$\theta_{min}/^\circ$	2.750	3.508
$\theta_{max}/^\circ$	27.500	29.484
Measured Refl.	68508	26035
Independent Refl.	11892	12326
$R_{int}$	0.0319	0.0303
Parameters	708	760
Restraints	81	0
Largest Peak/ $\text{e \AA}^{-3}$	0.424	0.925
Deepest Hole/ $\text{e \AA}^{-3}$	-0.315	-1.093
GooF	1.144	1.020
$wR_2$ (all data)	0.0493	0.0846
$wR_2$	0.0460	0.0757
$R_1$ (all data)	0.0360	0.0846
$R_1$	0.0266	0.0590

Table 8.3 - Crystallographic data of clathrochelates **3.28** and **3.29**.

Compound	3.28	3.29
Formula	C <sub>220</sub> H <sub>252</sub> B <sub>8</sub> Fe <sub>8</sub> K <sub>4</sub> N <sub>24</sub> O <sub>44</sub>	C <sub>60</sub> H <sub>75</sub> B <sub>2</sub> Fe <sub>2</sub> KN <sub>6</sub> O <sub>10</sub>
$D_{calc}/\text{g cm}^{-3}$	1.103	1.313
$\mu/\text{mm}^{-1}$	4.300	4.891
Formula Weight	4626.12	1212.68
Size/mm <sup>3</sup>	0.843 x 0.389 x 0.324	0.206 x 0.173 x 0.116
$T/\text{K}$	140.00(10)	140.00(10)
Crystal System	triclinic	monoclinic
Space Group	$P-1$	$P2_1/n$
$a/\text{\AA}$	12.5096(2)	16.5593(2)
$b/\text{\AA}$	23.8866(4)	20.6902(4)
$c/\text{\AA}$	24.3813(7)	18.0097(5)
$\alpha/^\circ$	83.6378(19)	90
$\beta/^\circ$	78.305(2)	96.1888(18)
$\gamma/^\circ$	78.1089(16) <sup>o</sup>	90
$V/\text{\AA}^3$	6963.0(3)	4488.37(6)
$Z$	1	4
Wavelength/ $\text{\AA}$	1.54184	1.54184
$\Theta_{min}/^\circ$	2.746	3.838
$\Theta_{max}/^\circ$	73.699	73.518
Measured Refl.	48627	44033
Independent Refl.	27134	12202
$R_{int}$	0.0420	0.0715
Parameters	1461	810
Restraints	165	132
Largest Peak/ $\text{e \AA}^{-3}$	0.664	0.494
Deepest Hole/ $\text{e \AA}^{-3}$	-0.697	-0.324
GooF	0.969	1.012
$wR_2$ (all data)	0.1575	0.1260
$wR_2$	0.1514	0.1099
$R_1$ (all data)	0.0637	0.0759
$R_1$	0.0571	0.0469

**Table 8.4** - Crystallographic data of clathrochelates **4.2**, **4.3** and **4.6**.

Compound	4.2	4.3	4.6
Formula	C <sub>28</sub> H <sub>28</sub> B <sub>2</sub> FeN <sub>6</sub> O <sub>6</sub>	C <sub>34</sub> H <sub>34</sub> B <sub>2</sub> FeN <sub>6</sub> O <sub>6</sub>	C <sub>33</sub> H <sub>33</sub> B <sub>2</sub> Br <sub>4</sub> FeN <sub>6</sub> O <sub>6</sub>
$D_{calc}/\text{g cm}^{-3}$	1.429	1.360	1.572
$\mu/\text{mm}^{-1}$	4.631	3.979	4.158
Formula Weight	622.03	700.14	1006.76
Size/mm <sup>3</sup>	0.76×0.60×0.04	0.87×0.12×0.06	0.72×0.52×0.20
$T/\text{K}$	140.00(10)	100.01(10)	140.00(10)
Crystal System	monoclinic	monoclinic	orthorhombic
Space Group	$P2_1/c$	$P2_1/a$	$P2_12_12$
$a/\text{\AA}$	10.8991(2)	30.5087(8)	14.0642(6)
$b/\text{\AA}$	16.1046(3)	9.8259(2)	17.8345(8)
$c/\text{\AA}$	16.9882(3)	46.0071(17)	16.9600(8)
$\alpha/^\circ$	90	90	90
$\beta/^\circ$	104.090(2)	97.269(3)	90
$\gamma/^\circ$	90	90	90
$V/\text{\AA}^3$	2892.17(10)	13681.0(7)	4254.1(3)
$Z$	4	16	4
Wavelength/ $\text{\AA}$	1	2	1
$\theta_{min}/^\circ$	1.54184	1.54184	0.71073
$\theta_{max}/^\circ$	3.838	3.704	2.581
Measured Refl.	76.244	63.685	33.065
Independent Refl.	18388	44155	56046
$R_{int}$	5928	11115	14690
Parameters	0.0610	0.0443	0.0686
Restraints	394	1000	506
Largest Peak/ $\text{e \AA}^{-3}$	0	1384	29
Deepest Hole/ $\text{e \AA}^{-3}$	0.834	1.281	0.955
GooF	-0.939	-0.833	-0.999
$wR_2$ (all data)	1.049	1.067	1.029
$wR_2$	0.1762	0.3377	0.2005
$R_1$ (all data)	0.1700	0.3284	0.1659
$R_1$	0.0640	0.1281	0.1377
Formula	0.0603	0.1170	0.0680

## Chapter 9 References

- [1] J. D. Curry, D. H. Busch, *J. Am. Chem. Soc.* **1964**, *86*, 592–594.
- [2] D. R. Boston, N. J. Rose, *J. Am. Chem. Soc.* **1968**, *90*, 6859–6860.
- [3] M. D. Wise, A. Ruggi, M. Pascu, R. Scopelliti, K. Severin, *Chem. Sci.* **2013**, *4*, 1658–1662.
- [4] S. M. Jansze, K. Severin, *Acc. Chem. Res.* **2018**, *51*, 2139–2147.
- [5] Y. Z. Voloshin, O. A. Varzatskii, N. G. Strizhakova, E. Y. Tkachenko, *Inorg. Chim. Acta* **2000**, *299*, 104–111.
- [6] Y. Z. Voloshin, O. A. Varzatskii, A. V. Palchik, N. G. Strizhakova, I. I. Vorontsov, M. Y. Antipin, D. I. Kochubey, B. N. Novgorodov, *New J. Chem.* **2003**, *27*, 1148–1155.
- [7] S. V. Dudkin, N. R. Erickson, A. V. Vologzhanina, V. V. Novikov, H. M. Rhoda, C. D. Holstrom, Y. V. Zatsikha, M. S. Yusubov, Y. Z. Voloshin, V. N. Nemykin, *Inorg. Chem.* **2016**, *55*, 11867–11882.
- [8] Y. Z. Voloshin, A. S. Belov, A. V. Vologzhanina, G. G. Aleksandrov, A. V. Dolganov, V. V. Novikov, O. A. Varzatskii, Y. N. Bubnov, *Dalton Trans.* **2012**, *41*, 6078–6093.
- [9] G. E. Zelinskii, A. S. Belov, A. V. Vologzhanina, I. P. Limarev, P. V. Dorovatovskii, Y. V. Zubavichus, E. G. Lebed, Y. Z. Voloshin, A. G. Dedov, *Polyhedron* **2019**, *160*, 108–114.
- [10] I. N. Denisenko, O. A. Varzatskii, R. A. Selin, A. S. Belov, E. G. Lebed, A. V. Vologzhanina, Y. V. Zubavichus, Y. Z. Voloshin, *RSC Adv.* **2018**, *8*, 13578–13587.
- [11] R. K. K. Y.Z. Voloshin, N.A. Kostromina, *Clathrochelates: Synthesis, Structure and Properties*, Elsevier, **2002**.
- [12] R. Voloshin, Yan, Belaya, Irina, Krämer, *Cage Metal Complexes: Clathrochelates Revisited*, Springer, **2017**.
- [13] G. E. Zelinskii, A. S. Belov, I. G. Belaya, A. V. Vologzhanina, V. V. Novikov, O. A. Varzatskii, Y. Z. Voloshin, *New J. Chem.* **2018**, *42*, 56–66.
- [14] V. V. Novikov, O. A. Varzatskii, V. V. Negrutska, Y. N. Bubnov, L. G. Palchykovska, I. Y. Dubey, Y. Z. Voloshin, *J. Inorg. Biochem.* **2013**, *124*, 42–45.

- [15] O. A. Varzatskii, V. V. Novikov, S. V. Shulga, A. S. Belov, A. V. Vologzhanina, V. V. Negrutska, I. Y. Dubey, Y. N. Bubnov, Y. Z. Voloshin, *Chem. Commun.* **2014**, 50, 3166–3168.
- [16] V. B. Kovalska, M. Y. Losytskyy, O. A. Varzatskii, V. V. Cherepanov, Y. Z. Voloshin, A. A. Mokhir, S. M. Yarmoluk, S. V. Volkov, *Bioorganic Med. Chem.* **2014**, 22, 1883–1888.
- [17] V. Kovalska, M. Kuperman, M. Losytskyy, S. Vakarov, S. Potocki, S. Yarmoluk, Y. Voloshin, O. Varzatskii, E. Gumienna-Kontecka, *Metallomics* **2019**, 11, 338–348.
- [18] A. V. Dolganov, O. V. Tarasova, A. Y. Ivleva, O. Y. Chernyaeva, K. A. Grigoryan, V. S. Ganz, *Int. J. Hydrogen Energy* **2017**, 42, 27084–27093.
- [19] A. V. Dolganov, A. S. Belov, V. V. Novikov, A. V. Vologzhanina, G. V. Romanenko, Y. G. Budnikova, G. E. Zelinskii, M. I. Buzin, Y. Z. Voloshin, *Dalton Trans.* **2015**, 44, 2476–2487.
- [20] Y. Z. Voloshin, A. V. Dolganov, O. A. Varzatskii, Y. N. Bubnov, *Chem. Commun.* **2011**, 47, 7737–7739.
- [21] V. V. Novikov, A. A. Pavlov, A. S. Belov, A. V. Vologzhanina, A. Savitsky, Y. Z. Voloshin, *J. Phys. Chem. Lett.* **2014**, 5, 3799–3803.
- [22] T. R. Cook, Y. R. Zheng, P. J. Stang, *Chem. Rev.* **2013**, 113, 734–777.
- [23] M. M. J. Smulders, I. A. Riddell, C. Browne, J. R. Nitschke, *Chem. Soc. Rev.* **2013**, 42, 1728–1754.
- [24] S. Saha, I. Regeni, G. H. Clever, *Coord. Chem. Rev.* **2018**, 374, 1–14.
- [25] S. Pullen, G. H. Clever, *Acc. Chem. Res.* **2018**, 51, 3052–3064.
- [26] Y. Sun, C. Chen, P. J. Stang, *Acc. Chem. Res.* **2019**, 52, 802–817.
- [27] S. Yuan, L. Feng, K. Wang, J. Pang, M. Bosch, C. Lollar, Y. Sun, J. Qin, X. Yang, P. Zhang, et al., *Adv. Mater.* **2018**, 30, 1–35.
- [28] M. D. Wise, J. J. Holstein, P. Pattison, C. Besnard, E. Solari, R. Scopelliti, G. Bricogne, K. Severin, *Chem. Sci.* **2015**, 6, 1004–1010.
- [29] S. M. Jansze, G. Cecot, M. D. Wise, K. O. Zhurov, T. K. Ronson, A. M. Castilla, A. Finelli, P. Pattison, E. Solari, R. Scopelliti, et al., *J. Am. Chem. Soc.* **2016**, 138, 2046–2054.
- [30] G. Cecot, M. Marmier, S. Geremia, R. De Zorzi, A. V. Vologzhanina, P. Pattison, E. Solari, F. Fadaei Tirani, R. Scopelliti, K. Severin, *J. Am. Chem. Soc.* **2017**, 139, 8371–8381.
- [31] G. Cecot, B. Alameddine, S. Prior, R. De Zorzi, S. Geremia, R. Scopelliti, F. T. Fadaei, E. Solari, K. Severin, *Chem. Commun.* **2016**, 52, 11243–11246.
- [32] G. Cecot, M. T. Doll, O. M. Planes, A. Ramorini, R. Scopelliti, F. Fadaei-Tirani, K. Severin, *Eur. J. Inorg.*

- Chem.* **2019**, 2972–2976.
- [34] S. M. Jansze, D. Ortiz, F. Fadaei Tirani, R. Scopelliti, L. Menin, K. Severin, *Chem. Commun.* **2018**, 54, 9529–9532.
- [35] S. Khanra, T. Weyhermüller, E. Bill, P. Chaudhuri, *Inorg. Chem.* **2006**, 45, 5911–5923.
- [36] M. Marmier, M. D. Wise, J. J. Holstein, P. Pattison, K. Schenk, E. Solari, R. Scopelliti, K. Severin, *Inorg. Chem.* **2016**, 55, 4006–4015.
- [37] M. Pascu, M. Marmier, C. Schouwey, R. Scopelliti, J. J. Holstein, G. Bricogne, K. Severin, *Chem. - A Eur. J.* **2014**, 20, 5592–5600.
- [38] M. Marmier, G. Cecot, A. V. Vologzhanina, J. L. Bila, I. Zivkovic, H. M. Ronnow, B. Nafradi, E. Solari, P. Pattison, R. Scopelliti, et al., *Dalton Trans.* **2016**, 45, DOI 10.1039/c6dt02758j.
- [39] M. Marmier, G. Cecot, B. F. E. Curchod, P. Pattison, E. Solari, R. Scopelliti, K. Severin, *Dalton. Trans.* **2016**, 45, 8422–8427.
- [40] G. Aromí, P. Gamez, P. C. Berzal, W. L. Driessen, J. Reedijk, *Synth. Commun.* **2003**, 33, 11–18.
- [41] M. Marmier, G. Cecot, A. V. Vologzhanina, J. L. Bila, I. Zivkovic, H. M. Ronnow, B. Nafradi, E. Solari, P. Pattison, R. Scopelliti, et al., *Dalton Trans.* **2016**, 45, 15507–15516.
- [42] J. Gong, C. Li, M. R. Wasielewski, *Chem. Soc. Rev.* **2019**, 48, 1862–1864.
- [43] G. Centi, G. Iaquaniello, S. Perathoner, *BMC Chem. Eng.* **2019**, 1, 1–16.
- [44] A. Sharma, **2019**, 210006, 1–6.
- [45] J. Mohtasham, *Energy Procedia* **2015**, 74, 1289–1297.
- [46] X. Wei, W. Pan, W. Duan, A. Hollas, Z. Yang, B. Li, Z. Nie, J. Liu, D. Reed, W. Wang, et al., *ACS Energy Lett.* **2017**, 2, 2187–2204.
- [47] J. Winsberg, T. Hagemann, T. Janoschka, M. D. Hager, U. S. Schubert, *Angew. Chem. - Int. Ed.* **2017**, 56, 686–711.
- [48] P. Leung, A. A. Shah, L. Sanz, C. Flox, J. R. Morante, Q. Xu, M. R. Mohamed, C. Ponce de León, F. C. Walsh, *J. Power Sources* **2017**, 360, 243–283.
- [49] R. Ye, D. Henkensmeier, S. J. Yoon, Z. Huang, D. K. Kim, Z. Chang, S. Kim, R. Chen, *J. Electrochem. Energy Convers. Storage* **2018**, 15, 1–21.
- [50] X. Ke, J. M. Prahl, J. I. D. Alexander, J. S. Wainright, T. A. Zawodzinski, R. F. Savinell, *Chem. Soc. Rev.* **2018**, 47, 8721–8743.



- 
- [51] A. Z. Weber, M. M. Mench, J. P. Meyers, P. N. Ross, J. T. Gostick, Q. Liu, *J. Appl. Electrochem.* **2011**, *41*, 1137–1164.
- [52] Q. Xu, Y. N. Ji, L. Y. Qin, P. K. Leung, F. Qiao, Y. S. Li, H. N. Su, *J. Energy Storage* **2018**, *16*, 108–115.
- [53] Q. Lai, H. Zhang, X. Li, L. Zhang, Y. Cheng, *J. Power Sources* **2013**, *235*, 1–4.
- [54] J. Zhang, G. Jiang, P. Xu, A. Ghorbani Kashkooli, M. Mousavi, A. Yu, Z. Chen, *Energy Environ. Sci.* **2018**, *11*, 2010–2015.
- [55] B. Li, Z. Nie, M. Vijayakumar, G. Li, J. Liu, V. Sprenkle, W. Wang, *Nat. Commun.* **2015**, *6*, 1–8.
- [57] C. Xie, H. Zhang, W. Xu, W. Wang, X. Li, *Angew. Chem. - Int. Ed.* **2018**, *57*, 11171–11176.
- [58] H. Chen, G. Cong, Y. C. Lu, *J. Energy Chem.* **2018**, *27*, 1304–1325.
- [59] K. Gong, Q. Fang, S. Gu, S. F. Y. Li, Y. Yan, *Energy Environ. Sci.* **2015**, *8*, 3515–3530.
- [60] Y. Matsuda, K. Tanaka, M. Okada, Y. Takasu, M. Morita, T. Matsumura-Inoue, *J. Appl. Electrochem.* **1988**, *18*, 909–914.
- [61] B. Yang, L. Hooper-Burkhardt, F. Wang, G. K. S. Prakash, S. R. Narayanan, *J. Electrochem. Soc.* **2014**, *161*, DOI 10.1149/2.1001409jes.
- [62] Y. Xu, Y. Wen, J. Cheng, G. Cao, Y. Yang, *Electrochem. commun.* **2009**, *11*, 1422–1424.
- [63] Y. Xu, Y. H. Wen, J. Cheng, G. P. Cao, Y. S. Yang, *Electrochim. Acta* **2010**, *55*, 715–720.
- [64] W. Wang, W. Xu, L. Cosimbescu, D. Choi, L. Li, Z. Yang, *Chem. Commun.* **2012**, *48*, 6669–6671.
- [65] T. Janoschka, M. D. Hager, U. S. Schubert, *Adv. Mater.* **2012**, *24*, 6397–6409.
- [66] Y. Liang, Z. Tao, J. Chen, *Adv. Energy Mater.* **2012**, *2*, 742–769.
- [67] H. Nishide, S. Iwasa, Y. J. Pu, T. Suga, K. Nakahara, M. Satoh, *Electrochim. Acta* **2004**, *50*, 827–831.
- [68] X. Wei, W. Xu, M. Vijayakumar, L. Cosimbescu, T. Liu, V. Sprenkle, W. Wang, *Adv. Mater.* **2014**, *26*, 7649–7653.
- [69] Z. Li, S. Li, S. Liu, K. Huang, D. Fang, F. Wang, S. Peng, *Electrochem. Solid-State Lett.* **2011**, *14*, 176–178.
- [70] A. P. Kaur, N. E. Holubowitch, S. Ergun, C. F. Elliott, S. A. Odom, *Energy Technol.* **2015**, *3*, 476–480.
- [71] F. R. Brushett, J. T. Vaughey, A. N. Jansen, *Adv. Energy Mater.* **2012**, *2*, 1390–1396.
- [72] J. Huang, L. Su, J. A. Kowalski, J. L. Barton, M. Ferrandon, A. K. Burrell, F. R. Brushett, L. Zhang, *J. Mater. Chem. A* **2015**, *3*, 14971–14976.

- [73] J. Huang, L. Cheng, R. S. Assary, P. Wang, Z. Xue, A. K. Burrell, L. A. Curtiss, L. Zhang, *Adv. Energy Mater.* **2015**, *5*, 1–6.
- [74] X. Wei, W. Xu, J. Huang, L. Zhang, E. Walter, C. Lawrence, M. Vijayakumar, W. A. Henderson, T. Liu, L. Cosimbescu, et al., *Angew. Chem. - Int. Ed.* **2015**, *54*, 8684–8687.
- [75] B. Hu, C. Debruler, Z. Rhodes, T. L. Liu, *J. Am. Chem. Soc.* **2017**, *139*, 1207–1214.
- [76] S. Zhang, X. Li, D. Chu, *Electrochim. Acta* **2016**, *190*, 737–743.
- [77] T. Liu, X. Wei, Z. Nie, V. Sprenkle, W. Wang, *Adv. Energy Mater.* **2016**, *6*, DOI 10.1002/aenm.201501449.
- [78] E. S. Beh, D. De Porcellinis, R. L. Gracia, K. T. Xia, R. G. Gordon, M. J. Aziz, *ACS Energy Lett.* **2017**, *2*, 639–644.
- [79] B. Hu, C. Seefeldt, C. Debruler, T. L. Liu, *J. Mater. Chem. A* **2017**, *5*, 22137–22145.
- [80] C. DeBruler, B. Hu, J. Moss, X. Liu, J. Luo, Y. Sun, T. L. Liu, *Chem* **2017**, *3*, 961–978.
- [81] C. Qu, Y. Cheng, F. Zhang, Y. Zhang, H. Zhang, X. Li, H. Zhang, *Int. J. Hydrogen Energy* **2015**, *40*, 16429–16433.
- [82] C. Xie, W. Xu, H. Zhang, X. Hu, X. Li, *Chem. Commun.* **2018**, *54*, 8419–8422.
- [83] S. Hwang, H. seung Kim, J. H. Ryu, S. M. Oh, *J. Power Sources* **2018**, *395*, 60–65.
- [84] B. Hwang, M. S. Park, K. Kim, *ChemSusChem* **2015**, *8*, 310–314.
- [85] G. M. Duarte, J. D. Braun, P. K. Giesbrecht, D. E. Herbert, *Dalton Trans.* **2017**, *46*, 16439–16445.
- [86] X. Xing, Y. Zhao, Y. Li, *J. Power Sources* **2015**, *293*, 778–783.
- [87] R. Shukla, S. V. Lindeman, R. Rathore, *Chem. Commun.* **2009**, *6*, 5600–5602.
- [88] K. P. Chiang, S. M. Bellows, W. W. Brennessel, P. L. Holland, *Chem. Sci.* **2014**, *5*, 267–274.
- [89] Y. Yuan, G. Zhu, *ACS Cent. Sci.* **2019**, *5*, 409–418.
- [90] T. Ben, S. Qiu, *CrystEngComm* **2013**, *15*, 17–26.
- [91] Z. Xiang, D. Wang, Y. Xue, L. Dai, J. F. Chen, D. Cao, *Sci. Rep.* **2015**, *5*, 1–8.
- [92] Y. Yuan, F. Sun, L. Li, P. Cui, G. Zhu, *Nat. Commun.* **2014**, *5*, 1–8.
- [93] M. Li, H. Ren, F. Sun, Y. Tian, Y. Zhu, J. Li, X. Mu, J. Xu, F. Deng, G. Zhu, *Adv. Mater.* **2018**, *30*, 1–7.
- [94] G. Li, L. Qin, C. Yao, Y. Xu, *Sci. Rep.* **2017**, *7*, 1–9.

- [95] S. Lu, Y. Jin, H. Gu, W. Zhang, *Sci. China Chem.* **2017**, *60*, 999–1006.
- [96] Y. Yuan, H. Huang, L. Chen, Y. Chen, *Macromolecules* **2017**, *50*, 4993–5003.
- [97] W. Zhang, B. Aguila, S. Ma, *J. Mater. Chem. A* **2017**, *5*, 8795–8824.
- [98] W. Zhao, F. Zhang, L. Yang, S. Bi, D. Wu, Y. Yao, M. Wagner, R. Graf, M. R. Hansen, X. Zhuang, et al., *J. Mater. Chem. A* **2016**, *4*, 15162–15168.
- [99] C. Xu, W. Zhang, J. Tang, C. Pan, G. Yu, *Front. Chem.* **2018**, *6*, 1–12.
- [100] S. Bracco, D. Piga, I. Bassanetti, J. Perego, A. Comotti, P. Sozzani, *J. Mater. Chem. A* **2017**, *5*, 10328–10337.
- [101] H. BİLDİRİR, *Turkish J. Chem.* **2019**, *43*, 730–739.
- [102] D. Wu, F. Xu, B. Sun, R. Fu, H. He, K. Matyjaszewski, *Chem. Rev.* **2012**, *112*, 3959–4015.
- [103] K. Cousins, R. Zhang, *Polymers (Basel)*. **2019**, *11*, DOI 10.3390/polym11040690.
- [104] G. Xing, T. Yan, S. Das, L. Ye, K. Ye, *RSC Adv.* **2018**, *8*, 20434–20439.
- [105] A. Efrem, K. Wang, P. N. Amaniampong, C. Yang, S. Gupta, H. Bohra, S. H. Mushrif, M. Wang, *Polym. Chem.* **2016**, *7*, 4862–4866.
- [106] H. W. Lee, S. K. Ji, I. Y. C. Lee, J. H. Lee, *J. Org. Chem.* **1996**, *61*, 2542–2543.
- [107] R. K. Pandey, R. K. Upadhyay, S. S. Shinde, P. Kumar, *Synth. Commun.* **2004**, *34*, 2323–2329.
- [108] J. Lozada, Z. Liu, D. M. Perrin, *J. Org. Chem.* **2014**, *79*, 5365–5368.
- [109] G. A. Molander, L. N. Cavalcanti, B. Canturk, P. S. Pan, L. E. Kennedy, *J. Org. Chem.* **2009**, *74*, 7364–7369.
- [110] R. S. Sprick, B. Bonillo, M. Sachs, R. Clowes, J. R. Durrant, D. J. Adams, A. I. Cooper, *Chem. Commun.* **2016**, *52*, 10008–10011.
- [111] M. Xue, B. Li, S. Qiu, B. Chen, *Mater. Today* **2016**, *19*, 503–515.
- [112] S. Bhattacharjee, M. I. Khan, X. Li, Q. L. Zhu, X. T. Wu, *Catalysts* **2018**, *8*, DOI 10.3390/catal8030120.
- [113] Z. Han, W. Shi, P. Cheng, *Chinese Chem. Lett.* **2018**, *29*, 819–822.
- [114] P. Zhang, S. Dai, *J. Mater. Chem. A* **2017**, *5*, 16118–16127.
- [115] P. Peluso, V. Mamane, S. Cossu, *J. Chromatogr. A* **2014**, *1363*, 11–26.
- [116] D. Asnaghi, R. Corso, P. Larpent, I. Bassanetti, A. Jouaiti, N. Kyritsakas, A. Comotti, P. Sozzani, M. W.

- Hosseini, *Chem. Commun.* **2017**, 53, 5740–5743.
- [117] M. G. Rabbani, H. M. El-Kaderi, *Chem. Mater.* **2012**, 24, 1511–1517.
- [118] D. S. Ahmed, G. A. El-Hiti, E. Yousif, A. A. Ali, A. S. Hameed, *J. Polym. Res.* **2018**, 25, DOI 10.1007/s10965-018-1474-x.
- [119] B. Alameddine, S. Shetty, N. Baig, S. Al-Mousawi, F. Al-Sagheer, *Polymer (Guildf)*. **2017**, 122, 200–207.
- [120] P. Mohanty, L. D. Kull, K. Landskron, *Nat. Commun.* **2011**, 2, 401–406.
- [121] Y. Wei, W. Chen, X. Zhao, S. Ding, S. Han, L. Chen, *Polym. Chem.* **2016**, 7, 3983–3988.
- [122] B. Alameddine, S. Shetty, R. S. Anju, F. Al-Sagheer, S. Al-Mousawi, *Eur. Polym. J.* **2017**, 95, 566–574.
- [123] W. Q. Wang, M. Y. Li, Q. X. Zeng, *Trans. Nonferrous Met. Soc. China (English Ed.)* **2012**, 22, 2831–2839.
- [124] S. Wu, Y. Ge, Y. Wang, X. Chen, F. Li, H. Xuan, X. Li, *Environ. Technol. (United Kingdom)* **2018**, 39, 1937–1948.
- [125] U. O. Aigbe, R. Das, W. H. Ho, V. Srinivasu, A. Maity, *Sep. Purif. Technol.* **2018**, 194, 377–387.
- [126] P. A. Kumar, M. Ray, S. Chakraborty, *J. Hazard. Mater.* **2007**, 143, 24–32.
- [127] C. Gao, X. Zhang, Y. Yuan, Y. Lei, J. Gao, S. Zhao, C. He, L. Deng, *Ecotoxicol. Environ. Saf.* **2018**, 166, 285–293.
- [128] S. Deng, R. Bai, *Water Res.* **2004**, 38, 2424–2432.
- [129] S. Rapti, A. Pournara, D. Sarma, I. T. Papadas, G. S. Armatas, A. C. Tsipis, T. Lazarides, M. G. Kanatzidis, M. J. Manos, *Chem. Sci.* **2016**, 7, 2427–2436.
- [130] M. Owlad, M. K. Aroua, W. A. W. Daud, S. Baroutian, *Water. Air. Soil Pollut.* **2009**, 200, 59–77.
- [131] A. D. Dwivedi, R. Permana, J. P. Singh, H. Yoon, K. H. Chae, Y. S. Chang, D. S. Hwang, *Chem. Eng. J.* **2017**, 328, 629–638.
- [132] L. Dupont, E. Guillon, *Environ. Sci. Technol.* **2003**, 37, 4235–4241.
- [133] B. Qiu, J. Guo, X. Zhang, D. Sun, H. Gu, Q. Wang, H. Wang, X. Wang, X. Zhang, B. L. Weeks, et al., *ACS Appl. Mater. Interfaces* **2014**, 6, 19816–19824.
- [134] S. Rapti, D. Sarma, S. A. Diamantis, E. Skliri, G. S. Armatas, A. C. Tsipis, Y. S. Hassan, M. Alkordi, C. D. Malliakas, M. G. Kanatzidis, et al., *J. Mater. Chem. A* **2017**, 5, 14707–14719.
- [135] S. Saini, S. Arora, Kirandeep, B. P. Singh, J. K. Katnoria, I. Kaur, *J. Environ. Chem. Eng.* **2018**, 6, 2965–2974.



## Curriculum vitae

**PROFILE***Nationality: Mozambican**Birthday: 27.11.1989**Swiss Permit B***ADDRESS**

*Ch. des jonchets 10  
1030 Bussigny, VD  
Switzerland*

**CONTACT***+41 78 837 99 35**joseluisbila@gmail.com**ORCID: 0000-0002-1260-064X***LANGUAGES***Portuguese – native**Shangaan – native**English – fluent**Turkish – fluent**French – B2+***TECHNICAL SKILLS***MATLAB**Python**Web design***SOFT SKILLS***Communication**Problem-solving**Leadership**Mentoring**Negotiation***EDUCATION***Sep 2019 École Polytechnique Fédérale de Lausanne - Switzerland**Present PhD in Chemistry**Aug 2015 Bilkent University - Turkey**Sep 2013 MSc in Chemistry**Aug 2015 Anadolu University - Turkey**Sep 2012 MSc in Chemical Engineering (incomplete)**Jan 2012 Aarhus University - Denmark**Aug 2011 Erasmus exchange program**Jun 2012 Middle East Technical University - Turkey**Sep 2008 BSc in Chemistry***RESEARCH AND TEACHING EXPERIENCE***Sep 2019 École Polytechnique Fédérale de Lausanne - Switzerland**Present Doctoral Assistant*

- Developed porous networks based on iron cage complexes and successfully employed them in gas storage, water purification and chiral recognition.
- Designed and synthesized iron based cage complexes for redox flow battery applications
- Oversaw 2 Masters student projects and performed as teaching assistant (600+ hours)

*Aug 2015 Bilkent University - Turkey**Sep 2013 Research and teaching assist.*

- Designed and synthesized heavy atom-free organic dyes photodynamic therapy
- Supervised Bachelors research projects (6 months).

**WORK EXPERIENCE***Jan 2018 Haltrie LLC - USA**Apr 2017 Business development Manager (Part-time)*

- Coordinated and directed the tender application proposal to USAID to supply water in 11 hospitals in rural areas of Ethiopia ( \$4 Million worth)
- Built a network of relevant manufacturers for tender applications between the USA and Turkey.

*Sep 2014 Pierre Cardin Office Furniture - Turkey**Apr 2014 Regional Sales Manager (Part-time)*

- Developed strategies for sales in 15 Sub-Saharan African countries resulting in the signing of business agreements in five countries.
- Oversaw international tender applications in Ghana, Mozambique and Uganda.

*Mar 2014 Yiğit Akü automotive battery manufacturer - Turkey**Feb 2012 Foreign Sales Assistant (Part-time)*

- Conducted customer search resulting in the acquisition of a leading Ghanaian customer (First deal signed worth \$50k+)
- Participated in Auto Parts Trade Fair in Lagos, Nigeria (1000+ visitors)

**INSTRUMENTS**

NMR, GC-MS, HPLC, SEM-EDX,  
Cyclic Voltammetry, TGA, UV-vis,  
Fluorimeter, FT-IR, Autosorb.

**HOBBIES**

Reading political magazines  
Playing berimbau

**REFERENCES**

Kay Severin

PhD Thesis Supervisor, EPFL  
Tel: +41 21 693 93 02  
e-mail: kay.severin@epfl.ch

Zeki Gündoğdu

Export Manager, Yiğit Akü  
Tel: +90 312 267 08 61  
e-mail: zekig@yigitaku.com

Engin U. Akkaya

Masters thesis supervisor, Bilkent  
University  
Tel: +90 312 290 24 50  
e-mail: eua.fen@bilkent.edu.tr

Jul 2011 **Senkron Plastik - Turkey**  
May 2011 *Quality Assurance Assistant (Internship)*

- Conducted quality control tests on raw materials and products
- Managed the laboratory reporting system

**EXTRACURRICULAR ACTIVITIES**

Present **The Consulting Society at EPFL - Switzerland**  
Jun 2018 *President*

- Leading a team of 20+ students to organize consulting related workshops and undertake communication with major sponsors (e.g.: BCG, McKinsey, Bain, etc.)
- Establishing a case interview platform intended for EPFL and Unil students
- Overseeing the organization of 30+ consulting events (case-study evenings, consulting career development workshops, Sponsoring company events)

Present **Capoeira Luanda de Renens - Switzerland**  
Nov 2017 *Vice-President*

- Co-organized the annual roda event in 2017 (50+ attendees)
- Created marketing campaigns leading in increase of students by 100%

**AWARDS**

- Awarded a Master's scholarship: Turkish government – 2012 (Top 10%)
- Bronze medal in African Karate championships – 2007 (Kumite male – 55 kg)
- Bronze medal in Turkish Language Olympiads – 2006 (300+ participants)

**CONFERENCES**

- SCS Fall meeting: poster presentation – 2019
- Challenges and opportunities in energy research: Oral presentation – 2018
- Conference of chromogenic and emissive materials: Poster presentation - 2014

**PUBLICATIONS**

- Ozdemir, T., **Bila, J. L.**, Sozmen, F., Yildirim, L. T. and Akkaya, E. U., *Org. Lett.*, **2016**, 18, 4821-4823.
- Marmier, M., Cecot, G., Vologzhanina, A. V., **Bila, J. L.**, Zivkovic, I., Ronnow, H. M., . . . Severin, K., *Dalton Trans.* **2016**, 45, 15507-15516.
- Eymann, L. Y., Tskhovrebov, A. G., Sienkiewicz, A., **Bila, J. L.**, Živković, I., Rønnow, H. M., . . . Severin, K., *J. Am. Chem. Soc.*, **2016**, 138, 15126-15129.
- **Bila, J. L.**, Marmier, M., Zhurov, K.O., Scopelliti, R., Zivkovic, I., Ronnow, H. M., . . . Severin, K., *Eur. J. Inorg. Chem.*, **2018**, 3118-3125.
- **Bila, J. L.**, Pijeat, J., Ramorini, A., Fadei-Tirani, F., Scopelliti, R., Baudat, E. and Severin, K., *Dalton Trans.* **2019**, 48, 4582-4588.